Uncovering Mechanisms Behind Simple Steatosis Progression to Non-Alcoholic Steatohepatitis

Nancy Magee Emole

B.Sc., Chemistry, Dillard University, 2014

Submitted to the graduate degree program in Toxicology and the Graduate Faculty of the University of Kansas in partial fulfillment of the requirements for the degree of Doctor of Philosophy.

____

Chair: Yuxia Zhang, PhD

____

Wen-Xing Ding, PhD

____

Bruno Hagenbuch, PhD

____

Michele Pritchard, PhD

____

Chad Slawson, PhD

Date Defended: 19 May 2020

The dissertation committee for Nancy Magee Emole certifies that this is the approved version of the following dissertation:

Uncovering Mechanisms Behind NAFL Progression to NASH

Chair: Yuxia Zhang, PhD

Graduate Director: Bruno Hagenbuch, PhD

Date Approved: 05 June 2020

Abstract

Non-alcoholic fatty liver disease (NAFLD) is the most common type of chronic liver disease in the Western countries. NAFLD encompasses the entire spectrum of fatty liver disease in individuals without significant alcohol consumption, ranging from nonalcoholic fatty liver (NAFL) to non-alcoholic steatohepatitis (NASH) and cirrhosis. The molecular events that influence disease progression from NAFL to aggressive NASH remain poorly understood; leading to a lack of mechanism-based targeted treatment options for NASH. Therefore, an increased understanding of NASH pathogenesis is pertinent to improve disease interventions in the future.

The first objective of this dissertation was to identify key signatures associated with disease progression from NAFL to NASH. Using a diet high in fructose, cholesterol, and fat (HFCF) for up to 9 months, we were able to induce NAFLD spectrum similar to humans in C57BL/6J mice. Specifically, the mice sequentially developed steatosis, steatohepatitis, steatohepatitis with fibrosis, and eventually spontaneous liver tumor as time on the HFCF diet progressed. These data indicate this NAFLD mouse model with disease progression from NAFL to NASH recapitulates key metabolic, and histologic changes seen in humans and could be used for further studies.

It is well known that NASH is characterized by steatosis plus inflammation with or without fibrosis. Nuclear receptor, small heterodimer partner (*SHP*, *NR0B2*), plays a complex role in lipid metabolism and inflammation. The expression of SHP is negatively correlated with NAFLD progression, indicative of a biological relevance of SHP in NAFLD. Therefore, the second objective of this dissertation was to understand the mechanism behind SHP suppression in NAFLD. Using palmitic acid (PA) or lipopolysaccharide (LPS) combined with pathway inhibitors, we observed that only the inhibition of c-Jun N-terminal kinase (JNK) activation rescued *Shp* expression. Mechanistically, we found that the downstream target of JNK, c-JUN, directly binds to the promoter region of *Shp*, preventing activation of *Shp* by liver receptor homolog-1.

The next objective of this dissertation was to understand the role of hepatic SHP in NAFLD. By treating mice that lack or overexpress hepatic SHP with normal chow or HFCF diet, we sought to determine SHP's role in regulating steatosis and inflammation. We

uncovered that hepatocyte *Shp* deletion (*Shp*$^{Hep-/-}$) in mice resulted in increased chemokine (C-C motif) ligand 2 (CCL2) secretion which led to a massive infiltration of macrophages and CD4^{+} T cells to the liver. Additionally, *Shp*$^{Hep-/-}$ mice developed reduced steatosis, but surprisingly increased hepatic inflammation and fibrosis after being fed the HFCF diet. Supporting this data was the RNA-seq analysis which revealed that pathways involved in inflammation and fibrosis were significantly activated in the livers of *Shp*$^{Hep-/-}$ mice fed a chow diet. After being fed the HFCF diet, wildtype mice displayed up-regulated peroxisome proliferator-activated receptor g (*Pparg*) signaling in the liver; however, this response was completely abolished in the HFCF-fed *Shp*$^{Hep-/-}$ mice. Additionally, *Shp*$^{Hep-/-}$ mice had consistent hepatic nuclear factor κB (NF-κB) activation. To further characterize the role of *Shp* specifically in the transition of steatosis to NASH, mice were fed the HFCF diet for 4 weeks followed by *Shp* deletion. Surprisingly, *Shp* deletion after steatosis development exacerbated hepatic inflammation and fibrosis without affecting liver steatosis.

RNA sequencing of hepatic mRNA from mice on the HFCF for 1 month (NAFL) and 3 months (transitioning to NASH) revealed that the key signatures associated with the progression of steatosis to steatohepatitis were related to extracellular matrix organization and immune responses such as leukocyte aggregation, chemotaxis, phagocytosis, and dendritic cell differentiation. Interestingly, our data also revealed that genes regulated by transcription factor forkhead box M1 (*Foxm1*) and negative elongation factor complex member E (*Nelfe*) were significantly altered during the disease progression. This was observed in a mouse NAFLD model as well as in patients with NAFLD. As of now, both regulators have been explored in hepatocellular carcinoma, and studies indicating FOXM1 as a regulator of insulin signaling are surfacing. However, the paucity of studies relating FOXM1 and NELFE to NAFLD development and progression warrants additional investigation.

The data presented within this dissertation indicate that the decrease of SHP in NAFLD is due to JNK activation of c-Jun which inhibits *Shp* transcription. Importantly, we demonstrate that, depending on the stage of NASH, hepatic *Shp* plays an opposing role in steatosis and inflammation. Mechanistically, *Shp* deletion in hepatocytes activates NF-κB and impairs *Pparg* activation, leading to the dissociation of steatosis, inflammation, and fibrosis in NASH development. Lastly, RNA-seq analysis of our mouse NAFL and early-stage NASH models reveals the prospective involvement of transcription factors, FOXM1 and NELFE in NASH development. Overall, this dissertation research provides new insights into understanding the regulation of NAFLD progression from NAFL to NASH with the intention to aid in development of novel preventative, diagnostic, and therapeutic strategies for NASH.

Acknowledgments

During all stages of life, it takes a village of support to achieve your goals. I am forever grateful for my mom, mentors, lab mates, family, numerous friends, co-workers-turned-family (i.e. Diana Kalinowska), and the night-shift janitors—my village—who constantly encouraged me along the way. To my precious daughter, Amarachi, thank you for waiting patiently for mommy to come home. Thank you for always brightening up my days with your laughter and cheerfulness. May you to grow to become much greater than I could ever know. You are the sun in my shine. I love you forever.

Thank you, my committee members, for your kindness and extensive help through the years. Dr. Wen-Xing Ding, thank you for bringing calmness and simplicity into the meeting room. Dr. Chad Slawson, thank you for teaching me that intelligence is not boastful. Dr. Pritchard, thank you for always lending your helpful advice. Dr. Hagenbuch, thank you for all of your *gentle* reminders and putting/keeping me on track. The most special "THANK YOU" belongs to the *World's Greatest Mentor*, Dr. Yuxia (Lisa) Zhang. You are truly a *SUPER* woman, mom, and scientist.

Thank you for accepting me into your lab when I had little experience;

Thank you for mentoring and for teaching me proper lab and life-balancing techniques;

Thank you for your never-ending concern and consideration;

Thank you, for your patience;

Thank you, for your kindness;

Thank you, for your diligence;

Thank you for *all* the time you spent helping me;

Thank you for going above and beyond expectations during these times; and

Thank you, most of all, for your ever-renewing faith in me.

I will always cherish your words of wisdom, and I hope to be as great a mentor as you.

This work would not be possible without funding support. This dissertation was supported by National Institutes of Health grants R01DK119131, K22CA184146, P20 GM103549, P30GM118247, P20GM103418, T32ES007079, UL1 TR002366 and KUMC Enhancement Award, American Association for the Study of Liver Diseases (AASLD) Bridging Award, and American Cancer Society (ACS) Institutional Research Grant (IRG) 16-194-07.

Table of Contents

List of Tables

List of Figures

Abbreviations

ABBREVIATION	TERM
AAV8	Associated Virus Serotype 8
ABCA1	ATP Binding Cassette Subfamily A Member 1
ABCG5	ATP Binding Cassette Subfamily G Member 5
ACC	Acetyl-CoA Carboxylase
ACLY	ATP Citrate Lyase
ALB	Albumin
ALT	Alanine Aminotransferase
APOB	Apolipoprotein B
ARG1	Arginase 1
AST	Aspartate Aminotransferase
ATF4	Activating Transcription Factor 4
BA	Bile Acid
BAFF	B-Cell-Activating Factor
BSA	Bovine Serum Albumin
CCL2	Chemokine (C-C Motif) Ligand 2
ChIP	Chromatin Immunoprecipitation
CHOP	C/EBP Homologous Protein
CIDEC	Cell Death Inducing Dffa Like Effector C
COL1A1	Collagen Type 1 Alpha 1
COL1A2	Collagen Type 1 Alpha 2
CPT1A	Carnitine Palmitoyltransferase 1a
CTGF	Connective Tissue Growth Factor
DAMP	Damage-Associated Molecular Patterns
DEG	Differentially Expressed Genes
ER	Endoplasmic Reticulum
eIF2a	Eukaryotic Translation Initiation Factor 2 alpha
FABP1	Fatty Acid-Binding Protein 1
FBS	Fetal Bovine Serum
FDR	False-Discovery Rate
FPKM	Fragments per Kilobase of exon model per Million reads mapped
FOXM1	Forkhead Box M1
FXR	Farnesoid X Receptor
GEO	Gene Expression Ominbus
GLP-1	Glucagon-Like Peptide 1
GSH	Glutathione
GTT	Glucose Tolerance Test
HCC	Hepatocellular Carcinoma
HFCF	High Fat, Cholesterol, and Fructose
HHIP	Hedgehog Interacting Protein
HNF4a	Hepatocyte Nuclear Factor 4 Alpha
HPRT1	Hypoxanthine Phosphoribosyl Transferase 1

HSC	Hepatic Stellate Cell
IFNg	Interferon Gamma
IL	Interleukin
ITT	Insulin Tolerance Test
JNK	c-Jun N-Terminal Kinase
KEGG	Kyoto Encyclopedia of Genes and Genomes
LPS	Lipopolysaccharide
LRH1	Liver Receptor Homolog-1
LXR	Liver X Receptor
LXRE	Liver X Receptor Response Element
MAPKK	Mitogen-Activated Protein Kinase Kinase
MCD	Methionine Choline Deficient
ME1	Malic Enzyme 1
MMP	Matrix Metallopeptidase
MR	Mineralocorticoid Receptor
MTTP	Microsomal Triglyceride Transfer Protein
NAFL	Nonalcoholic Fatty Liver
NAFLD	Nonalcoholic Fatty Liver Disease
NAS	NAFLD Activity Score
NASH	Nonalcoholic Steatohepatitis
NELFE	Negative Elongation Factor
NF-κB	Nuclear Factor Kappa B
NLRP3	NLR Family Pyrin Domain Containing 3
NOS	Nitric Oxide Synthase
OX-LDL	Oxidized Low-Density Lipoprotein
PA	Palmitic Acid
PBS	Phosphate Buffered Saline
PDGF	Platelet-Derived Growth Factor
PI3K	Phosphoinositide 3-Kinase
PPAR	Peroxisome Proliferator-Activated Receptor
qPCR	Quantitative Polymerase Chain Reaction
ROS	Reactive Oxygen Species
RXR	Retinoid X Receptor
SCD1	Stearoyl-CoA Desaturase-1
SHH	Sonic Hedgehog
SHP	Small Heterodimer Partner
$Shp^{Hep-/-}$	Hepatocyte-Specific *Shp* Knockout
SREBP1c	Sterol Regulatory Element Binding Protein 1 C
SREBP2	Sterol Regulatory Element Binding Protein 2
STC2	Stanniocalcin 2
T2DM	Type II Diabetes Mellitus
TBG	Thyroxine-Binding Globulin
TF	Transcription Factor
TGF-b	Transforming Growth Factor Beta
TLR	Toll-Like Receptor

TNFa	Tumor Necrosis Factor Alpha
TRE	Tetradecanoylphorbol-13-Acetate Response Element
TUNEL	Terminal Deoxynucleotidyl Transferase DUTP Nick End Labeling
VLDL	Very Low-Density Lipoprotein
XBP1	X-box Binding Protein 1

Chapter 1: Introduction

This chapter is adapted from our previously-published article in an open-access journal: Magee N, Zou A, Zhang Y. Pathogenesis of nonalcoholic steatohepatitis: interactions between liver parenchymal and nonparenchymal cells. BioMed research international, 2016, 2016: 5170402. PMCID: PMC5086374. www.hindawi.com/

Non-alcoholic fatty liver disease

Non-alcoholic fatty liver disease (NAFLD) is the most common type of chronic liver disease in Western countries and is a major health concern in both adults and, tragically, in children (1,2). The most recent study found that the global prevalence of NAFLD was 25% and in patients with type 2 diabetes mellitus (T2DM), 55.5% (3). Encompassing the entire spectrum of fatty liver disease in individuals without significant alcohol consumption, NAFLD is further histologically categorized into nonalcoholic fatty liver (NAFL; steatosis without hepatocellular injury) and nonalcoholic steatohepatitis (NASH) which is characterized by the presence of hepatic steatosis and inflammation with hepatocyte injury (ballooning) with or without fibrosis (4). NAFL is considered the benign and reversible stage, which arises due to an excessive accumulation of triglycerides in hepatocytes (4). In contrast, NASH is a more advanced stage of NAFLD, since the chances of developing more serious diseases such as cirrhosis, hepatocellular carcinoma (HCC), and cardiovascular diseases increase in patients with NASH (4). A study showed the mean annual rate of fibrosis progression in NASH is 9%, and NASH overall mortality is 25.6 per 1,000 person-years (5).

The pathogenesis of NASH is complex (6-8). Additional progress has been made to understand the role of the immune system during NASH progression. For example, inflammation, which occurs in NASH patients and in animal models of human NASH, is induced by various mediators including endotoxins, adipokines, inflammatory cytokines, chemokines, and other inflammatory mediators (9). The cellular sources of these molecules are broad and include hepatocytes, hepatic stellate cells, portal fibroblasts, adipocytes, and immune cells such as neutrophils, macrophages, natural killer cells, natural killer T cells, and lymphocytes (10). Moreover, what has greatly improved our understanding of NASH is an increasing recognition of the importance of interactions between liver parenchymal and nonparenchymal cells as well as crosstalk between various immune cell populations in liver as well as other organs such as brain, adipose, and gut (11-13).

Hypotheses describing pathogenesis of NASH

The mechanisms leading to NASH are multifactorial. A retrospective study using liver biopsies from patients with NAFL or NASH suggests that rather than being distinct entities, NAFL and NASH represent different stages in the progression of NAFLD (14). It is known that an important factor which drives NAFLD progression is hepatocyte damage (15). In the initial phase, hepatocyte damage triggers the release of damage-associated molecular pattern molecules (DAMPs) into the microenvironment, which stimulates macrophage activation (16). This process is influenced by both direct metabolic effects in the liver, such as excessive oxidative stress driven by lipotoxic metabolites (17,18), as well as indirect effects coming from other tissues such as inflammatory initiators released by adipose tissue (19), the intestine (20), and the immune system (21). As a result of these complicated effects, there have been multiple hypotheses describing the pathogenesis of NASH, such as the "two-hit", "three-hit", and "multiple-hit" hypotheses.

The "two-hit" hypothesis was originally proposed in 1998 (22). This hypothesis infers that the first hit is insulin resistance which leads to aberrant lipid accumulation in the liver, and is followed by a second hit driven by lipotoxic metabolite-induced mitochondrial dysfunction and oxidative stress leading to hepatocyte death and inflammation (22,23). In the healthy liver, dead hepatocytes are normally replaced by replication of existing, mature hepatocytes; thus, normal liver function is maintained. In NASH, however, the replication of mature hepatocytes is inhibited and accompanied by the expansion of a progenitor cell population (24). The progenitor cells can either differentiate into hepatocyte-like cells or into cholangiocytes, which aid in the recovery of normal liver function. However, the abnormal expansion of progenitor cells contributes to more unfavorable outcomes such as HSC activation and liver fibrosis (25). Thus, a "third hit", which drives NASH pathogenesis, involves inadequate hepatocyte proliferation after cell death triggered by insulin resistance-induced aberrant lipid accumulation and excessive oxidative stress (26).

More recently, several different inflammatory mediators released from adipose tissue and the liver/gut axis have been implicated in NASH pathogenesis. Thus, a "multiple-hit" hypothesis involving organ-organ interactions in NASH is also appreciated (27). In this model, NASH pathogenesis is initiated through triggering excessive oxidative stress by lipotoxic metabolites. This, in turn, drives hepatocyte death, inflammation, and fibrosis. Additional pathogenic factors from other organs, such as gut-derived endotoxins resulting from increased gut permeability and gut dysbiosis, adipokines secreted from adipose tissue, are all considered crucial to NASH pathogenesis (28).

Lipotoxic hepatocyte injuries, oxidative stress and ER stress

Lipotoxicity, characterized by excessive free fatty acid accumulation within hepatocytes, is known to generate toxic lipid metabolites and cause hepatocyte injury via ballooning, and, consequently, initiation of NASH. Ballooned hepatocytes are a cardinal histologic feature of lipotoxic hepatic injury, and the magnitude of ballooned hepatocytes correlates with disease severity. In fact, semi-quantitation of hepatocyte ballooning is used to calculate the NAFLD activity score (NAS), a measure of disease severity (29), supporting the importance of this phenomenon in disease progression.

Increased dietary intake of free fatty acids, as well as *de novo* lipogenesis and adipose lipolysis, together with impaired free fatty acid oxidation, cause an increase in the accumulation of free fatty acids in hepatocytes. Hepatocytes store free fatty acids as triglycerides. An interesting study indicated that triglycerides themselves are unlikely to be the cause of hepatocyte injury in NASH (30). Instead, hepatocyte triglyceride accumulation may act as a protective mechanism to counter free fatty acid-induced lipotoxicity (30,31). However, once the threshold of lipid storage is exceeded, the excessive accumulation of free fatty acids leads to production of toxic lipid metabolites, such as ceramides, diacylglycerols, lysophosphatidylcholine, and oxidized cholesterol metabolites (24,30). These toxic lipid metabolites promote the overproduction of reactive oxygen species (ROS), which cause liver injury.

Of all the mechanisms related to NASH, oxidative stress has been most widely studied (17,18,32,33). Oxidative stress is triggered by an imbalance between pro-oxidants and antioxidants. It is now clear that oxidative stress can mediate liver injury through at least two major mechanisms, direct cell injury and indirect changes of cell signaling pathways. For example, ROS induces activation of nuclear factor κB (NF-κB), a master regulator in the production of proinflammatory cytokines including interleukin-1b (IL-1b), tumor necrosis factor a (TNF-a), and interleukin-6 (IL-6) (34). Liver-specific inhibition of NF-κB is expected to ameliorate high fat diet (HFD)-induced hepatic inflammation (35,36). However, the role of NF-κB in NASH pathogenesis is more complicated than researchers originally thought. There is also evidence to suggest that inflammation is required for liver regeneration, which is mediated through anti-apoptotic and pro-proliferative characteristics of NF-κB (37).

Free fatty acid-induced oxidative stress also acts as an upstream mechanism to activate endoplasmic reticulum (ER) stress in NASH. ER stress is initiated by conditions associated with protein overload or increased amount of unfolded proteins. Activation of ER stress response causes adaptation and recovery of homeostasis; however, severe or prolonged ER stress can ultimately lead to cell death. Recently, attention has turned to the ER due to increasing evidence demonstrating that ER stress is a common feature in NAFLD (38). For example, one study showed that two ER stress markers, X-box binding protein 1 (*XBP1*) and stanniocalcin 2 (*STC2*), are increased in human NASH (39). This study also found that other ER stress proteins, including activating transcription factor 4 (ATF4), C/EBP homologous protein (CHOP), and phosphorylated c-Jun N-terminal kinase (JNK) and eukaryotic translation initiation factor 2 alpha (eIF2a), were not significantly changed in NASH samples (39). Additional studies found activation of ER stress can trigger various inflammatory pathways, such as JNK and NF-κB signaling pathways, further enhancing NASH progression (38,40,41). On the other hand, reduced inflammation ameliorates ER stress-induced liver injury. Kandel-Kfir (2015) showed that interleukin-1 alpha (*Il-1a)* deficient mice display reduced inflammation, hepatocyte death, and liver damage in an ER stress-induced steatohepatitis model (42). Intuitively, researchers have used various natural antioxidants found in coffee, tea, and soy in several rodent NAFLD models and found beneficial effects on lipid metabolism, glucose metabolism, fibrosis, and even HCC (43). These studies help to understand a complex puzzle of NASH pathogenesis, aiding in the elucidation of ER stress risk factors involved in NASH development. Nonetheless, further study is needed and encouraged.

Inflammatory mediators and immune alterations

Accumulated studies demonstrate that immunological mechanisms, including innate immunity (mediated by neutrophils, macrophages, natural killer cells and natural killer T cells), adaptive immunity (mediated by T and B cells), NLR family pyrin domain containing 3 (NLRP3) inflammasome activation, and the gut-liver axis, are implicated in the NAFLD progression (44,45). For example, portal inflammatory infiltrates in human NASH patients are characterized by both broad leukocyte subset markers (CD68, CD3, CD8, CD4, CD20, and neutrophil elastase) and selected inflammatory markers (matrix metalloproteinase 9 and interleukin [IL]-17) (46). The balance of the various immune cell populations and their products involved in inflammatory signaling pathways is crucial as it is a determinant of NASH attenuation or progression (47).

Macrophages and gut microbiota

Macrophages, also termed mononuclear phagocytes, represent a major cell type of innate immunity. Hepatic macrophages consist of resident macrophages called Kupffer cells and infiltrated bone marrow-derived monocytes/macrophages. Kupffer cells are named after their discoverer, Carl Wilhelm von Kupffer, who originally identified the cells as “sternzellen” or “star cells,” now known to be HSC, but later were correctly identified as macrophages by scientist Tadeusz Browicz (48,49). Kupffer cells, dendritic, natural killer and natural killer T cells, are located within the sinusoidal space of the liver. Given that Kupffer cells are the body’s primary line of defense against microorganisms that would cause a gut-derived immune response, this location is optimal for the macrophages to carry out their functions in liver. During liver injury, Kupffer cells are important in the initial response by rapidly producing cytokines and chemokines which induce the recruitment of other immune cells, including monocytes, into the liver. Both the infiltrating macrophages and the resident Kupffer cells produce proinflammatory and anti-inflammatory cytokines, contributing to the chronic inflammation such as that seen in alcoholic liver disease, NAFLD, and other pathological conditions affecting liver (50-52).

The liver is constantly exposed to antigens and low levels of endotoxins from the gut as 70% of the liver’s blood is supplied from the portal vein. In normal conditions, small amounts of endotoxins from the gut bacteria enter the liver and most of them are eliminated by Kupffer cells. Thus, the resident Kupffer cells play a critical role in maintaining liver homeostasis and immunological tolerance in the liver. However, the altered composition of microbiota, increase of gut permeability, and hyper responsibility of Kupffer cells to the gut-derived endotoxin can interrupt this tolerance. Recently, gut microbiota analysis revealed that individuals with NAFLD have a lower percentage of *Bacteroidetes* with higher levels of *Prevotella* and *Porphyromonas* species compared to healthy controls (53). Another study found that the inflammasome-mediated dysbiosis of gut microbiota exacerbates hepatic steatosis and inflammation through enhancing liver TNFa production (54). The prolonged exposure to ethanol is known to promote hepatic macrophage hypersensitivity to LPS from the gut and induce a high production of TNFa, leading to alcoholic liver disease (55). Interestingly, patients with NASH harbor modified microbiota that produce endogenous ethanol, suggesting a role for alcohol-producing microbiota in the pathogenesis of NASH (56).

The contribution of macrophages to NAFLD progression is a late outcome of steatosis but an early participant in NASH development, although altered macrophage function has been documented in many stages of NAFLD (57). Macrophages are extraordinarily versatile cells and exhibit various phenotypes ranging from a pro-inflammatory classical M1 type to an anti-inflammatory alternative M2 type, depending on the conditions of local microenvironment (58). The M1 macrophages are abundant in HFD liver and play a critical role in driving inflammation and hepatocyte injury (59). M2-polarized macrophages counterbalance M1 macrophage-induced inflammation, promoting resolution of inflammation and tissue repair (60). Increasing M2 macrophages promotes M1 macrophages apoptosis which protects against NAFLD progression (59). The influence of hepatocyte on macrophages polarization was recently demonstrated in human differentiated macrophage THP-1 cells (61). In this study, HepG2 cells, a human hepatoblastoma-derived cell line, were pretreated with ER-stress inducers tunicamycin and thapsigargin. The THP-1 cells were then exposed to the conditional medium from HepG2 cells and subsequently displayed a M2 phenotype, mediated by the peroxisome proliferator-activated receptor g (PPARg) signaling pathway. The authors further demonstrated that macrophage M2 activation is initiated by cytokines IL-10 and IL-4 releasing from prolonged ER stressed hepatocytes.

Macrophage-mediated inflammation in NASH is associated with toll-like receptor (TLR) activation; this is particularly true for TLR4 (62). During liver injury, macrophages release proinflammatory cytokines such as IL-1b, TNFa, and IL-6 through the activation of TLR4 (63). When prolonged, this contributes to T cell activation and results in hepatocyte death and subsequent activation of hepatic stellate cells (64). Accordingly, TLR4 inhibition or macrophage depletion reduces hepatic damage and prevents NASH development (65,66). Interestingly, during NASH, liver macrophages engulf an excessive amount of oxidized low-density lipoprotein (ox-LDL) and form "foam cells" (67). These macrophage-derived foam cells predominantly contain enlarged lysosomes filled with cholesterol and cholesterol crystals. Additional evidence showed that increased cholesterol storage inside lysosomes of Kupffer cells is associated with hepatic inflammation in the context of NASH (68,69)

Taken together, hepatic macrophages play a critical role in maintaining immune homeostasis of the liver. The important function they play in the pathogenesis of NASH makes them an attractive therapeutic target for NASH treatment. More research on macrophage phenotypes and functions is required to better understand these cells to develop novel macrophage-based therapeutic interventions.

Neutrophils

Neutrophils (also known as neutrophilic granulocytes or polymorphonuclear leukocytes) are the first immune cells to infiltrate the liver after acute injury. The contribution of neutrophils in NASH pathogenesis is studied in human NASH and in mouse models. One study found neutrophils infiltrate into the livers of patients with NASH and frequently surround steatotic hepatocytes, resembling the crown-like structures in obese adipose tissue (70). Moreover, the neutrophil-to-lymphocyte ratio is higher in patients with advanced fibrosis (71). Transgenic mice expressing human neutrophil peptide-1 (HNP-1) display enhanced hepatic fibrosis through inducing hepatic stellate cells proliferation in a choline-deficient and L-amino acid-defined diet-induced mouse model of NASH (72). In contrast, deletion of elastase, a protease secreted by neutrophils in HFD-induced obese mice, improves liver tissue inflammation with a lower infiltration of neutrophils and macrophages (73). Beyond this, a better understanding of neutrophil function in the pathophysiology of NASH is still needed and requires further study.

T and B lymphocytes

T and B lymphocytes mediate the adaptive immune response. For instance, T helper cells, a sub-group of T lymphocytes, can drive the activation of the other immune cells. They accomplish this through, for example, by helping B cells switch antibody classes, by activating cytotoxic T cells, and by maximizing macrophage phagocytosis through cytokine release (74). Depending on the cytokine environment, T helper cells can assume a proinflammatory phenotype (Th1), characterized by the release of INF-g and transforming growth factor-b (TGF-b) or an anti-inflammatory phenotype (Th2), characterized by the release of IL-4, IL-5, and IL-10 (75). The balance between Th1 and Th2 T cells is important to maintain immune system homeostasis. For example, Th1 and Th2 enhancement can affect macrophage polarization; in particular, Th1 induces macrophages M1 polarization via the release of INF-g (75).

The distinct role of different T cell populations in the pathogenesis of NASH has been recently appreciated (8). For instance, in human NASH liver biopsy sections, the portal tract infiltrates are dominated by CD8 (+) lymphocytes (46). Limiting CD8 (+) T-cell expansion by dendritic cells protects mouse liver from NASH development (76). Th17 cells, a subtype of T helper cells, facilitate leukocyte recruitment through the secretion of various cytokines including IL-17 (IL-17A, IL-17F), IL-21, IL-22, and TNF-a. Hepatic Th17 cell infiltration is found in NASH (77). In addition, IL-17 secretion exacerbates hepatic steatosis and inflammation, whereas IL-17 neutralization attenuates LPS-induced liver injury (77). Furthermore, *Il-17a*$^{-/-}$ mice were resistant to the development of steatohepatitis, whereas wild-type mice showed progression from NAFL to NASH via the induction of the *Il-17* and downstream mediators (78). Another study reports the progression from NAFL to NASH is marked by an increase of ratio of Th17/resting regulatory T cells in peripheral blood and liver (79).

By driving T cell activation and secreting proinflammatory cytokines or chemokines, B cells play a critical role in NASH pathogenesis (8,80). Lipid peroxidation products, arisen from phospholipid oxidation, interact with cellular proteins and are one of the sources of neo-antigens able to promote an adaptive immune response in NASH (81). As evidence, 40%-60% of patients with NASH have circulating antibodies against lipid peroxidation-derived antigens such as malonyldialdehyde or 4-hydroxynonenal (82). Furthermore, the high titers of these antibodies are in parallel with increased risk to develop advanced liver fibrosis (33). Recently, the contributions of B cells to obesity, diabetes and NAFLD are extensively examined using animal models. Winer (2011) demonstrated that B cells rapidly increase in serum and adipose tissue of mice fed a HFD (83). In this study, B cell deficient mice (B null) fed HFD display a reduced insulin resistance, and adoptive transfer of B cells or IgG isolated from mice fed HFD into B null mice can reverse that phenotype and induce insulin resistance (83). B-cell-activating factor (BAFF, TNFSF13B) is a cell survival and maturation factor for B cells, and overproduction of BAFF is associated with systemic autoimmune disease (84). Recently, an increase of serum level of BAFF was identified in human NASH, and the serum BAFF level correlates with B cell content in liver (85). In addition, BAFF receptor deficient mice display improved obesity and insulin resistance induced by HFD but also, unexpectedly, show enhanced hepatic steatosis, which indicates a protective role of BAFF in hepatic steatosis (85,86). However, contradictory observations on the B-cell's contribution to insulin resistance and NAFLD have also emerged. Bhattacharjee (2014) found that B cell defect mice [CBA/CaHN-Btk$^{xid/J}$ (xid mice)] fed high fructose drinking water develop the same level of glucose intolerance and insulin resistance as wild-type mice (87), which suggests that B cells do not play a role in NAFLD progression. The reason for these contradictory observations could be, in part, due to the differences in B cell deficient mutant mouse strains and different diet-induced NAFLD models.

NLRP3 inflammasome

NLRP3 inflammasome is a large, intracellular multiprotein complex expressed in both parenchymal and non-parenchymal cells of the liver. In response to various cellular danger signals, NLRP3 inflammasomes activate caspase-1 and release mature IL-1b and IL-18 (88). Interestingly, recent studies revealed NLRP3 inflammasome activation as an emerging factor contributes to NASH development. For example, the expressions of NLRP3 components, *pro-Il-1b* and *pro-Il-18*, are markedly increased both in mouse models and humans with NASH (89,90). Moreover, *Nlrp3* knockout mice or *Il-1a* or *Il-1b* knockout mice are protected from diet-induced liver injury, inflammation, and fibrosis (90,91). Another study demonstrates that selective inhibition of caspase-1 alleviates hepatic steatosis, inflammation, and fibrosis in a diet-induced mouse model of NASH (92). These studies strongly suggest that NLRP3 inflammasome may serve as a potential therapeutic target for the treatment of NASH.

HSCs and Fibrosis in NASH Progression

Liver fibrosis is a condition in which an excessive amount of extracellular matrix (ECM) proteins, like type I collagen, accumulate in the liver. This buildup of ECM occurs in most types of chronic liver diseases including NAFLD (93). Although many cell types, including the hepatocytes and sinusoidal endothelial cells have been identified as contributors of ECM components, liver myofibroblasts, originally from HSCs (from the word of Latin origin, *stella*, meaning *star*), portal fibroblasts (PFs) or mesothelial cells are the major source of ECM (94). The role HSCs play in fibrosis is unequivocal. Data have demonstrated that HSC activation precedes fibrogenesis and that a lack of HSC activation halts the process (95-97). Lipid accumulation, as that seen in NAFLD, triggers a profibrogenic response from HSCs (98), therefore an overview of fibrogenesis in NASH is critical to understanding NASH progression.

HSC activation involves two phases: the initiation phase and the perpetuation phase (99). During the initiation phase, HSCs proliferate and become myofibroblast-like in response to proliferative and fibrogenic cytokines. Only activated HSCs express alpha2-macroglobulin, P100, CD95L, and reelin, making these proteins good identifiers for HSC activity (96,100,101). There are many cells involved in activating HSC. For example, hepatocytes, liver sinusoidal endothelial cells, macrophages, NK cells and lymphocytes play roles in the activation process (102). Those cells secrete mediators that affect HSC activation. Of the mediators that are released, platelet-derived growth factor (PDGF) and transforming growth factor beta (TGF-β) are the two best-described growth factors. PDGF is involved in the signaling process required for HSC proliferation, while TGF-β promotes collagen production (103). The increase of ECM components (fibrillar collagens such as type I collagen) and inhibitors of matrix-degrading enzymes, like tissue inhibitor of matrix metalloproteinases (TIMP), occurs in the second phase of

HSC activation—an event resulting in matrix accumulation, especially at sites where many activated HSCs reside (93).

Extensive studies have investigated how HSCs are activated in NAFLD. Lipid metabolites accumulation in hepatocytes induces TGF-β signaling and impairs adiponectin activity, supporting a key role for lipotoxicity in the development of hepatic fibrosis (104). Recent data demonstrate a positive correlation between the Notch signaling pathway and HSC activation. In TGF-β-activated HSCs, Notch pathway components are significantly increased and inhibition of Notch signaling decreases HSC activation (105). Bernd *et al.*, demonstrated that TGF-β-activated kinase 1 (TAK1)/c-Jun N-terminal kinase (JNK) and p38 pathways work collaboratively in HSC activation. TAK1/JNK promotes HSC proliferation while p38 decreases HSC proliferation (106). Another recent study suggests that osteopontin and high mobility group box 1 (HMGB1) releasing from necrotic hepatocyte also play a key role in HSC activation (107). Most recently, Dr. Diehl and co-workers discovered that ballooned hepatocytes generate sonic hedgehog (Shh), a ligand of the hedgehog-signaling pathway, which promotes HSC activation and drives NASH progression in mice (108). Those studies support the notion that HSCs shift from a quiescent state to an ECM-producing machine in NASH, and the regulation for that process is quite complex. Interestingly, one study reported that SHP inhibits the transcription and nuclear translocation of hedgehog effector protein, glioma-associated oncogene homologue (Gli), which is a contributor to several malignancies in humans(109). Therefore, whether SHP prevents HSC activation via inhibition of the hedgehog/Gli signaling is worth exploring.

Transcriptional regulators in NAFLD

To date, there are more than 1,600 known transcription factors and their general structures and functions are highly conserved amongst metazoans (110,111). The general structure of a TF includes a transactivation domain, signal-sensing domain, and DNA-binding domain. The DNA-binding sequences for more than two-thirds of TFs have been identified and research efforts towards uncovering others are highly encouraged (110). Expectedly, TFs play important roles in regulating critical processes such as cell growth, development, and mobility, nutrient sensing and homeostasis, inflammation, as well as obesity and insulin sensitivity (112). Hence, it is highly probable that alterations of TFs can lead to the onset of diseases such as NAFLD.

Nuclear receptors are ligand-activated transcription factors. Structurally, nuclear receptors contain a variable N-terminal transactivation domain, a DNA-binding domain, and a conserved C-terminal ligand-binding domain (113,114). There are 48 nuclear receptors identified in humans thus far, which are categorized into four mechanistic subtypes (I-IV) (115). Nuclear receptors are popular targets for drug development since endogenous ligands for up to 24 nuclear receptors have been identified (115), and their critical roles in disease progression or amelioration are surfacing (116). Generally, type I nuclear receptors are steroid receptors, including the estrogen receptor, androgen receptor, progesterone receptor, mineralocorticoid receptor, and glucocorticoid receptor. Type I nuclear receptors reside within the cytosol of the cell bound to chaperone proteins when inactive. Once bound by a ligand, the type I nuclear receptor enters the nucleus where it forms a homodimer and binds to hormone response elements within the promoter of a target gene (117).

Type II nonsteroidal nuclear receptors are located within the cell's nucleus regardless of activation state. Once bound by a ligand, the type II nuclear receptors undergo a conformational change and target respective response elements on DNA. Typically, the type II nuclear receptors form heterodimers with retinoid X receptor (RXR) to carry out their functions (118). Many metabolism-regulating nuclear receptors belong to the type II nuclear receptors, such as the well-studied peroxisome proliferator-activator receptors (PPAR), liver X receptors (LXR), and farnesoid X receptors (FXR). PPARs (alpha, beta, and gamma) are regulated by different genes and are expressed more abundantly in specific tissues. PPARa is highly expressed in the liver, PPARg in adipose tissue, and PPARb/δ within the skeletal muscle. Together, the PPARs regulate lipid metabolism, glucose homeostasis, and insulin sensitivity (119). LXRs are most abundantly expressed in liver and are master regulators of *de novo* lipogenesis. Mechanistically, LXRs bind to the LXR response element (LXRE) on sterol regulatory element-binding protein 1c (*SREBP1C*), a central regulator of lipid synthesis (120). Interestingly, one study demonstrated that PPARa, a main regulator of fatty acid beta-oxidation, directly inhibits LXR/RXR binding to LXRE on *SREBP1c* by competing with the LXR ligand. The study not only demonstrated another mechanism of regulation of SREBP1c but also that nuclear receptors can interact with the ligand binding region of other nuclear receptors (121). This is important since there is a class of nuclear receptors with no known endogenous ligand. Further studies addressing whether nuclear receptors may serve as “ligands” or activators of orphan nuclear receptors are encouraged.

Types III and IV nuclear receptors include nuclear receptors with unknown endogenous ligands, classified as “orphan” nuclear receptors. These receptors can form homodimers or heterodimers but do not require dimerization to bind to DNA (118). Evolutionarily, orphan nuclear receptors are most common type of nuclear receptors in the most primitive invertebrate species. In fact, Evans and Mangelsdorf indicated that of the all nuclear receptors found in *C. elegans* and *Drosophila*, less than 1% are found to be ligand-dependent (122). Small heterodimer partner (*SHP*, *NR0B2*) is an orphan nuclear receptor whose role is regulating various metabolic pathways are becoming illuminated (123-125). However, *SHP* lacks the DNA-binding domain which classical nuclear receptors contain; thus, it remains unclear whether SHP is a type III or IV nuclear receptor. In this dissertation, we thoroughly investigate the role of hepatocyte-specific SHP in our murine NAFLD model.

Therapeutic options

There is no Food and Drug Administration (FDA)-approved pharmacological treatment for NASH. However, therapeutic options exist to manage NASH symptoms such as probiotics for gut dysbiosis, physical activity and weight loss for obesity and diabetes (126). Targeting PPARs are of specific interest due to the suspected roles that these nuclear receptors have in preventing hypertriglyceridemia and type 2 diabetes (two risk factors for NAFLD) (127,128). Targeting hepatic macrophages is also one of the focus areas for therapeutic options (129). This is especially true since hepatic macrophages are involved in many processes throughout NAFLD progression. Another suggestion is to target the main cells responsible for hepatic fibrosis, hepatic stellate cells. Proposed methods include, but are not limited to targeting TGF-b1, PDGF, and PPARs (specifically PPARg) (130).

As we have discussed, oxidative stress is a key feature of NAFLD progression. Vitamin E is an antioxidant, which prevents oxidative stress associated with JNK activation. In 2010, NIDDK sponsored a PIVENS trial (PPARg agonist pioglitazone, Vitamin E, or Placebo for NASH, NCT00063622) in 247 adults with NASH without diabetes. The improvement in histologic features of NASH was assessed with the use of a composite of standardized scores for steatosis, lobular inflammation, hepatocellular ballooning, and fibrosis. It turned out vitamin E was superior to placebo for the treatment of NASH in adults without diabetes (131). A later study found that the treatment response in vitamin E group is correlated with the loss of sonic hedgehog positive (Shh+) hepatocytes and an improvement against hedgehog (Hh)-promoted NASH progression (132,133). Another promising therapeutic option includes glucagon-like peptide-1 (GLP-1)-based therapies, which promote hepatocyte survival via reduction of hepatic fat accumulation and unfolded-protein response (126,134).

Statement of purpose

Our knowledge of NASH pathogenesis has been greatly advanced through animal models and *in vitro* studies, as well as through the examination of liver specimens from patients with NAFLD. The pathogenesis of NASH and its progression to fibrosis are very complex and occur in response to a chronic inflammatory state in the setting of obesity, insulin resistance, hepatic steatosis and oxidative stress (*Fig.* 1-1). In any case, the ability to treat a disease relies heavily on the knowledge of disease etiology. So far, the main treatment options are to relieve or prevent the symptoms of NAFLD via changing diet, weight loss, exercise, or bariatric surgery (135). Progress in this aspect has greatly improved recently. However, more remains to be uncovered regarding the connections between, and the orders of, the pathways involved in NASH pathogenesis particularly for patients whose liver disease does not respond to these behavioral or surgical options. Additionally, when these proposed treatment options were considered, there was not sufficient data or evidence to show the treatments are effective to ameliorate NASH in human patients (136). As we have discussed above, the pathogenesis of NASH involves multiple mechanisms that affect both liver parenchymal and nonparenchymal cells, thus a multi-pronged strategy to design and implement multimodality pharmacologic approaches targeting multiple mechanisms could possibly be more successful than single-agent use. Nonetheless, it is hoped that this dissertation will provide an increased understanding of NASH pathogenesis and progression, particularly, on the mechanisms triggering immune response and liver fibrosis. In all, we aim to provide better targets for therapeutic intervention in this increasingly common disease.

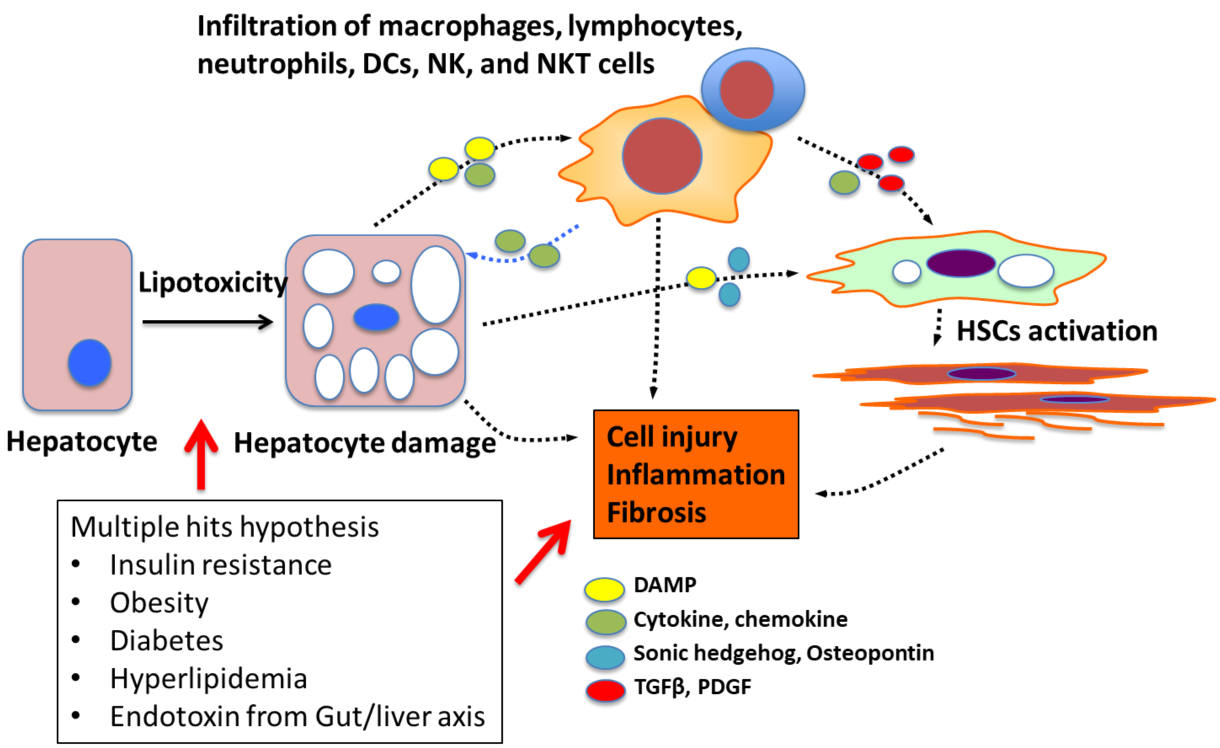

Figure 1-1: Schematic illustration of NASH pathogenesis.

Multiple hits lead to hepatocyte damage involving excessive oxidative stress driven by lipotoxic metabolites. Injured hepatocytes release damage-associated molecular pattern molecules (DAMPs) that initiate an inflammatory response leading to direct recruitment of neutrophils, macrophages, and other components of the innate immune response. Macrophages and damaged hepatocytes, especially ballooned hepatocytes, instigate the release of pro-fibrogenic cytokines and ligands, such as Hedgehog and osteopontin. Hepatic stellate cells are subsequently activated and produce excessive extracellular matrix leading to progressive fibrosis. In addition, macrophages promote a proinflammatory microenvironment that initiates an adaptive immune response, likely mediated by T and B lymphocytes.

Chapter 2: Materials and Methods

Animal studies

NAFLD mouse model

C57BL/6J (#000664) mice were purchased from Jackson Laboratory. *Shp*$^{flox/flox}$ mice were generously provided by Drs. Johan Auwerx and Kristina Schoonjans at the Ecole Polytechnique de Lausanne and backcrossed into C57BL/6J background for 10 generations. Mice were exposed to a standard 12-hr light/dark cycle (light on 6 AM to 6 PM) and maintained in a temperature-controlled (22-23°C) facility with free access to food and water. Experiments on mice were performed on males at the age of 8-10 weeks unless stated otherwise (n=5-6/group). To generate hepatocyte-specific *Shp* knockout (*Shp*$^{Hep-/-}$) and wildtype (WT) controls, *Shp*$^{flox/flox}$ mice were administered with either Adeno-Associated Virus serotype 8 (AAV8) expressing Cre recombinase driven by the thyroxine-binding globulin (*Tbg*) promoter (AAV8-*Tbg*-Cre) or control AAV8 (AAV8-*Tbg*-null) at a dose of 2 x10^{11} genome copies/mouse through tail vein injection. Both AAV8-*Tbg*-Cre (AV-8-PV1090) and AAV8-*Tbg*-null (AV-8-PV0148) were obtained from University of Pennsylvania Vector Core. Blood and liver samples were collected after mice had been fasted for 16 hours. All experiments were performed in accordance with relevant guidelines and regulations approved by the Institutional Animal Care and Use Committee (IACUC) at the University of Kansas Medical Center.

In dietary NAFLD models, C57BL/6J mice were either placed on a methionine choline-deficient (MCD) diet (Harlan Laboratories, TD. 90262) for 1 month or placed on a diet enriched in high-fat, cholesterol and fructose (Research Diet, D09100301, 40 kcal% fat, 2% cholesterol, 20 kcal% fructose, HFCF) for 1 to 9 months. In a steatosis-to-NASH transition model, *Shp*$^{\text{flox/flox}}$ mice were fed HFCF diet for 4 weeks to develop liver steatosis and followed by tail vein injection of AAV8-*Tbg*-Cre or AAV8-*Tbg*-null control. Mice remained on the HFCF diet for an additional 8 weeks. In the SHP-overexpression experiment, AAV8 including AAV8-*Tbg*-Flag-SHP and AAV8-*Tbg*-GFP were obtained from University of Pennsylvania Vector Core. C57BL/6J mice were on the HFCF diet for 1 month, followed by administration of either AAV8-*Tbg*-Flag-SHP or control AAV8-*Tbg*-GFP at a dose of 2x10^{11} genome copies/mouse through tail vein injection. The mice remained on the HFCF diet for 3 months. In each experiment, the control mice were fed normal chow (Research Diet #D12450J, 10 kcal% fat).

Mouse primary hepatocyte culture and adenovirus infection

The University of Kansas Medical Center Cell Isolation Core performed hepatocyte isolation from *Shp*$^{flox/flox}$ mice using the method described (137) with a slight modification. In brief, mouse liver was perfused with 25 ml of solution I (9.5 g/l Hank's balanced salt solution, 0.5 mmol/l EGTA, pH 7.2), followed by 50 ml of solution II (9.5 g/l Hank's balanced salt solution, 0.14 g/l collagenase IV, and 40 mg/l trypsin inhibitor, pH 7.5). After digestion, single-cell suspension was filtered through a 100-μm Falcon cell strainer (Fisher scientific 08-771-19), and the cells were centrifuged at 50g for 5 min at 4°C to pellet hepatocytes. Hepatocytes were then seeded in collagen type 1 coated dishes. After 2-hour incubation, cell culture medium was replaced with fresh William's E medium (Sigma W4128) with various adenoviruses at a multiplicity of infection (MOI) of 20. At second day hepatocytes were either treated with 5μM of NF-κB inhibitor BAY 11-7082 (Sigma, B5556) for 6 hours or 0.5 mM of oleic Acid (Sigma, O1008) conjugated with bovine serum albumin (Fisher, BP9704-100) for 24 hours. Cells were then collected for RNA isolation or oil red O staining.

Perfusion and separation of hepatocytes, HSCs, and Kupffer cells

Cell isolation and purification was performed at Kansas University Medical Center Cell Isolation Core using the method described above. After centrifugation, the supernatant was then centrifuged at 300g for 10 min at 4°C to enrich non-parenchymal cells. To isolate hepatic stellate cells and Kupffer cells, the non-parenchymal cells were gently resuspended in phosphate buffered saline (PBS) solution containing 1% bovine serum albumin (BSA) and mixed with Percoll (Sigma P1644), followed by a two-step Percoll gradient (50% Percoll and 35% Percoll) and centrifuged at 900 g for 30 min at 4°C. Three different cell bands were obtained after centrifugation. Hepatic stellate cells were enriched on top of the Percoll gradient and Kupffer cells were located near the bottom of the centrifugation tube. Cell fractions were then harvested and washed twice.

Cell lines, chemicals, plasmids, adenoviruses, and antibodies

Mouse macrophage RAW 264.7 (ATCC TIB-71) was maintained in Dulbecco's modified Eagle's medium (DMEM) with 100 U of penicillin G-streptomycin sulfate/ml and 10% heat-inactivated fetal bovine serum (FBS). AML12 (ATCC CRL-2254), a cell line established from hepatocytes from a mouse transgenic for human TGF alpha, was maintained in DMEM containing 10 % FBS supplemented with 0.005 mg/ml insulin, 0.005 mg/ml transferrin, 5 ng/ml selenium, and 40 ng/ml dexamethasone. Reagents including palmitic acid (P5585), lipopolysaccharide (L2654), JNK inhibitor SP600125 (S5567), NFκB inhibitor BAY 11-7082 (B5556), phosphatidylinositol 3-kinase (PI3K) inhibitor LY294002 (440202), and D-Glucose anhydrous (346351) were purchased from Sigma. The luciferase reporters containing a 2-kb fragment of mouse *Shp* proximal promoter (*Shp*-Luc) or a 3-kb fragment of mouse *Ccl2* proximal promoter (*Ccl2*-Luc) were engineered in our laboratory and confirmed by sequencing, respectively. Expression plasmids for c-Jun, Flag-LRH1, Flag-SHP, HA-p65, and EIA-like inhibitor of differentiation 1 (EID1), and adenoviruses for GFP and SHP were described previously (138). The *Pparg* adenovirus (#1354), Cre adenovirus (#1045), and vector control adenovirus (#1240) were purchased from Vector Biolabs.

Raw cell migration assay

Raw cells were serum-starved for 24 h and 200,000 cells were seeded on Transwell inserts (8-μm-pore size; Corning 24 well format, Fisher Scientific, 07-20-150) in FBS free medium. The lower chamber of transwell contained conditional medium from hepatocyte culture, supplemented with or without recombinant mouse CCL2 (40 ng/ml) or anti-mouse CCL2 antibody (500 ng/ml). Cells were cultured at 37 °C for 12-hour or 24 h. The migrated cells were fixed in 10% neutral buffered? formalin (Fisher scientific SF100) for 10 min before staining with 0.1% crystal violet (Fisher Scientific, AC21212-0250) for 10 min, followed by washing with PBS. A cotton swab removed the cells on topside of the filter. The pictures of migrated cells were taken by Microfire/Qcam CCD Olympus BX60 microscope (Olympus, Lake Success, NY). Five fields per sample were captured at 10×

magnification. Quantitation of cell migration was determined by measuring pixel density of crystal violet-stained cells using Image J software.

Transient transfection and promoter activity assays

AML12 cells in 24 well plates were transfected with luciferase reporters along with various expression plasmids using Lipofectamine 2000 (Invitrogen). Firefly luciferase and *Renilla* luciferase were examined in cells after 24 h transfection using dual luciferase (Firefly-*Renilla)* assay system (Promega, Madison, WI). Data are displayed as the ratio of firefly luminescence divided by *Renilla* luminescence. Each point was the average of triplicate and one representative was shown.

Histological examinations of NAFLD features

NAS Scoring

Fresh liver tissues were fixed with 10% neutral buffered formalin (Fisher scientific SF100). Paraffin sections at 4 µm were stained with hematoxylin and eosin (H&E) to assess liver histology. A pathologist reviewed and scored the severity of steatosis, inflammation, cell death, and fibrosis according to the NASH-Clinical Research Network (CRN) criteria (139). In brief, the amount of steatosis was scored as 0 (<5%), 1 (5-33%), 2 (>33-66%) and 3 (>66%). Hepatic cell death was scored as 0 (none), 1 (few) and 2 (many cells). Foci of lobular inflammation were scored as 0 (no foci), 1 (<2 foci), 2 (2-4 foci) and 3 (>4 foci). Fibrosis was scored as 0 (no fibrosis), 1 (perisinusoidal or periportal fibrosis), 2 (perisinusoidal and portal/periportal fibrosis), 3 (bridging fibrosis) and 4 (cirrhosis).

Immunohistochemistry

Paraffin sections at 4 µm or frozen sections at 6 µm were incubated with 0.3% H_2O_2 in methanol for 15 minutes to block endogenous peroxidase activity. Antigen retrieval was performed by incubation of slides in 20 µg/ml proteinase K solution (Fisher scientific PRMC5005) for 3 min at room temperature or heat-induced antigen retrieval using citrate buffer (pH 6) for 10 min. Slides were then treated with 10% normal serum for 30 min, followed by incubation with primary antibody overnight at 4°C. ImmPRESS peroxidase polymer detection kit (Vector Laboratories MP-7444) and ImmPACT 3,3'-

diaminobenzidine (DAB) peroxidase substrate (Vector Laboratories, SK-4105) were used for the final detection. Sections were then counterstained with hematoxylin, dehydrated, cleared, and mounted. Images were acquired with an Olympus BX60 microscope.

Oil red O staining of lipids

Fresh liver tissues were immediately embedded in O.C.T. compound (VWR 25608-930, Tissue-Tek). Frozen sections were cut at 8 µm and fixed with 10% neutral buffered formalin, followed by staining with oil red O (Sigma O0625) and counter stained with hematoxylin. Images were acquired with an Olympus BX60 microscope.

Picrosirius red staining of liver fibrosis

Paraffin sections at 4 µm were rehydrated and incubated in 0.1% Sirius red F3B (Sigma, Direct red 80, 365548) containing saturated picric acid (Sigma, p6744) for 1 h. After washing three times in 0.5% glacial acetic acid, sections were briefly dehydrated, cleared, and mounted. Images were acquired with a BX60 microscope.

Detection of cell death by TUNEL staining

TUNEL staining for detection of cell death in the liver was performed using an *in-situ* cell death detection kit-alkaline phosphatase (Sigma 11684809910) according to the manufacturer’s suggestions.

Serum measurements

Blood samples were collected from anesthetized animals via cardiac puncture and deposited into blood collection tubes (Fisher Scientific, 22-225516). After 20 minutes, blood was centrifuged (5,000rpm, 2min) and serum was transferred into 500 µL tubes. Various kits were used to determine serum levels of triglycerides (Pointe scientific, T7532), total cholesterol (Pointe scientific, C7510), glucose (Pointe scientific, G7521), AST (Pointe scientific, A7561), and ALT (Pointe scientific, A7526)

Glucose tolerance test (GTT) and insulin tolerance test (ITT)

For the GTT assay, mice were fasted for 16 hours, followed by intraperitoneal injection of glucose (Sigma, #346351) at 2g/kg body weight. Blood was collected by minor tail clipping and glucose levels were determined before and at 30, 60, 90, 120, and 180 minutes after glucose administration. In the ITT assay, mice were fasted for 4 hours from 8 am-12 pm, followed by intraperitoneal injection of insulin (Sigma, # I0516) at 0.75 U/kg body weight. Blood glucose was measured before and at 30, 60, 90, and 120 minutes post insulin injection.

Hepatic triglycerides and cholesterol measurements

Liver tissues (100 mg) were homogenized in 300 µL of chloroform: methanol (1:2 in volume) for 2 min, followed by a second homogenization for 30 sec with an addition of 300µL chloroform. The homogenates were mixed with 100 µL of H_2O and homogenized again for 30 sec. The lipid layer (~600 µL) was separated via centrifugation at 800g for 10 min at room temperature. The lower phase enriched in lipid was transferred and dried using nitrogen gas. The lipid extract was suspended in 300 µL of 5% Triton X-100 in PBS (pH 7.4). The measurement was performed using respective kit for triglycerides (Pointe scientific, T7532) and cholesterol (Pointe scientific, C7510). The hepatic triglyceride or cholesterol content was defined as µg of triglyceride or cholesterol/mg of liver tissue.

Determine hepatic collagen content by hydroxyproline assay

Liver tissues (10 mg) were homogenized in 100 µL of H_2O. The homogenates were mixed with 100 µL of 12 M HCl and incubated at 120°C for 3 hours for acid hydrolysis. The homogenates were then centrifuged at 10,000g for 10 minutes. Aliquots of the hydrolyzed samples (10 µL) were incubated with 100 µL of chloramine T solution (1.27% chloramine T and 10% isopropanol in acetate-citrate buffer, pH 6.0) at room temperature for 25 minutes, followed by a second incubation with 100 µL of Ehrlich's solution (Sigma, 03891) at 60°C for 35 minutes. A plate reader measured sample absorbance at 550 nm. The hepatic hydroxyproline content was defined as µg of hydroxyproline per mg of liver tissue.

Analysis of bile acid (BA) pool size and fecal BA extraction rate

To determine BA pool size, fresh mouse tissues including gallbladder, liver, and entire small intestine were minced and extracted in 75% ethanol at 50 °C for 2-hours. The extract was then centrifuged, diluted with 75% ethanol, and further diluted with PBS before the BA measurement using a BA colorimetric assay BQ kit (Thermo Fisher

Scientific, # BQ092A-EALD). The pool size was expressed as micromoles of bile acid/g of body weight. To determine fecal bile acid excretion, the feces from individually housed mouse over 72 hours were collected, weighed, dried, and extracted in 75% ethanol. The extract was then diluted with PBS and subjected to bile acid measurement. The daily fecal output (g/day/g of body weight) and fecal bile acid content (μm/g) were used to calculate the rate of bile acid excretion (μm/day/g of body weight).

General western blot procedure

Mouse tissues (liver or fat) were homogenized using PowerGen 700 homogenizer (Fisher Scientific) in lysis buffer (50 mm Tris, pH 7.5, 1% Nonidet P-40, 150 mm NaCl, 0.5% sodium deoxycholate, 0.1% SDS) containing protease inhibitors (Fisher Scientific, protease inhibitor cocktail PI78410) to obtain whole protein lysates. Nuclear and cytoplasmic protein extraction was carried out using a commercial kit (Fisher Scientific, PI78833). Protein lysates (60μg) were resolved by SDS-PAGE. Following standard SDS-PAGE and transfer procedures, nitrocellulose membranes were blocked, incubated with primary antibodies followed by horseradish peroxidase-conjugated corresponding secondary antibody incubation. Antibody binding was visualized using either SuperSignal West Pico Plus Chemiluminescent Substrate (Fisher Scientific, PI34580) or SuperSignal West Femto Chemiluminescent Substrate (Fisher Scientific, PI34094). Equal loading of protein was verified by loading controls such as b-actin, a-Tubulin, or histone H3. Quantitative analysis of band intensity was performed by Image Studio Lite software and relative expression levels were normalized to loading controls.

Immunoprecipitation to detect protein-protein interactions

For the immunoprecipitation (IP) experiment, 800 µg of whole protein lysates from AML12 cells overexpressing Flag-SHP or HA-p65 were incubated with 2 µg of anti-p65 antibody and immune complexes were captured by sheep anti-rabbit IgG M-280 Dynabeads (Fisher scientific 11-203-D). The immune complexes were then eluted by 2xSDS loading buffer. The pull down of p65 and Flag-SHP were detected by Western blot. A TrueBlot® anti-Rabbit IgG HRP (Rockland, RL18-8816-33) was used as a secondary antibody to detect p65; this antibody does not interfere with the immunoprecipitating immunoglobulin heavy or light chains.

TABLE 2-1: Antibody List

Antibody	Company	Catalog #
CD19	Bio-Rad	MCA1439T
CD3	Bio-Rad	MCA500GT
CD4	Bio-Rad	MCA2691T
CD8	Bio-Rad	MCA2694T
F4/80	Bio-Rad	MCA497R
LY6G/GR1	Bio-Rad	MCA2387T
p-JNK (Thr183/Tyr185)	Cell Signaling	4668p
HISTONE 3	Cell Signaling	14269
JNK	Cell Signaling	9252S
NFκB	Cell Signaling	8242
p-C-JUN	Cell Signaling	3270
p-P65	Cell Signaling	4764
P65	Cell Signaling	8242p
CCL2	R&D Systems	AF-479-SP
LRH1	R&D Systems	PP-H2325-00
Recombinant CCL2 protein	R&D Systems	479-JE-010
SHP	Santa Cruz	SC-30169 and SC-271511
FLAG-HRP	Sigma	A-8592
a-TUBULIN	Sigma	T6074
b-ACTIN	Sigma	A1978

Real-time quantitative PCR

The real-time quantitative PCR (qPCR) was carried out using the SYBR Green PCR master mix (Applied Biosystems) as described (140). The amount of PCR products was measured by threshold cycle (Ct) values, and the relative ratio of specific genes to either beta-actin or housekeeping gene hypoxanthine guanine phosphoribosyl transferase 1 (*Hprt1*) was calculated and presented as a fold change in the tested group relative to the control group.

TABLE 2-2: Primer List

Species	Genes	Forward (5'-3')	Reverse (5'-3')
Human	*HPRT1*	TGACACTGGCAAAACAATGCA	GGTCCTTTTCACCAGCAAGCT
Human	*SHP*	GGTGCCCAGCATACTCAAGAA	GGACTTCACACAGCACCCAGT
Mouse	*Abca1*	AAAACCGCAGACATCCTTCAG	CATACCGAAACTCGTTCACCC
Mouse	*Abcg5*	AGGGCCTCACATCAACAGAG	GCTGACGCTGTAGGACACAT
Mouse	*Acc1*	ATGGGCGGAATGGTCTCTTTC	TGGGGACCTTGTCTTCATCAT
Mouse	*Acc2*	CCTTTGGCAACAAGCAAGGTA	AGTCGTACACATAGGTGGTCC
Mouse	*Acly*	CAGCCAAGGCAATTTCAGAGC	CTCGACGTTTGATTAACTGGTCT
Mouse	*Alb*	TGCTTTTTCCAGGGGTGTGTT	TTACTTCCTGCACTAATTTGGCA
Mouse	*ApoB*	TTGGCAAACTGCATAGCATCC	TCAAATTGGGACTCTCCTTTAGC
Mouse	*Arg1*	CTCCAAGCCAAAGTCCTTAGAG	AGGAGCTGTCATTAGGGACATC
Mouse	*Ccl2*	TTAAAAACCTGGATCGGAACCAA	GCATTAGCTTCAGATTTACGGGT
Mouse	*Cd163*	TGGGTGGGGAAAGCATAACT	AAGTTGTCGTCACACACCGT
Mouse	*Cd36*	ATGGGCTGTGATCGGAACTG	GTCTTCCCAATAAGCATGTCTCC
Mouse	*Cidec*	ATGGACTACGCCATGAAGTCT	CGGTGCTAACACGACAGGG
Mouse	*c-Jun ChIP P1*	CCCTGGTACAGCCTGGGTTA	ATGAAGTGGCCATTGCAGG
Mouse	*c-Jun ChIP P2*	GGCTGGCCTTGAACTCAGAA	TGGTGTCTCTTCACAGCAAT
Mouse	*Col1a1*	GACGCCATCAAGGTCTACTGC	GGAAGGTCAGCTGGATAGCG
Mouse	*Col1a2*	GCAGGGTTCCAACGATGTTG	GCAGCCATCGACTAGGACAGA
Mouse	*Cpt1a*	CTCCGCCTGAGCCATGAAG	CACCAGTGATGATGCCATTCT
Mouse	*Ctgf*	GGGCCTCTTCTGCGATTTC	ATCCAGGCAAGTGCATTGGTA
Mouse	*Adgre1*	CCCCAGTGTCCTTACAGAGTG	GTGCCCAGAGTGGATGTCT
Mouse	*Fabp1*	ATGAACTTCTCCGGCAAGTACC	CTGACACCCCCTTGATGTCC
Mouse	*Fxr*	GCTTGATGTGCTACAAAAGCTG	CGTGGTGATGGTTGAATGTCC
Mouse	*Hhip*	TGAAGATGCTCTCGTTTAAGCTG	CCACCACACAGGATCTCTCC
Mouse	*Hnf4a*	TGGCCAAGATTGACAACCTG	AGGTGAGAGGGCATCGTGTT
Mouse	*Hprt1*	CGTCGTGATTAGCGATGATGA	CACACAGAGGGCCACAATGT
Mouse	*Ifng*	ATTACTACCTTCTTCAGCAACAG	CGAATCAGCAGCGACTCC
Mouse	*Il1*	CCTGTGTTTTCCTCCTTGCCT	GCCTAATGTCCCCTTGAATCAA
Mouse	*Il6*	AACGATGATGCACTTGCAGA	GAGCATTGGAAATTGGGGTA
Mouse	*Lrh1*	TTGCCAAATTGACAAAACGCA	GGCTCGAATGAGGGCTTTCTT
Mouse	*Lrh1 ChIP L1*	TGGCTCCTTGGCTCAGTGA	TACCAGGGCACCAAGGTCTC
Mouse	*Lrh1 ChIP L2+3*	GGTCAGCGTGTATGCATTGTG	TTTATATCCTTGATGGGCGGG
Mouse	*Lxra*	CTCAATGCCTGATGTTTCTCCT	TCCAACCCTATCCCTAAAGCAA
Mouse	*Lxrb*	ATGTCTTCCCCCACAAGTTCT	GACCACGATGTAGGCAGAGC

Species	Genes	Forward (5'-3')	Reverse (5'-3')
Mouse	*Me1*	GTCGTGCATCTCTCACAGAAG	TGAGGGCAGTTGGTTTTATCTTT
Mouse	*Mmp12*	CTGCTCCCATGAATGACAGTG	AGTTGCTTCTAGCCCAAAGAAC
Mouse	*Mmp13*	TGTTTGCAGAGCACTACTTGAA	CAGTCACCTCTAAGCCAAAGAAA
Mouse	*Mttp*	CATGCTTCTTCATCTGGTCCG	CACTTTGTCTTGCTGGGCCT
Mouse	*Nos2*	AATCTTGGAGCGAGTTGTGG	CAGGAAGTAGGTGAGGGCTTG
Mouse	*Pparg*	TCGCTGATGCACTGCCTATG	GAGAGGTCCACAGAGCTGATT
Mouse	*Ppara*	AGAGCCCCATCTGTCCTCTC	ACTGGTAGTCTGCAAAACCAAA
Mouse	*Scd1*	TTCTTGCGATACACTCTGGTGC	CGGGATTGAATGTTCTTGTCGT
Mouse	*Shp*	TGAGCTGGGTCCCAAGGA	CCTGGCACATCTGGGTTGA
Mouse	*Srebp1c*	GATGTGCGAACTGGACACAG	CATAGGGGGCGTCAAACAG
Mouse	*Srebp2*	GCAGCAACGGGACCATTCT	CCCCATGACTAAGTCCTTCAACT
Mouse	*Tgfb1*	CTCCCGTGGCTTCTAGTGC	GCCTTAGTTTGGACAGGATCTG
Mouse	*Tnfa*	CGTGGAACTGGCAGAAGAG	ACAAGCAGGAATGAGAAGAGG

Chromatin immunoprecipitation (ChIP) assays

AML12 cells were fixed in 1% formaldehyde, followed by nuclei isolation and sonication. Chromatin samples were precleared and subjected to immunoprecipitation with specific antibodies or rabbit normal IgG, respectively. The chromatin immune complexes were captured by sheep anti-rabbit IgG Dynabeads (Fisher scientific 11-203-D) and eluted. After reversing cross-links by incubation with 3 M NaCl and 10 mg/mL RNase A at 65 ^{o}C for 4-hours, DNA fragments were purified and used as templates in qPCR. Four sets of primers were designed for ChIP assays and listed in Table 2-2. P1 was specific for the TRE site (*c-Jun* binding site) on mouse *Shp* promoter, whereas P2 was located 4 kb upstream from TSS thus served as a negative control. L1 and L2+3 were specific to amplify LRH1 sites on mouse *Shp* promoter.

RNA sequencing: RNA isolation, DEG parameters, and analysis

Total RNA for Illumina sequencing was extracted from mouse liver tissues using a Direct-zol RNA kit (Zymo Research, R2071) according to the manufacturer's protocol. During RNA isolation, the samples were treated with RNase-free DNase to avoid DNA contamination. The purity, concentration and integrity of the RNA were examined using a NanoDrop 1000 spectrophotometer (Thermo Fisher, USA) and an Agilent Bioanalyzer 2100 system (Agilent Technologies, USA). Three biological replicates in each group were submitted for RNA sequencing. The RNA integrity number (RIN) values of all samples used for RNA-seq were >6.0. The High Throughput Genomics Core at the Huntsman Cancer Institute, University of Utah performed library preparation and sequencing. cDNA libraries were prepared using the Illumina TruSeq stranded RNA kit with Ribo-Zero Gold. Fifty-cycle single-read sequencing was performed with an Illumina HiSeq 2500 (San Diego, CA) and reads were aligned to a mouse reference sequence genome mm10 using the Novalign short-read alignment software. Sample reads were visualized and differentially expressed genes (DEGs) were identified based on the log transformed false discovery rate (FDR) of >1.3 and ≥± 1.5-fold change in expression relative to controls using the USeq application as previously described (141).

Three biological replicates from 1-month WT Chow, 1-month WT HFCF, 3-month WT Chow, 3-month WT HFCF, *Shp*$^{flox/flox}$ WT Chow, *Shp*$^{flox/flox}$ WT HFCF, *Shp*$^{Hep-/-}$ Chow, and *Shp*$^{Hep-/-}$ HFCF were submitted for RNA sequencing. All RNA-seq data generated in this work were deposited into the Gene Expression Omnibus (GEO) database (GSE135050 and GSE133566). Gene Ontology (GO) term enrichment and Kyoto Encyclopedia of Genes and Genomes (KEGG) pathway analyses were performed in Enrichr web server using DEGs to identify significantly enriched biological functions and pathways. Enrichr is freely available at: http://amp.pharm.mssm.edu/Enrichr/. GO terms and KEGG pathways with P-value < 0.05 were considered significantly different. An Enrichr combined score calculated based on adjusted p value and Z score was used to select top enriched GO terms and KEGG pathways.

Human NAFLD microarray dataset

The microarray dataset of human livers in various stages of NAFLD is accessible in NCBI GEO database (GSE48452). The dataset contains 14 normal, 14 NAFL, and 18 NASH.

Human Liver Samples

Human liver specimens were obtained through the Liver Center at the University of Kansas, including 12 normal, 12 NAFL, and 8 NASH. The exclusion criteria were excessive alcohol use (>20 g of alcohol daily for women and >30 g for men) and chronic liver diseases, including chronic viral hepatitis, autoimmune, Wilson's disease, and drug-induced hepatitis. A NAFLD activity score (NAS) which represents the sum of scores for steatosis, lobular inflammation, and ballooning (29) was applied in our study. Cases with NAS 0 were classified as normal. Cases with steatosis score ≥ 1 without inflammation, ballooning, or fibrosis were defined as NAFL. Cases with NAS ≥ 5 were classified as NASH. Studies were approved by the University of Kansas Medical Center Institutional Review Board for Human Research Committee and abide by the Declaration of Helsinki principles. All liver samples were de-identified, and the researchers were not able to ascertain individual identities associated with the samples.

Statistical Analysis

Quantitative data were presented as the mean ± SEM. The statistical difference in data obtained between two groups was determined by Student's T-test. Multiple groups were compared by One-Way ANOVA and followed by Duncan's test. Statistical significance was accepted within 95% confidence limits.

Chapter 3: Development of Mouse NAFLD Model

This chapter is adapted from Magee N, Zou A, He L, Ghosh P, Ahamed F, Delker D, Zhang Y. Hepatic transcriptome profiling reveals key signatures associated with disease progression from nonalcoholic steatosis to steatohepatitis. (*Manuscript under revision*)

Introduction

NAFLD is becoming a leading cause of chronic liver disease worldwide due to the increasing prevalence of obesity, hyperlipidemia, and diabetes (142). To date, remarkable progress has been made to understand the pathogenesis of NAFLD; however, there remains a paucity of insight into the molecular events that influence the transition of NAFL to NASH. Therefore, there remains a lack of mechanism-based targeted treatment options for NASH. Thus, understanding the molecular machinery that causes the transition of simple steatosis to NASH is essential to develop effective prevention and therapeutic strategies for this unresolved disease.

Several dietary animal models have been used to characterize the pathogenesis of NAFLD, including animals fed a methionine choline-deficient (MCD) diet or Western-type diets with excess of saturated fats, trans fats, and cholesterol; either individual use or in combination with sugars such as fructose and sucrose (143-145). Ideally, a preclinical animal model for NASH should be associated with the same risk factors seen in humans such as obesity, insulin resistance, dyslipidemia, and endocrine dysfunction. The animal model should also match NASH in humans with respect to histological characteristics (steatosis, hepatocyte damage, inflammation, and fibrosis) as well as alterations on gene expression signatures and signaling pathways relevant to humans.

Mice fed an MCD diet develop steatosis, inflammation and fibrosis; however, this model lacks features of metabolic syndrome like obesity, dyslipidemia, and insulin resistance (143). Mice fed a high-fat and high-cholesterol diet feature obesity, insulin resistance, dyslipidemia, and steatosis with liver inflammation, but do not develop liver fibrosis (143). Recently, a diet enriched in fat, cholesterol, and fructose has been implicated in the development of obesity and NASH in humans (146,147). Similarly, the high-fat diet enriched in cholesterol and fructose has been reported to effectively induce key features of NASH in mice (125,148,149). In such diet, excess fat alone contributes to the development of steatosis while the addition of fructose and cholesterol enhance oxidative stress; combined, these diet components predispose animals to hepatocyte damage, inflammation and fibrosis.

In the current chapter, we demonstrate how we established our NAFLD model by feeding mice a high-fat diet enriched in cholesterol and fructose (HFCF, 40 kcal% fat, 2% cholesterol, 20 kcal% fructose) for up to 9 months. We found that HFCF-fed mice sequentially developed steatosis (1 month), early steatohepatitis (3 months), steatohepatitis with fibrosis (5 months), steatohepatitis with progressive fibrosis (7 months onwards), and spontaneous liver tumor development (9 months). In summary, we developed a NAFLD mouse model with disease progression from NAFL to NASH that recapitulates key metabolic and histologic changes seen in humans.

Results

HFCF-fed mice develop obesity, dyslipidemia, and insulin resistance

To develop a mouse model that carries the disease progression from NAFL to NASH, we fed C57BL/6J mice a HFCF diet for up to 9 months, collecting samples at 1, 3, 5, 7, and 9 months after diet administration (*Fig.* 3-1A). As shown in *Fig.* 3-1B, animals gained weight rapidly on the HFCF diet with the maximum weight gain at 7 months, after which growth remained stable. The weights between HFCF-fed and chow-fed animals were significantly different at all time points throughout the 9-month feeding period. Paralleling body weight gains, both liver weight and liver-to-body weight ratio increased rapidly in HFCF-fed mice, becoming significantly different from chow-fed mice as early as 3 months following feeding (*Fig.* 3-1C). Meanwhile, HFCF diet feeding led to a persistent increase in liver injury markers such as alanine aminotransferase (ALT) and aspartate aminotransferase (AST) starting at 3-months post diet initiation (*Fig.* 3-1D). Additionally, mice fed HFCF diet developed an increase in fasting cholesterol from the 3-months time point throughout the experimental period (*Fig.* 3-1E). Interestingly, mice fed 1 month of HFCF diet developed hypertriglyceridemia, after which serum levels of triglycerides declined to values noted in chow-fed mice (*Fig.* 3-1E). Moreover, HFCF-fed mice developed significant glucose intolerance and insulin resistance at 3 months post diet feeding (*Fig.* 3-2A and B). Collectively, these results indicate that HFCF-fed mice develop liver injury with obesity, dyslipidemia, and insulin resistance.

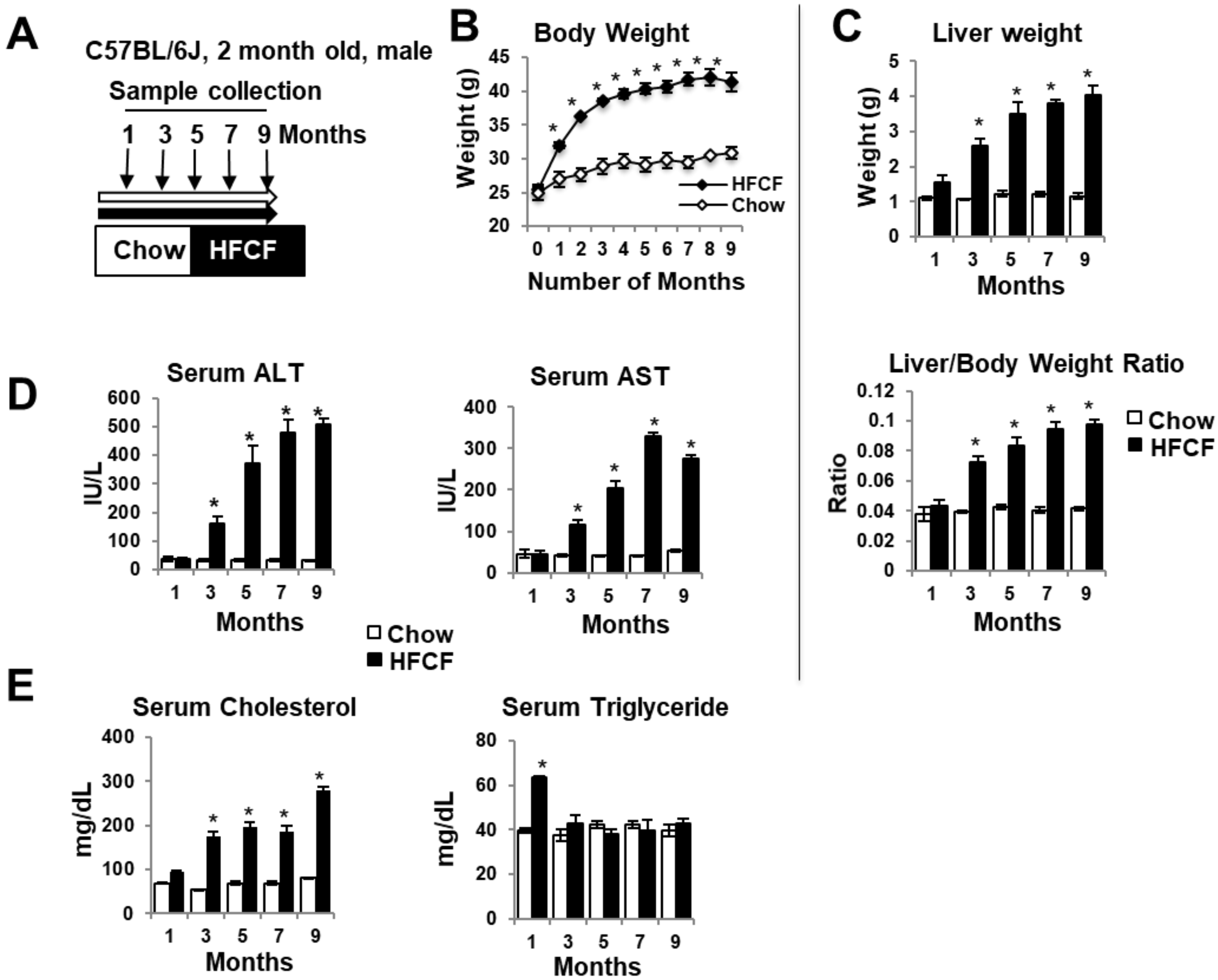

Figure 3-1: HFCF-fed mice develop obesity, dyslipidemia, and liver injury.

C57Bl/6J mice were fed chow or a high-fat diet enriched in cholesterol and fructose (HFCF diet contains 40 kcal% fat, 2% cholesterol, 20 kcal% fructose) for up to 9 months. **A**: Experimental design shows diet feeding and time when samples were collected. **B**: Body weight change. **C**: Liver weight and liver to body weight ratio. **D**: Serum alanine aminotransferase (ALT) and aspartate aminotransferase (AST). **E**: Fasting serum levels of cholesterol and triglycerides. Data presented in B-E are expressed as mean ± SEM for 5 mice per group. *P < 0.05 versus chow controls.

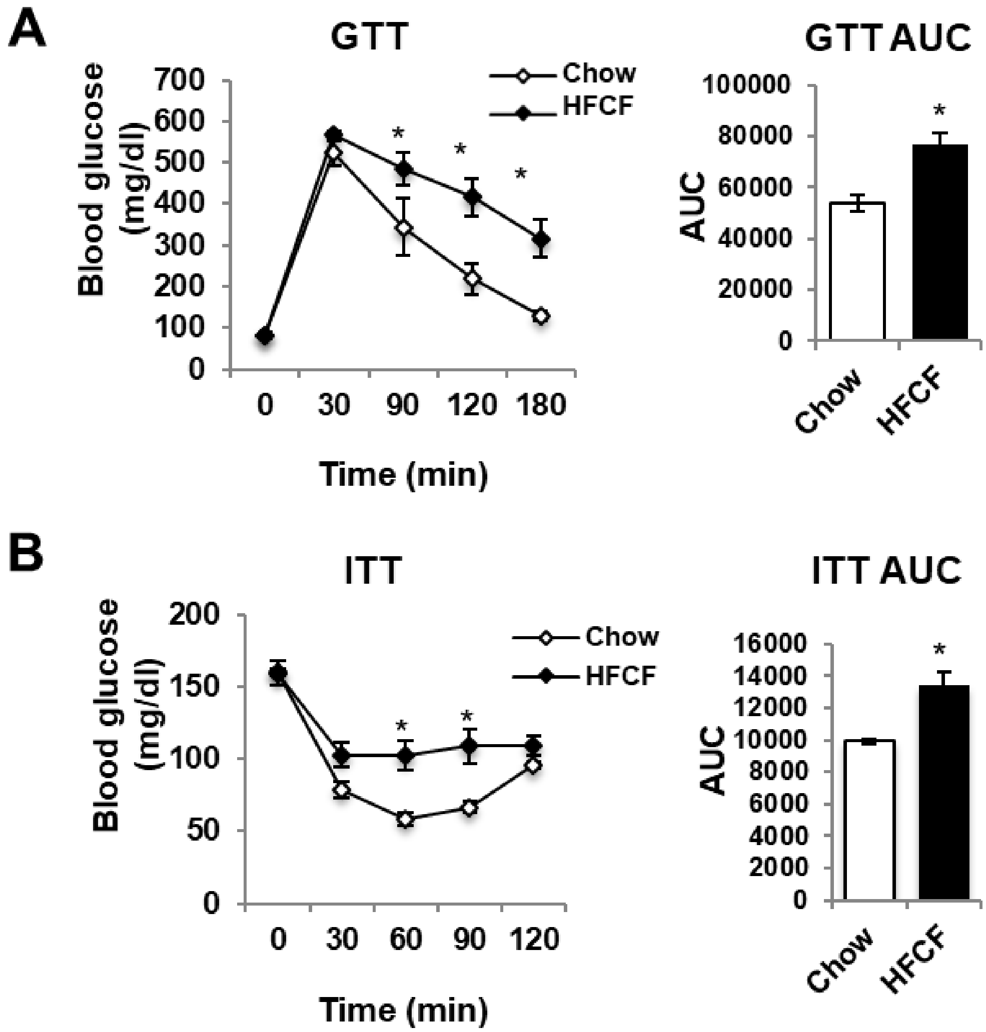

Figure 3-2: HFCF-fed mice develop glucose intolerance and insulin resistance.

C57Bl/6J mice were on a chow or HFCF diet. **A:** Glucose tolerance test (GTT). **B:** Insulin tolerance test (ITT). Data presented are expressed as mean ± SEM for 5 mice per group. *$P < 0.05$ versus chow controls.

Liver steatosis is present throughout the HFCF diet feeding

Mice fed HFCF diet rapidly developed both microvesicular steatosis and macrovesicular steatosis after 1-month diet administration (*Fig.* 3-3A). The latter predominated from 3-months onwards and was seen commonly in zone 1 (periportal region). These findings were confirmed by oil red O staining (*Fig.* 3-3A) and by quantification of hepatic triglyceride and cholesterol after hepatic lipid extraction (*Fig.* 3-3B).

Pparg, a master transcriptional regulator of lipid synthesis and storage, sustained an increase in the livers of HFCF-fed mice (*Fig.* 3-4). In parallel, *Pparg*-regulated direct targets such as fatty acid transporter CD antigen 36 (*Cd36*) and lipid droplet membrane protein cell death-inducing DFFA-like effector c (*Cidec*, also called Fsp27) were significantly increased at all time points throughout the 9-month feeding period (*Fig.* 3-4). We next examined expression of genes involved in *de novo* lipogenesis, including acetyl-Coenzyme A carboxylase alpha (*Acaca*, also called *Acc1*) and fatty acid synthase (*Fasn*). Interestingly, both *Acc1* and *Fasn* were decreased in HFCF-fed mice within 3 months of introducing the diet, but increased robustly by 5-months and thereafter remained 2- to 4-fold elevated (*Fig.* 3-4). In contrast, stearoyl-Coenzyme A desaturase 1 (*Scd1*), a rate-limiting enzyme for lipogenesis that converts saturated fatty acids to monounsaturated fatty acids, sustained increased expression levels throughout the 9-month feeding period (*Fig.* 3-4). *Ppara*, a key transcriptional regulator of genes involved in peroxisomal and mitochondrial b-oxidation, was transiently induced in HFCF-fed mice within 1 month of diet administration, and thereafter decreased to the levels noted in the chow-fed groups (*Fig.* 3-4). Moreover, the expression of carnitine palmitoyltransferase I (*Cpt1*), which is a direct target of *Ppara* and transports fatty acids through the inner mitochondrial membrane for beta-oxidation, was significantly increased in the 1-month HFCF-fed group but decreased throughout the 9-month feeding period (*Fig.* 3-4), suggesting that short-term HFCF feeding increases fatty acid oxidation but long-term feeding represses it. The expression of genes involved in synthesis of very-low-density lipoprotein (VLDL) that carries lipids in the plasma, apolipoprotein B (*ApoB*) and microsomal triglyceride transfer protein (*Mttp*), were both unchanged during the first 3 months of HFCF diet administration, but thereafter decreased significantly (*Fig.* 3-4), consistent with changes of serum triglyceride levels observed in HFCF-fed animals (*Fig.* 3-1E). Taken together, the above data suggest that HFCF feeding induces liver steatosis and coordinately alters expression of genes involved in fatty acid uptake, biosynthesis, storage, b-oxidation, and lipid secretion.

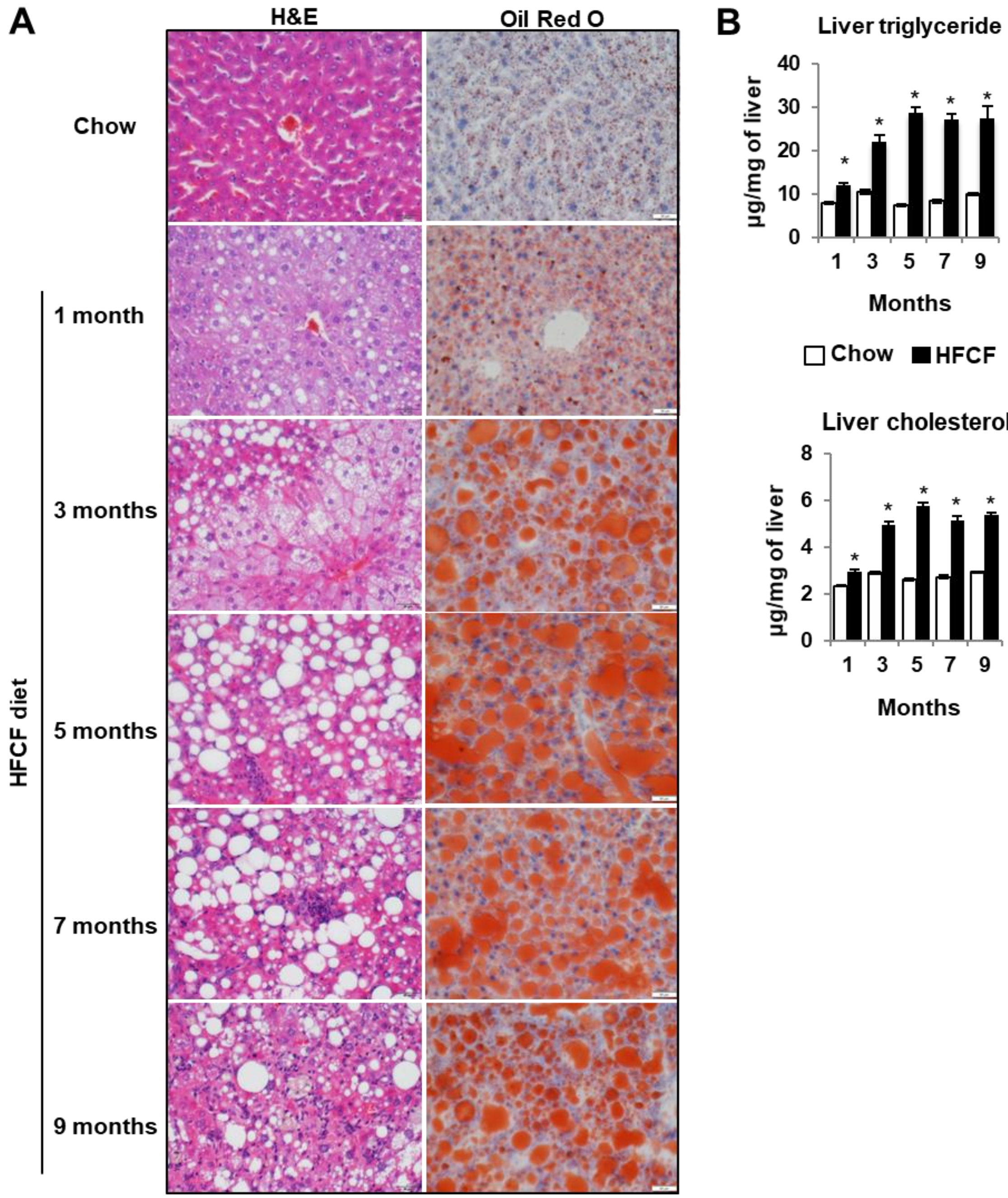

Figure 3-3: HFCF-fed mice develop liver steatosis.

Two-month-old C57BL/6J male mice were fed chow or a HFCF diet for up to 9 months. **A**: Representative images of liver sections stained with hematoxylin-eosin (H&E) or oil red O, respectively. Original magnification, 400X. **B**: Liver triglycerides and cholesterol content. Data presented in B are expressed as mean ± SEM for 5 mice per group. *P < 0.05 versus chow controls.

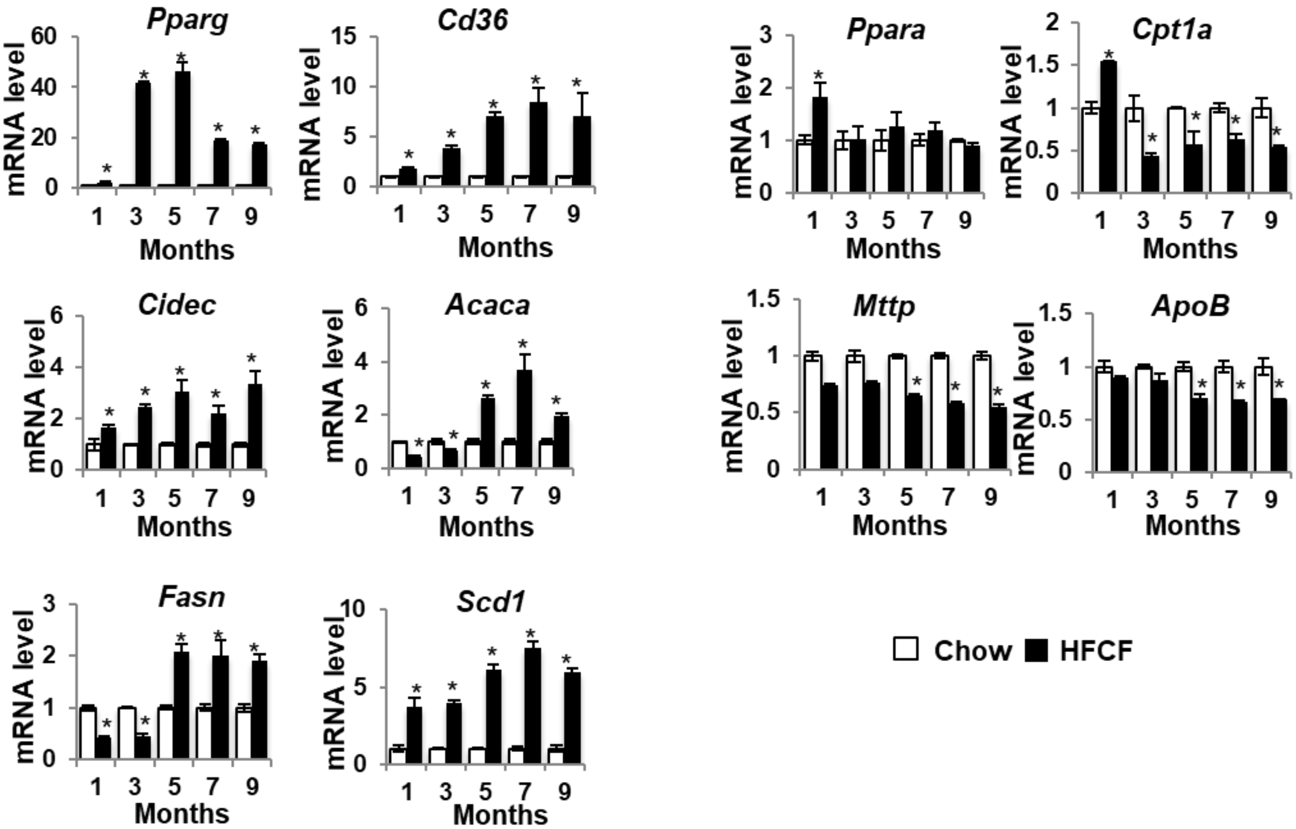

Figure 3-4: Lipid-regulating gene expression is altered in HFCF-fed mice.

Two-month-old C57BL/6J male mice were fed chow or a HFCF diet for up to 9 months. Relative mRNA levels of genes related to lipid metabolism in the liver were determined by qPCR. Data presented in are expressed as mean ± SEM for 5 mice per group. *$P <$ 0.05 versus chow controls.

HFCF feeding gradually induces hepatocyte cell death, inflammation, fibrosis, and tumor development over time

We next assessed the extent of cell death, inflammation, and fibrosis in HFCF-fed groups. In correlation with increased serum AST and ALT levels, TUNEL staining detected increased cell death in HFCF-fed mice, starting 3-months after diet initiation, and remained elevated throughout the 9-month feeding period (*Fig.* 3-5A). In parallel, liver inflammation and fibrosis dramatically increased in HFCF-fed groups, which were detected by immunostaining of macrophage marker F4/80 and Picosirius staining, respectively (*Fig.* 3-5A).

At the molecular level, gene expression of tumor necrosis factor a (*Tnfa*) and chemokine (C-C motif) ligand 2 (*Ccl2*) were both significantly increased in the 3-months HFCF group and sustained increased expression over time of diet feeding (*Fig.* 3-6A). Meanwhile, HFCF-fed groups showed a progressive increased expression of M1 macrophage marker nitric oxide synthase 2 (*Nos2*) and decreased expression of M2 markers *CD163* and arginase-1 (*Arg1*) (*Fig.* 3-6A). Similarly, fibrosis marker collagen 1 alpha 1 (*Col1a1*) increased in HFCF-fed animals (*Fig.* 3-6A), supporting the increase in collagen deposition detected by both Picrosirius red staining (*Fig.* 3-6A) and the quantification of hydroxyproline extracted from liver (*Fig.* 3-5B). Finally, spontaneous hepatic tumors developed in 20% (2/10) of mice maintained on the HFCF diet for 9 months (*Fig.* 3-6B).

Taken together, the above data indicate that mice developed steatosis after 1 month on the HFCF diet, which was more extensive at 3-months and accompanied by inflammation and collagen accumulation. The extent of steatosis remained unchanged in mice fed the HFCF diet for 5 to 9 months, but the presence of inflammation and fibrosis were enhanced over time. We then examined the NAFLD activity score (NAS) in HFCF-fed mice over the course of diet feeding. As shown in *Fig.* 3-6C, NAS increased by 1-month and remained significantly higher than chow-fed mice by 9-month. In particular, steatosis was the major contributor to NAS at early time point; however, the increase in NAS at late time points was mainly attributed by inflammation, cell death, and fibrosis. In HFCF-fed mice, the NAS of 1-month, 3-month, 5-month, 7-month, and 9-month were

1.09±0.01, 3.26±0.26, 5.20±0.75, 6.50±0.58, and 7.63±0.69, respectively. Per NASH-Clinical Research Network (CRN) criteria (139,150), NAS of 1-2 is NAFL, 3-4 indicates borderline NASH and 5-8 means definitely NASH. Therefore, our results indicate that HFCF-fed mice developed a transition phase of NAFL progression to NASH at the 3- to 5-month post HFCF diet administration.

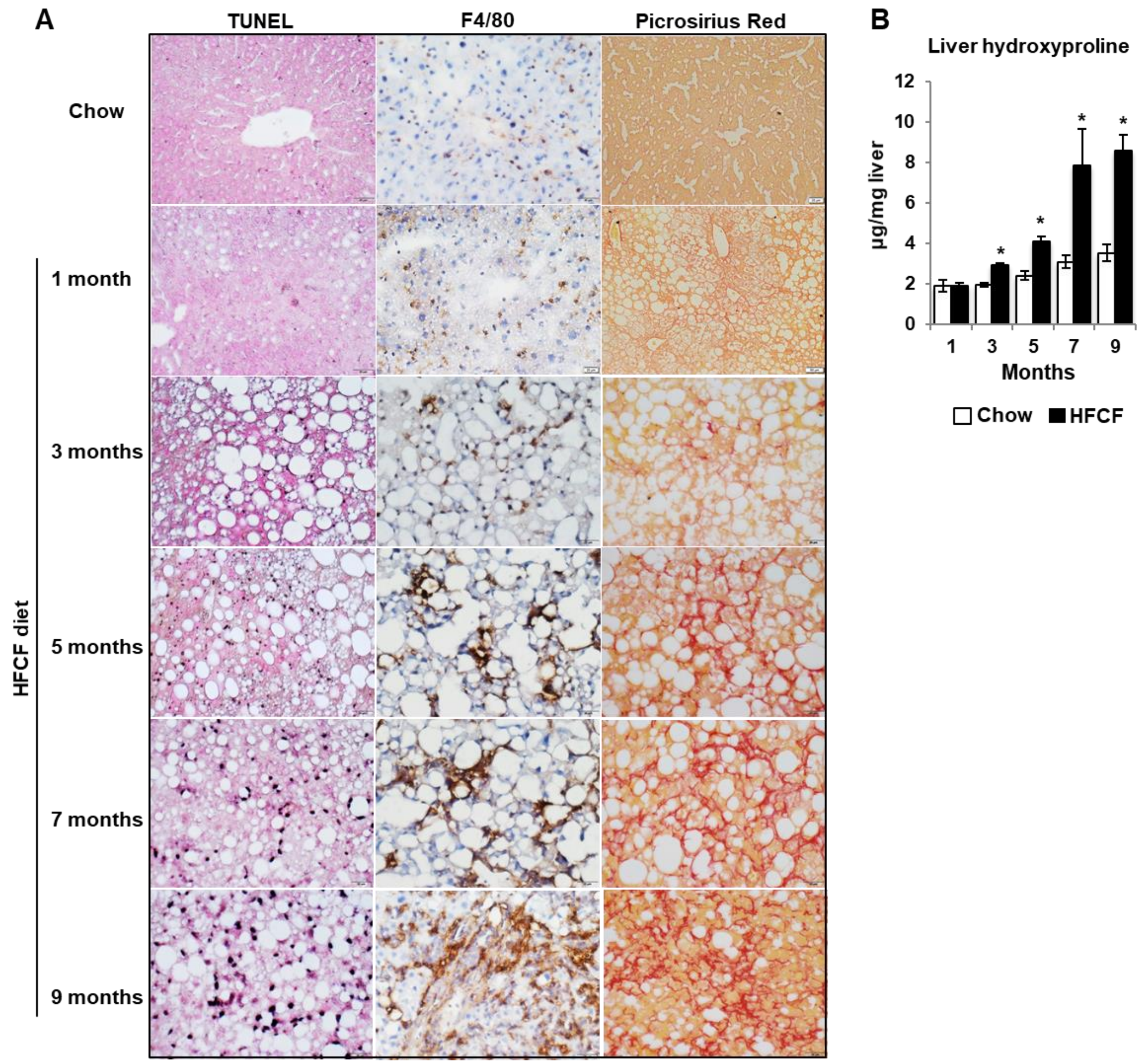

Figure 3-5: The development of cell death, inflammation, and fibrosis in livers from HFCF-fed mice.

Two-month-old C57BL/6J male mice were fed chow or a HFCF diet for up to 9 months. **A:** Representative images of liver sections stained with TUNEL, F4/80, or Picrosirius Red. Original magnification, 400X. **B:** Liver hydroxyproline content was determined by hydroxyproline assay. Data presented in B is expressed as mean ± SEM for 5 mice per group. *$P < 0.05$ versus chow controls.

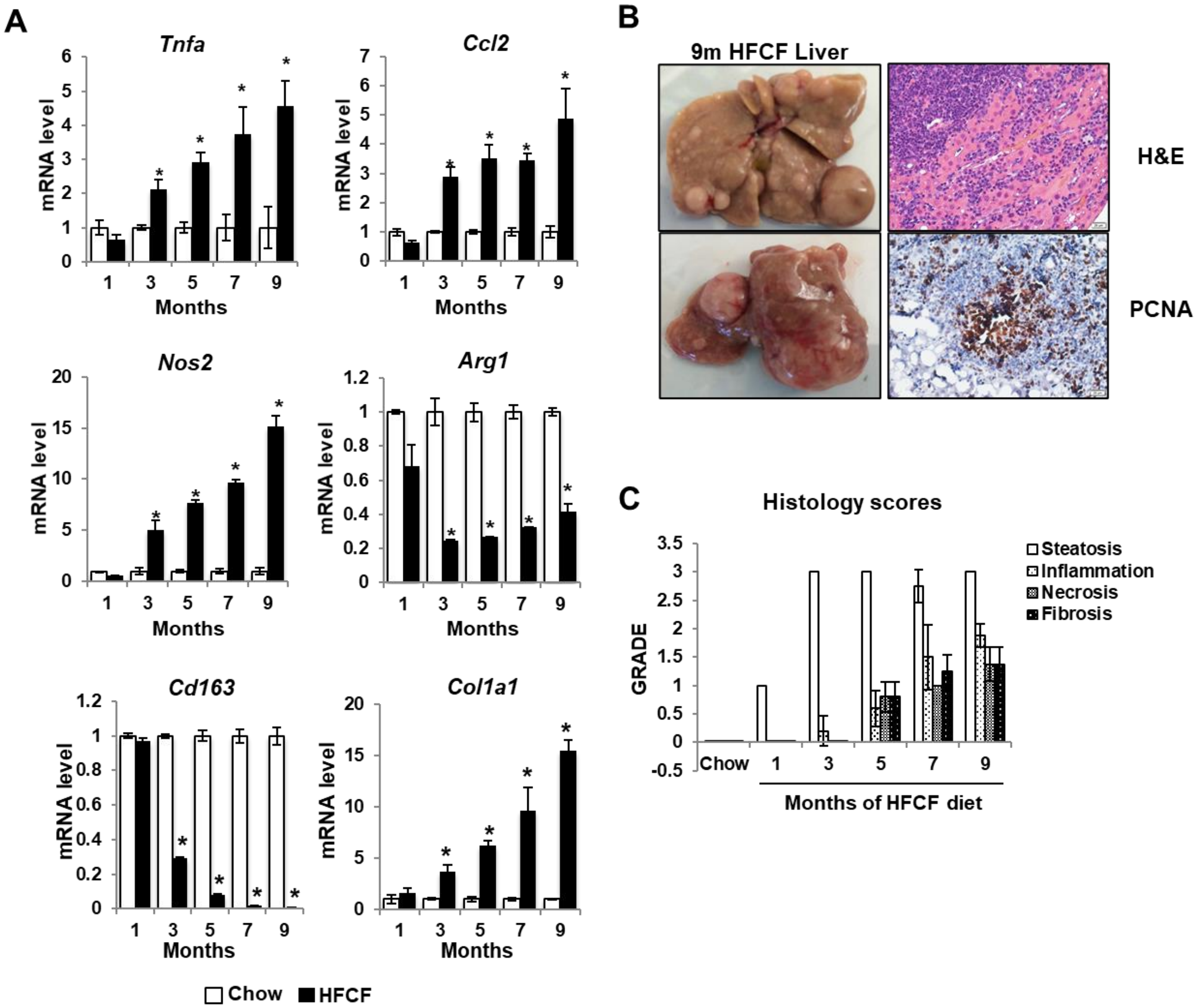

Figure 3-6: HFCF feeding induces the expression of genes involved in inflammation and fibrosis, and promotes tumor development over time.

Two-month-old C57BL/6J male mice were fed chow or a HFCF diet for up to 9 months. **A:** Relative mRNA levels of genes related to inflammation and fibrosis in liver were determined by qPCR. **B:** Gross liver appearance and representative images of liver sections stained with hematoxylin-eosin (H&E) or proliferating cell nuclear antigen (PCNA) from the 9-month HFCF-fed mice. **C:** Liver histology scores of steatosis, inflammation, cell death, and fibrosis. Data presented in A and C are expressed as mean ± SEM for 5 mice per group. *$P < 0.05$ versus chow controls.

Discussion

In the present study, we provide an overview of the dynamic changes of NAFLD progression in C57Bl/6J mice that were fed a HFCF diet—a model which closely recapitulates the key physiological, metabolic, and histologic changes seen in humans. We demonstrated that upon the initiation of HFCF diet, mice became obese and developed dyslipidemia with insulin resistance. Notably, HFCF-fed mice sequentially developed simple steatosis, steatohepatitis, steatohepatitis with progressive fibrosis, and eventually liver tumor within the timeframe of 9 months. These stages are consistent with NAFLD progression in humans. Therefore, we anticipate that our HFCF-fed mice can serve as a relevant model to identify therapeutic targets and test preventive and therapeutic approaches against NASH.

NAFLD development is strongly associated with obesity. In this study, we found that, upon introduction of HFCF diet, mouse body weight increased rapidly, becoming significantly different from the chow-fed group as early as 1 month after feeding. However, the increases in liver weight as well as the liver-to-body weight ratio became significant after 3 months of HFCF diet feeding. Similarly, histology showed that lipid accumulation in liver was severe after 3 months of HFCF diet feeding. These data suggest that liver steatosis in HFCF-fed mice developed after the excessive abdominal fat accumulation.

A key feature of NAFLD is triglyceride accumulation in hepatocytes. *Pparg* is a master transcriptional regulator of adipogenesis and lipid storage. Disruption of the *Pparg* gene in hepatocytes ameliorates steatosis, whereas its overexpression promotes the development of fatty liver through the activation of various lipogenic genes such as fatty acid uptake-related gene, *Cd36*, and lipid droplet formation-related gene, *Cidec* (151,152). We found that HFCF-fed mice displayed sustained upregulation of *Pparg* and its downstream targets, *Cd36* and *Cidec*, throughout the 9-month feeding period. This indicates that liver steatosis development in HFCF-fed mice could be mainly attributed to the increase of fatty acid uptake regulated by *Pparg*.

De novo lipogenesis is a tightly regulated process for fatty acid biosynthesis, in which both *Acc1* and *Fasn* are important. ACC1 is involved in the carboxylation of acetyl-CoA to generate malonyl-CoA and FASN catalyzes malonyl-CoA to produce new saturated fatty acid. In healthy, lean individuals, *de novo* lipogenesis contributes to < 5% of total triglyceride synthesis in fasting conditions but the rate can be 25% or greater in fed conditions (153). Notably, in HFCF-fed mice, both *Acc1* and *Fasn* were decreased at early time points (1 month and 3 months) after diet initiation but increased at later time points (5 to 9 months) when the liver displayed severe steatosis. Our data here support the notion that augmented *de novo* lipogenesis is an important contributor to the development of NASH.

To remove lipids from the liver, lipids can either be secreted as VLDL particles or oxidized through fatty acid oxidation. In HFCF-fed mice, both *Apob* and *Mttp* were unchanged during the first 3 months of diet administration but decreased thereafter, accompanied by severe lipid accumulation in the liver. This result indicates that the decreased VLDL secretion exacerbates lipid accumulation in the liver during NASH development. CPT1 is a regulatory enzyme that transports fatty acid from cytosol to mitochondria for beta-oxidation. In NAFLD patients, *CPT1* expression has been found to decrease by 50% (154). Consistently, our study showed that *Cpt1* was transiently increased in the 1-month HFCF-fed group but decreased thereafter. The transient induction of *Cpt1* by short-term HFCF feeding could be due to *Ppara* activation induced by fatty acids; however, long-term HFCF feeding results in augmented *de novo* lipogenesis and malonyl-CoA formation which could downregulate *Cpt1* (155-157).

Taken together, the working summary of lipid metabolism in HFCF-fed mice is that fatty acid uptake into liver is augmented after the HFCF diet initiation, resulting in subsequent accumulation of lipids in the liver. The lipid accumulation drives the upregulation of genes involved in fatty acid oxidation and decreases lipogenic genes related to *de novo* lipogenesis by a feedback mechanism. However, long-term feeding causes excessive hepatic lipid accumulation driven by both augmented fatty acid uptake and *de novo* lipogenesis. This results in decreased VLDL secretion and fatty acid oxidation which potently worsen steatosis and drive disease progression. In summary, our study provides a unique overview of the dynamic changes in NAFLD developed in mouse that is consistent with disease progression in humans.

Chapter 4: Uncovering the Role of Hepatocyte-Specific SHP in NAFLD and Its Contribution to NAFL to NASH Transition

This chapter is adapted from our previously-published articles in open-access journals: Zou A, Magee N, Deng F, Lehn S, Zhong C, Zhang Y. Hepatocyte nuclear receptor SHP suppresses inflammation and fibrosis in a mouse model of nonalcoholic steatohepatitis. *J Biol Chem* 2018; 293: 8656-8671. PMCID: PMC5986206. www.jbc.org/cellbiology_gene_regulation

and

Magee N, Zou A, Ghosh P, Ahamed F, Delker D, Zhang Y. Disruption of hepatic small heterodimer partner induces dissociation of steatosis and inflammation in experimental nonalcoholic steatohepatitis. J Biol Chem 2020; 295: 994-1008. PMCID: PMC6983844. www.jbc.org/MolecularBasisofDisease_gene_regulation

Introduction

Nuclear receptor small heterodimer partner (*Nr0b2*, Homo sapiens *SHP*; *Mus musculus Shp*) is highly expressed in normal hepatocytes and acts as an important transcriptional regulator for bile acid, glucose and lipid metabolism (123). In support of a critical role of SHP in metabolic diseases, *SHP* mutation is associated with an increase in body weight and morbidity risk of type 2 diabetes in Japanese populations (158). More recently, SHP is shown to suppress toll-like receptor 4 (TLR4)-induced (159) and NLRP3 inflammasome-mediated (160) inflammatory responses in monocytes, which suggest a connection between SHP and inflammation. Now, hepatocytes are gradually being recognized as important players involved in the initiation of inflammation in NASH (161,162). However, whether hepatocyte SHP plays a role in this process remains unexplored.

C-Jun N-terminal kinase (JNK) is well known for its roles in acetaminophen-induced hepatotoxicity, inflammation, and apoptosis. Activated by monounsaturated and saturated free fatty acids, cellular stress and oxidative stress, JNK has also been shown to play an important role in the advancement of inflammation and apoptosis seen in NAFL/NASH (163). Within the last two decades, the involvement of JNK in insulin resistance, metabolic inflammation and obesity has become clearer. These effects of JNK are due to its direct phosphorylation of insulin receptor substrates 1 and 2 (164,165), promotion of proinflammatory macrophage phenotype (166), and negative regulation of PPARa and fibroblast growth factor 21 (FGF21) (167). Studies and clinical trials employing specific inhibition of JNK using SP600125 were able to ameliorate NAFLD amongst other diseases in various animal models (168). Here, we explore whether JNK activation in our mouse NAFLD model is correlated to SHP downregulation observed along disease progression.

NFκB is a major regulator of the inflammatory response in various cell types. In macrophages, NFκB is bound to SHP. Upon TLR stimulation, SHP is dislodged and NFκB can translocate to the nucleus to induce transcription of cell survival or proinflammatory genes such as TNFa (159,169). Crosstalk between JNK and NFκB is well described and there appears to be feedback mechanism based upon stimuli and cell-types. In regards to cell survival, several studies demonstrate the role of NFκB in inhibiting apoptosis by negatively regulating the JNK signaling cascade (170-172). On the other hand, JNK has been implicated in the inhibition of NFκB-mediated inflammation in macrophages, human monocytic cell lines, and renal epithelial cells (173-175). However, the connection between hepatic JNK and NFκB in NASH is incompletely understood. In this dissertation, we explore a possible link between NFκB, JNK and SHP in hepatocytes and the importance of their interactions in NASH development.

Inflammatory chemokine (C-C motif) ligand 2, CCL2, (also known as monocyte chemoattractant protein 1, MCP1) is responsible for attracting monocytes and T cells during liver injury (176). It is well known that NFκB mediates CCL2 release in various organs, and many types of liver cells can produce CCL2, including hepatocytes, stellate cells and Kupffer cells (177-180). Studies have shown that high levels of CCL2 in NAFLD contribute to the conversion of NAFL to NASH (181) and pharmacological inhibition of CCL2 reduces liver macrophage infiltration in NASH (182), which makes CCL2 a good therapeutic target for NASH prevention and treatment. However, how CCL2 is produced during the disease progression from NAFL to NASH is incompletely understood. A recent study has demonstrated that the activation of SHP by a small molecule activator inhibits liver cancer cell migration via blocking CCL2 signaling (183) which potentially links SHP to CCL2 production.

Here, we show that SHP was markedly decreased in the livers of patients with NASH and in diet-induced mouse NASH, which was due to JNK-induced c-JUN inhibition on *Shp* transcription. In addition, we employed a clinically relevant dietary mouse NASH model and investigated the role of SHP in NASH development. We demonstrated that the loss of SHP in hepatocytes resulted in NFκB p65-mediated induction of CCL2, leading to macrophage activation. Meanwhile, hepatic *Shp* disruption dampened *Pparg* signaling, leading to the dissociation of steatosis, inflammation, and fibrosis during NAFLD development. Additionally, we found that ablation of hepatic *Shp* after the development of steatosis exacerbated liver inflammation and fibrosis. On the other hand, hepatic SHP overexpression could attenuate liver inflammation and fibrosis. Taken together, our study has uncovered a novel regulatory network in hepatocytes, consisting of JNK/SHP/NFκB/CCL2, which controls macrophage recruitment during the disease progression from NAFL to NASH. Our finding that hepatic *Shp* could play distinct roles at different stages of NAFLD provides some new mechanistic insights into our understanding of NAFLD pathogenesis and progression, which may benefit the development of new management or prevention strategies for NASH.

Results

SHP decreases in human NASH liver

To determine whether the expression of SHP is associated with NAFLD pathogenesis, we examined *SHP* mRNA levels in two sets of human liver specimens. The first set was obtained through the University of Kansas Liver Center. The liver histology of human NAFL and NASH is shown in *Fig.* 4-1A. NAFL is characterized by the deposition of triglycerides as lipid droplets in hepatocytes. NASH is distinguished from NAFL by the presence of hepatocyte injury (hepatocyte ballooning and cell death), inflammation, and/or collagen deposition (fibrosis). Perisinusoidal /pericellular (chicken wire) fibrosis is the characteristic pattern of liver fibrosis in NASH, which typically begins in zone 3 due to the deposition of collagen along the sinusoids and around the hepatocytes. As shown in *Fig.* 4-1A, Picrosirius red staining showed the chicken-wire pattern of perisinusoidal/pericellular fibrosis and periportal fibrosis in human NASH. While there were similar *SHP* mRNA levels in the liver of normal and NAFL, a significant decrease in *SHP* mRNA was observed in NASH samples compared to NAFL samples (*Fig.* 4-1A). Consistently, the analysis of microarray dataset GSE48452 also revealed a significant decrease in *SHP* mRNA levels in patients with NASH compared to NAFL and normal controls (*Fig.* 4-1B). Western blotting analysis confirmed the decrease of SHP protein in NASH samples compared to NAFL and normal livers (*Fig.* 4-1C). Collectively, our results strongly suggest a biological relevance of SHP downregulation during the disease progression from NAFL to NASH in humans.

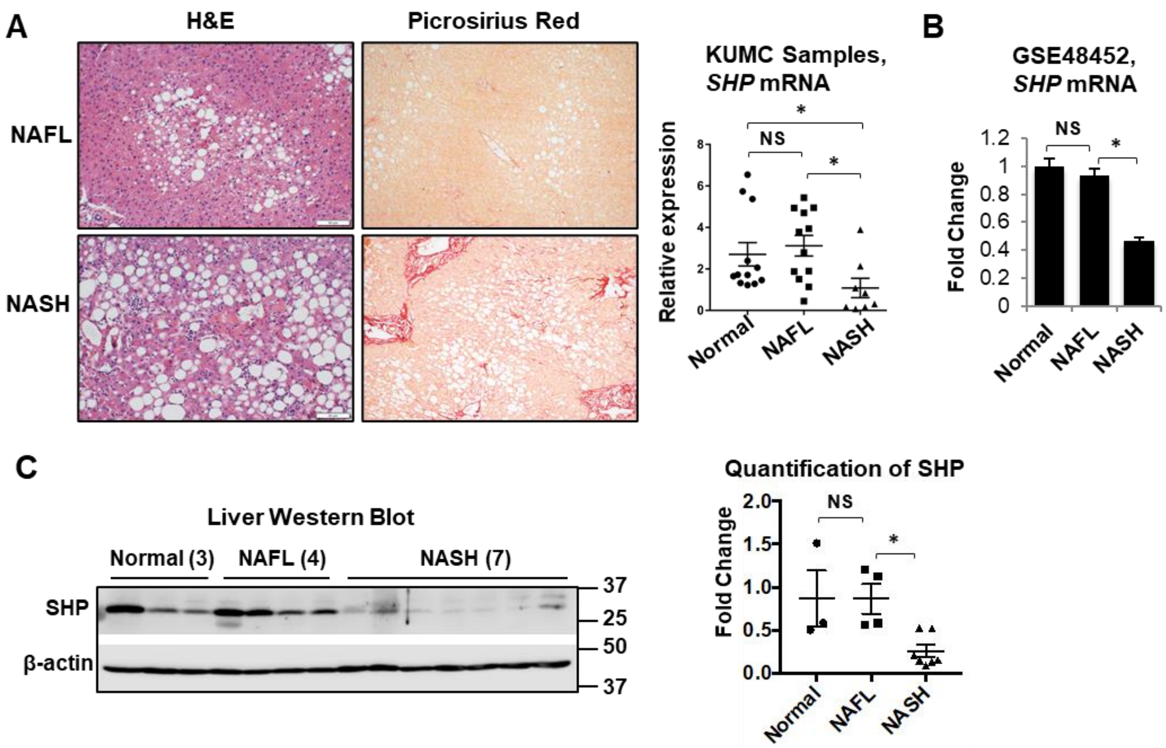

Figure 4-1: Decrease of SHP in human NASH compared to NAFL.

A: Human liver specimens were obtained from the University of Kansas Liver Center, including 12 normal livers, 12 NAFL livers, and 8 NASH livers. (Left) Representative images of liver sections stained with H&E or Picrosirius red from patients with NAFL or NASH. Original magnification, 100x. (Right) Relative *SHP* mRNA level was determined by qPCR. *$p < 0.05$. **B:** Analysis of SHP expression in a microarray database (GEO GSE48452). The no. of specimens in each group was as follows: normal (n=14), steatosis (n=14), and NASH (n=18). Data are represented as mean ± SEM. *$p < 0.05$. **C:** (Left) Western blotting analysis of SHP in human livers. (Right) Band intensities were calculated using Image J software. The relative expression of SHP was normalized to the expression of loading control b-actin. Data are presented as fold changes relative to that of the control. *$p < 0.05$

Decrease of SHP in HFCF diet-induced mouse NASH

We next examined SHP expression in the liver of HFCF-dietary mouse model. As shown in *Fig.* 4-2A, 1 month of HFCF feeding did not change liver *Shp* mRNA level compared to chow controls; however, a significant decrease in *Shp* mRNA was observed after mice were on the HFCF diet for 5 months. SHP protein is a rapidly degraded protein with a very short half-life (184). We employed two anti-SHP antibodies in Western blot to determine SHP protein levels in the liver. SHP (H-160) is a rabbit polyclonal antibody while SHP (H-5) is a mouse monoclonal antibody. Both antibodies recognize the epitope corresponding to amino acids 1-160 mapping at the N-terminus of SHP protein. As shown in *Fig.* 4-2B, both antibodies detected a significant decrease in SHP protein in the livers of 5-month HFCF-fed mice.

The MCD diet induces NASH-like liver pathology including liver steatosis, inflammation, and fibrosis, despite weight loss and insulin sensitivity (143). Next, we explored SHP expression in livers of mice fed MCD diet. As shown in *Fig.* 4-2C, the liver morphology indicated the development of liver steatosis, inflammation, and fibrosis in mice fed MCD diet for 1 month. Consistently, the expression of genes involved in inflammation and fibrosis such as *Adgre1*, *Tnfa*, *Ccl2*, *Il-1b*, and *Col1a1* were all increased in mice on the MCD diet (*Fig.* 4-2D). Importantly, we observed a significant decrease in *Shp* mRNA level in the livers of MCD-fed mice compared to chow controls (*Fig.* 4-2D). Collectively, our results indicate that the expression of SHP is dramatically decreased in the liver of mouse NASH. Moreover, our HFCF-dietary mouse studies provide convincing evidence that SHP is suppressed during NAFL progression to NASH.

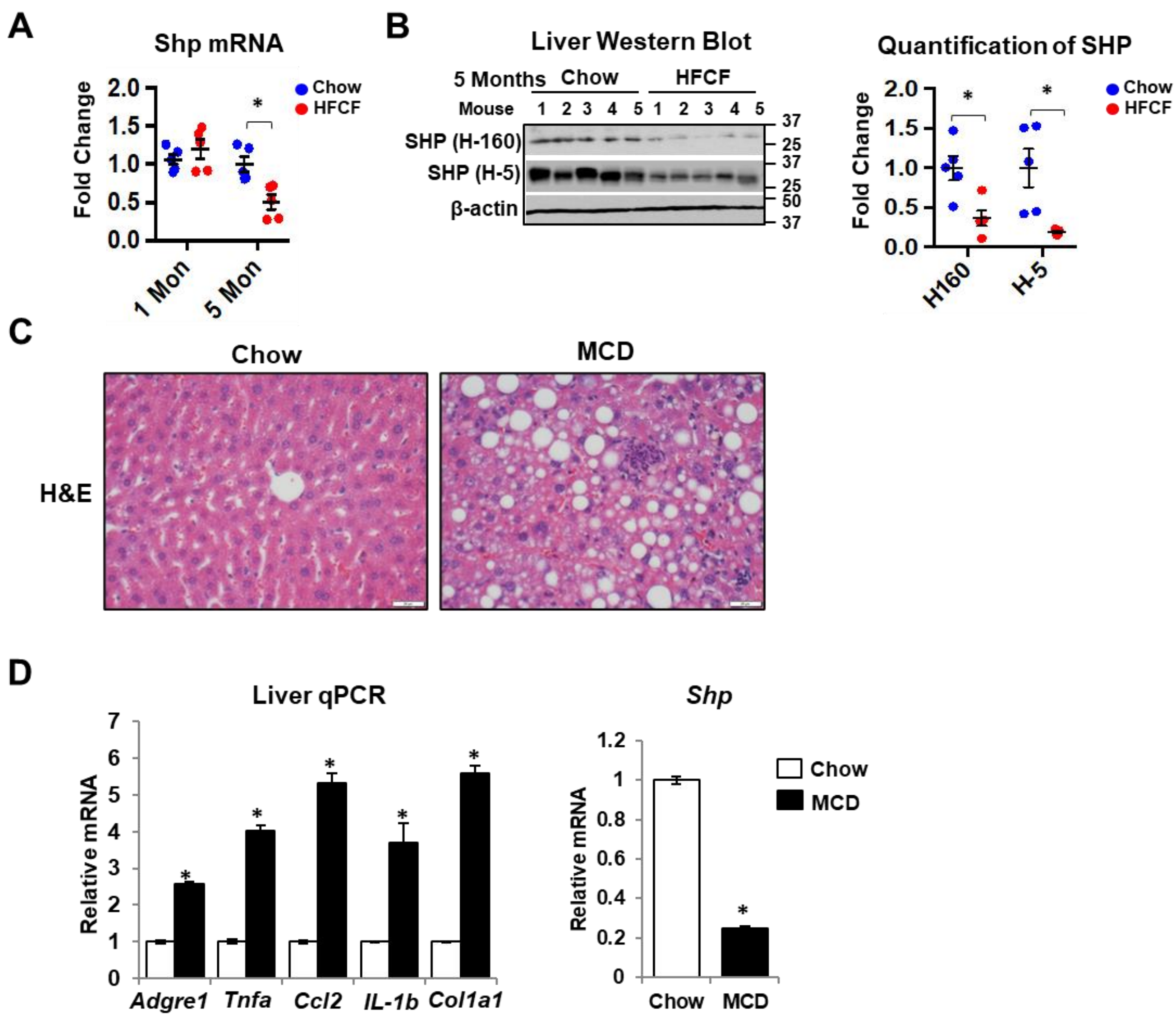

Figure 4-2: Hepatic SHP levels decrease in mouse models of NASH.

A: qPCR analysis of *Shp* mRNA level in the liver of mice fed chow or HFCF diet. **B:** (Left) Western blot of SHP protein in the liver of mice fed chow or HFCF diet for 5 months. (Right) Band intensities were measured by densitometry, and the intensities relative to that of the controls were plotted. **C:** Representative images of liver sections stained with hematoxylin-eosin (H&E) in mice fed chow or methionine-choline deficient (MCD) diet for 1 month. Original magnification, 400X. **D:** qPCR analysis of gene expression in the liver of mice fed chow or MCD diet for 1 month. Data in A, B, and D are represented as mean ± SEM for 5 mice per group. *$p < 0.05$ MCD or HFCF versus respective controls.

JNK inhibits SHP expression in hepatocytes

Since SHP is highly expressed in hepatocytes (185), we speculate that SHP suppression during NAFL transition to NASH is mainly from the decrease of SHP in hepatocytes. To begin to test our hypothesis, we isolated hepatocytes, hepatic stellate cells (HSC), and macrophages from mouse liver and compared SHP expression. The cell purification was confirmed by the detection of various cell specific markers by qPCR, including hepatocyte marker albumin (Alb), quiescent HSC marker Hedgehog interacting protein (Hhip), and macrophage marker F4/80 (Adgre1). As expected, *Shp* mRNA is abundantly expressed in hepatocytes and low in macrophages and hepatic stellate cells (*Fig.* 4-3A).

We next sought to investigate the potential mechanisms of SHP suppression in NASH. We employed a primary mouse hepatocyte culture as an *in vitro* lipotoxicity model and explored whether palmitic acid (PA) or TLR4 ligand lipopolysaccharide (LPS) could alter SHP expression. PA (0.5 mM) or LPS (100 ng/ml) treatment for 6h significantly decreased *Shp* mRNA expression (*Fig.* 4-3B). To further investigate the potential mechanisms of SHP suppression by PA and LPS, we superimposed various signaling pathway inhibitors including a JNK inhibitor SP600125 (50 μM), NFκB inhibitor BAY 11-7082 (5 μM), and phosphatidylinositol 3-kinase (PI3K) inhibitor LY294002 (50 μM) on a PA or LPS treatment regimen. Interestingly, co-treatment with the JNK inhibitor completely rescued the decrease of *Shp* mRNA by PA or LPS (*Fig.* 4-3B). Thus, our results indicate that JNK activation mediates the suppression of SHP by PA and LPS in hepatocytes.

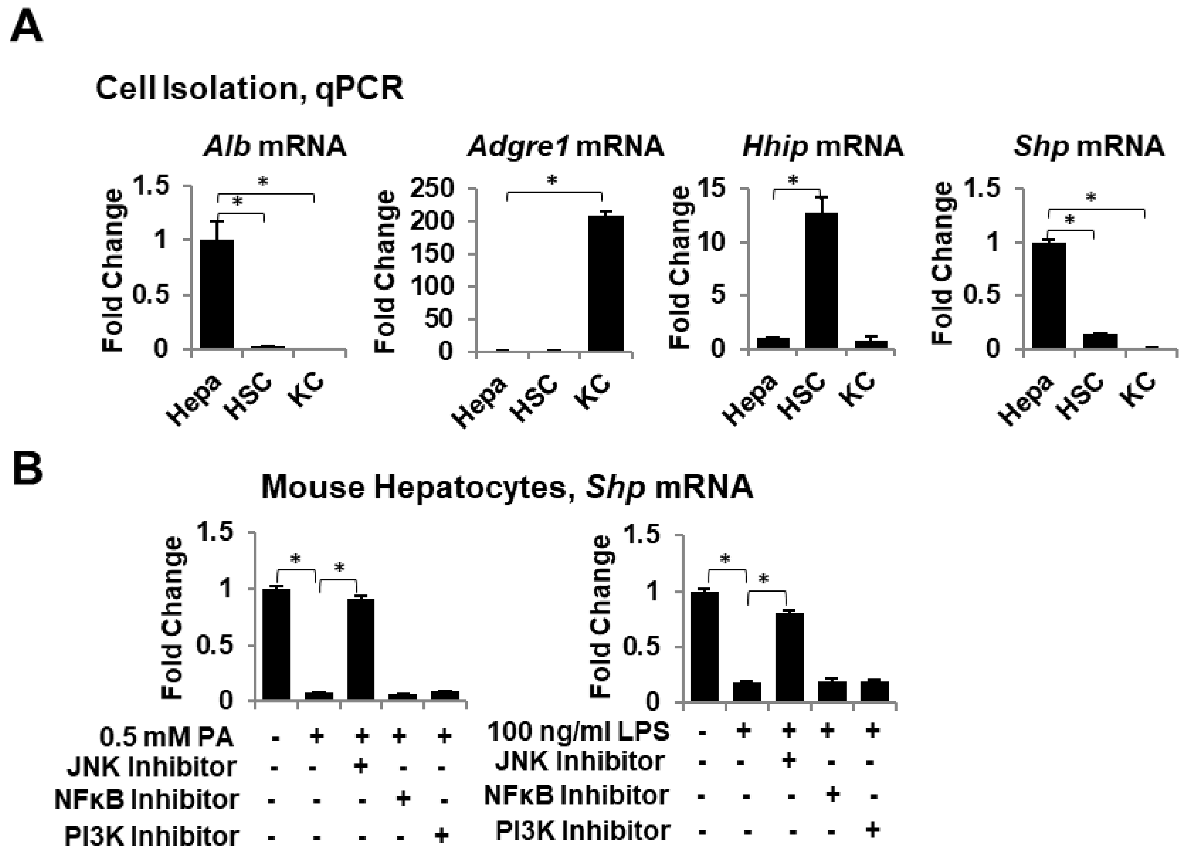

Figure 4-3: *Shp* is highly expressed in hepatocytes and JNK activation inhibits *Shp* expression.

A: qPCR in primary hepatocytes (Hepa), hepatic stellate cells (HSC), and resident macrophage Kupffer cells (KC) isolated from mouse liver. **B:** qPCR analysis of *Shp* mRNA levels in mouse hepatocytes. Hepatocytes were incubated with 0.5 mM PA or 100 ng/ml LPS for 6 h in the presence or absence of various inhibitors such as JNK inhibitor SP600125 (50 μM), NF-κB inhibitor BAY 11-7082 (5 μM), and phosphatidylinositol 3-kinase (PI3K) inhibitor LY294002 (50 μM). Data are represented as mean ± SEM. *p < 0.05 versus respective controls.

C-Jun is activated by JNK and targets *Shp* promoter for *Shp* suppression

In our study, JNK activation was observed in the livers of mice fed HFCF for 5 months, evidenced by the induction of phosphorylated JNK (p-JNK, activated form of JNK) (*Fig.* 4-4A). Activation of JNK was accompanied by c-Jun phosphorylation at Ser73 (*Fig.* 4-4A), potentially connecting JNK activation and c-Jun phosphorylation to *Shp* suppression during NAFLD progression. The *SHP* gene contains a consensus 12-O-tetradecanoylphorbol-13-acetate response element (TRE, core sequence TGAGTCA) located on its promoter region (–295 to –289 on human SHP gene and -333 to -326 on mouse *Shp* gene) which is predicted to be a c-Jun response element (*Fig.* 4-4B). We cloned the mouse *Shp* proximal promoter (2 kb) into a luciferase reporter (*Shp*-Luc) and examined c-Jun's effect on *Shp* promoter activity in mouse hepatocyte cell line AML12 cells. Nuclear receptor LRH1 binds to the *Shp* promoter and induces *Shp*-Luc activity (*Fig.* 4-4B); thus, LRH1 was included as a positive activator. Overexpressing c-Jun decreased the basal activity as well as the induction of *Shp*-Luc by LRH1, which was completely blocked in the reporter construct containing a mutated TRE site (*Shp*-Luc Mut) (*Fig.* 4-4C), suggesting that c-Jun inhibits *Shp* promoter activity through the TRE site. Moreover, blocking JNK activation by a specific inhibitor, SP600125, increased *Shp*-Luc activity which was completely disrupted in the *Shp*-Luc Mut (*Fig.* 4-4C), indicating for the first time that the suppression of *Shp* by JNK was primarily facilitated by c-Jun.

A chromatin immunoprecipitation (ChIP) assay was performed in AML12 cells overexpressed with c-Jun and confirmed the recruitment of c-Jun to the *Shp* promoter (*Fig.* 4-5A). Additionally, PA (0.5 mM) treatment in AML12 cells dramatically stimulated the recruitment of endogenous c-Jun to the *Shp* promoter, which was completely abrogated by the co-treatment of a specific JNK inhibitor SP600125 (*Fig.* 4-5A). The mouse *Shp* proximal promoter contains three LRH1 binding sites (*Fig.* 4-4B, GAGACCTTGG at –383 to –374; TCAAGGTTG at -116 to -108, TCAAGGATA at -83 to -75) which are close to the TRE site. To understand how c-Jun inhibits LRH1-induced *Shp*-Luc activity, we performed ChIP assay to examine whether c-Jun would interfere with the recruitment of LRH1 to *Shp* promoter. As shown in *Fig.* 4-5B, overexpressing c-Jun in AML12 cells dramatically decreased the recruitment of LRH1 to all three LRH1 sites on *Shp* promoter. Similarly, PA treatment in AML12 cells also significantly decreased the recruitment of LRH1 to the *Shp* promoter (*Fig.* 4-5B). Thus, our data suggests that the binding of c-Jun to the *Shp* promoter inhibits LRH1 recruitment to the *Shp* promoter.

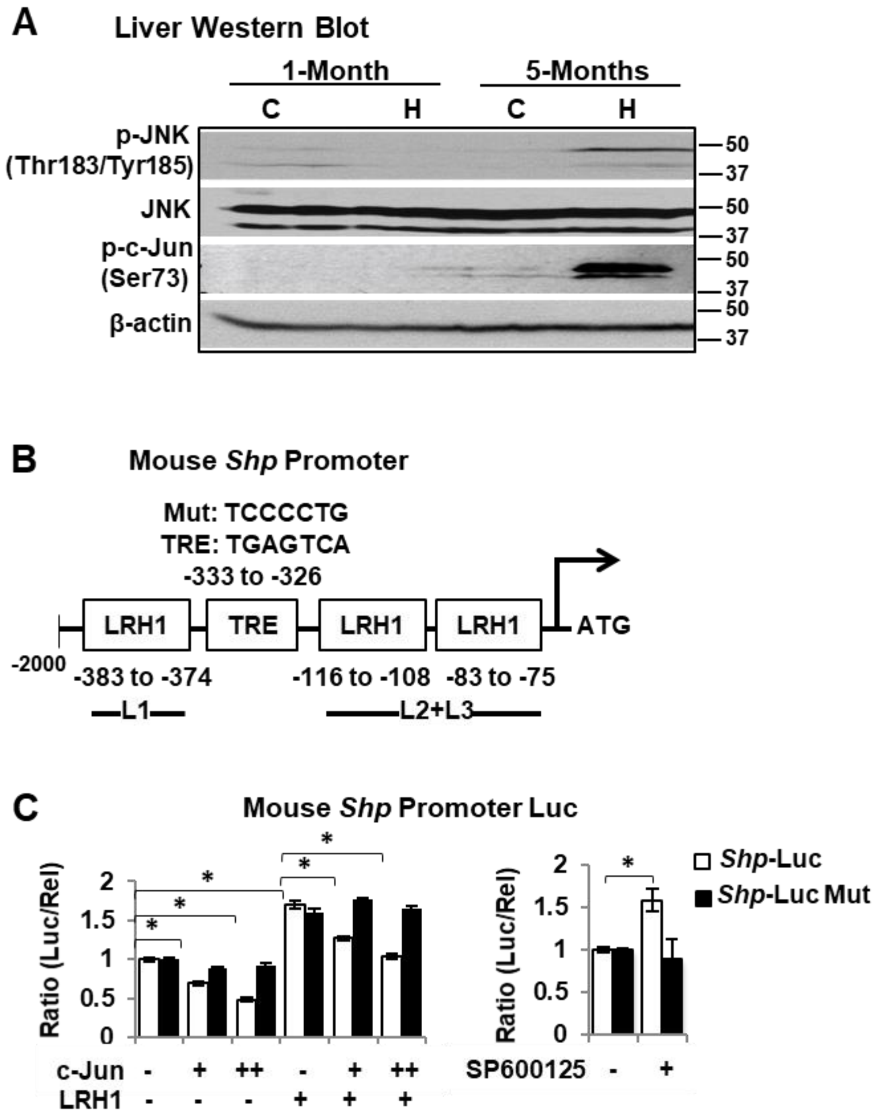

Figure 4-4: JNK activates c-Jun which targets *Shp* promoter.

A: Western blot in the liver of mice fed chow or HFCF for 1 and 5 months. **B:** Diagram showing the location of 12-O-tetradecanoylphorbol-13-acetate response element (TRE, core sequence TGAGTCA) site on the *Shp* promoter reporter (*Shp*-Luc) and its mutant. **C:** (Left) AML12 cells were transfected with *Shp*-Luc or its mutant with or without various expression plasmids. Luciferase activities were determined at 24 h post transfection. (Right) AML12 cells were transfected with *Shp*-Luc or its mutant for 24 h, followed by incubation with SP600125 (50 μM) for 6 h. Data are displayed as the ratio of firefly luminescence divided by *Renilla* luminescence and are represented as mean ± SEM for triplicate per group. *p < 0.05.

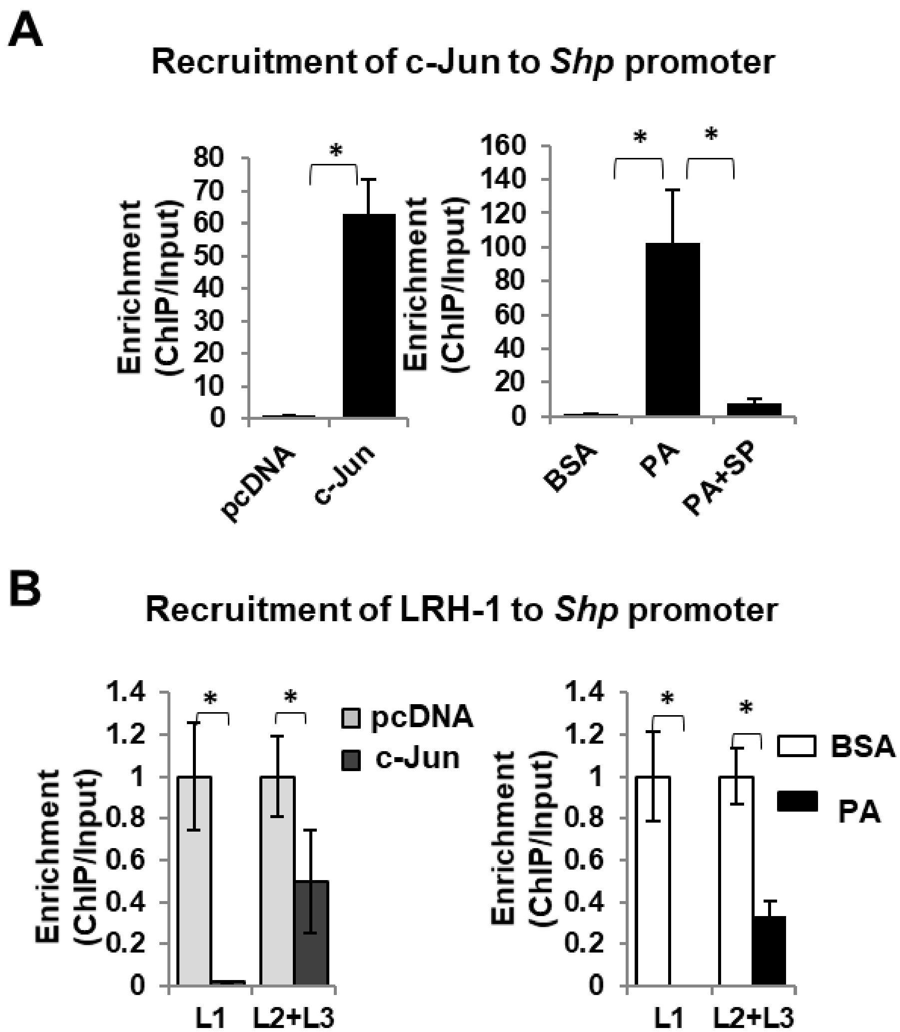

Figure 4-5: ChIP assay to determine the enrichment of c-Jun and LRH1 to the *Shp* promoter.

A: ChIP assay to determine the enrichment of c-Jun to the *Shp* promoter. (Left) AML12 cells overexpressed with c-Jun were harvested at 24 h post-transfection. pcDNA served as a transfection control. (Right) AML12 cells were incubated with BSA control or 0.5 mM PA with or without JNK inhibitor SP600125 (50 μM) for 6 h. The cross-linked chromatin was immunoprecipitated by an antibody against c-Jun. The enriched DNA was amplified by qPCR and normalized to the input. The fold changes relative to that of the controls are plotted and represented as mean ± SEM. *$p < 0.05$. **B:** The enrichment of LRH1 to the *Shp* promoter was revealed by ChIP assay. (Left) AML12 cells overexpressed with c-Jun were harvested at 24 h post-transfection. (Right) AML12 cells were incubated with 0.5mM PA or BSA control for 6 h. The cross-linked chromatin was immunoprecipitated by an antibody against LRH1. The enriched DNA was amplified by qPCR and normalized to the input. The fold changes relative to that of the controls are plotted and represented as mean ± SEM. *$p < 0.05$.

Hepatic *Shp* disruption in adult mice induces liver injury, inflammation, and fibrogenesis

To generate hepatocyte-specific *Shp* knockout (*Shp*$^{Hep-/-}$) mice and wildtype (WT) controls, we injected 2-month-old *Shp*$^{flox/flox}$ mice with either AAV8-*Tbg*-Cre or AAV8-*Tbg*-null control for 1 or 12 weeks (*Fig.* 4-6A). The use of the *Tbg* promoter ensures that AAV8 specifically targets hepatocytes (186). Hepatic *Shp* deletion specifically in adult mice achieved a model in which a direct assessment of hepatic *Shp* function in the adult livers could be made. This is an advantage over using mice with a germline mutation in *Shp*, which could interfere with proper embryonic or neonatal development and alter adult hepatic function. This acute deletion approach also made it possible to distinguish the direct effects of *Shp* deletion from any secondary or compensatory effects.

The knockdown of *Shp* mRNA in the liver after Cre injection was confirmed by RT-PCR (*Fig.* 4-6A). Body weight gain, and lean and fat mass, were comparable between *Shp*$^{Hep-/-}$ mice and WT controls after 1 week or 12 weeks of AAV8 injection (*Fig.* 4-6B and 6C). To investigate whether ablation of hepatic *Shp* could affect glucose metabolism, we performed a GTT. As shown in *Fig.* 4-6D, no difference in GTT was observed between *Shp*$^{Hep-/-}$ mice and WT controls, which was further confirmed by the quantification of areas under the curves (AUC) of GTT (*Fig.* 4-6D Right). Additionally, the fasting serum triglycerides, cholesterol, and glucose were similar between *Shp*$^{Hep-/-}$ mice and WT controls; however, the liver injury marker ALT was significantly increased after 12 weeks of *Shp* deletion (*Fig.* 4-7A).

We next examined liver changes. Both liver weight and liver/body weight ratios were comparable between *Shp*$^{Hep-/-}$ mice and WT controls after AAV8 injection (*Fig.* 4-7B). No obvious histological change was observed after 1-week *Shp* deletion; however, after 12 weeks a massive infiltration of inflammatory cells occurred in the livers of *Shp*$^{Hep-/-}$ mice (*Fig.* 4-7C). Meanwhile, an increase in cell death was observed in *Shp*$^{Hep-/-}$ liver that was detected by terminal deoxynucleotidyl transferase dUTP nick end labeling (TUNEL) staining (*Fig.* 4-7D), supporting the elevated serum ALT shown in *Fig.* 4-7A. Taken together, the above data indicate that hepatic *Shp* deletion induces liver injury.

Immunohistochemistry staining of inflammatory cell markers CD3, CD4, CD8, CD19, F4/80, and Ly6G/Gr1 revealed an elevation of $CD4^+$ T cells, B cells, macrophages, and neutrophils in the *Shp*$^{Hep-/-}$ liver, respectively (*Fig.* 4-8). Meanwhile, an increase in liver fibrosis in *Shp*$^{Hep-/-}$ mice was detected by both trichrome staining and liver hydroxyproline measurement (*Fig.* 4-9A). Consistently, *Shp* deletion led to a robust induction of genes involved in inflammation and fibrosis, including lymphocyte antigen 6 family member D (*Ly6d*), interleukin 6 (*Il6*), interleukin 1 (*Il1*), tumor necrosis factor alpha (*Tnfa*), *Ccl2*, interferon gamma (*Ifng*), nitric oxide synthase 2 (*Nos2*), collagen type I alpha 1 chain (*Col1a1*), and collagen type I alpha 2 chain (*Col1a2*) (*Fig.* 4-9B). NF-κB signaling is a key regulator that controls inflammation (187). An increase in nuclear translocation of p65 was observed in the livers of *Shp*$^{Hep-/-}$ mice (*Fig.* 4-9C), supporting the overall increase of liver inflammation in *Shp*$^{Hep-/-}$ mice.

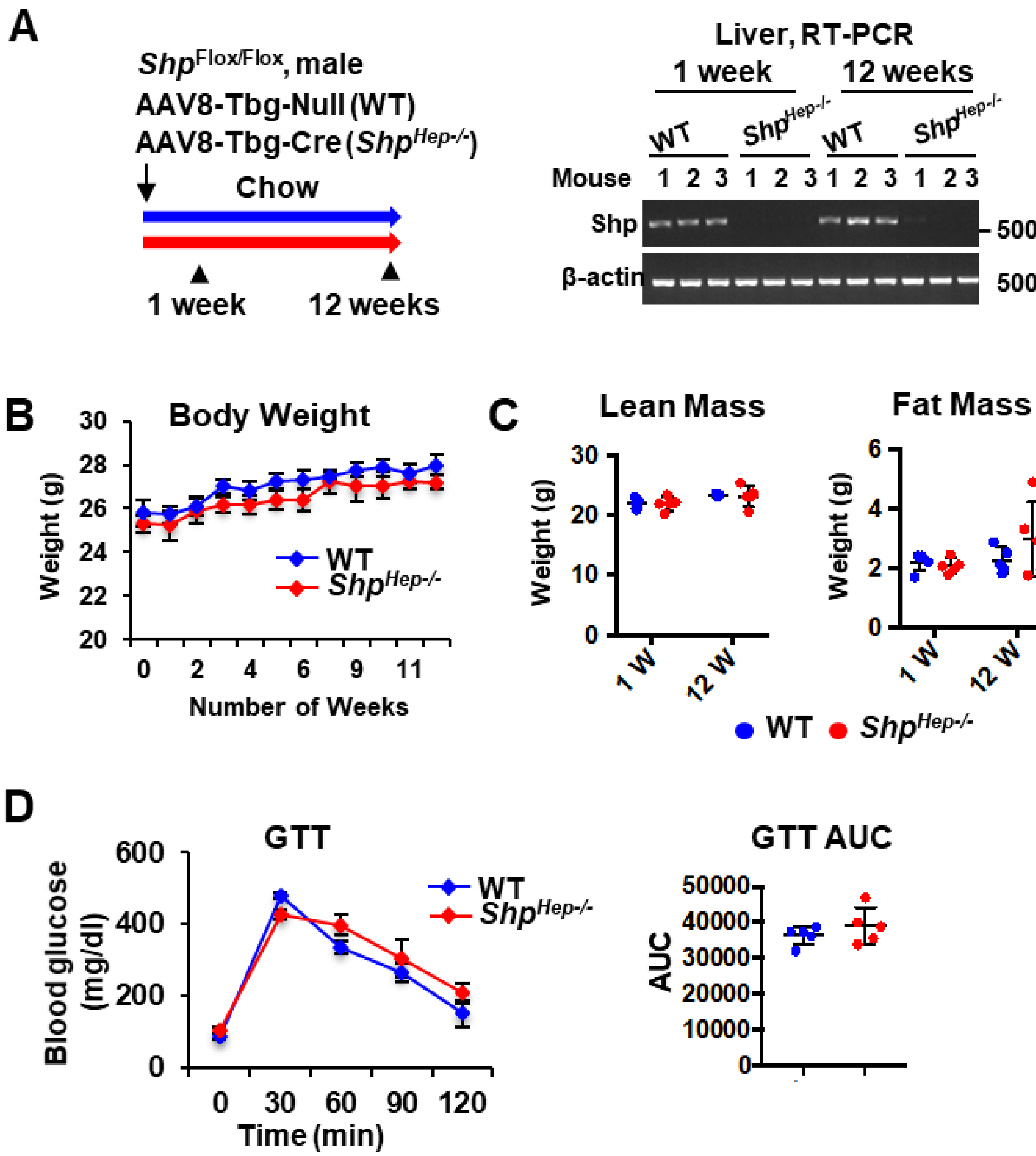

Figure 4-6: Hepatocyte-specific *Shp* disruption does not change body composition and glucose sensitivity.

A: (Left) schematic diagram showing experimental design. Two-month-old male *Shp*$^{flox/flox}$ mice were injected with either AAV8-*Tbg*-Cre or control AAV8-*Tbg*-null to generate hepatocyte-specific *Shp* knockout (*Shp*$^{Hep-/-}$) and wild type (WT) controls, respectively. Samples were collected at 1 week or 12 weeks post AAV8 injection. (Right) RT-PCR analysis of *Shp* mRNA levels in the liver. **B:** Mouse body weight change over time. **C:** Lean mass and fat mass were determined by EchoMRI™ system. **D:** (Left) Glucose tolerance test (GTT). (Right) Calculation of area under the curve (AUC) of GTT. Data are represented as mean ± SEM in B-D. n=5 mice/group.

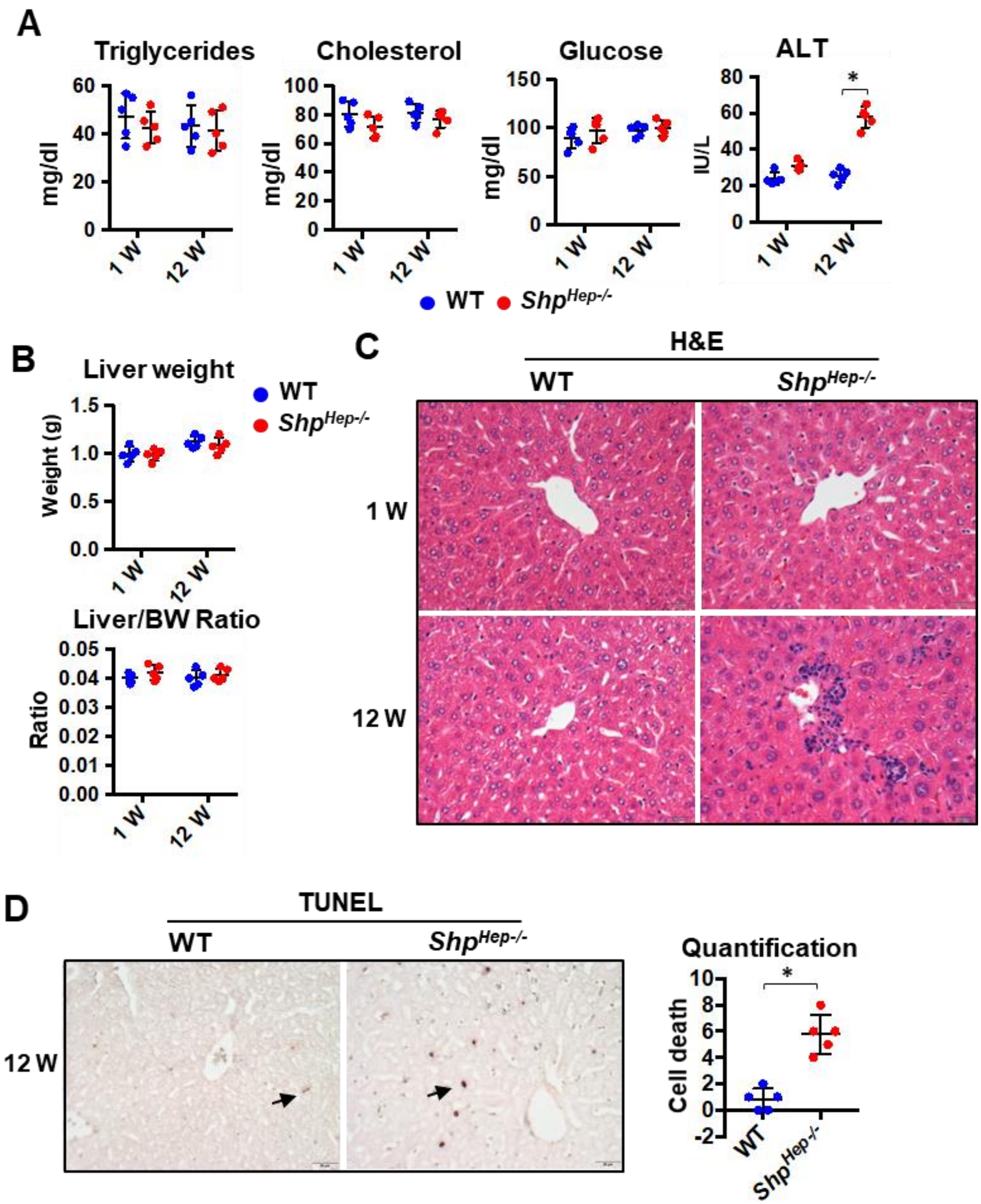

Figure 4-7: Hepatocyte-specific *Shp* deletion in adult mice causes liver injury.

A: Serum levels of fasting triglycerides, cholesterol, glucose, and ALT. **B:** Liver weight and liver/body weight ratios. **C:** Liver H&E stain. **D:** TUNEL stain and quantification. Data are represented as mean ± SEM in A, B, and D. n=3-5 mice/group. *, $p<0.05$ *Shp*$^{Hep-/-}$ versus WT.

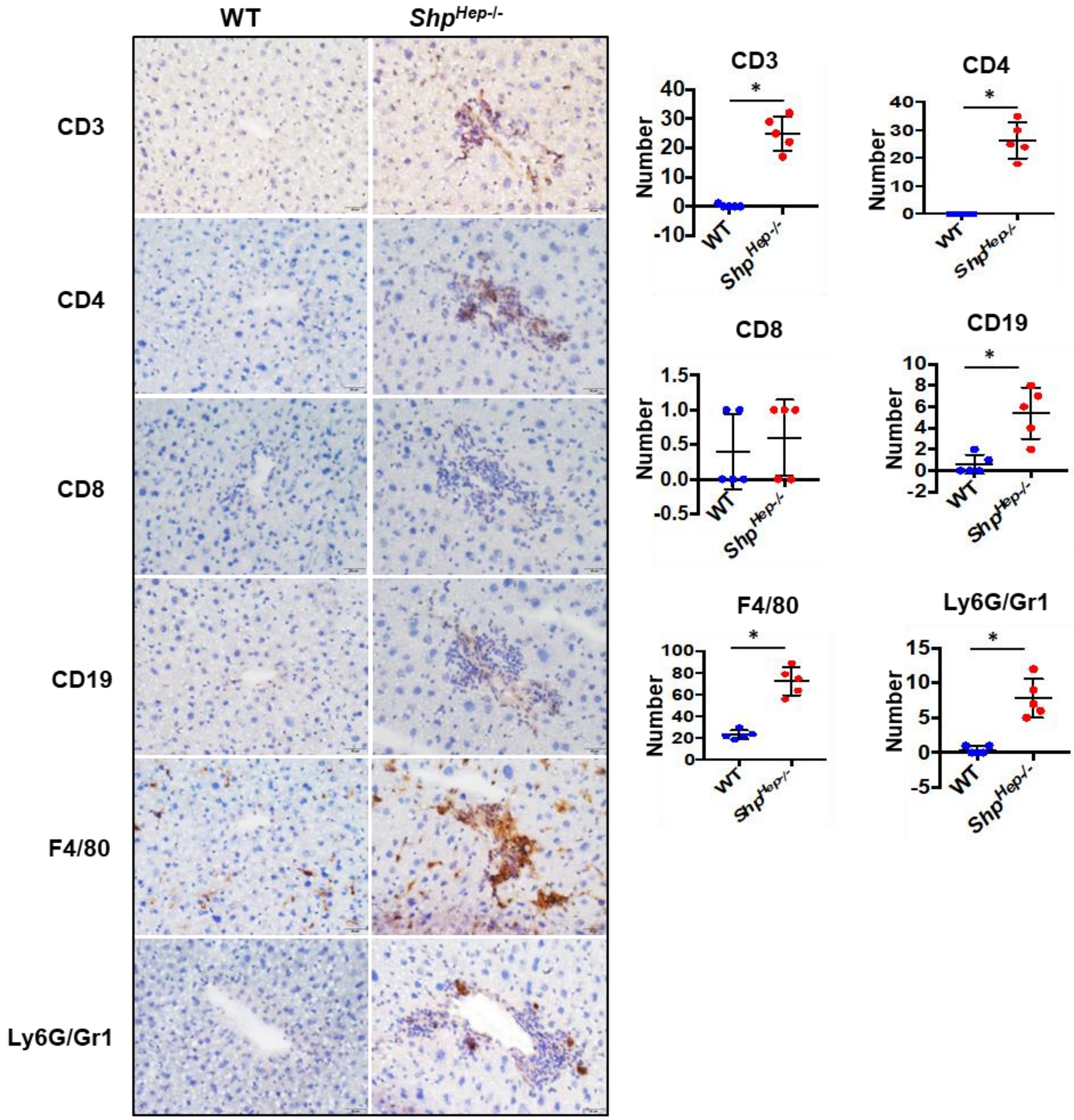

Figure 4-8: *Shp* deficiency in hepatocytes triggers proinflammatory immune cell infiltration.

Two-month-old male *Shp*$^{flox/flox}$ mice were injected with either AAV8-*Tbg*-Cre or control AAV8-*Tbg*-null to generate hepatocyte-specific *Shp* knockout (*Shp*$^{Hep-/-}$) and wild type (WT) controls, respectively. Samples were collected at 12 weeks post AAV8 injection. (Left) Representative images of immunohistochemistry staining of CD3 (T cells), CD4 (T-helper cells), CD8 (cytotoxic T cells), CD19 (B cells), F4/80 (macrophages), and Ly6G/Gr1 (neutrophils) in liver sections of WT and *Shp*$^{Hep-/-}$. Original magnification, 400X. (Right) Quantification of respective staining. Data are represented as mean ± SEM n=5 mice/group. *, p<0.05 *Shp*$^{Hep-/-}$ versus WT.

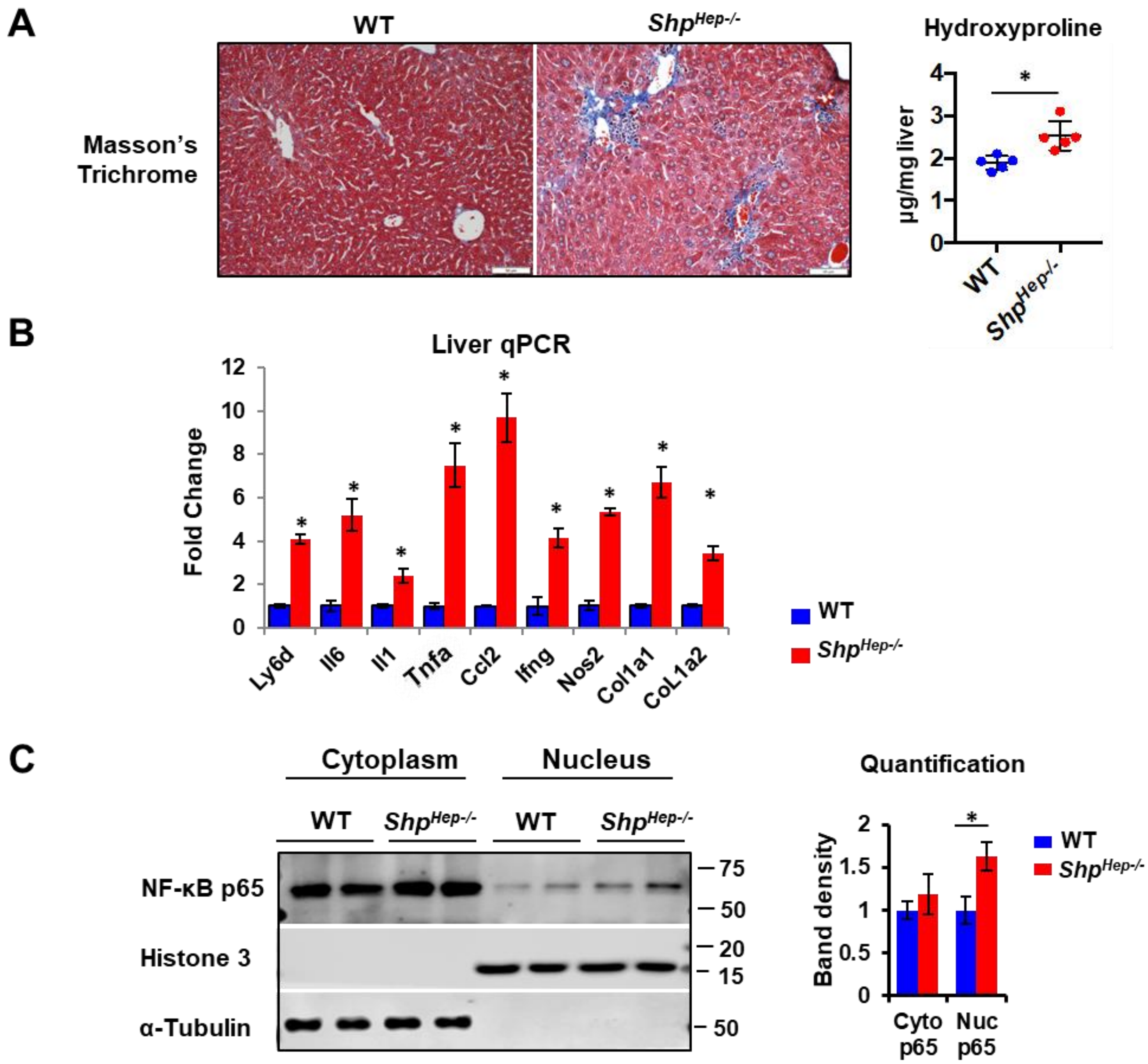

Figure 4-9: Hepatic *Shp* disruption induces liver fibrosis and NF-κB pathway activation.

Two-month-old male, *Shp*$^{flox/flox}$ mice were injected with either AAV8-*Tbg*-Cre or control AAV8-*Tbg*-null to generate hepatocyte-specific *Shp* knockout (*Shp*$^{Hep-/-}$) and wild type (WT) controls, respectively. Samples were collected at 12 weeks post AAV8 injection. **A:** (Left) Representative images of liver Masson's trichrome stain. Original magnification, 400X. (Right) Liver hydroxyproline content was determined by hydroxyproline assay. **B:** The relative mRNA levels of genes related to inflammation and fibrosis in liver tissues were determined by qPCR. **C:** (Left) Western blot analysis of cytoplasmic and nuclear proteins in the liver. (Right) Band intensities were calculated using Image J software and normalized by loading control. Band intensities in *Shp*$^{Hep-/-}$ mice relative to that in WT controls were plotted. Data are represented as mean ± SEM; n=5 mice/group. *, $p < 0.05$ *Shp*$^{Hep-/-}$ versus WT.

Hepatic *Shp* deletion reduces HFCF diet-induced liver steatosis but exacerbates liver inflammation and fibrosis

In Chapter 3, we described a mouse NASH model induced by a HFCF diet. We then superimposed hepatic *Shp* deletion by AAV8-*Tbg*-Cre on a HFCF feeding regimen (*Fig.* 4-10A). Both *Shp*$^{Hep-/-}$ mice and WT mice developed glucose intolerance after the HFCF diet for 12 weeks **(***Fig.* 4-10B). Meanwhile, body weight gain and fasting serum triglycerides were similar in *Shp*$^{Hep-/-}$ and WT mice after 12 weeks on the HFCF diet (*Fig.* 4-10C and 10D). However, a decrease in fasting serum cholesterol level was observed in the HFCF-fed *Shp*$^{Hep-/-}$ (*Fig.* 4-10D). In contrast, serum ALT was significantly increased in the HFCF-fed *Shp*$^{Hep-/-}$ mice compared to the HFCF-fed WT mice (*Fig.* 4-10D).

Both whole body *Shp*$^{-/-}$ mice and hepatocyte-specific *Shp*$^{-/-}$ mice are resistant to high fat diet-induced liver steatosis (188,189). Consistently, a decrease in liver weight and liver/body weight ratio was observed in the HFCF-fed *Shp*$^{Hep-/-}$ mice compared to the HFCF-fed WT controls (*Fig.* 4-11A). Additionally, both oil red O staining and liver lipid extraction quantification revealed reduced liver steatosis, triglyceride, and cholesterol in the HFCF-fed *Shp*$^{Hep-/-}$ mice (*Fig.* 4-11B and 11C), supporting the overall resistance to HFCF diet-induced liver steatosis triggered by hepatic *Shp* deletion.

Shp is a critical suppressor for bile acid synthesis through the direct inhibition of cytochrome P450 family 7 subfamily A member 1 (Cyp7a1) (190-192), a key rate-limiting enzyme that converts cholesterol to 7-alpha-hydroxycholesterol for bile acid synthesis (193,194). Knockout of *Shp* increases bile acid synthesis and decreases hepatic accumulation of cholesterol (123). Consistently, HFCF-fed *Shp*$^{Hep-/-}$ mice displayed increased bile acid pool size and fecal bile acid excretion rate (*Fig.* 4-11D) in parallel with the reduction of hepatic and serum cholesterol levels compared to HFCF-fed WT controls **(***Fig.* 4-10D and 4-11C). The data indicate that hepatic *Shp* deficiency increases cholesterol use for bile acid synthesis and decreases hepatic and serum cholesterol levels subsequently.

In contrast to the attenuation of liver steatosis, *Shp* deletion surprisingly exacerbated liver inflammation and fibrosis during NASH development, evidenced by increased macrophage infiltration as well as collagen formation in the HFCF-fed *Shp*$^{Hep-/-}$ liver compared to the HFCF-fed WT controls (*Fig.* 4-12A and 12B). At the mRNA level, an increase in expression of genes involved in inflammation (*Il6, Tnfa, Ccl2, Il1, Ifng, Nos2*) and fibrosis (*Col1a1, Col1a2, Col5a1, Mmp12, Mmp13*) was observed in the HFCF-fed *Shp*$^{Hep-/-}$ liver (*Fig.* 4-12C). Taken together, these data indicate that hepatocyte-specific *Shp* depletion in adult mice attenuates HFCF diet-induced steatosis but exacerbates liver inflammation and fibrosis.

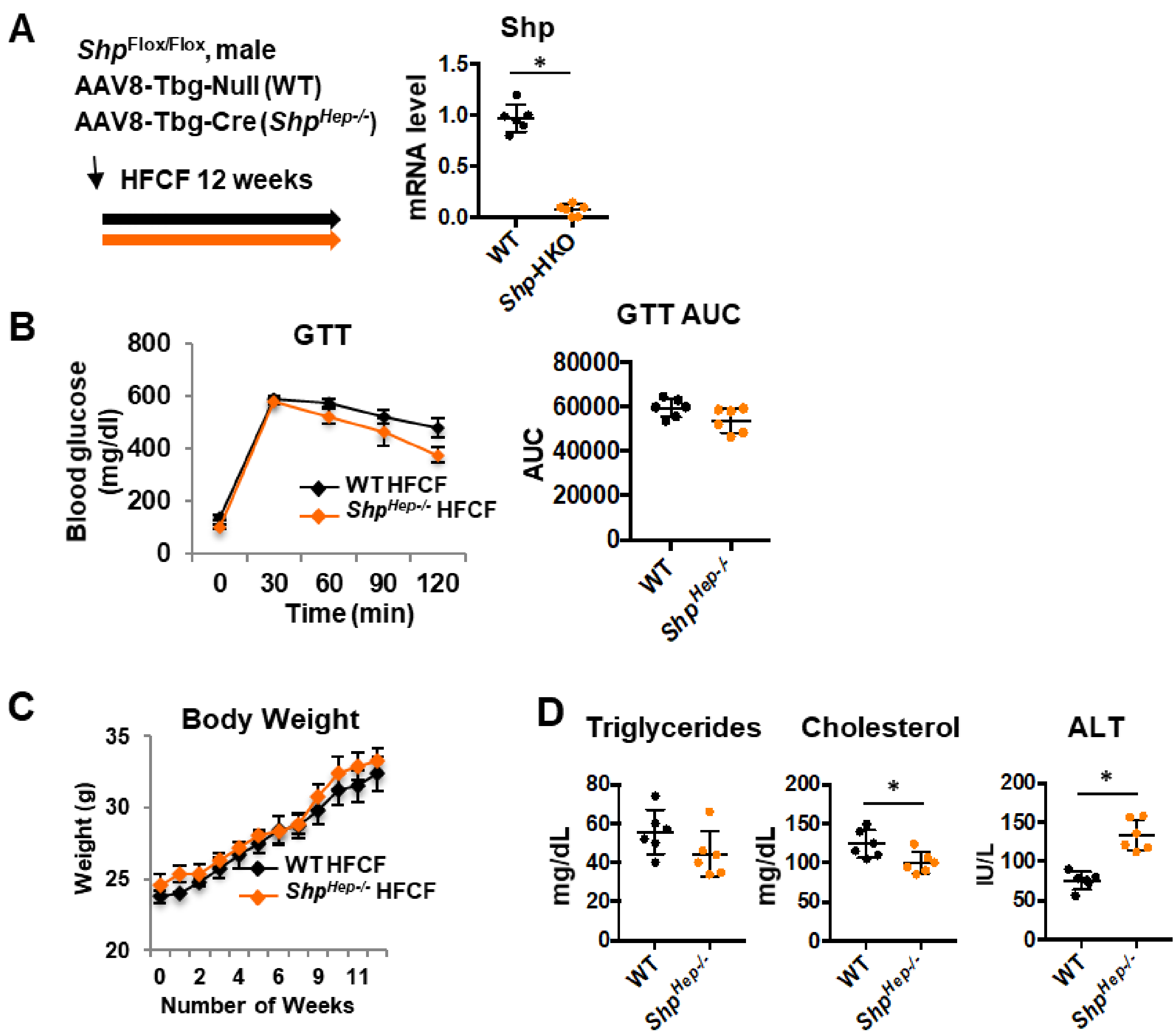

Figure 4-10: Body weight and blood lipid profile in HFCF-fed hepatocyte-specific Shp deficient mice and wild type controls

Two-month-old male *Shp*$^{flox/flox}$ mice were injected with either AAV8-*Tbg*-Cre or control AAV8-*Tbg*-null to generate hepatocyte-specific *Shp* knockout (*Shp*$^{Hep-/-}$) or wild type (WT) controls, respectively. Mice were then fed a HFCF diet for 12 weeks. **A:** (Left) schematic diagram showing experimental design. (Right) qPCR analysis of *Shp* mRNA levels in the liver. **B:** (Left) glucose tolerance tests (GTTs). (Right) Calculation of area under the curve (AUC) of GTT. **C:** Mouse body weight change over time. **D:** Serum levels of fasting triglycerides, cholesterol, glucose, and ALT. Data are represented as mean ± SEM. n=6 mice/group. *, *p*<0.05 *Shp*$^{Hep-/-}$ HFCF versus WT HFCF.

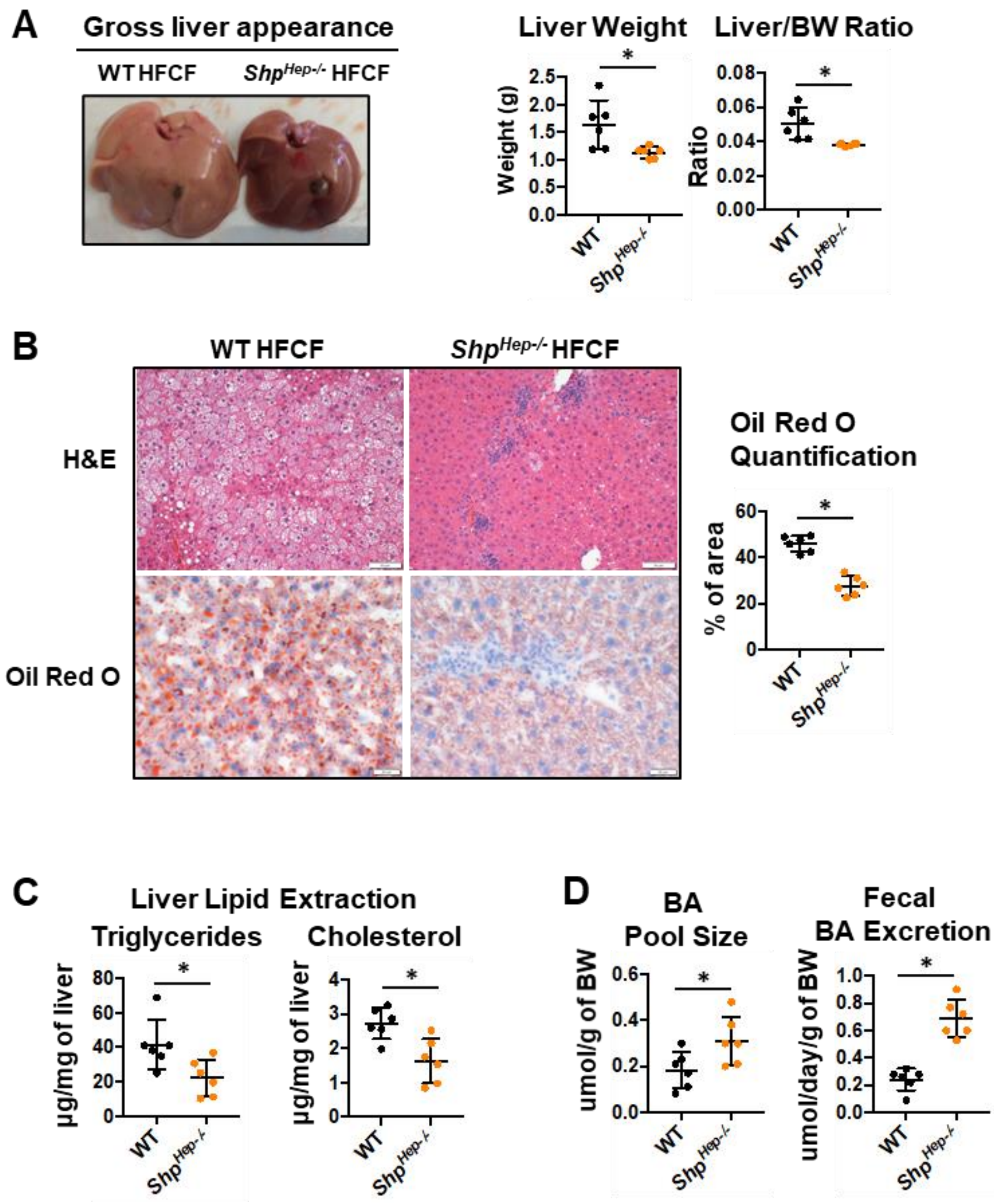

Figure 4-11: Hepatocyte-specific Shp deficiency attenuates HFCF-induced liver steatosis.

A: (Left) Gross liver appearance. (Right) liver weight and liver to body weight ratio. **B:** (Left) Representative images of liver sections stained with H&E and oil red O. Original magnification, 400X. (Right) Quantification of oil red O staining. **C:** Quantification of liver triglycerides and cholesterol contents. **D:** Quantification of bile acid (BA) pool size and BA in feces. Data are represented as mean ± SEM. n=6 mice/group. *, *p*<0.05 $Shp^{Hep-/-}$ HFCF versus WT HFCF.

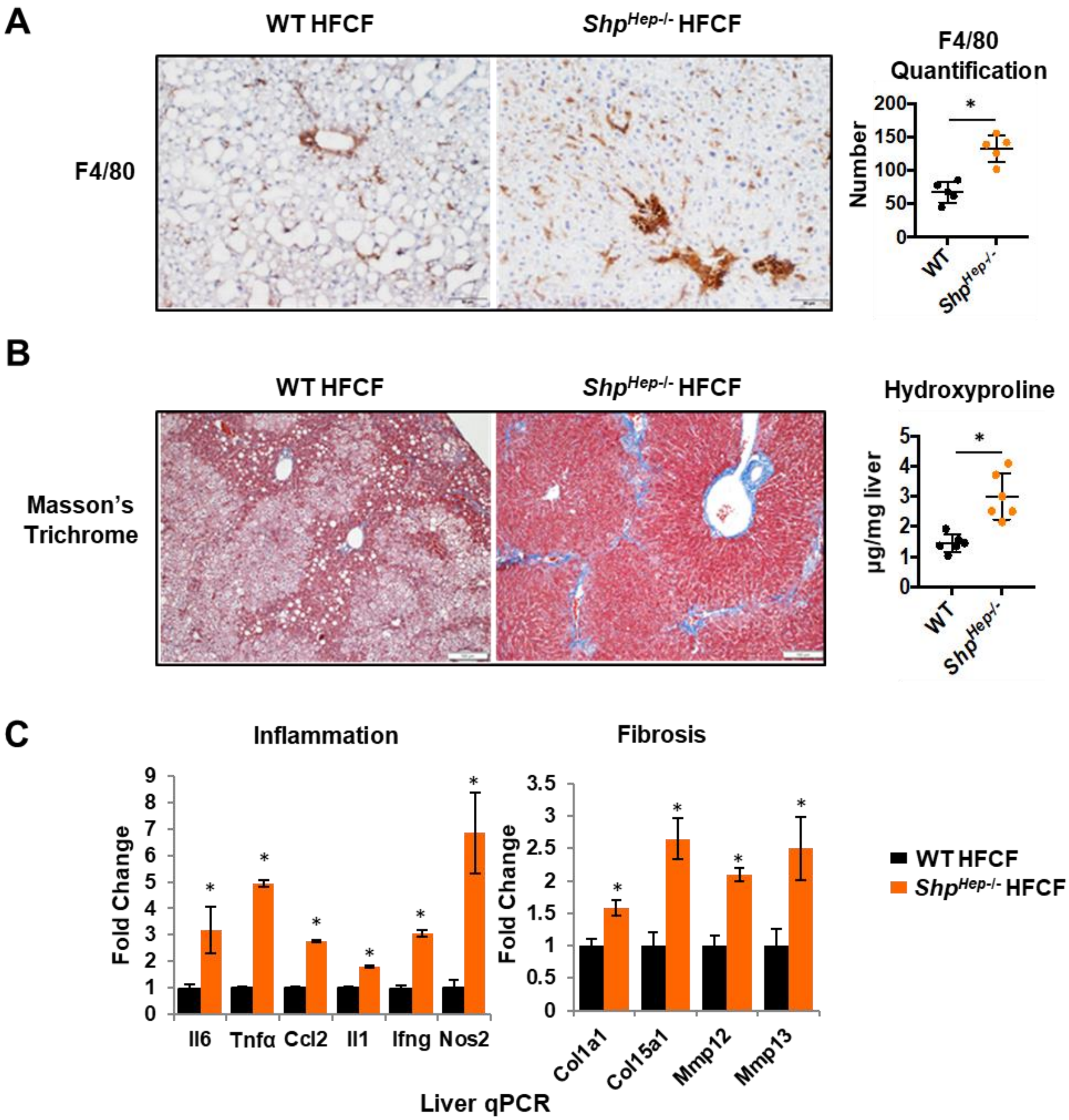

Figure 4-12: Disruption of *Shp* in hepatocytes exacerbates liver inflammation and fibrosis in HFCF-fed mice.

Liver samples of WT and *Shp*$^{Hep-/-}$ mice were collected at 12 weeks post HFCF diet feeding. **A:** (Left) Representative images of liver sections stained with F4/80. Original magnification, 400X. (Right) Quantification of F4/80 positive cells. **B:** (Left) Representative images of liver sections stained with Masson's trichrome. Original magnification, 400X. (Right) Liver hydroxyproline content was determined by hydroxyproline assay. **C:** Relative mRNA levels of genes related to inflammation and fibrosis in liver tissues were determined by qPCR. Data are represented as mean ± SEM. n=6 mice/group. *, $p<0.05$ *Shp*$^{Hep-/-}$ HFCF versus WT HFCF.

RNA sequencing reveals activation of inflammatory processes and pathways by hepatic *Shp* deletion

To pursue an unbiased investigation of mechanisms by which hepatocyte-specific *Shp* deletion induces the disconnection between steatosis and inflammation in NASH, we conducted RNA-seq analysis of liver obtained from WT and *Shp*$^{Hep-/-}$ mice after 12 weeks on the chow and HFCF diet (GEO number: GSE133566). The fragments per kilobase of exon model per million reads mapped (FPKM) was calculated to quantify the expression of genes in four groups, including WT Chow, *Shp*$^{Hep-/-}$ chow, WT HFCF, and *Shp*$^{Hep-/-}$ HFCF. The differentially expressed genes (DEG) were determined using fold change cutoff of 1.50 and false discovery rate (FDR) < 0.05.

The volcano plot analysis of gene expression revealed distinct differences between the WT groups and the *Shp*$^{Hep-/-}$ groups (*Fig.* 4-13A). Feeding mice the chow diet changed the expression of 1106 genes. After the HFCF treatment, *Shp*$^{Hep-/-}$ significantly altered the expression of 1,352 genes. Meanwhile, 794 genes were differentially expressed in the WT HFCF group compared to the WT chow group, and 324 genes were differentially expressed comparing the *Shp*$^{Hep-/-}$ HFCF group to the *Shp*$^{Hep-/-}$ chow group. The data indicate that *Shp* deletion induced significant changes to the hepatic transcriptome when compared to the WT groups, which was observed on both chow and HFCF feeding conditions,

A heat map with hierarchical clustering was used to determine the expression patterns of DEGs in livers of WT and *Shp*$^{Hep-/-}$ mice fed chow or HFCF diet. The idea is that genes with similar expression patterns may have similar functions or may be involved in the same biological process or cellular pathway; therefore, they are clustered into classes. In this study, we found *Shp*$^{Hep-/-}$ groups were distinctly separated from WT groups on both chow and HFCF conditions (*Fig.* 4-13B). The DEGs in four groups were clustered into two major types, one with higher expression in the WT groups but lower expression in the *Shp*$^{Hep-/-}$ groups, and the other with lower expression in the WT groups but higher expression in the *Shp*$^{Hep-/-}$ groups.

We next conducted Gene Ontology (GO) enrichment and KEGG (Kyoto Encyclopedia of Genes and Genomes) pathway analysis of DEGs using Enrichr. The DEGs in each group were assigned to GO terms describing biological processes, cellular components and molecular functions. The enriched GO terms and KEGG pathways with adjusted p-values < 0.05 were selected. As shown in *Figs.* 4-14a and 4-14b, the GO enrichment analysis indicated that a major effect of genes involved in proinflammatory and fibrogenic processes, such as extracellular matrix organization, cytokine, type I interferon, neutrophil degranulation, and cellular response to interferon gamma were induced by *Shp* deletion under chow diet.

Furthermore, KEGG pathway analysis of DEGs demonstrated that multiple pathways were differentially altered in $Shp^{Hep-/-}$ chow compared to WT chow, with cytokine-cytokine receptor interaction, hematopoietic cell lineage, chemokine signaling, T cell receptor signaling, and NF-κB signaling as the top five enriched KEGG pathways based on statistical significance (*Fig.* 4-14a, top). To further characterize HFCF diet-induced biological pathways and disease processes that are directly influenced by *Shp* deletion, we compared gene expression between the WT HFCF and the $Shp^{Hep-/-}$ HFCF groups (*Fig.* 4-14a, lower). As expected, biological processes and pathways involved in inflammation (type I interferon, cytokine, exocytosis, chemokine, T cell receptor, NF-κB signaling) were distinctly affected by hepatic disruption of *Shp*. In addition, HFCF-induced PPAR signaling, the key pathway involved in lipid metabolism, was largely altered by the absence of *Shp* (*Fig.* 4-14a, lower). The top five biological processes and pathways altered by HFCF diet feeding in WT and $Shp^{Hep-/-}$ mice are displayed in *Fig.* 4-14b, respectively. Among them are several common metabolic processes and pathways such as steroid and cholesterol biosynthesis, regulation of triglyceride, and PPAR signaling. Each of these processes is related to NASH development or progression.

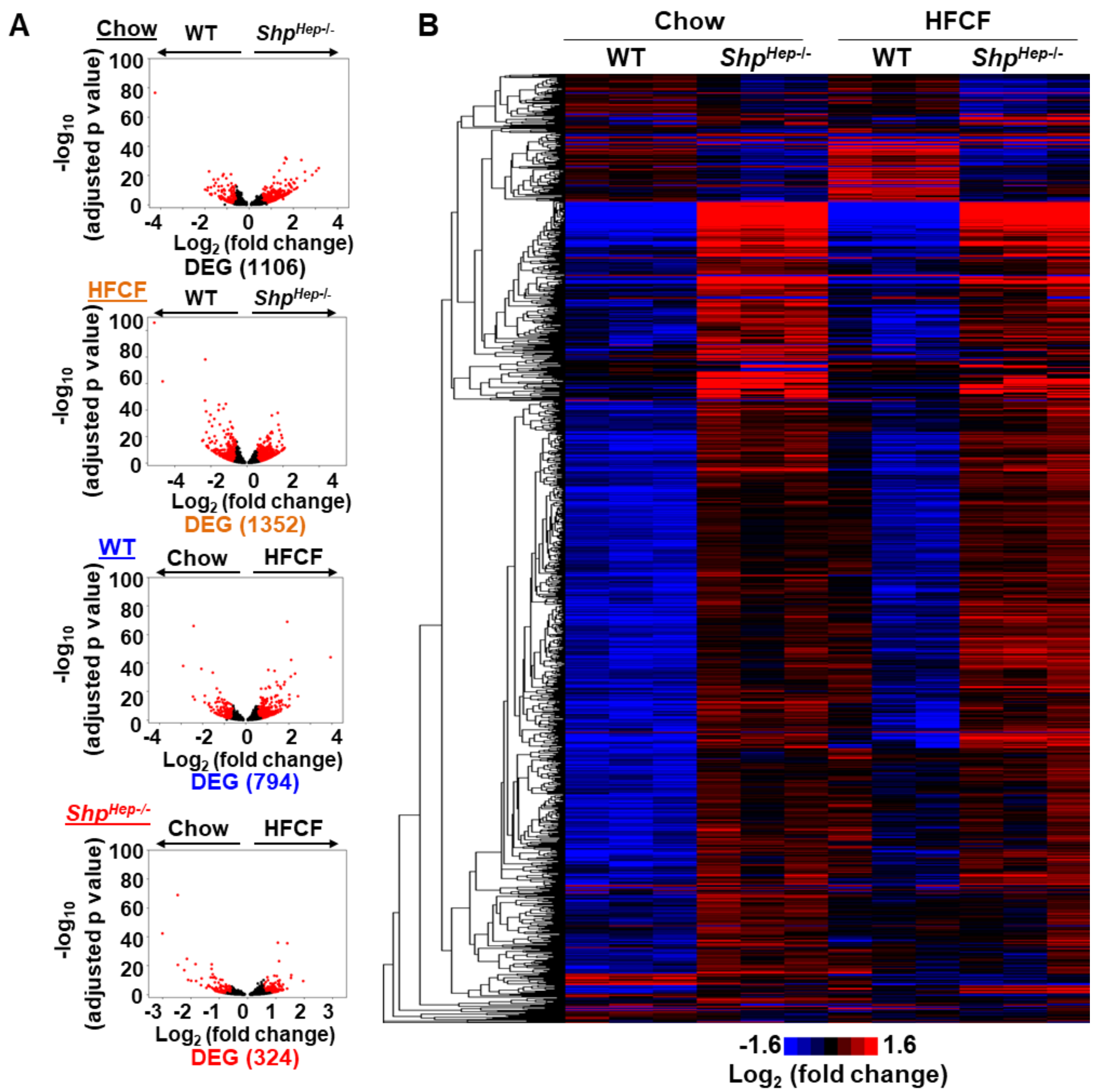

Figure 4-13: RNA-seq analysis of livers from WT and *Shp*$^{Hep-/-}$ mice after chow or HFCF diet.

Wild-type and *Shp*$^{Hep-/-}$ mice were generated by injection of AAV8-*Tbg*-null or AAV8-*Tbg*-Cre into two-month-old *Shp*$^{flox/flox}$ male mice, respectively. Liver samples were collected after 12 weeks of chow or HFCF diet. **A:** Volcano plot of differentially expressed genes (DEGs). The plots were constructed by plotting –$\log_{10}$ (adjusted p value) on the y-axis and $\log_2$ (fold change) on the x-axis. Red dots represent DEGs and grey blots represent gene expression without significant difference. **B:** Hierarchical clustering of DEGs in WT and *Shp*$^{Hep-/-}$ mice fed chow or HFCF diet. Red and blue colors indicate high and low gene expression, respectively.

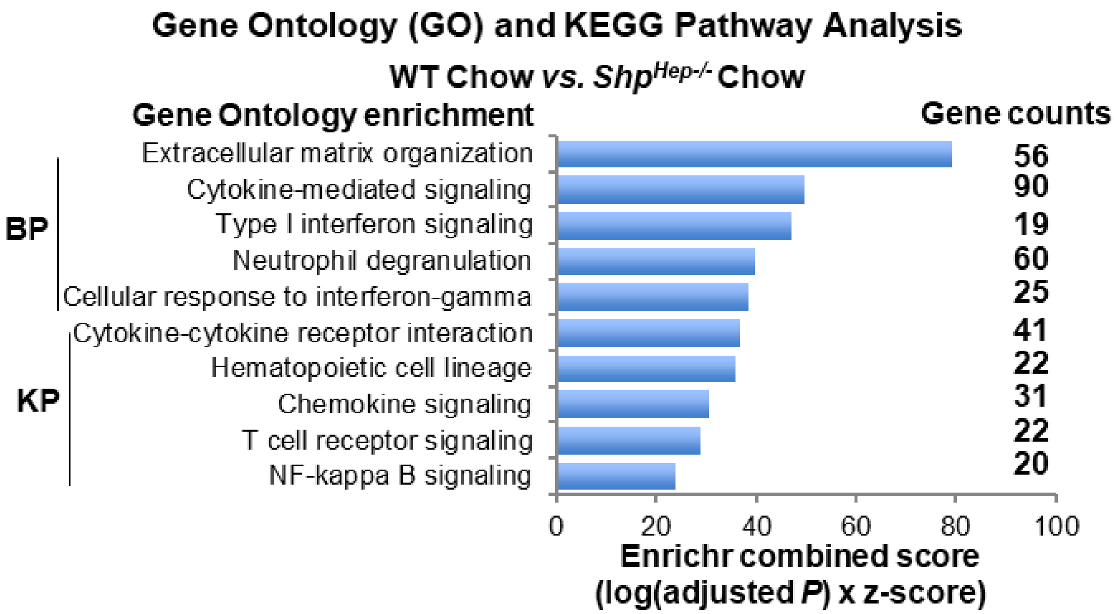

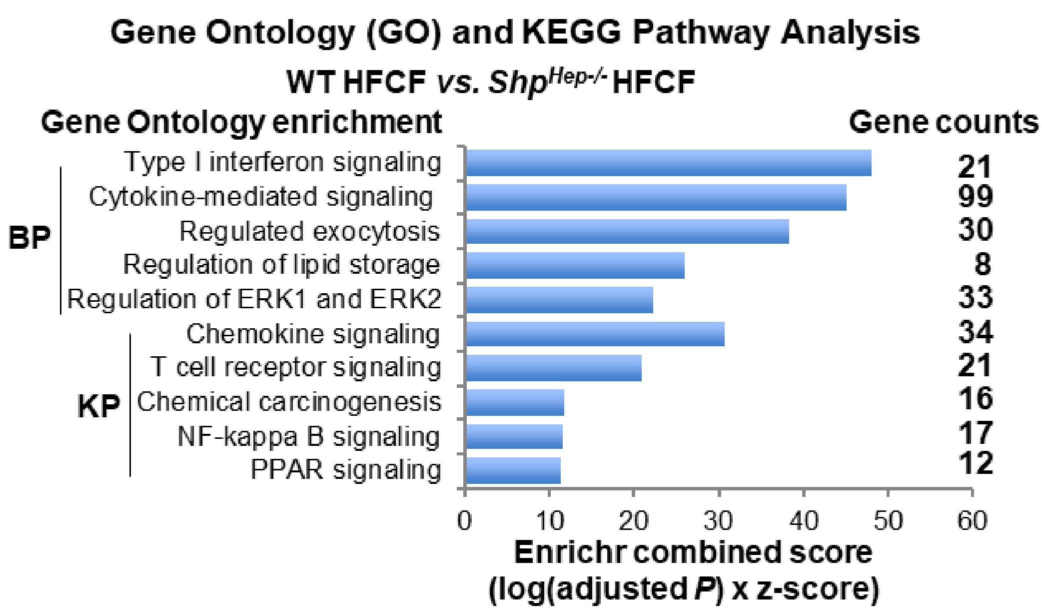

Figure 4-14a: Gene Ontology and pathway analysis of DEGs from WT and *Shp*$^{Hep\text{-}/\text{-}}$ mice after chow or HFCF diet.

Wild-type and *Shp*$^{Hep\text{-}/\text{-}}$ mice were generated by injection of AAV8-*Tbg*-null or AAV8-*Tbg*-Cre into two-month-old *Shp*$^{flox/flox}$ male mice, respectively. Liver samples were collected after 12 weeks on chow or HFCF diet. Gene Ontology and pathway analysis of DEGs were selected by Enrichr combined score using Enrichr. The x-axis represents Enrichr combined scores and the y-axis represents GO terms and KEGG pathways. **Top:** WT Chow vs *Shp*$^{Hep\text{-}/\text{-}}$ Chow. **Lower:** WT HFCF vs *Shp*$^{Hep\text{-}/\text{-}}$ HFCF. BP, Biological Process; KP, KEGG pathway.

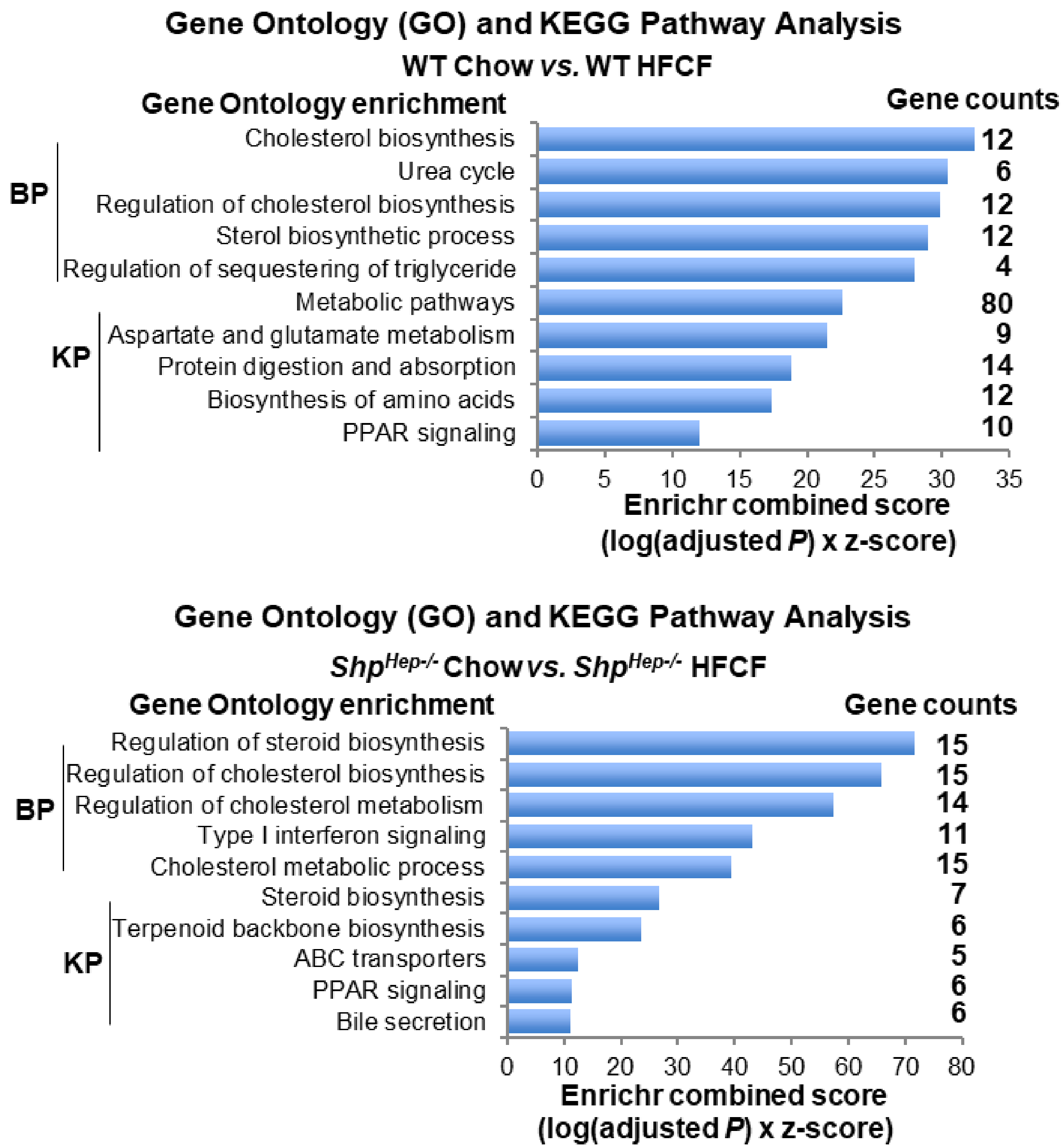

Figure 4-14b: Gene Ontology and pathway analysis of DEGs from WT and *Shp*$^{Hep\text{-}/\text{-}}$ mice after chow or HFCF diet.

Wild-type and *Shp*$^{Hep\text{-}/\text{-}}$ mice were generated by injection of AAV8-*Tbg*-null or AAV8-*Tbg*-Cre into two-month-old *Shp*$^{flox/flox}$ male mice, respectively. Liver samples were collected after 12 weeks on chow or HFCF diet. Gene Ontology and pathway analysis of DEGs were selected by Enrichr combined score using Enrichr. The x-axis represents Enrichr combined scores and the y-axis represents GO terms and KEGG pathways. **Top:** WT Chow vs WT HFCF. **Lower:** *Shp*$^{Hep\text{-}/\text{-}}$ Chow vs *Shp*$^{Hep\text{-}/\text{-}}$ HFCF. BP, Biological Process; KP, KEGG pathway.

Activation of NF-κB signaling in HFCF-fed *Shp*$^{Hep-/-}$ mice

Among genes involved in NF-κB signaling most significantly induced by loss of *Shp* were phosphatidylinositol-4-phosphate 3-kinase catalytic subunit type 2 gamma (*Pik3c2g*), fibroblast growth factor receptor 1 (*Fgfr1*), NF-κB inhibitor delta (*NFκBid*), lymphocyte protein tyrosine kinase (*Lck*), TNF alpha induced protein 3 (*Tnfaip3*), interleukin 33 (*Il33*), toll-like receptor 8 (*Tlr8*), TNF receptor superfamily member 11a (*Tnfrsf11a*), interleukin 1 beta (*Il1b*), phosphoinositide-3-kinase regulatory subunit 5 (*Pik3r5*), phosphatidylinositol-4,5-bisphosphate 3-kinase catalytic subunit gamma (*Pik3cg*), toll-like receptor 8 (*Tlr2*), phospholipase C gamma 2 (*Plcg2*), interleukin 1 receptor antagonist (*Il1rn*), caspase recruitment domain family member 11 (*Card11*), phosphatidylinositol-4,5-bisphosphate 3-kinase catalytic subunit delta (*Pik3cd*), *Cd40*, *Tnfa*, toll-like receptor 3 (*Tlr3*), mitogen-activated protein kinase kinase kinase 8 (*Map3k8*), and epidermal growth factor receptor (*Egfr*) (*Fig.* 4-15A). In contrast, neurotrophic receptor tyrosine kinase 1 (*Ntrk1*) was dramatically downregulated by the hepatic disruption of *Shp* (*Fig.* 4-15A).

To clarify the causative role of NF-κB signaling in *Shp* deletion-induced inflammation, we isolated hepatocytes from *Shp*$^{flox/flox}$ mice and deleted *Shp* (*Shp*$^{-/-}$) using adenovirus expression Cre recombinase. The infection of adenovirus vector control was used to generate wildtype (WT) hepatocytes. We chose Ad-Cre for *in vitro Shp*$^{flox/flox}$ hepatocyte infection is based on our experience that Ad-Cre is more potent compared to AAV8-Cre to knockdown *Shp in vitro*. The real-time PCR confirmed the successful knockdown of *Shp* in hepatocytes (*Fig.* 4-15B Left). As expected, loss of *Shp* in hepatocytes significantly increased the expression of *Tnfa*, an established NF-κB target (*Fig.* 4-15B Right). Most importantly, the induction of *Tnfa* in the *Shp*$^{-/-}$ hepatocytes was markedly inhibited by the co-treatment of a specific NF-κB inhibitor BAY 11-7082 (*Fig.* 4-15B Right). The above data indicate that NF-κB activation plays a critical role in *Shp* deletion-induced initiation of inflammation.

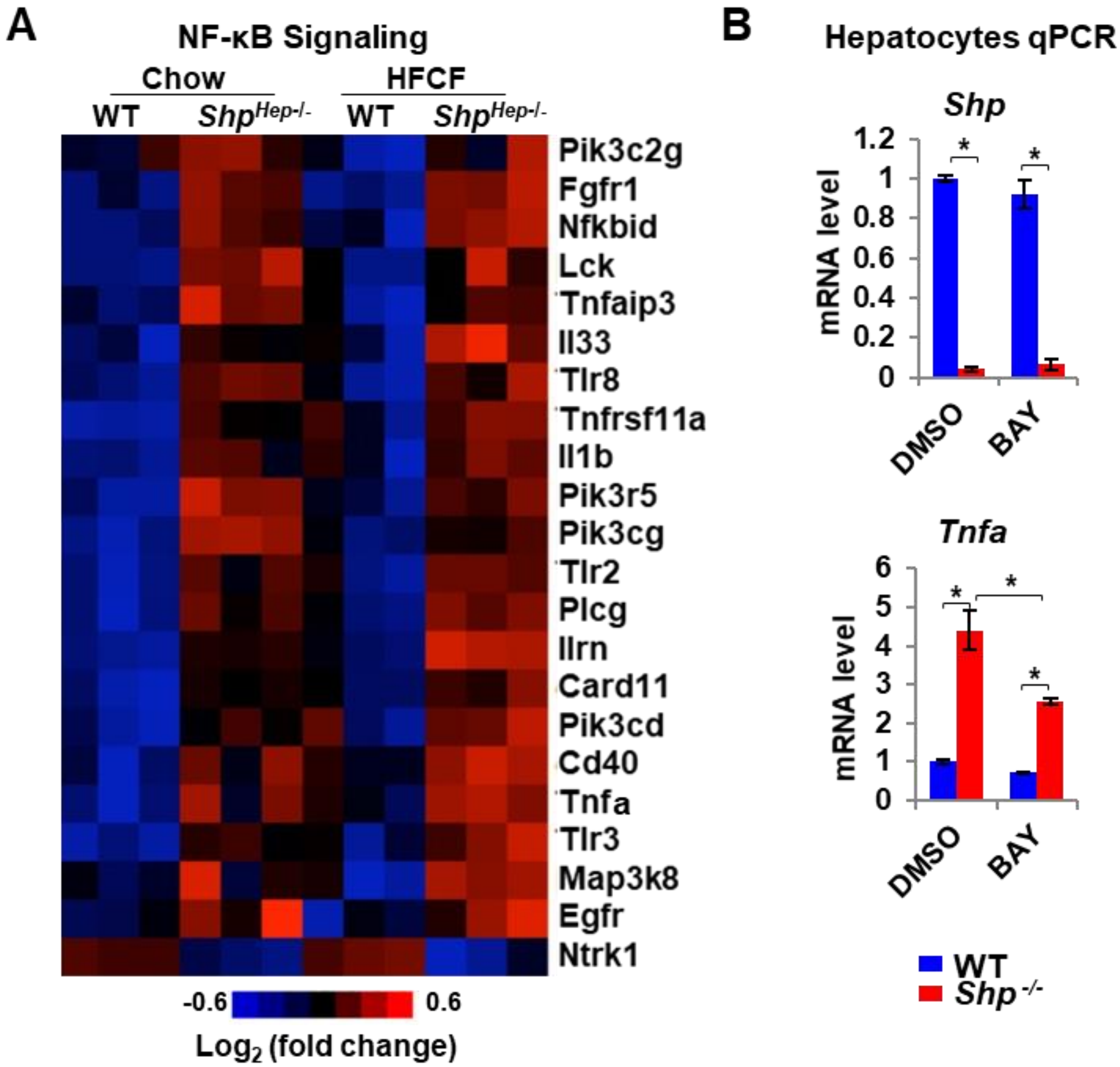

Figure 4-15: Hepatocyte-specific *Shp* deletion activates NF-kB signaling.

A: Heat map depicts genes differently regulated by NF-κB in wild type and *Shp*$^{Hep-/-}$ mice fed chow or a HFCF diet. **B**: qPCR analysis of *Shp* (Left) and *Tnfa* (Right) in wild-type or *Shp* deficient mouse primary hepatocytes treated with DMSO or 5μM of NF-κB inhibitor BAY 11-7082 for 6 hours. Data are represented as mean ± SEM. *, *p*<0.05 for *Shp*$^{-/-}$ versus WT.

***In vitro* deletion of *Shp* increases CCL2 production leading to proinflammatory M1 macrophage polarization**

To understand how hepatocyte SHP regulates liver inflammation, we isolated hepatocytes from *Shp*$^{flox/flox}$ mice and deleted *Shp* using adenovirus expressing Cre recombinase (Ad-Cre). We wanted to assess the effect of hepatocyte conditional medium (CM) on macrophage M1 or M2 polarization and migration (*Fig.* 4-16A). The knockdown of *Shp* mRNA in hepatocytes was confirmed by real-time PCR (*Fig.* 4-16B). Consistently, loss of SHP in hepatocytes dramatically induced p65 nuclear translocation (*Fig.* 4-16B), suggesting an activation of p65 in *Shp* deficient hepatocytes. A significant increase in *Ccl2* mRNA and protein was subsequently detected in *Shp* deficient hepatocytes and conditional medium (*Fig.* 4-16C), indicating that loss of *Shp* in hepatocytes induces the secretion of CCL2.

Next, we treated Raw264.7 cells, a mouse macrophage cell line, with hepatocyte CM for 6h and assessed their polarization status. The CM from *Shp* deficient hepatocytes increased the expression of M1 markers such as *Nos2*, *IL1*, *IL6*, and *Tnfa*, and repressed the expression of M2 marker arginase 1 (*Arg1*) in Raw264.7 cells (*Fig.* 4-17a), suggesting that the CM from *Shp* deficient hepatocytes stimulated proinflammatory M1 polarization. In addition, the CM from *Shp* deficient hepatocytes stimulated a significant increase in migration of Raw264.7 cell (*Fig.* 4-17b), which is mimicked by the exposure to control CM supplemented with 40 ng/ml of recombinant mouse CCL2 protein or inhibited by blocking CCL2 action by a CCL2 antibody (500 ng/ml) (*Fig.* 4-17b). Thus, our findings suggest a novel mechanism in which loss of *Shp* in hepatocytes stimulates macrophage proinflammatory M1 polarization that is mediated through CCL2 secretion from hepatocytes.

To understand how *Shp* represses *Ccl2* expression, we analyzed the proximal promoter of mouse *Ccl2*, and identified two IκB sites (*Fig.* 4-18A). We cloned a 3kb mouse *Ccl2* proximal promoter fragment into a luciferase reporter and examined SHP's effect on *Ccl2* promoter activity in AML12 cells. Overexpression of p65 increased *Ccl2* promoter activity that was inhibited by co-expression of SHP (*Fig.* 4-18A). EIA-like inhibitor of differentiation 1 (EID1) is a common co-repressor that interacts with SHP (195). Co-expression of SHP and EID1 synergistically diminished p65-induced activation of the *Ccl2* promoter (*Fig.* 4-18A). Additionally, we overexpressed Flag-SHP and HA-p65 in AML12 cells and the immune precipitation results showed the protein-protein interactions between SHP and p65 (*Fig.* 4-18B). Taken together, the results suggest that SHP interacts with p65 and inhibits p65-induced *Ccl2* transcription.

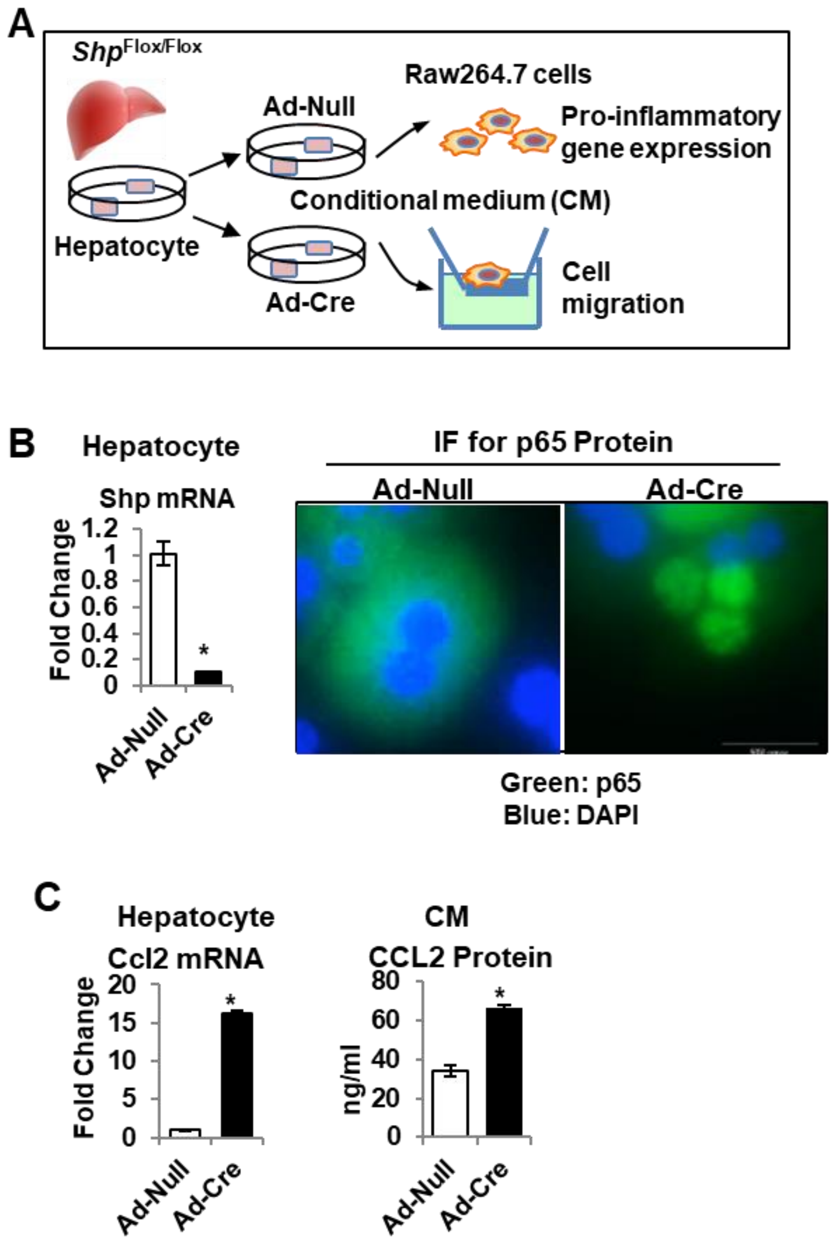

Figure 4-16: *Shp* deficiency causes p65 nuclear translocation and CCL2 release from mouse primary hepatocytes.

A: Schematic diagram shows experimental design. Primary hepatocytes were isolated from *Shp*$^{flox/flox}$ mice and infected with adenovirus expressing Cre recombinase (Ad-Cre) or vector control (Ad-Null). Conditional medium (CM) were collected at 24 h post infection and used for RAW cell treatment. **B: (**Left) Relative *Shp* mRNA levels were determined by qPCR. (Right) Representative images of immunofluorescence staining of p65 in hepatocytes. **C: (**Left) Relative *Ccl2* mRNA levels in hepatocytes were determined by qPCR. (Right) CCL2 protein level in CM of hepatocyte culture was measured by ELISA. Data are represented as mean ± SEM for triplicate per group; *$p < 0.05$.

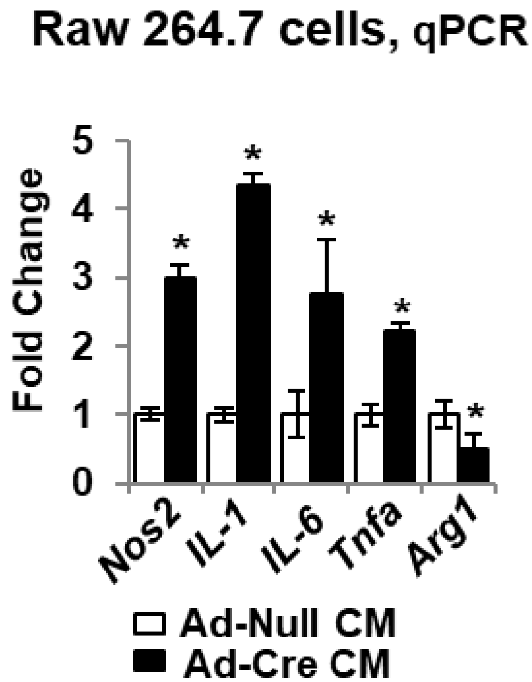

Figure 4-17a: CCL2 production from *Shp* deficient hepatocytes increases macrophage proinflammatory response

RAW264.7 cells were incubated with the conditional medium (CM) from hepatocyte culture for 6 h and the relative expression of genes involved in inflammation was determined by qPCR. Data are represented as mean ± SEM for triplicate per group; $*p < 0.05$

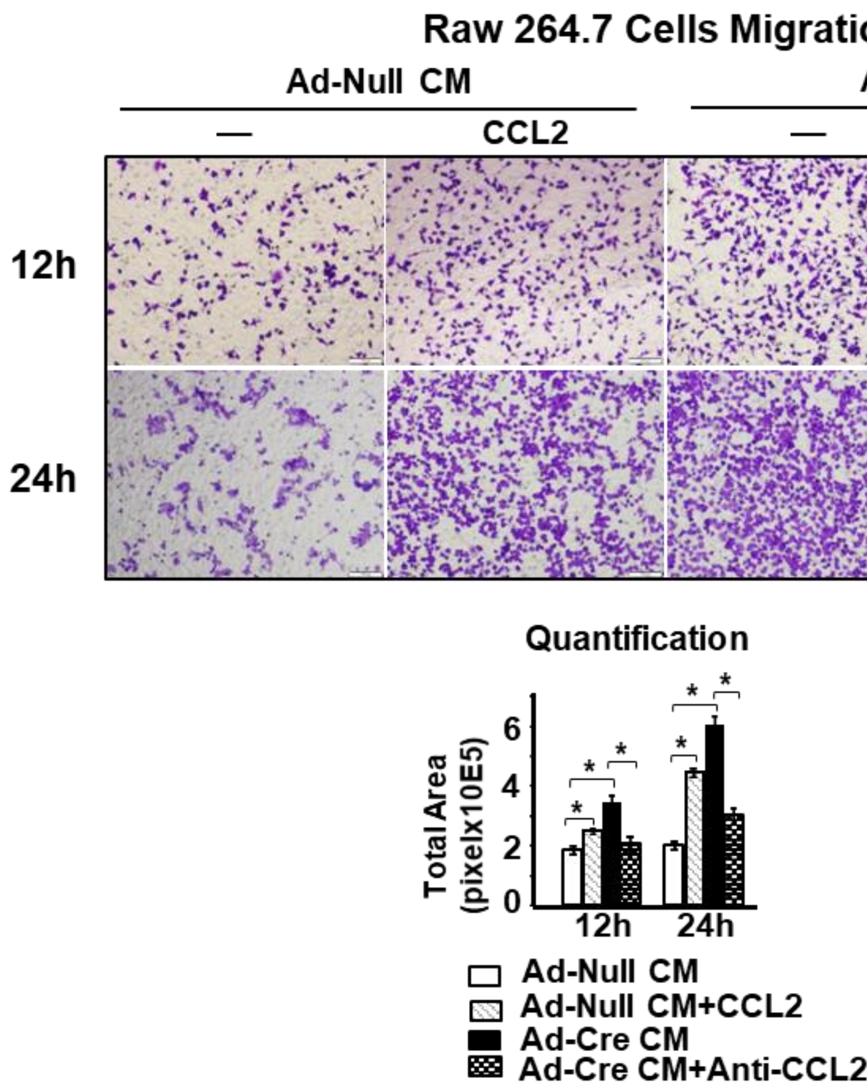

Figure 4-17b: CCL2 production from *Shp* deficient hepatocytes increases macrophage migration

(Top) Representative images of RAW cell migration. RAW cells were incubated with hepatocytes CM in the presence or absence of recombinant mouse CCL2 (40 ng/ml) or anti-mouse CCL2 antibody (500 ng/ml). Migration was assessed after incubation for 12-hrs and 24-hrs, respectively. (Bottom) Quantification of cell migration was determined by measuring pixel density of crystal violet-stained cells using Image J software and is represented as mean ± SEM for 5 fields per sample. *$p < 0.05$.

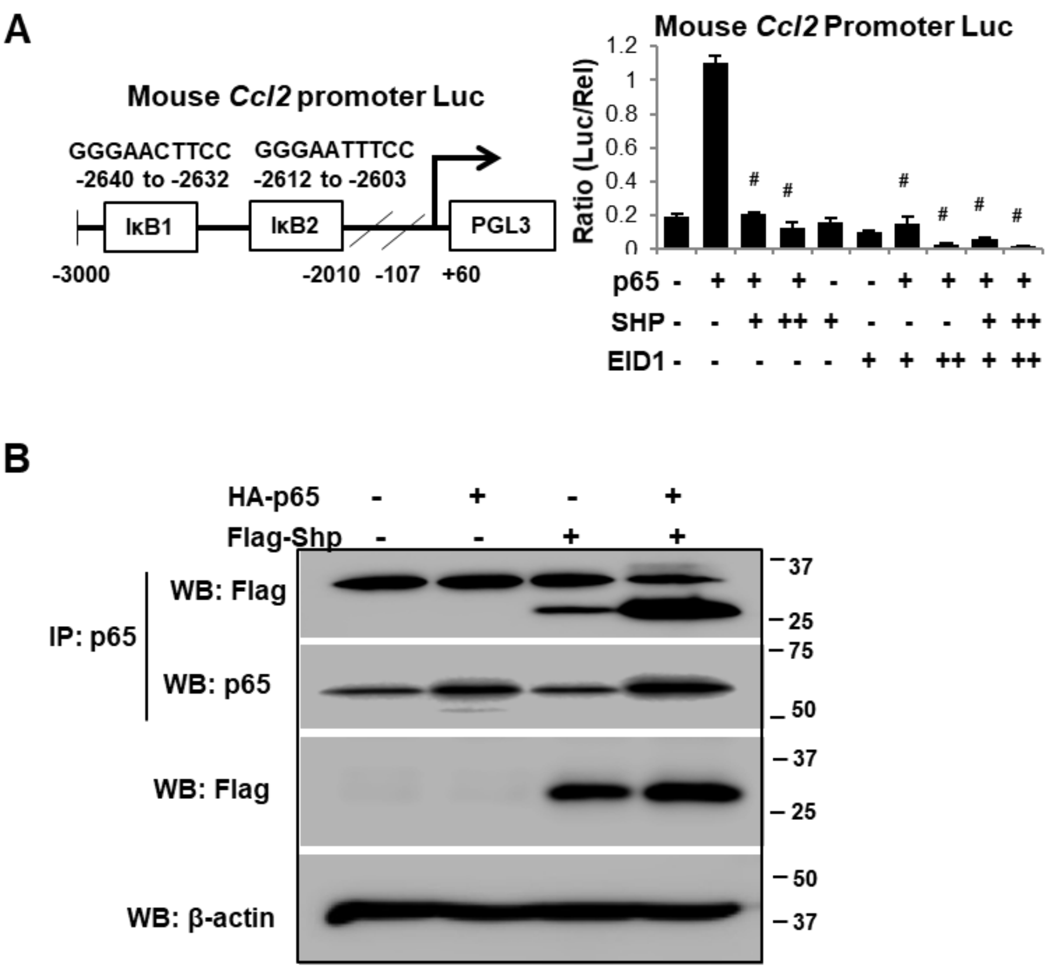

Figure 4-18: SHP interacts with p65 and reduces p65-induced transcription of *Ccl2*.

A: (Left) Diagram shows the location of two IκB sites on the mouse *Ccl2* promoter reporter (*Ccl2*-Luc). (Right) AML12 cells were transfected with *Ccl2*-Luc with or without various expression plasmids. Luciferase activities were determined at 24 h post transfection. Data are calculated as the ratio of firefly luminescence divided by *Renilla* luminescence and represented as mean ± SEM for triplicate per group. $*p < 0.05$. **B:** AML12 cells were overexpressed with Flag-*Shp* or HA-p65 and harvested at 24 h post-plasmid transfection. Immunoprecipitation (IP) followed by Western blotting (WB) was employed to detect protein-protein interactions between Flag-SHP and HA-p65.

Suppression of *Pparg* signaling in HFCF-fed *Shp*$^{Hep-/-}$ mice

Ppar family members (*Ppara, Pparb/δ, and Pparg*) control the transcription of genes in lipid and carbohydrate metabolism. As shown in *Fig.* 4-19A and 19B, major genes involved in lipid metabolism, including sterol regulatory element binding transcription factor 1 (*Srebp1c*), stearoyl-Coenzyme A desaturase 1 (*Scd1*), *Ppara*, *Pparg*, and some *Pparg* targets such as fatty acid binding protein 1 (*Fabp1*), cell death-inducing DFFA-like effector c (*Cidec*), and *Cd36* were significantly induced in the livers of HFCF-fed WT mice, but decreased in the absence of hepatic *Shp*. The above data support the overall resistance of *Shp*$^{Hep-/-}$ mice to HFCF-induced liver steatosis.

SHP interacts with and alters the function of many nuclear receptors in lipid metabolism, including *Pparg, Ppara, Lrh1, Hnf4a, Fxr, Lxra,* and *Lxrb* (123). Strikingly, hepatic *Shp* disruption specifically decreased *Pparg* expression in both chow and HFCF conditions (*Fig.* 4-19C). In contrast, hepatic *Shp* deletion abolished HFCF-induced upregulation of *Ppara* but did not impact *Ppara* expression in the chow-fed mice. Moreover, neither HFCF diet nor *Shp* deletion altered hepatic expression of *Lrh1, Hnf4a, Fxr, Lxra,* and *Lxrb* (*Fig.* 4-19C). *Pparg* is expressed at a low level in normal liver but markedly increased in fatty liver (196). *Pparg* overexpression upregulates various lipogenic genes which promotes liver steatosis, and hepatocyte *Pparg* deletion ameliorates liver steatosis (151,197). Similarly, here we show that hepatic *Shp* deletion results in *Pparg* downregulation that is correlated with the decrease of liver steatosis in HFCF-fed mice.

We next examined *Pparg* and its target gene *Cd36* in WT and *Shp*$^{-/-}$ hepatocytes. As shown in *Fig.* 4-20A, the mRNA levels of *Pparg* and *Cd36* were significantly decreased in *Shp*$^{-/-}$ hepatocytes compared to WT hepatocytes. We then treated WT and *Shp*$^{-/-}$ hepatocytes with oleic acid (0.5 mM) for 24 hours to assess steatosis. Strikingly, though oleic acid dramatically increased steatosis in WT hepatocytes, lipid accumulation was largely inhibited in *Shp*$^{-/-}$ hepatocytes (*Fig.* 4-20B). Interestingly, overexpressing *Pparg* by adenovirus greatly increased lipid contents in oleic acid-treated WT hepatocytes, and this response was maintained in *Shp*$^{-/-}$ hepatocytes overexpressed with *Pparg* (*Fig.* 4-20B). The overexpression of *Pparg* in WT and *Shp*$^{-/-}$ hepatocytes was confirmed by real-time PCR shown in *Fig.* 4-20C. Taken together, the above data clearly indicate that *Pparg* plays a critical role in *Shp* deficiency-induced resistance to steatosis.

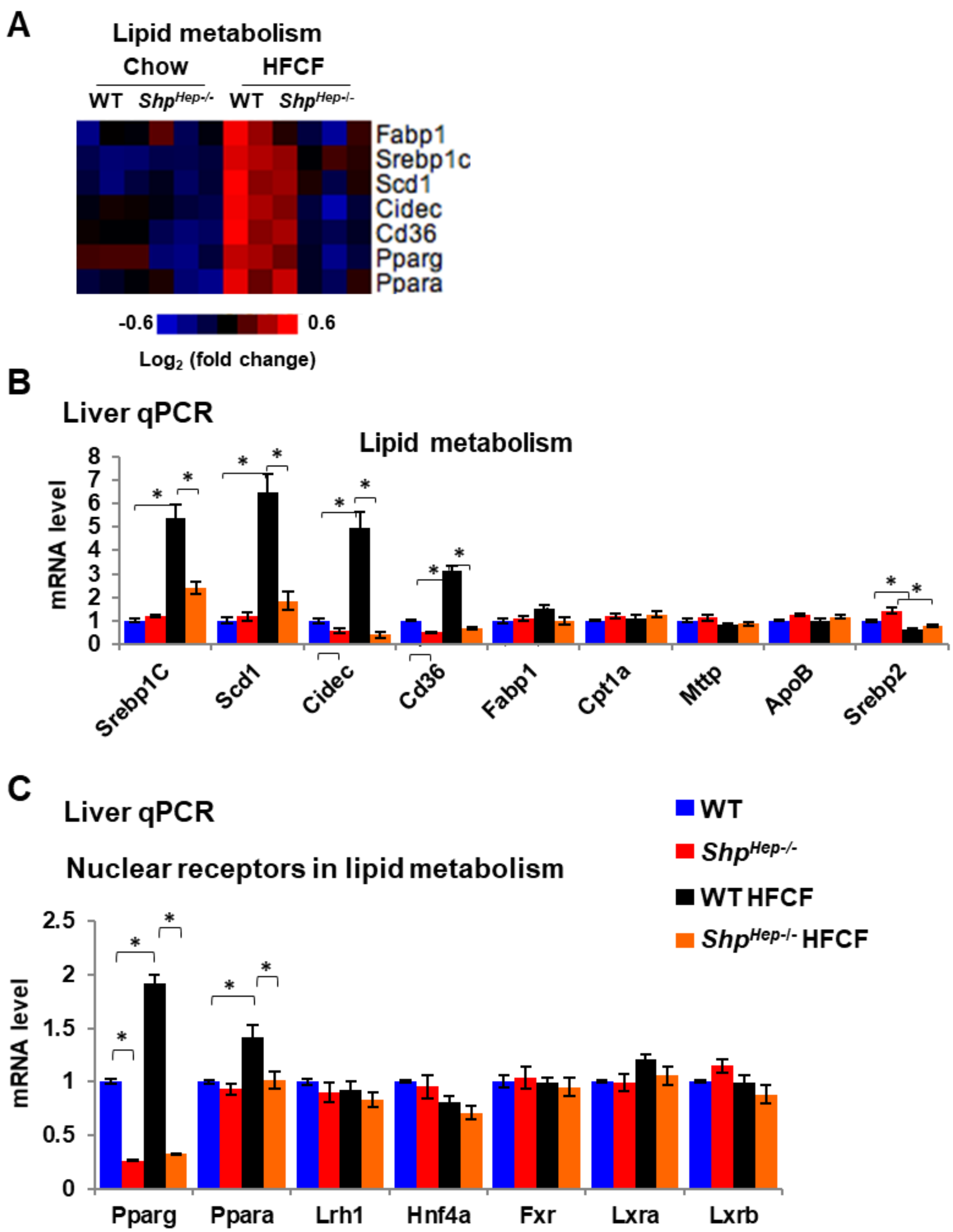

Figure 4-19: Hepatocyte-specific *Shp* deletion results in repression of PPARg signaling in HFCF-fed mice.

A: Heat map depicts genes differently regulated by Ppars in wild type and *Shp*$^{Hep-/-}$ mice fed chow or a HFCF diet. **B-C:** The relative gene expression in liver tissues was determined by qPCR. Data in B and C are represented as mean ± SEM. n=6 mice/group. *, *p*<0.05.

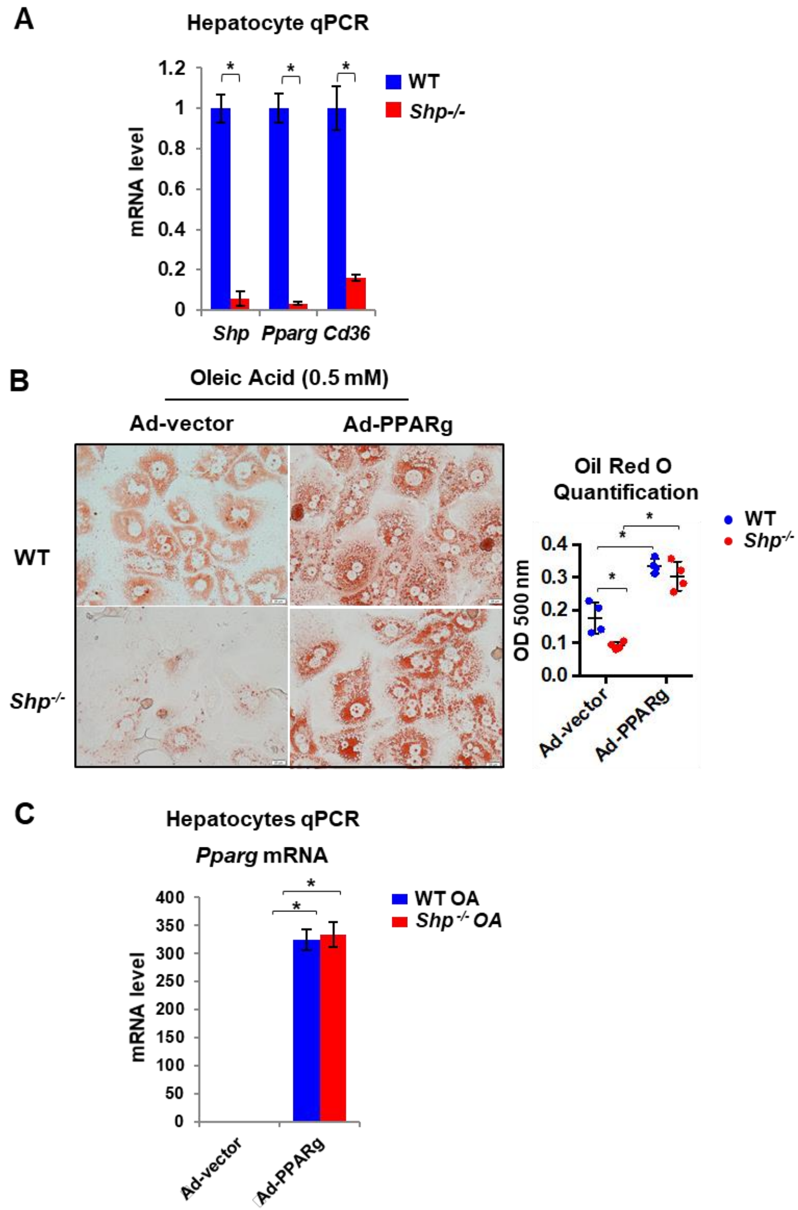

Figure 4-20: Overexpressing *Pparg* increases lipid content in oleic acid-treated hepatocytes.

A: Primary hepatocytes from *Shp*$^{flox/flox}$ mice were infected with adenovirus expressing Cre recombinase or vector control to generate *Shp*$^{-/-}$ and WT hepatocytes respectively. The relative expression of *Shp*, *Pparg*, and *Cd36* was determined by qPCR. **B:** Wild-type or *Shp*$^{-/-}$ hepatocytes overexpressing PPARg (Ad-PPARg) or vector (Ad-vector) by adenovirus were treated with 0.5 mM of oleic acid for 24 hours. (Left) Representative images of cells stained with oil red O. Original magnification, 400X. (Right) Oil red O was dissolved and quantified by the measurement of absorbance at $OD_{500\ nm}$. **C:** Relative expression of *Pparg* was determined by qPCR**.** Data is represented as mean ± SEM. *p < 0.05

Ablation of hepatic *Shp* after the development of steatosis enhances liver inflammation and fibrosis in HFCF-fed mice without affecting liver steatosis

Since we noticed that 4 weeks of HFCF feeding does not alter hepatic *Shp* expression (*Fig.* 4-2A), we began to investigate the role of *Shp* specifically in the transition of steatosis to NASH. $Shp^{flox/flox}$ mice were fed a HFCF diet for 4 weeks followed by *Shp* deletion in hepatocytes by injection of AAV8-*Tbg*-Cre and remained on the HFCF diet for an additional 8 weeks (*Fig.* 4-21A). The knockdown of hepatic *Shp* was confirmed by real-time PCR (*Fig.* 4-21A). No differences in body weight, serum fasting triglycerides, cholesterol, and glucose were noticed between $Shp^{Hep-/-}$ and WT controls (*Fig.* 4-21B and 21C). However, serum ALT was consistently increased in $Shp^{Hep-/-}$ mice (*Fig.* 4-21C). Interestingly, hepatic *Shp* disruption after steatosis development did not alter liver weight and liver/body weight ratio compared to WT controls (*Fig.* 4-21D).

Both H&E staining and lipid extraction revealed a similar extent of liver steatosis developed in $Shp^{Hep-/-}$ mice and WT controls in this steatosis-to-NASH transition model (*Fig.* 4-22A). However, the livers of $Shp^{Hep-/-}$ mice displayed marked increase in F4/80$^+$ macrophages and collagen accumulation (*Fig.* 4-22B and 22C). Consistently, the expression of genes involved in inflammation (*Ccl2*, *Tnfa*, *Nos2*) and fibrosis (*Col1a1*, *Col1a2*) were significantly increased in the livers of HFCF-fed $Shp^{Hep-/-}$ mice (*Fig.* 4-23). Next, we examined hepatic *Pparg* expression. Surprisingly, although there were similar levels of liver steatosis in HFCF-fed $Shp^{Hep-/-}$ mice and WT controls, the expression of hepatic *Pparg* was consistently lower in $Shp^{Hep-/-}$ mice (*Fig.* 4-23), supporting a strong regulation of *Shp* on *Pparg's* expression that is independent of liver steatosis. Meanwhile, our data also indicated that after steatosis development, disruption of hepatic *Shp* decreases *Pparg* expression, but did not alter liver steatosis; instead, other PPARg-independent mechanisms may contribute significantly to liver steatosis. Taken together, the above data support *Shp* as a key player that prevents NASH progression by inhibiting both liver inflammation and fibrosis.

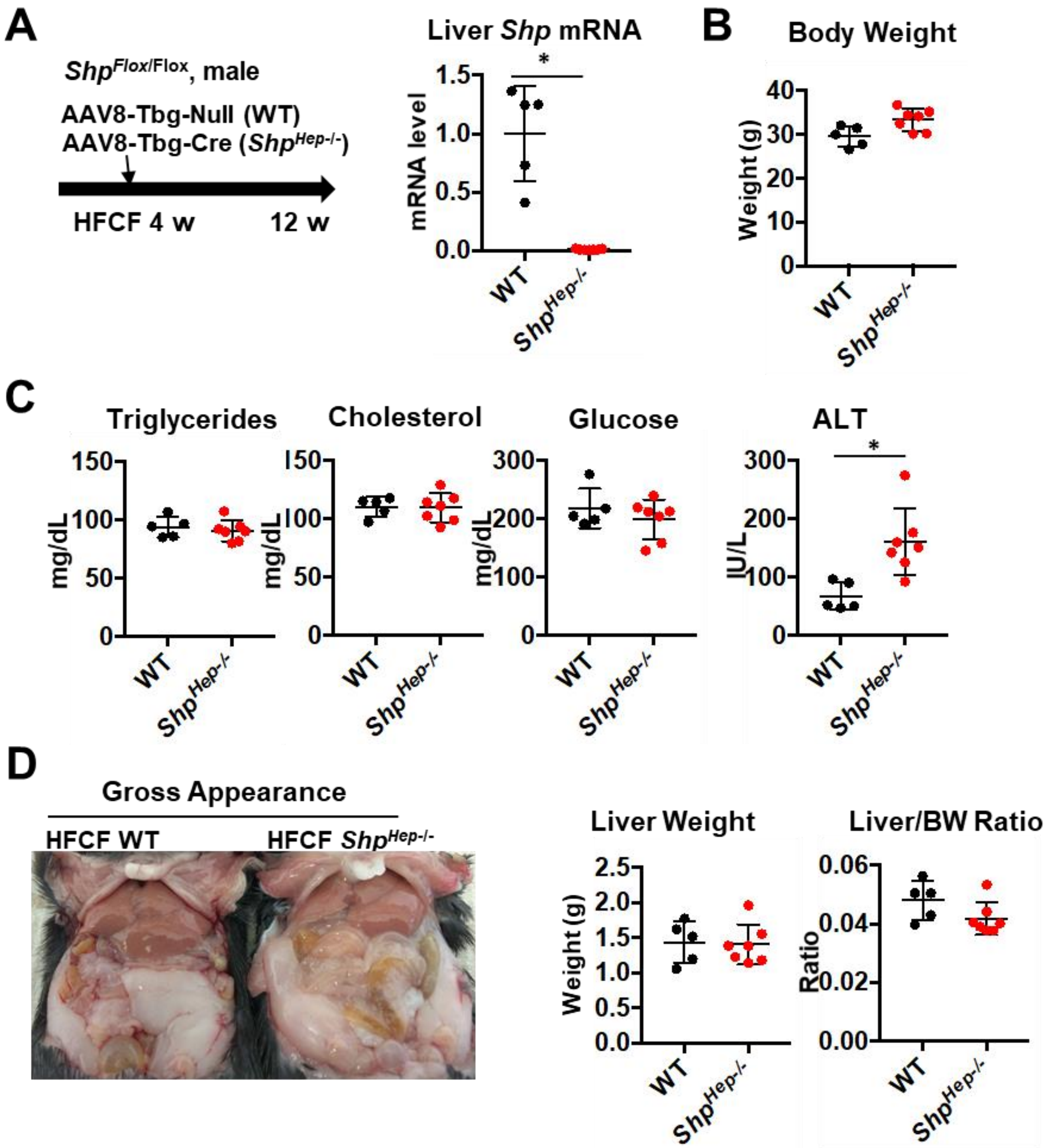

Figure 4-21: Disruption of hepatic *Shp* after steatosis development exacerbates liver injury.

Two-month-old male *Shp*$^{flox/flox}$ mice were fed a HFCF diet for 4 weeks to develop liver steatosis followed by tail vein injection of AAV8-*Tbg*-Cre or AAV8-*Tbg*-null control. Mice remained on the HFCF diet for an additional 8 weeks. **A:** (Left) schematic diagram shows experimental design. (Right) qPCR analysis of *Shp* mRNA levels in the liver. **B:** Body weight. **C:** Serum levels of fasting triglycerides, cholesterol, glucose, and ALT. **D:** (Left) Gross liver appearance. (Right) Liver weight and liver to body weight ratio. Data are represented as mean ± SEM. n=7 mice/group. *, $p<0.05$ HFCF *Shp*$^{Hep-/-}$ versus HFCF WT.

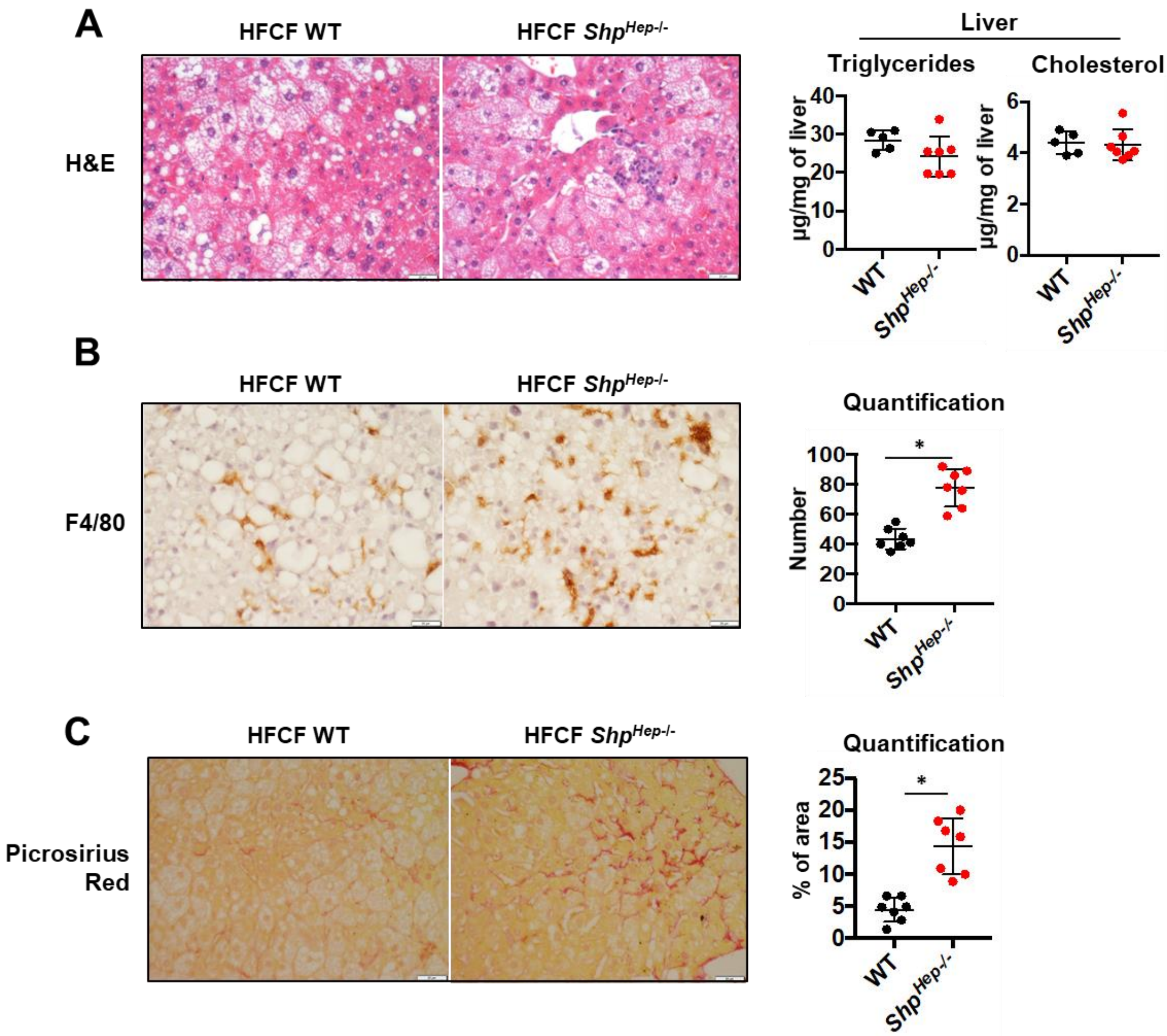

Figure 4-22: Hepatic *Shp* deletion after steatosis development exacerbates liver inflammation and fibrosis.

A: (Left) Representative images of liver H&E staining. (Right) Quantification of liver triglycerides and cholesterol content. **B:** Liver F4/80 staining and quantification. **C:** Liver Picrosirius Red staining and quantification. Original magnification, 400X. Data are represented as mean ± SEM. n=7 mice/group. *, $p<0.05$ HFCF *Shp*$^{Hep-/-}$ versus HFCF WT.

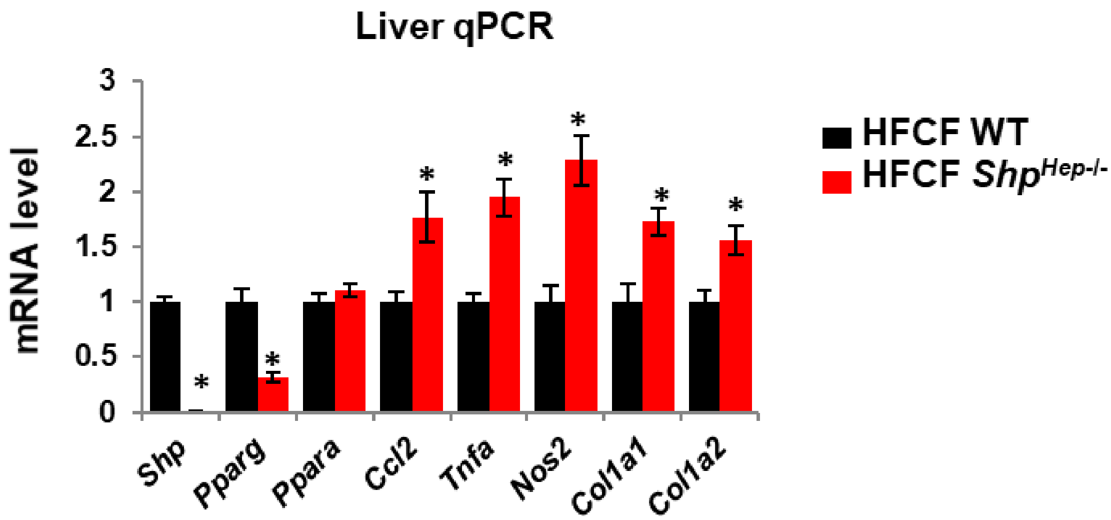

Figure 4-23: Hepatic *Shp* deletion after steatosis development increases the expression of genes involved in inflammation and fibrosis.

Hepatic expression of genes involved in lipid metabolism (*Pparg, Ppara*), inflammation (*Ccl2, Tnfa, Nos2*), and fibrosis (*Col1a1, Col1a2*) were determined by qPCR. Data are represented as mean ± SEM. n=7 mice/group. *, p<0.05 HFCF *Shp*$^{Hep-/-}$ versus HFCF WT.

Increasing hepatocyte SHP levels in steatotic livers does not alter liver steatosis

We next asked whether overexpressing SHP in hepatocytes could prevent the progression of NAFL to NASH. For this purpose, we used an AAV8 vector in which Flag-tagged SHP was driven by a hepatocyte-specific *Tbg* promoter (AAV8-*Tbg*-FlagSHP). C57Bl/6J mice were placed on the HFCF diet for 1 month to induce liver steatosis, followed by tail vein administration of AAV8-*Tbg*-FlagSHP or control vector AAV8-*Tbg*-GFP. The mice remained on the HFCF diet for an additional 3 months (*Fig.* 4-24A). SHP overexpression in liver was confirmed by qPCR (*Fig.* 4-24A). The body weight, liver weight, liver to body weight ratio, and serum levels of fasting cholesterol and triglycerides were similar in SHP and GFP mice (*Fig.* 4-24B and C). However, serum ALT and AST, two markers of liver injury, were significantly decreased in SHP-overexpressing mice compared to GFP control mice (*Fig.* 4-24C).

To investigate whether overexpressing SHP could affect glucose metabolism, we performed a glucose tolerance test. The result showed that SHP-overexpressing mice displayed no differences in glucose tolerance when compared to GFP control mice (*Fig.* 4-25). Further quantification of areas under the curves (AUC) of GTT showed no statistical differences in GFP and SHP-overexpression groups (*Fig.* 4-25).

We next examined liver histology. Liver steatosis and inflammation were apparent in the livers of GFP mice fed a HFCF diet (*Fig.* 4-26A). As expected, IHC staining of Flag-tagged SHP protein revealed SHP overexpression in hepatocytes (*Fig.* 4-26A). A similar level of lipid accumulation was observed in the livers of HFCF-fed SHP-overexpression mice compared to GFP controls (*Fig.* 4-26A); however, there was less inflammation in SHP-overexpressing liver (*Fig.* 4-26A). Consistently, liver triglycerides and cholesterol levels were similar in GFP and SHP mice fed the HFCF diet (*Fig.* 4-26B). Taken together, our results suggest that overexpressing SHP in steatotic livers improves liver injury without altering liver steatosis and glucose tolerance.

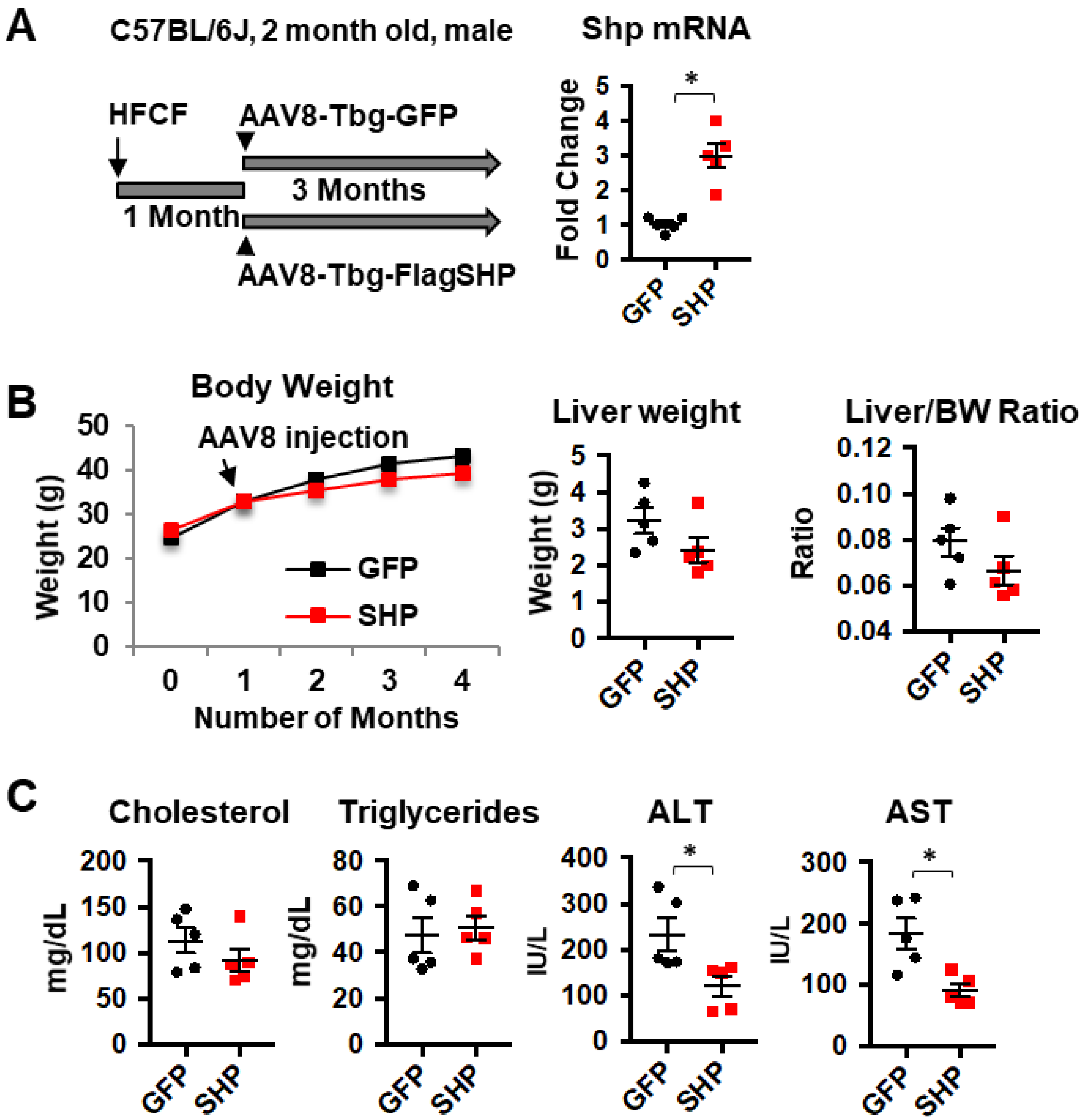

Figure 4-24: Hepatic SHP overexpression reduces liver injury in HFCF-fed mice.

Two-month-old male C57BL6J mice were fed a HFCF diet for 1 month to develop liver steatosis, followed by tail vein administration of AAV8-*Tbg*-FlagSHP or control vector AAV8-*Tbg*-GFP. Mice were continued on HFCF diet for 3 months. **A:** (Left) Schematic diagram shows experimental design. (Right) qPCR of *Shp* mRNA levels in the liver. **B:** (Left) Body weight change over time. (Middle) Liver weight. (Right) Liver weight to body weight ratio. **C:** Serum levels of fasting cholesterol, triglycerides, ALT and AST. Data are represented as mean ± SEM for 5 mice per group; *$p < 0.05$ SHP *vs.* GFP.

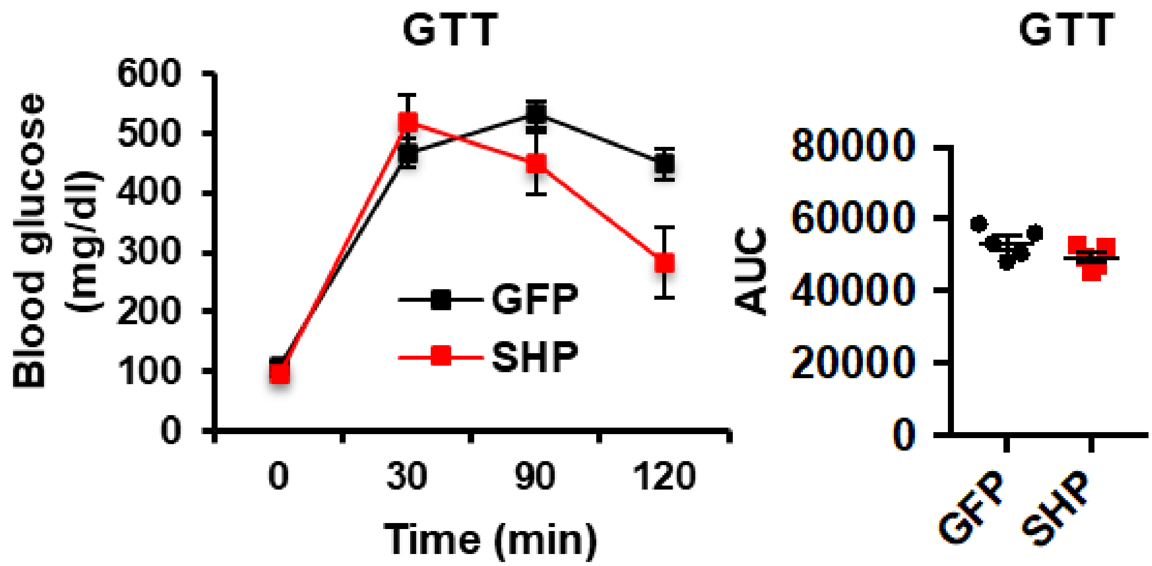

Figure 4-25: Hepatic SHP overexpression does not alter glucose tolerance of HFCF-fed mice.

Two-month-old male C57BL/6J mice were fed a HFCF diet for 1 month to develop liver steatosis followed by tail vein administration of AAV8-*Tbg*-FlagSHP or control vector AAV8-*Tbg*-GFP. The mice were remained on the HFCF diet for an additional 3 months. Mice were fasted overnight before glucose tolerance test (GTT). (Left) Blood glucose was measured at 0, 30, 90, or 120 minutes after glucose injection. (Right) The calculation of area under the curve (AUC) of GTT is represented as mean ± SEM for 5 mice per group.

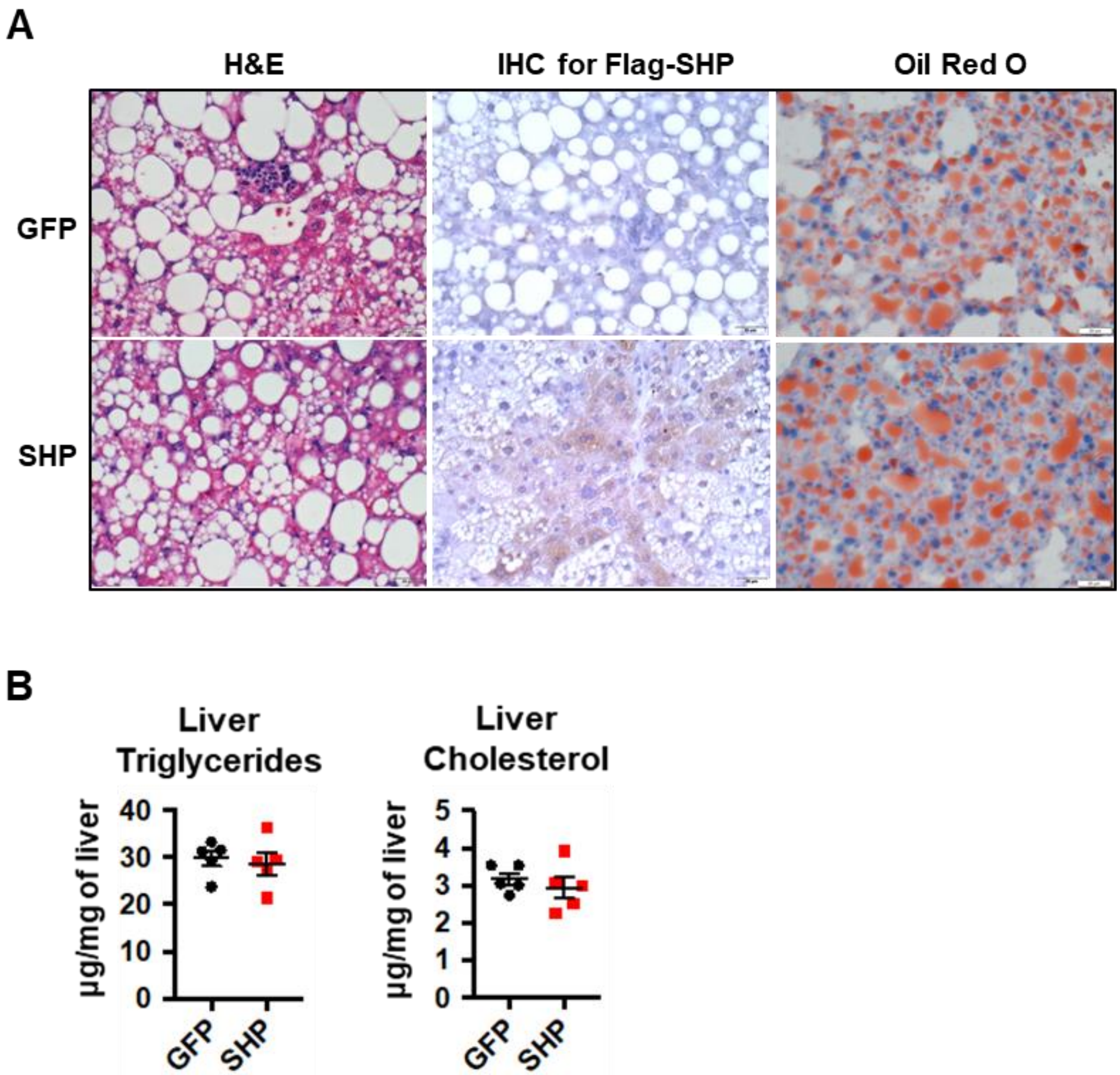

Figure 4-26: Increasing hepatocyte SHP level in steatotic liver does not affect steatosis.

A: Representative images of liver sections of hematoxylin-eosin (H&E) staining, immunohistochemistry staining of Flag-SHP, and oil red O staining. Original magnification, 400X; Scale Bar = 20 micrometers. **B:** Liver triglycerides and cholesterol contents. Data in B are represented as mean ± SEM for 5 mice per group.

Hepatocyte SHP overexpression prevents NAFL progression to NASH by attenuating liver inflammation and fibrosis

Next, we evaluated the extent of liver inflammation and fibrosis in GFP and SHP-overexpressing mice. The results showed that increasing hepatocyte SHP levels dramatically attenuated liver inflammation and fibrosis in mice fed a HFCF diet, evidenced by the marked reduction in the staining of F4/80 positive macrophages and collagen accumulation in the livers of SHP-overexpressing mice (*Fig.* 4-27A). Consistently, the liver hydroxyproline level was reduced in SHP-overexpression mice (*Fig.* 4-27B). At the mRNA level, overexpressing SHP in HFCF diet-fed mice led to a robust reduction in liver expression of genes related to inflammation such as *Il6*, *Tnfa*, and *Ccl2* (*Fig.* 4-28A). Meanwhile, overexpressing SHP altered macrophage polarization in the liver with a decrease in expression of proinflammatory M1 marker *Nos2* and increases in expression of anti-inflammatory M2 markers such as *Arg1* and *Cd163* (*Fig.* 4-28A). Furthermore, overexpressing SHP significantly decreased the expression of genes related to fibrosis, including *Tgfb1, Ctgf, Col1a1,* and *Col1a2* (*Fig.* 4-28A), without altering mRNAs of genes related to lipid metabolism such as fatty acid biosynthesis (*Pparg, Srebp-1c, Me1, Acc1, Acly*), fatty acid oxidation (*Cpt1a, Acc2*), VLDL secretion (*Mttp, ApoB*), and cholesterol metabolism (*Srebp2, Abca1, Abcg5*) (*Fig.* 4-28B). Thus, hepatic SHP-overexpression improved key parameters of NASH progression that are related to liver inflammation and fibrosis without affecting liver steatosis.

We next sought to explore potential mechanisms by which hepatocyte SHP inhibits liver inflammation. NF-κB signaling controls inflammation (198) and growing evidence indicates that NF-κB p65 activation contributes to the pathogenesis of NASH (199). SHP inhibits TLR4-triggered activation of NF-κB p65 signaling in monocytes (159). We, therefore, hypothesized that increasing SHP in hepatocytes may lead to a repression of NF-κB p65 signaling and, subsequently, inhibit liver inflammation. As expected, overexpressing SHP in hepatocytes dramatically decreased HFCF-induced nuclear translocation of total p65 and phospho-p65 (Ser536) (*Fig.* 4-29), an active form of p65, supporting the overall decrease in liver inflammation in SHP-overexpressing mice compared to GFP controls.

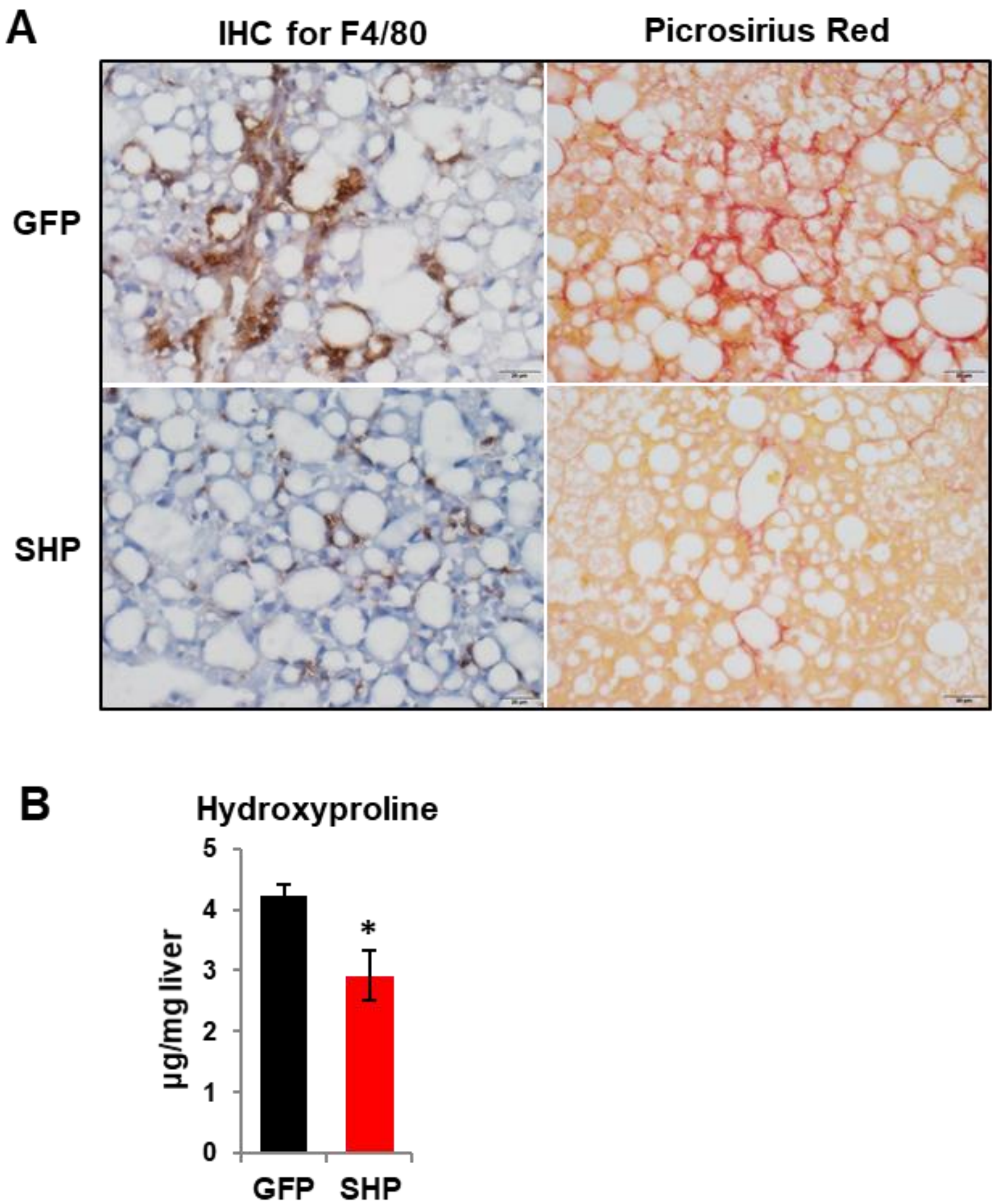

Figure 4-27: Hepatocyte SHP overexpression attenuates liver inflammation and fibrosis.

Two-month-old male C57BL6J mice were fed a HFCF diet for 1 month to develop liver steatosis, followed by tail vein administration of AAV8-*Tbg*-FlagSHP or control vector AAV8-*Tbg*-GFP. Mice were continued on the HFCF diet for 3 months. **A:** Representative images of liver sections of immunohistochemistry staining of F4/80 and Picrosirius Red staining. Original magnification, 400X. **B:** Liver collagen content was estimated by the hydroxyproline assay. Data in B is represented as mean ± SEM for 5 mice per group; **p* < 0.05 SHP *vs.* GFP.

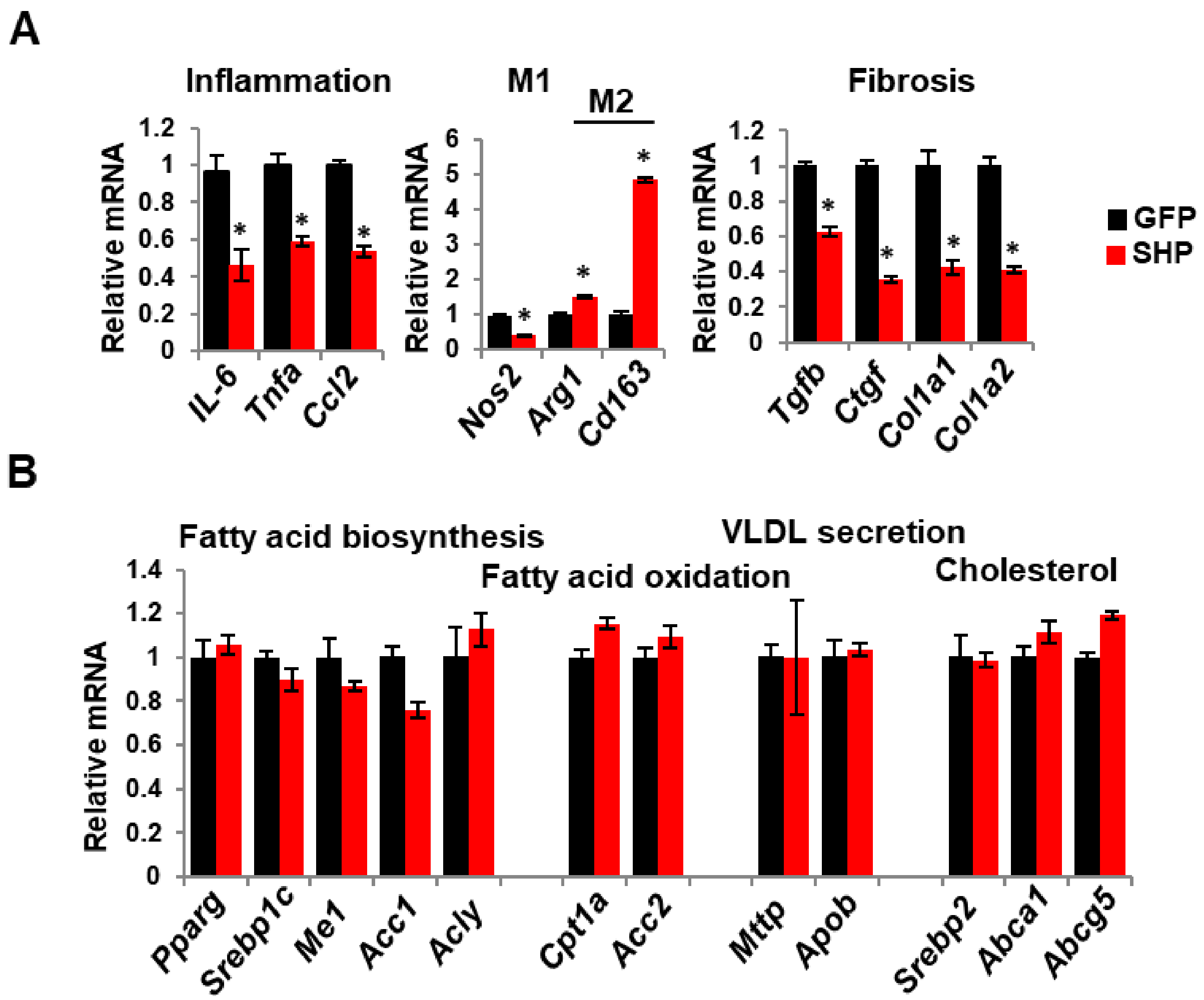

Figure 4-28: Hepatic SHP overexpression reduces pro- inflammatory and fibrotic gene expression but does not alter genes involved in lipid metabolism.

Relative mRNA levels of genes related to inflammation and fibrosis (A), as well as lipid metabolism (B) in the liver were determined by qPCR. Data are represented as mean ± SEM for 5 mice per group; *$p < 0.05$ SHP *vs.* GFP

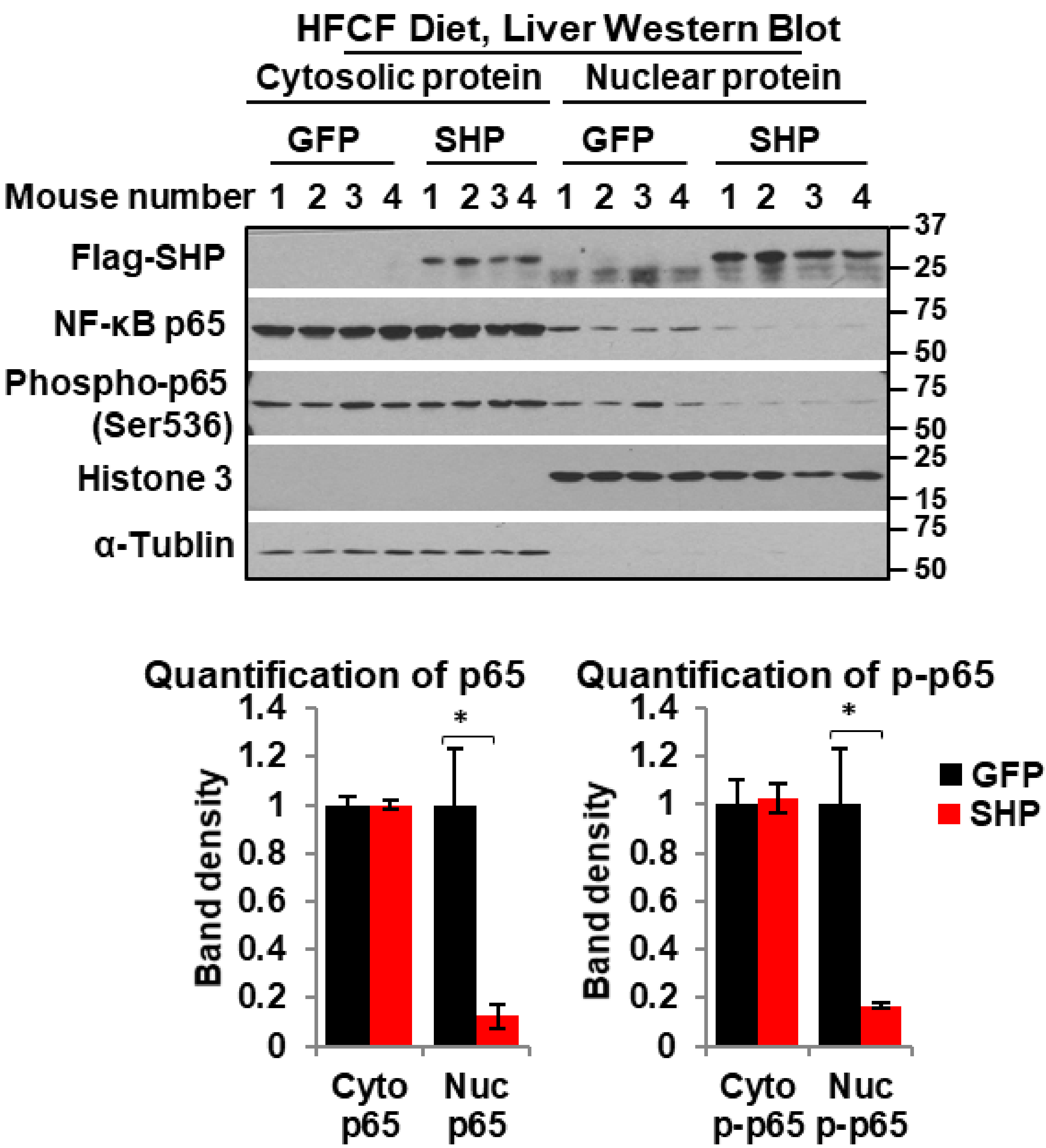

Figure 4-29: Hepatic SHP overexpression reduces p65 nuclear translocation.

Western blot of cytosolic and nuclear proteins in the liver (Top). Band intensities were measured by densitometry, and the intensities relative to that of the control were plotted (Bottom). Data are represented as mean ± SEM; n= 4/group, **p* < 0.05 SHP *vs.* GFP.

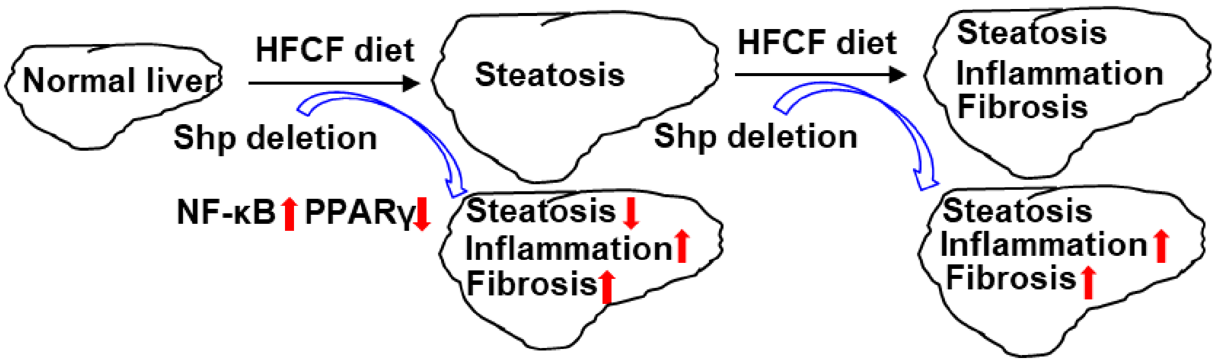

Figure 4-30: Schematic of the complex role of *Shp* in NAFLD.

Depending on NAFLD stage, hepatic *Shp* plays an opposing role in regulating steatosis, inflammation, and fibrosis. *Shp* disruption in hepatocytes activates *NF-κB* signaling and impairs *Pparg* activation, leading to the dissociation of steatosis, inflammation, and fibrosis in NAFLD development. *Shp* deletion after steatosis development exacerbates hepatic inflammation and fibrosis without affecting liver steatosis.

Discussion

One important finding in our study is the demonstration that SHP is markedly decreased during the progression of NAFL to NASH, which is observed in the livers of patients with NAFLD and in our diet-induced mouse NAFLD model. SHP expression in NAFLD is inconsistently reported in literature. One earlier study showed that SHP protein levels are reduced in NASH while mRNA levels are upregulated (200). Another study demonstrated that *SHP* mRNA is similarly reduced in obese patients with NAFL or NASH compared to the lean NAFLD (201). These discrepancies could be because SHP protein is not stable and degrades rapidly (184), thus protein expression and mRNA levels may not change in parallel. Additionally, not all commercial SHP antibodies are good to detect SHP protein, which may explain inconsistent results reported. In a recent study, Benet (2015) compared SHP expression levels in different mouse models of NAFLD and demonstrated that SHP is repressed in advanced NAFLD livers (NASH with fibrosis), such as tetracycline-treated rat livers, MCD diet livers, and glycine N-methyltransferase-deficient (*Gnmt*$^{-/-}$) mouse livers, but is not suppressed in the steatotic livers of methionine adenosyltransferase 1A-deficient (*Mat1a*$^{-/-}$) mice (202). Similarly, our study shows that SHP is not suppressed in NAFL but in NASH, suggesting a gradual decrease of SHP occurred during the disease progression.

Several signaling pathways have been implicated in the regulation of SHP. For instance, literature shows that mitogen activated protein kinase kinase 1/2 (MAPKK 1/2) pathway activates, while the phosphatidylinositol 3 kinase (PI3K) pathway suppresses SHP expression (202). Our studies contribute yet another regulator of hepatic SHP in NAFLD, JNK. As previously mentioned, JNK is activated by saturated fatty acids in a TLR-dependent manner. In the setting of excessive free fatty acid traffic in hepatocytes, especially saturated fatty acids, lipotoxicity occurs which is the major mechanism underlying hepatocyte dysfunction in NAFLD (203). One of the most abundant saturated fatty acids presented in diets and in serum is PA (204). PA can bind to TLR4 and lead to JNK activation (205,206). We demonstrated that TLR4 activation of JNK in mouse hepatocytes reduces *Shp* mRNA expression which is recovered upon JNK inhibition. In contrast, the rescue of hepatocyte *Shp* mRNA expression was not possible by inhibiting

NFκB or PI3K, indicating that JNK is predominantly responsible for *Shp* repression in the event of PA or LPS-induced TLR4 activation.

JNK was originally identified due to its ability to specifically phosphorylate c-Jun on its N-terminal transactivation domain at two serine residues, Ser63 and Ser73 (207). We confirmed that phosphorylated c-Jun is increased in the livers of 5-month HFCF-fed mice and this abundance of c-Jun reduces SHP expression by binding to the TRE site within the *Shp* promoter region. *In vitro,* the saturated fatty acid, PA, led to an increase of c-Jun recruitment to the *Shp* promoter which was abrogated upon addition of a JNK inhibitor. These results bridge the gap between JNK and hepatic SHP in NASH and indicate that JNK activation induces the binding of c-Jun to the *Shp* promoter, leading to suppression of *Shp* transcription. Further investigation is warranted to explore whether inhibition of JNK could rescue SHP suppression and ameliorate disease progression of NAFLD.

Steatosis alone is considered little to no risk for progressive liver disease, while NASH can progress into irreversible cirrhosis and hepatocellular carcinoma without effective treatments. Given the clinical significance of NASH, identifying key factors and pathways that promote the progression of steatosis to NASH is critically important for developing effective prevention and therapeutic strategies. Using a clinically relevant dietary mouse NASH model, we investigated the role of SHP in NASH development. We demonstrate that disruption of hepatic *Shp* activates NF-κB signaling and impairs *Pparg* activation, leading to the dissociation of steatosis, inflammation, and fibrosis during NAFLD development. Interestingly, ablation of hepatic *Shp* after the development of steatosis exacerbates liver inflammation and fibrosis without affecting steatosis (*Fig.* 4-30). Our finding that hepatic *Shp* plays a crucial role in steatosis-to-NASH transition provides some new mechanistic insights into our understanding of NASH pathogenesis and progression and may present a new target for NASH treatment.

An important finding from this study is that *Shp* disruption in hepatocytes induces liver inflammation, which is supported by several pieces of evidence. First, immunohistochemistry staining confirmed an increase in $CD4^+$ T cells, B cells, macrophages, and neutrophils in the liver after 12 weeks of SHP deletion. Second, deletion of *Shp* led to a robust induction of genes involved in liver inflammation, such as

Ly6d, Il6, Il1, Tnfa, Ccl2, Ifng, and *Nos2*. Most importantly, RNA-seq revealed that absence of *Shp* significantly altered biological processes and pathways involved in inflammation. Finally, loss of *Shp* induced NF-κB signaling activation in hepatocytes that can be blocked by a specific NF-κB inhibitor.

SHP plays an important anti-inflammatory role in monocytes by negatively regulating inflammation induced by toll-like receptor 4 (TLR4) and NLRP3 inflammasomes (159,160). Here, we found that in hepatocytes, SHP also plays an anti-inflammatory role. Our finding is important, as the hepatocyte is being recognized as a key cell type involved in innate immunity by secreting innate immunity proteins such as bactericidal proteins, opsonins, iron-sequestering proteins, coagulation factor fibrinogen, and cytokines (208). The dysregulation of these innate immunity proteins contributes significantly to the pathogenesis and progression of chronic liver diseases including NASH. For instance, palmitic acid induces the production of proinflammatory cytokine interleukin-8 from hepatocytes, contributing to hepatic inflammation and liver injury subsequently (162). Lipotoxicity induces the release of chemokine (C-X-C motif) ligand 10 (CXCL10)-bearing vesicles from hepatocytes, resulting in macrophage recruitment into the liver (161). Moreover, in a recent study, hepatocytes were found to secrete CXCL1/interleukin-8 which causes neutrophil infiltration and alcoholic liver injury (209).

One well-known, powerful proinflammatory chemokine is CCL2 which is responsible for attracting monocytes/macrophages and T cells during liver injury. An increase in CCL2 secretion from hepatocytes has been shown in both alcohol-associated fatty liver disease (210) and obesity-associated NAFLD (211), which exacerbates liver injury and inflammation. Similarly, our study demonstrates that disruption of SHP in hepatocytes induces NF-κB signaling activation, resulting in CCL2 production and secretion from hepatocytes, leading to macrophage recruitment and proinflammatory M1 polarization (*Fig* 4-16). Consistently, SHP deletion in hepatocytes also causes liver inflammation *in vivo*. Therefore, we speculate that the increase in CCL2 secretion from *Shp* deficient hepatocytes may contribute to the liver inflammation developed in *Shp*$^{Hep-/-}$ mice. Further investigation is warranted to explore whether blocking CCL2 production from hepatocytes or repressing CCL2 function could inhibit or ameliorate liver inflammation developed in *Shp*$^{Hep-/-}$ mice.

The role of hepatic *Shp* in the development of NAFLD has been extensively studied in mouse models. For instance, earlier studies showed that both whole body *Shp* knockout mice and hepatic *Shp* knockout mice are resistant to high fat diet-induced hepatic steatosis (188,189,212). Given that all these fatty liver models are associated with little or no inflammation and fibrosis, the role of hepatic SHP in mouse NASH remains obscure. Here, we fed mice a HFCF diet that induces many biochemical and histopathological hallmarks of NASH, to study the role of SHP in modulating liver steatosis, inflammation, and fibrosis during NASH development. One striking observation was that hepatic *Shp* disruption activates NF-κB signaling and impairs *Pparg* activation, leading to the dissociation of steatosis, inflammation, and fibrosis during NAFLD development.

To elucidate the role of SHP specifically in the disease transition from steatosis to NASH, we developed a steatosis-to-NASH transition model where mice were fed HFCF diet for 4 weeks to induce liver steatosis followed by disrupting *Shp* in hepatocytes. Interestingly, hepatic *Shp* deletion after steatosis development exacerbated liver inflammation and fibrosis without affecting liver steatosis, though *Pparg* expression was consistently decreased in this model. The results support the notion that SHP plays distinct roles in different stages of NAFLD and the sustained decrease in SHP expression could worsen disease progression. Our results also support the complexity of steatosis development in NAFLD; both *Pparg*-dependent *and Pparg*-independent mechanisms could contribute significantly during the disease progression.

SHP was decreased during NAFL transition to NASH, indicating that SHP may play a protective role during NAFLD progression. To test our hypothesis, we induced liver steatosis using the HFCF diet and overexpressed SHP specifically in hepatocytes. As expected, increasing hepatocyte SHP levels in steatotic liver dramatically attenuated liver inflammation and fibrosis —two critical events responsible for NAFLD progression, indicating a protective role of SHP during NAFLD progression. The finding that overexpressing SHP in steatotic liver did not change hepatic lipid content is in line with observations showing no changes in the expression of genes involved in fatty acid biosynthesis, oxidation, and VLDL secretion in steatotic livers with SHP overexpression.

These data reconfirm the critical anti-inflammatory and anti-fibrotic role of SHP in the progression of fatty liver to NASH.

In summary, our study provides compelling evidence that a novel regulatory network in hepatocytes, consisting of JNK/SHP/NF-κB/CCL2, is critical to regulate macrophage recruitment and initiation of inflammation for NAFLD progression. Additionally, we have demonstrated that hepatic *Shp* disruption in adult mice induces the dissociation of steatosis, inflammation, and fibrosis during NASH development. In contrast, SHP overexpression in steatotic liver prevents NAFL progression to NASH. Our study provides new mechanistic insights into our understanding of NASH pathogenesis and progression. However, we also noticed that the complex effects of SHP on hepatic steatosis, inflammation, and fibrosis could compromise the potential use of SHP as a therapeutic target for NAFLD treatment. Any approaches increasing or decreasing SHP should be cautiously used. For instance, inhibition of hepatic *Shp*, while beneficial for the amelioration of liver steatosis, could exacerbate liver inflammation and fibrosis during NAFLD progression.

Chapter 5: RNA-Sequencing Reveals Key Signatures Involved in NAFL and NASH-Afflicted Mouse Livers.

This chapter is adapted from Magee N, Zou A, He L, Ghosh P, Ahamed F, Delker D, Zhang Y. Hepatic transcriptome profiling reveals key signatures associated with disease progression from nonalcoholic steatosis to steatohepatitis. (*Manuscript under revision*)

Introduction:

Over the past decades, bioinformatics tools and techniques such as genome-wide associated studies (GWAS) and RNA sequencing (RNA-seq) have been widely employed as powerful tools to investigate molecular mechanisms that influence NASH development in humans and in mouse models (140,213,214). One study reported genomic comparisons between NASH in humans and in 9 different mouse models, including mice fed: 1) a high-fat diet with fructose, 2) an MCD diet, 3) a high-fat diet with streptozotocin, or in mice with disruption of the hepatic *Pten* gene (213). Surprisingly, the comparisons yielded few overlaps between NASH in humans and in mouse models, indicating that NASH development in mouse models does not significantly correlate with NASH developed in humans at the transcriptome level. However, a recent study employed high-throughput RNA sequencing to explore mRNA expression profiling in a NAFLD mouse model developed in an isogenic strain derived from a cross of C57BL/6J (B6) and 129S1/SvImJ (S129) mice fed a high fat, cholesterol, and fructose diet (150). They found that this model recapitulates transcriptomic and cell-signaling changes seen in humans with progressive NASH, suggesting some similarities between NASH development in humans and in this mouse dietary model.

NASH development involves both hepatocytes and non-parenchymal cell types such as hepatic stellate cells, macrophages, and other immune cells. However, the changes within the hepatic transcriptome profile during NAFL transition to NASH is incompletely understood. Since we captured the stage-wise progression of NAFLD in our HFCF mouse model, we next employed RNA-seq to identify key signatures involved in disease progression. Specifically, we used the livers from the 1- and 3- month chow- and HFCF-fed mice to explore the transcriptomic changes which occur during the NAFL to NASH transition. We observed a strong induction of gene signatures related to NASH such as those involved in immune response and extracellular matrix organization. Our results are consistent with previous hepatic transcriptomic studies in mouse NASH models and in NASH patients (214-216). We, therefore, anticipate that the findings from our studies may help pave the way to develop novel preventative, diagnostic, and therapeutic strategies for NASH.

Results

HFCF diet induces significant changes to hepatic transcriptome

To pursue an unbiased investigation of early events associated with the transition of NAFL to NASH, we conducted RNA-seq analysis of livers obtained from chow-fed and HFCF-fed mice at 1-month and 3-month time points (data were deposited into GSE135050). The fragments per kilobase of exon model per million reads mapped (FPKM) was calculated to quantify the expression levels of genes in four groups, including 1-month chow, 1-month HFCF, 3-month chow, and 3-month HFCF. The differentially expressed genes (DEG) were determined using fold change cutoff of 1.50 and false discovery rate (FDR) < 0.05.

Volcano plots demonstrated distinct differences between chow-fed and HFCF-fed groups at both 1-month and 3-month time points (*Fig.* 5-1A). In particular, 460 genes were significantly differentially expressed between the chow-fed group and the HFCF-fed group at the 1-month time point. At the 3-month time point, the hepatic gene expression in the HFCF-fed group was also different from the chow-fed group resulting in 2,167 DEGs. Meanwhile, 78 genes were differentially expressed in the 1-month chow compared to the 3-month chow group, and 1,869 genes were differentially expressed comparing the 1-month HFCF group to the 3-month HFCF group. A heat map visualization of the hepatic transcriptome with hierarchical clustering was used to determine the expression patterns of different genes in chow-fed and HFCF-fed groups (*Fig.* 5-1B). As shown in the heat map, the DEGs were clustered into two major types, one with higher expression in the HFCF groups but lower expression in the chow groups, and the other with higher expression in the chow groups but lower expression in the HFCF groups. The data indicate that HFCF diet feeding induces significant changes to the hepatic transcriptome when compared to the chow-fed groups. Feeding duration also made a difference especially for the HFCF groups.

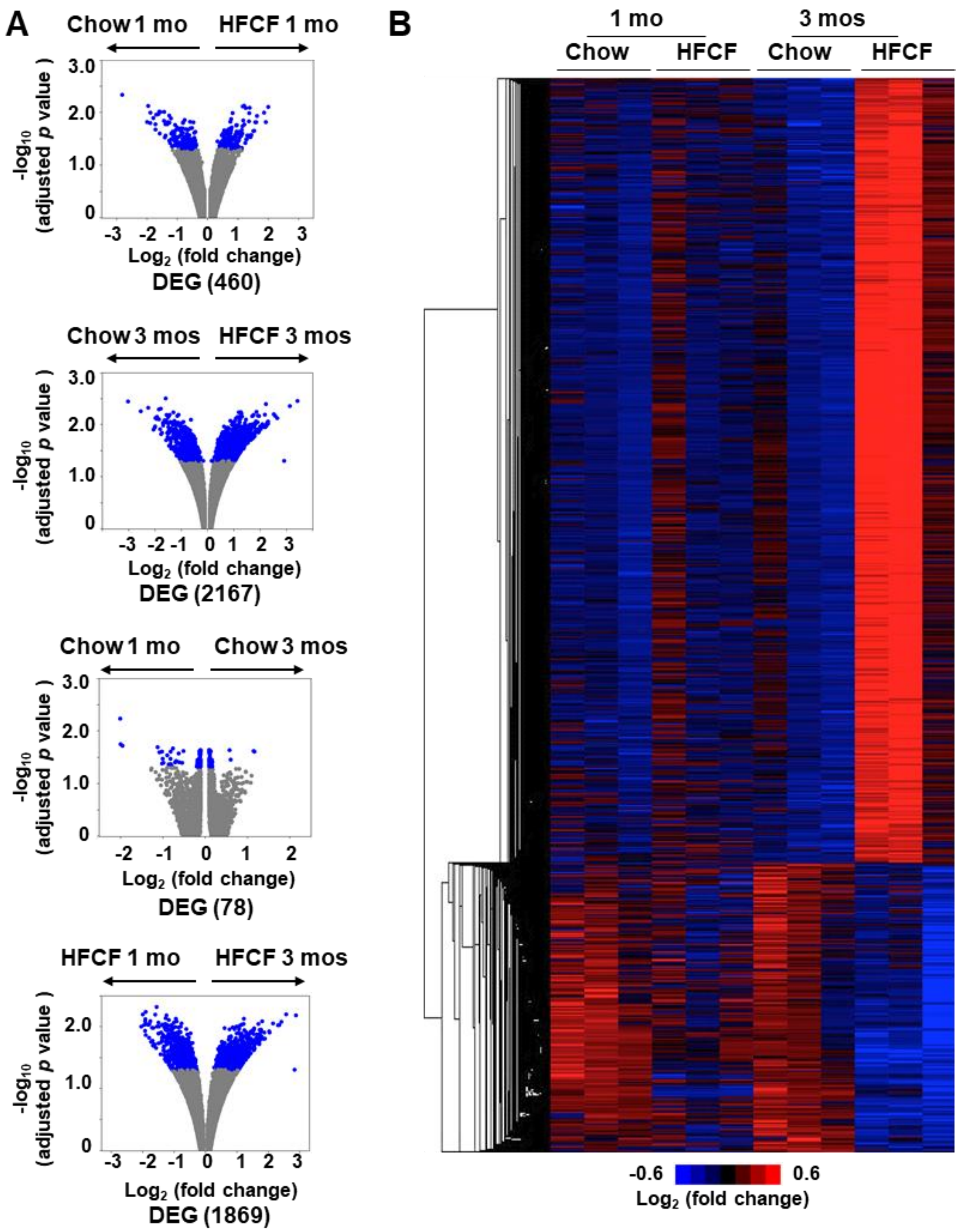

Figure 5-1: Dynamic gene changes in mice fed chow or HFCF diet for 1 month or 3 months.

RNA-seq analysis of livers from mice fed a chow or HFCF diet for 1 month or 3 months. **A:** volcano plots of mRNAs. The plots were constructed by plotting $-\log_{10}$ (adjusted p value) on the y-axis and $\log_2$ (fold change) on the x-axis. Blue dots represent differentially expressed genes (DEGs) and grey blots represent mRNAs without significant difference. **B:** hierarchical cluster of representative mRNA expression across biological replicates. Red and blue colors indicate high and low gene expression, respectively.

RNA-seq reveals key gene signatures associated with NAFL transition to NASH in HFCF-fed mice

To identify key gene signatures responsible for NAFL transition to NASH, we conducted Gene Ontology (GO) enrichment and Kyoto Encyclopedia of Genes and Genomes (KEGG) pathway analysis using Enrichr. The DEGs were assigned to GO terms describing biological processes, cellular components, and molecular functions. A cutoff p-value of < 0.05 was used to select enriched GO terms and KEGG pathways.

Compared with the 1-month chow group, the GO terms identified a significant enrichment of genes involved in multiple metabolic processes in the 1-month HFCF group. The top 10 biological processes altered in the 1-month HFCF are displayed in *Fig.* 5-2A and indicate that most significant consequences of HFCF feeding for 1 month are alterations in lipid and cholesterol metabolism. KEGG pathway analysis of DEGs revealed that the significant pathways altered were related to the biological processes such as steroid biosynthesis, DNA replication, amino acid metabolism, and PPAR signaling (*Fig.* 5-2B). Notably, the KEGG pathways also signified that pathways related to cytochrome P450s, key enzymes important for drug metabolism, were significantly altered (*Fig*. 5-2B). The top 20 deregulated genes between the 1-month chow and the 1-month HFCF group are shown in *Fig.* 5-2C.

We next used GO enrichment and KEGG pathway analyses in the 3 months HFCF fed mice compared to the 3 months chow control groups. The top 10 biological processes and pathways altered indicate that, compared to chow controls, significantly altered genes are involved in lipid metabolism, inflammation, and fibrosis (*Fig.* 5-3A, 3B). The top 20 genes up- or down-regulated between the 3-month HFCF and the 3-month chow groups are shown in *Fig.* 5-3C. The above results demonstrate that HFCF feeding for 3 months causes an increase in gene signatures related to lipid metabolism, inflammation, and fibrosis, supporting our qPCR and histological findings in Chapter 3.

To identify key genes and pathways associated with the transition of NAFL to NASH, DEGs from the 3-month HFCF versus the 1-month HFCF comparison were used for GO enrichment and KEGG pathways analysis. Consistently, genes involved in inflammation and fibrosis were enriched by both analyses (*Fig.* 5-4A). Interestingly, amongst the top

10 pathways from the KEGG pathway analysis were known regulators of lipid metabolism and inflammation, PPAR and NF-κB signaling pathways (*Fig.* 5-4B). *Figure* 5-4C shows the top 20 deregulated genes selected based on their fold change differences between the 1-month HFCF and the 3-month HFCF groups.

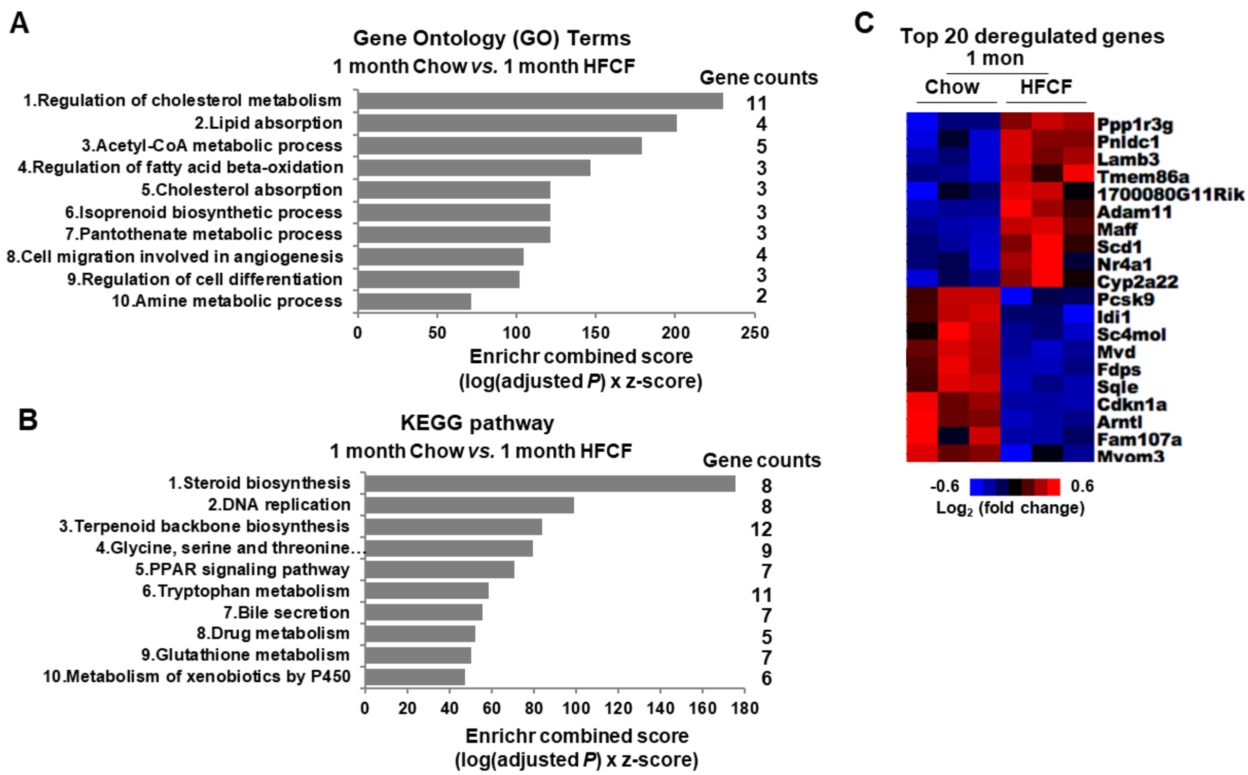

Figure 5-2: Gene Ontology (GO) enrichment and KEGG pathway analysis of DEGs for 1-month chow or HFCF diet.

A: The top 10 enriched GO terms were selected by Enrichr combined score using Enrichr. The x-axis represents Enrichr combined scores and the y-axis represents GO terms. **B**: The top 10 enriched KEGG pathways were selected by Enrichr combined score using Enrichr. The x-axis represents Enrichr combined scores and the y-axis represents KEGG pathway. **C**: Heatmap depicts top 20 deregulated genes between the 1-month chow and the 1-month HFCF groups.

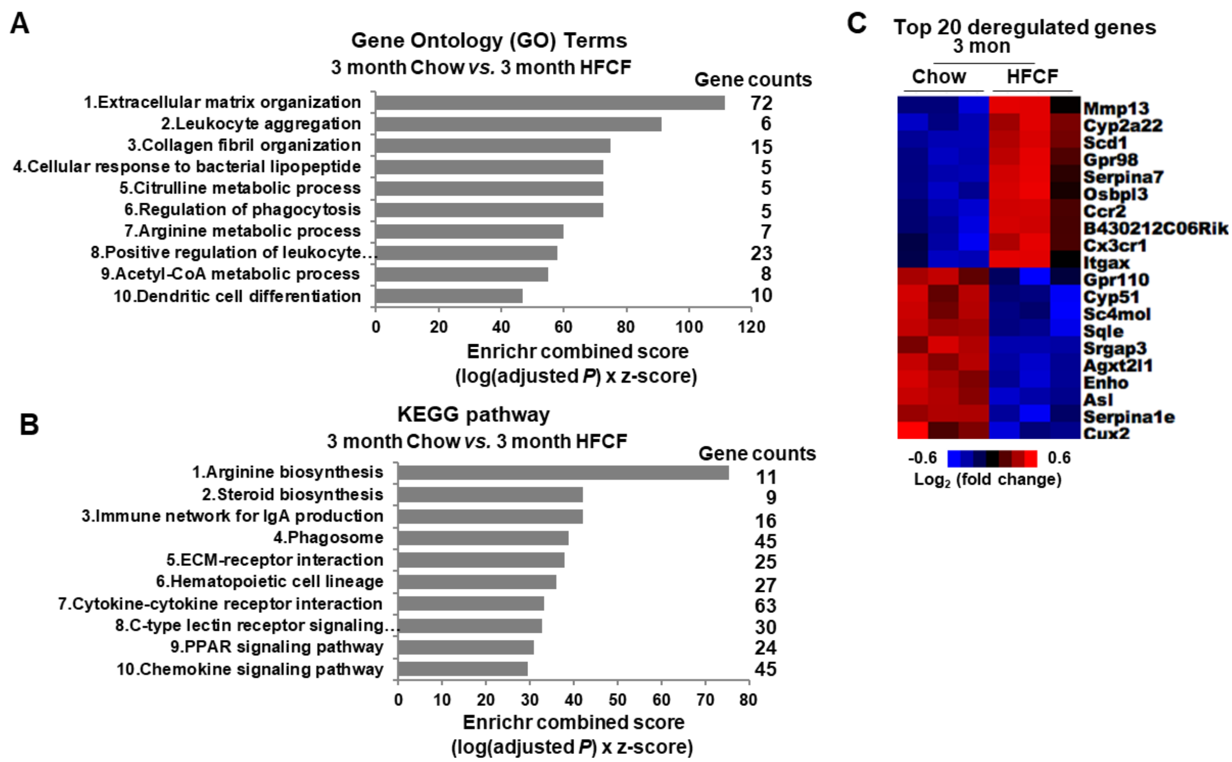

Figure 5-3: Gene Ontology (GO) enrichment and KEGG pathway analysis of DEGs for 3-months chow or HFCF diet.

A: The top 10 enriched GO terms were selected by Enrichr combined score using Enrichr. The x-axis represents Enrichr combined scores and the y-axis represents GO terms. **B:** The top 10 enriched KEGG pathways were selected by Enrichr combined score using Enrichr. The x-axis represents Enrichr combined scores and the y-axis represents KEGG pathway. **C:** Heatmap depicts top 20 deregulated genes between the 3-month chow and the 3-month HFCF groups.

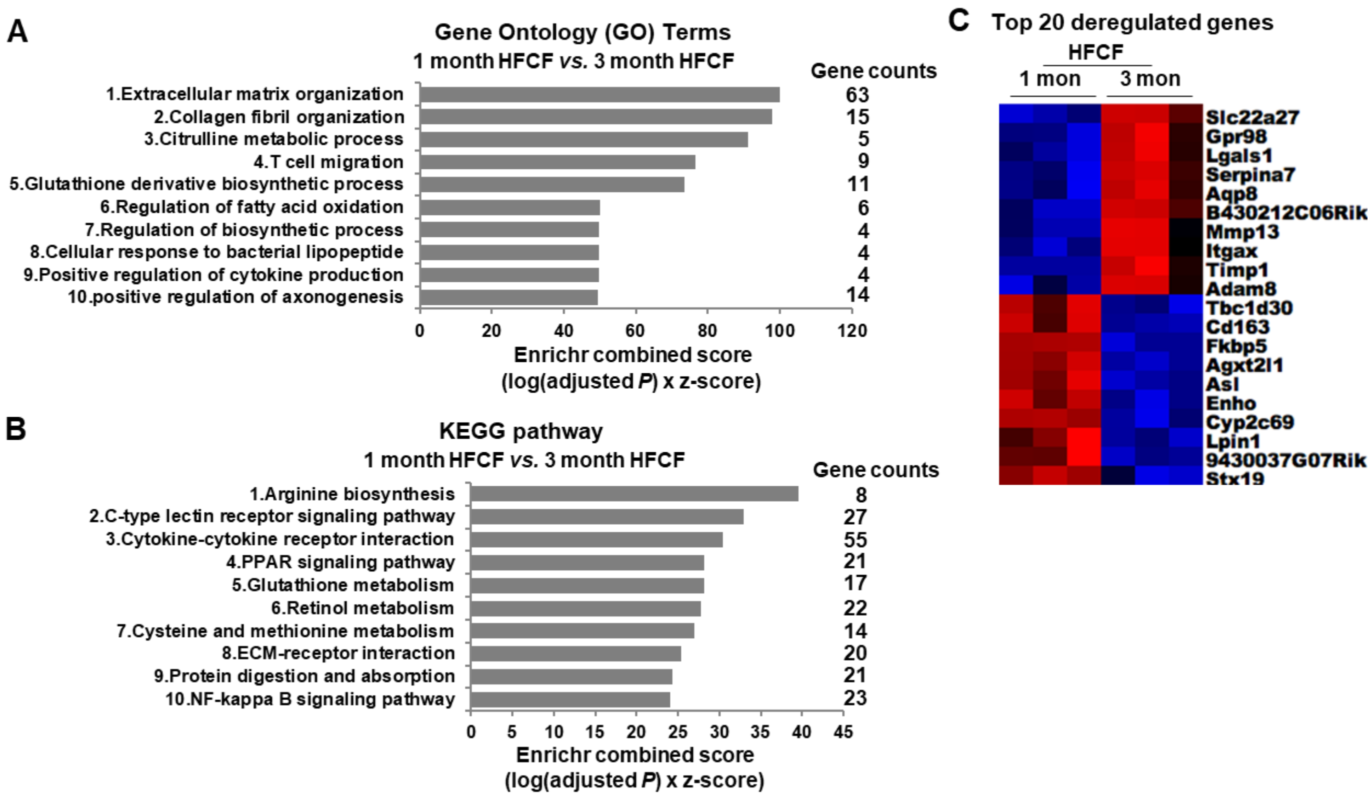

Figure 5-4: Gene Ontology (GO) enrichment and KEGG pathway analysis of DEGs for 1 or 3 months HFCF diet.

A: The top 10 enriched GO terms were selected by Enrichr combined score using Enrichr. The x-axis represents Enrichr combined scores and the y-axis represents GO terms. **B**: The top 10 enriched KEGG pathways were selected by Enrichr combined score using Enrichr. The x-axis represents Enrichr combined scores and the y-axis represents KEGG pathway. **C:** Heatmap depicts top 20 deregulated genes between the 1-month and the 3-month HFCF groups.

Deregulation of FOXM1 and NELFE targets during NAFL transition to NASH in a mouse NAFLD model

To understand which upstream regulators are responsible for the gene expression differences between NAFL and NASH, we performed Encyclopedia of DNA Elements (ENCODE) and ChIP enrichment analysis (ChEA) on DEGs obtained of the 1-month HFCF and the 3-month HFCF groups using Enrichr. The use of ENCODE and ChEA allowed us to identify consensus transcription factors. *Figure* 5-5A shows 15 consensus transcription factors whose regulation was most deregulated between the 1-month HFCF and the 3-month HFCF groups, including forkhead box M1 (*Foxm1*) and negative elongation factor (*Nefle*).

To verify whether consensus transcription factors identified during the transition of NAFL to NASH in our mouse model could be relevant to the NAFLD development in humans, we conducted ENCODE and ChEA analyses using DEGs obtained from a human liver microarray dataset (GSE48452). This dataset contains results of microarrays from human livers in different stages of NAFLD, including 14 steatotic livers and 18 NASH livers. Nine consensus transcription factors were identified by the comparison (*Fig.* 5-5B). Strikingly, both FOXM1 and NEFLE were identified from the NAFL versus NASH comparison, which was observed in the NAFLD mouse model and NAFLD patients (*Fig.* 5-5). The heat maps of target genes differently regulated by FOXM1 and NEFLE in the mouse NAFL to NASH transition are shown in *Fig.* 5-6, respectively. Table 5-1 shows the fold changes and significant p values of target genes regulated by FoxM1 or NEFLE from the human NASH versus human steatosis comparison.

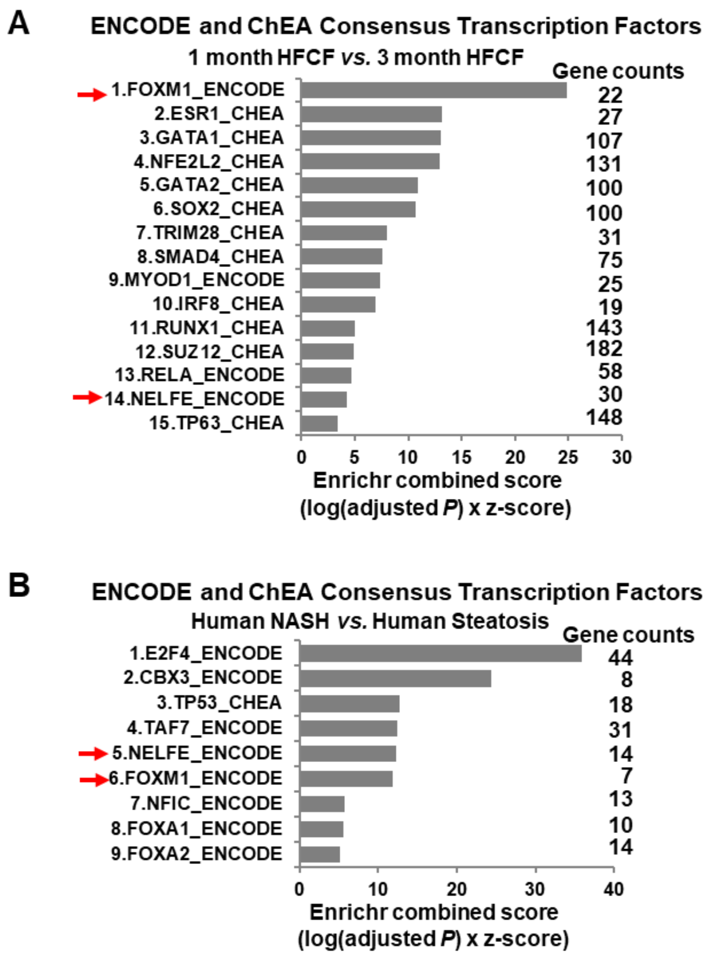

Figure 5-5: Results of screening for consensus transcription factors in NAFL to NASH transition.

ENCODE and ChEA were used to screen consensus transcription factors during NAFL to NASH transition. **A:** Consensus transcription factors identified in mouse NAFL to NASH transition. The DEGs from the 1-month versus the 3-month HFCF comparison were submitted to Enrichr. The consensus transcription factors were selected based on p value and Enrichr combined score. The x-axis represents Enrichr combined scores and the y-axis represents consensus transcription factors. **B:** Consensus transcription factors identified in human NAFL to NASH transition. The DEGs from the human NASH versus steatosis comparison were downloaded from GSE48452 and submitted to Enrichr. The consensus transcription factors were selected based on p value and Enrichr combined score. The x-axis represents Enrichr combined scores and the y-axis represents consensus transcription factors.

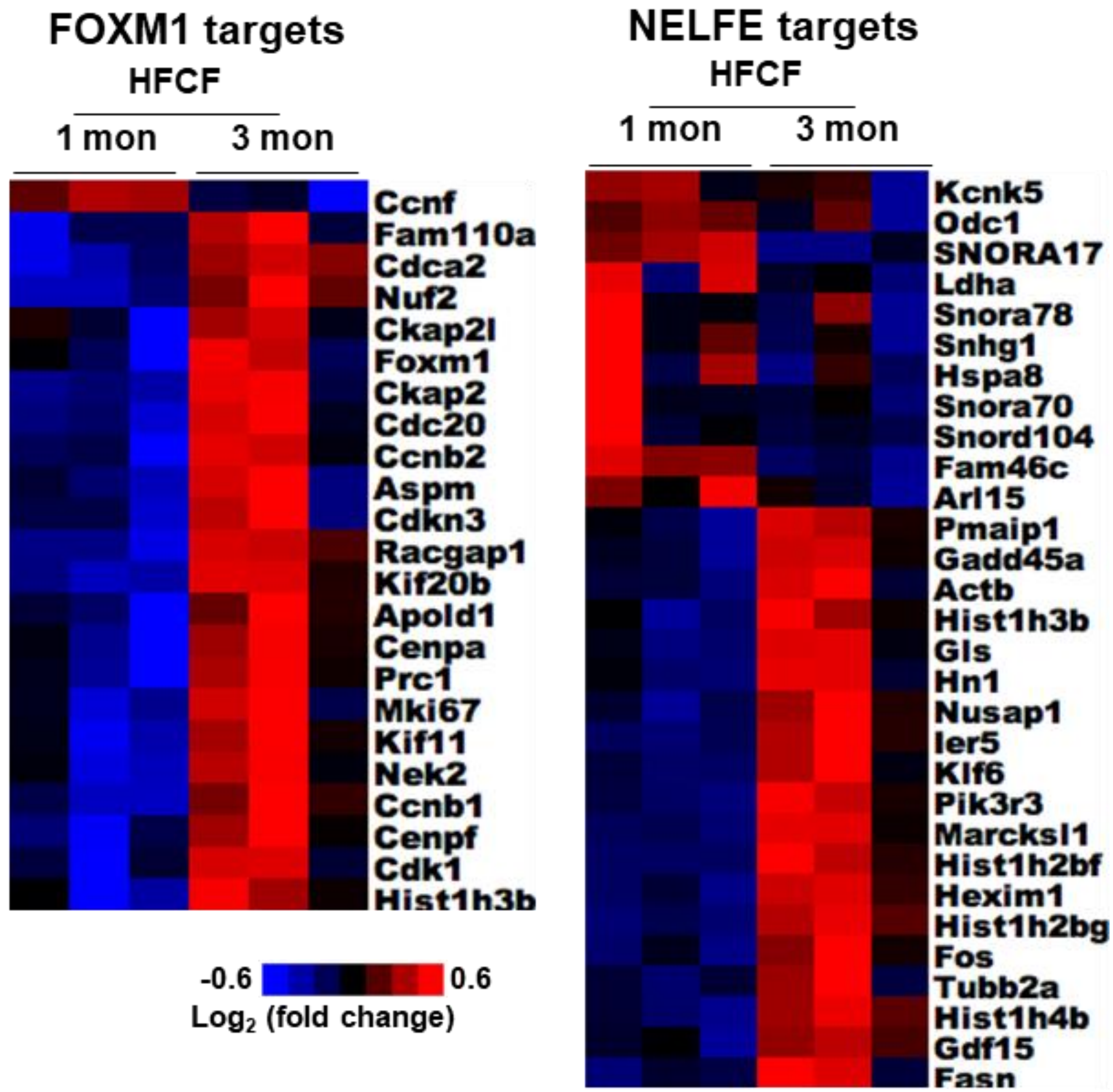

Figure 5-6: Heatmaps display genes differently regulated by FOXM1 and NELFE in mouse NASH livers.

Heat maps depict genes differently regulated by FoxM1 or NEFLE in the 1-month versus the 3-month HFCF comparison.

TABLE 5-1: Genes regulated by FOXM1 and NELFE were significantly altered in human NASH.

Human NASH *vs.* Human Steatosis

	Genes	Fold changes	P value
FOM1 targets	ASPM	1.82	0.0010
	RHEB	1.67	0.0004
	KPNA2	1.51	0.0083
	HIST1H3B	1.52	0.0063
	LMNB1	1.59	<0.0001
	SKA2	2.12	0.0003
NELFE targets	CBX5	1.50	0.0010
	HIST1H3B	1.52	0.0063
	GADD45B	0.52	0.0024
	DUSP1	0.58	0.0091
	WDR74	0.28	0.0036
	FOS	0.27	0.0164
	RNU11	0.55	0.0002
	SNORD43	0.47	0.0044
	EGR1	0.34	0.0286
	JUNB	0.58	0.0242
	SNORA44	0.63	0.0157
	GAS5	0.54	0.0058
	SNORA64	0.32	0.0014
	SNORD61	0.66	0.0121

The fold changes and significant p-values of target genes regulated by FoxM1 or NEFLE from the human NASH versus steatosis comparison.

Discussion

To further understand the molecular machinery responsible for the transition of simple steatosis to NASH, we examined the hepatic transcriptome profile of chow-fed and HFCF-fed mice at two different feeding periods (1 month and 3 months). We found that the HFCF diet induced remarkable transcriptomic changes in the liver which correlate with the observed histologic phenotypes (*Fig.*3-5A). Additionally, we revealed similarities between upstream regulators in both HFCF-fed mice and human patients with NAFLD.

Enrichr pathway analysis revealed relevant pathway changes in our three group comparisons (Group 1: 1-month HFCF vs 1-month Chow, Group 2: 3-month HFCF vs 3-month Chow, and Group 3: 3-month HFCF vs 1-month HFCF). Based upon Group 1 pathway comparison, the top pathways altered after 1-month HFCF feeding relate to cholesterol and steroid biosynthesis as well as lipid absorption. The top upregulated gene in the 1-month HFCF group is a key regulator of fatty acid synthesis, *Scd1* (*Fig.* 5-2). The upregulation of *Scd1* was maintained after 3 months on the HFCF diet. Together, these data portray an expected dietary response to overnutrition and increased lipids and carbohydrates. After prolonged feeding for 3 months, it was expected that the cells would become more stressed by the excess fat, sugar, and cholesterol. Group 2 pathway comparison confirmed the hypothesis in that the major pathways influenced after 3 months on the HFCF diet involve inflammatory response pathways (11 of 20 pathways) and fibrosis (3 of 20 pathways) (*Fig.* 5-3). Interestingly, pathway analysis of Group 3 reveals PPAR and NFκB signaling pathways are altered which supports the relevance of PPAR and NFκB signaling in disease transition.

One striking finding of this study is that the expression of genes regulated by transcription factors FOXM1 and NELFE were significantly different between NAFL and NASH, which was observed in both a mouse NAFLD model and NAFLD patients. FOXM1 is a proliferation-associated transcription factor expressed during the cell cycle (217). FOXM1 controls the critical expression of genes involved in cancer initiation, cancer progression, cancer metabolism, and drug resistance (218,219). Increase in hepatic FOXM1 is reported in human hepatocellular carcinoma (HCC) and inhibition of FOXM1 by targeting mevalonate pathway is beneficial for HCC treatment (220,221). Additionally, a recent study demonstrates that insulin signaling regulates the FoxM1/ polo like kinase 1 (PLK1)/ centromere protein A (CENP-A) pathway to promote adaptive pancreatic b cell proliferation that is an essential component to delay or prevent progression of diabetes (222), suggesting a potential role of FOXM1 in metabolic disease. However, the role of FOXM1 in NAFLD development especially in NAFL transition to NASH remains unknown and an important unsolved question.

NELFE is originally identified as part of a complex termed negative elongation factor that represses RNA polymerase II transcript elongation, but a recent study reveals NELFE as an RNA-binding protein (223). The molecular function of NELFE is largely unknown, but high NELFE levels have been demonstrated in HCC (224). Recently, NELFE was reported as an oncogenic protein that contributes to transcriptome imbalance of HCC through the regulation of MYC signaling (223). Whether NELFE-regulated pathways could contribute to the development and progression of NAFLD remains unknown.

In summary, the dynamic gene changes observed during NAFL to NASH transition confirm the importance and complexity of the inflammatory and fibrotic regulatory pathways involved in NAFLD progression. Our findings may provide new insights into the identification of potential targets for developing novel effectual NASH prevention and treatment strategies. However, several questions such as the changes of hepatic transcriptome profile and signaling pathway in the late stages of NAFLD remain to be resolved. We look forward to future scientific endeavors to answer these interesting questions.

Chapter 6: Overall Discussion

NAFLD is a burgeoning health problem worldwide, and its pathogenesis is complex. The studies performed in this dissertation aim to shed more insights into the mechanisms behind NAFLD development and progression through the development of a NAFLD mouse model, in-depth analysis of nuclear receptor SHP in NAFLD, and the use of RNA sequencing. The purpose of this dissertation is to aid in uncovering potential targets for effectual diagnostic and/or therapeutic interventions for NAFLD.

Murine HFCF model is relevant to NAFLD development in humans

The diagnosis of NAFLD requires a combination of invasive and noninvasive tests. Abnormal liver blood test values, such as liver enzymes ALT and AST, often trigger the evaluation of NAFLD. However, no single blood test is specific for NAFLD diagnosis. Patients who have normal liver enzymes but may be in the transition to mid stages of NAFLD could be overlooked and miss the opportunity for interventions (225). Otherwise, NAFLD discovery in a patient who has normal liver enzymes or is asymptomatic is secondary to another issue such as a patient getting a CT scan due to complaints of abdominal pain (226). Liver biopsy is often required for detecting and staging NAFLD. Once diagnosed with NAFLD, there is no FDA-approved drug available for NASH treatment. Classically, patients are advised to lifestyle changes such as diet and exercise whether obese or lean, and to take medications to relieve the symptoms associated with NAFLD such as anti-diabetic medications, vitamins, probiotics and other supplements (227,228). The studies performed in this dissertation aim to shed more insights into the mechanisms behind NAFLD development and progression with the hopes of uncovering potential targets for effectual diagnostic and/or therapeutic interventions.

One of the issues with studying NAFLD in rodents was developing a model which could depict and progress through each stage of the disease spectrum as humans do. Factors that affect NAFLD development include genetics, age, gender, and environment. Taking such components into account, several genetic and dietary models have been developed in an attempt to mimic one, some or all stages of the disease. We aimed to use a dietary model which carries the disease progression from simple steatosis to steatohepatitis. We, therefore, fed 2-month-old C57Bl6/J male mice a variation of the Western diet (HFCF: 40 kcal% fat, 2% cholesterol, 20 kcal% fructose) for 1, 3, 5, 7, and

9 months which we assess throughout Chapter 3. Using the histological scoring system to assess hepatic lipid, extracellular matrix content, and inflammation, we were able to capture simple steatosis at 1 month, transitioning period at 3 months, primary NASH at 5 months, complete NASH at 7 months, and NASH with fibrosis and spontaneous tumor development at 9 months.

We have shown that steatosis in HFCF-fed mice develops in parallel with the rapid increase of body weight. This observation is consistent with NAFLD development in humans, where studies showed that the prevalence of NAFLD is 58% in overweight individuals but can be as high as 98% in obese individuals (229). Triglyceride content in the liver cells can either derive from the *de novo* lipogenesis in hepatocytes or from the uptake of circulating fatty acids into the hepatocytes. Once formed, triglycerides can then be stored as lipid droplets (microvesicular or macrovesicular) within hepatocytes or secreted into the blood via VLDL to be used by other cells for energy. NAFLD arises from an imbalance between lipid acquisition (*de novo* lipogenesis or fatty acid uptake) and removal (fatty acid oxidation or export as VLDL particles), resulting in excessive fatty acid flux within hepatocytes which leads to liver steatosis.

We observed both micro- and macrovesicular steatosis in mice after 1 month of HFCF diet feeding; however, after 3 months of HFCF insult, the liver presents a predominant macrovesicular steatosis. This is due to the excessive accumulation of hepatic lipids. To understand the regulatory machinery that promotes liver steatosis in HFCF-fed mice, we examined the expression of genes responsible for fatty acid uptake, *de novo* lipogenesis, fatty acid b-oxidation, and VLDL secretion. We found that critical fatty acid biosynthesis enzymes, *Fas* and *Acc1* are decreased during earlier time points of mouse NAFLD model but increased after 5 months on HFCF diet when mice developed NASH. This suggests that *de novo* lipogenesis is initially suppressed in the early stage of steatosis but after long-term HFCF diet feeding it is augmented. Our study is consistent with previous publications which showed that, in NASH patients, *de novo* lipogenesis rates are increased and could contribute up to 25% of the fatty acid flux into the liver (230-232). Given the clinical importance of *de novo* lipogenesis to NASH development, approaches specifically inhibiting *de novo* lipogenesis are being tested to treat NASH in humans, including ACC1 inhibitors and liver X receptor (LXR) inverse agonists (233,234).

Moreover, our observation that the expression of genes involved in VLDL secretion was downregulated during NAFLD progression is in line with previous publications which demonstrated that VLDL secretion is decreased by excessive ER stress induced by lipotoxicity, eventually worsening steatosis and NASH progression (235,236).

Since NASH is the more advanced, progressive stage of NAFLD, many research efforts focus on establishing a comprehensive understanding of NASH development and progression. This entails gathering insights into the following questions: 1) When does hepatic lipid accumulation switch from protective to perilous? 2) At which instance(s) are inflammation and fibrosis triggered and which cells are involved? 3) Does the occurrence of inflammation and fibrosis happen independently or do they depend on one another? If they occur simultaneously, at which rate? Much progress has been made in answering these questions; however, gaps in detailed understanding of the disease remain. Therefore, in addition to phenotypic studies, in Chapter 5 we explored the transition phase of NAFLD by studying the genotypic changes occurred in 1- and 3-month chow and HFCF fed mice.

Pathway analysis of the 1-month *versus* the 3-month HFCF comparison revealed that the metabolic regulation of several amino acids (citrulline, arginine, cysteine and methionine) is altered by HFCF feeding over time. A recent study showed that blood cysteine level is positively correlated with NAFLD and severity of hepatic damage in children (237). In addition, amino acid supplementation is a strategy employed in treating humans with NAFLD. Clinical trials conducted using amino acid supplements such as serine and *N*-acetyl-l-cysteine (NAC) revealed amelioration of steatosis in NAFLD patients (238). Interestingly, cysteine was shown to increase the levels of antioxidant glutathione (GSH) in the liver (238). Given this information, it is possible that the changes in amino acid regulation pathways may account for the changes in the GSH pathway in our NAFL to NASH transition model signified by Enrichr. GSH supplementation was found to reduce triglyceride and serum ALT in humans with NAFLD (239). Further evaluation of GSH homeostasis in our HFCF-induced NASH model is pertinent as GSH was shown to reduce TNFa-induced cell injury in hepatocytes and NFκB suppression in HFD-fed mice (240).

SHP in NAFLD

SHP is an atypical nuclear receptor due to its lack of a DNA binding domain (241). As an orphan nuclear receptor without known ligand, SHP represses bile acid synthesis (191,242), controls energy metabolism (243), and regulates glucose homeostasis (244,245) via direct interactions with numerous nuclear receptors and transcription factors (123). In support of its important role in metabolic diseases, mutations in the *Shp* gene are correlated with obesity and susceptibility to type 2 diabetes (158). The role of SHP in the development of mouse NAFLD is very complicated. An earlier study demonstrated that acute liver-specific SHP overexpression in C57BL/6J mice decreased hepatic triglyceride levels (246). In contrast, other studies showed that whole body *Shp* knockout mice and hepatocyte-specific *Shp* knockout mice are resistant to high fat diet-induced hepatic steatosis (188,189,212). Given that the fatty liver models utilized in these studies are associated with little or no inflammation and fibrosis, the role of hepatic SHP in NAFLD progression, especially in NASH, remains obscure.

In Chapter 3 of this dissertation, we developed a HFCF dietary mouse model that carries the entire disease spectrum of NAFLD from NAFL to NASH. In Chapter 4, we employed this dietary mouse model to dissect the role of SHP in steatosis, inflammation, and fibrosis during NASH development. We found that the expression of *SHP* was markedly decreased in the livers of patients with NASH and in diet-induced mouse NASH, suggesting the biological relevance of SHP in the disease progression from NAFL to NASH (Chapter 4 part I). We demonstrated in Chapter 4 part II that *Shp* deletion in murine hepatocytes resulted in massive infiltration of macrophages in the liver. The data indicate that hepatic SHP plays a critical role in regulating liver immune homeostasis. One important observation is that after being fed a HFCF diet, *Shp*$^{\text{Hep-/-}}$ mice developed reduced steatosis compared to WT mice, but accelerated hepatic inflammation and fibrosis. To further characterize the role of *Shp* specifically in the transition of steatosis to NASH, mice were fed the HFCF diet for 4 weeks, followed by *Shp* deletion. Surprisingly, *Shp* deletion after steatosis development exacerbated hepatic inflammation and fibrosis without affecting liver steatosis. On the other hand, overexpressing SHP in hepatocytes prevented NAFL progression to NASH by attenuating liver Inflammation and fibrosis.

Together, our studies in Chapter 4 clearly indicate that, depending on NAFLD stages, hepatic *Shp* plays distinct roles in modulating liver steatosis, inflammation, and fibrosis.

SHP regulates lipid metabolism in NAFLD

Efforts towards elucidating mechanisms behind hepatic lipid accumulation reveal nuclear receptors as major players, particularly the constitutive androstane receptor (CAR), pregnane X receptor (PXR), LXR, PPAR, and FXR (116,127,247-251). This is expected since fasting and feeding regulate these nuclear receptors and their heterodimer partner, RXR (252). SHP is a regulator of many of these nuclear receptors.

Notorious for binding other transcription factors to carry out its functions, SHP is an inducible transcriptional corepressor (253). Thorough studies regarding the role of SHP in the regulation of lipid metabolism have been conducted (123). Goodwin and colleagues revealed the repressive effect of SHP binding to nuclear receptor LRH-1 which regulates *Cyp7a1*, an enzyme critical for the production of bile acids from cholesterol (191). In the same year, Lu and colleagues identified LRH1 as a competence factor that permits nuclear receptor LXRa transactivation of *Cyp7a1* (242). Interestingly, Brendel and colleagues provided insight into the interaction of SHP with LXRa also. Particularly, it was shown that SHP directly binds to LXRa and inhibits its transactivation (254). During the same decade, Wang and colleagues demonstrated that SHP is a repressor of PPARg co-factor 1a (*Pgc1a*) and uncovered the importance of SHP in lipid regulation. In particular, *Shp*-deficient mice were resistant to high fat diet-induced obesity (243).

Since *Shp* is most abundantly expressed in the liver—particularly in hepatocytes—our studies involved observing the effect of hepatocyte-specific functions of SHP in liver steatosis (Chapter 4). Interestingly, deletion of hepatocyte *Shp* before HFCF diet feeding resulted in decreased hepatic steatosis. In contrast, *Shp* deletion or overexpression after steatosis development did not alter the extent of steatosis. We, therefore, hypothesized that hepatic *Shp* is critical for liver steatosis formation in the early stage of NAFLD.

To understand how *Shp* disruption decreases liver steatosis in HFCF-fed mice, we conducted RNA-seq analysis of liver obtained from WT and *Shp*$^{Hep-/-}$ mice after 12 weeks on the chow or HFCF diet. WT mice displayed up-regulated *Pparg* signaling in liver after HFCF diet administration; however, this response was completely abolished in the HFCF-fed *Shp*$^{Hep-/-}$ mice (Chapter 4 part II). PPARg is highly expressed in adipose tissue but at a relative low level in normal liver (255). However, under conditions of nutrient overload such as obesity and diabetes, PPARg is quickly induced and activated in hepatocytes where it is essential for fatty acids uptake and storage as lipid droplets (256). At the molecular level, PPARg up-regulates several proteins associated with lipid uptake, storage, and formation of lipid droplets, such as fatty acid binding protein 4, Cidec, CD36, monacylglycerol O-acyltransferase 1, and perilipin 2 (257). The notion that hepatic PPARg expression promotes steatosis is supported by numerous studies which demonstrated up-regulation of PPARg in steatotic livers observed in both NAFLD animal models and NAFLD patients (197,258). It's becoming clear that the storage of excessive fatty acids as triglycerides is unlikely to be the cause of hepatocyte injury in NASH; instead, the triglyceride accumulation within hepatocytes acts as a protective mechanism against fatty acid-induced lipotoxicity (259). In support of this notion, inhibiting triglycerides synthesis improves hepatic steatosis but exacerbates liver damage and fibrosis in NASH (260). In hepatocyte-specific *Pparg* knock (*Pparg*$^{Hep-/-}$) mice, the expression of genes associated with lipid storage was down-regulated. Consequently, *Pparg*$^{Hep-/-}$ mice developed reduced liver steatosis but markedly exacerbated liver injury and fibrosis in a model of steatohepatitis (209).

In Chapter 4 part II, we observed a positive correlation between the expression of *Shp* and *Pparg* as deletion of hepatic *Shp* significantly decreased the expression of *Pparg* and its target gene, *Cd36*, in HFCF-fed mice. In addition, *Shp*$^{-/-}$ hepatocytes were resistant to oleic acid-induced steatosis; however, overexpressing PPARg largely increased lipid content in *Shp*$^{-/-}$ hepatocytes. Together, our data suggest a tight regulatory link between hepatic SHP and PPARg, and indicate that hepatic SHP, in a PPARg-dependent manner, plays an important role in hepatic steatosis.

The mechanism by which SHP regulates the expression of *Pparg* remains incompletely understood. One earlier study demonstrated that SHP increases hepatic *Pparg* gene expression through a transcriptional cascade where SHP inhibits hairy and enhancer of split 6 (*Hes6*), a transcriptional repressor that suppresses *Pparg* gene expression (212). Another study showed that in the rat immortalized HSC cell line HSC-T6, SHP is recruited to the *Pparg* gene promoter and activates *Pparg* transcription which facilitates the quiescence of HSC (261). Additionally, increasing SHP expression by 6-ethyl cheno-deoxycholic acid (INT-747) stimulates the expression and activity of *Pparg* in adipocytes (262). These data indicate that SHP is a strong transcriptional regulator of *Pparg* and multiple mechanisms may implicate in this regulation.

Interestingly, SHP deletion or overexpression after steatosis development did not affect liver lipid content (Chapter 4 part II), which is somehow unexpected since SHP is known to regulate hepatic lipid metabolism (123). It is crucial to note that hepatic SHP is a critical suppressor for bile acid synthesis through the direct regulation on *Cyp7a1* (191,242), a critical rate-limiting enzyme in bile acid synthesis (263). Accumulated evidence highlights an important role of bile acid in NAFLD. For instance, changes in bile acid synthesis and composition can alter gut microbiota, which may affect lipid metabolism and subsequent NAFLD development (264). Thus, SHP deletion or overexpression may affect bile acid synthesis, composition, and gut microbiota differently, resulting in distinct roles of SHP in different stages of NAFLD.

SHP prevents NAFLD progression though inhibiting liver inflammation and fibrosis

Another important finding from Chapter 4 part II is that the expression of hepatic SHP regulates chemokine CCL2 production from hepatocytes. Overnutrition-induced aberrant synthesis and accumulation of proinflammatory mediators within the liver is one of the major culprits for the pathogenesis of NASH (265). Particularly, an increased level of CCL2 is associated with a high risk of NASH in both animal models and humans (181). Here, we have identified that the expression of SHP in hepatocytes is essential to suppress overnutrition-induced CCL2 production. Importantly, our study demonstrates that the crosstalk between p65 and SHP in hepatocytes is one of the key events in regulating CCL2 production. On the molecular level, we have identified a novel regulatory network in hepatocytes that consists of SHP/NF-κB/CCL2 which regulates macrophage recruitment and initiation of inflammation for NAFLD progression.

Identification of this regulatory axis is important as it could shed light on our understanding of FXR, a very well-known up-stream regulator of SHP (124,266-268), in the alleviation of hepatic inflammation. FXR has been recognized as an interesting target for NAFLD treatment, and FXR agonist, obeticholic acid, has been used in NAFLD treatment (269). However, the mechanism underlying FXR-mediated inhibition of hepatic inflammation remains undetermined. Therefore, future research is warranted to determine whether the mechanism governed by SHP/NF-κB/CCL2 could contribute to FXR-mediated alleviation of hepatic inflammation in NAFLD.

Loss of hepatic SHP affects fibrogenic processes in the liver, which is another important observation from Chapter 4 part II of this dissertation. The critical anti-fibrotic role of SHP has been documented in the literature. An earlier study demonstrated that disruption of SHP exacerbates bile duct ligation (BDL)-induced cholestatic liver fibrosis (195), whereas SHP overexpression or increasing SHP expression by pharmacological compounds attenuate hepatic fibrosis induced either by hepatitis C virus infection (270) or by carbon tetrachloride and a-naphthyl-isothiocyanate (ANIT) (271). In addition, increasing *SHP* mRNA levels in hepatic stellate cells by FXR ligands abrogates thrombin and TGF-b1-induced upregulation of alpha1 collagen mRNA (272). Furthermore, SHP overexpression in hepatic stellate cells inhibits the expression of tissue metalloproteinase inhibitor 1 (Timp1) and promotes quiescent phenotype of hepatic stellate cells (273). All of these findings indicate that SHP is a critical anti-fibrotic factor in various liver diseases. Our results, obtained from hepatic *Shp* deficient and overexpressing animals, support this notion.

In summary, in this dissertation we employed a clinically relevant dietary mouse NAFLD model to investigate the role of SHP in NAFLD development. We demonstrate that disruption of hepatic *Shp* activates NF-κB signaling and impairs *Pparg* activation, leading to the dissociation of steatosis, inflammation, and fibrosis during NAFLD development. Our finding that hepatic *Shp* plays a critical role in the steatosis-to-NASH transition provides some new mechanistic insights into our understanding of NASH pathogenesis and progression and may present a new target for NASH treatment.

Chapter 7: Future Directions

The regulation between SHP and PPARg

Based upon the studies presented in this dissertation, SHP and PPARg expression in mouse hepatocytes are positively correlated. Using CV-1 and HeLa cells, Nishizawa demonstrated that SHP competes with nuclear receptor corepressor in binding to the DNA-binding domain/hinge region of *Pparg*, in a ligand-independent manner, enhancing its activity (274). Later, another study indicated that the human *SHP* promoter contains a PPAR response element to which PPARg binds and enhances *SHP* transcription (275). A very recent study investigating the anti-obesity effects of soybean in high fat diet-fed Sprague-Dawley rats supports that hepatic PPARg positively regulates *Shp* expression (276). Mechanistic studies are needed in order to elucidate 1) whether there is positive feedback regulation between hepatic SHP and PPARg in hepatocytes and 2) which factors lead to SHP recruitment to *PPARg* promoter or PPARg recruitment to *SHP* promoter.

RNA-seq of mouse NAFLD model

We have preliminarily demonstrated using RNA-seq that processes involving lipid absorption and oxidation, cell cycle, inflammation and fibrosis are aberrantly regulated in livers of 1- and 3-month HFCF-fed mice. Since the livers of 3-month HFCF-fed mice resemble the early transition from NAFL to NASH, this observation is expected. However, to gather a more detailed understanding of the mechanisms leading to NASH, RNA-seq of the livers of 5-month HFCF-fed mice must be conducted since it is the earliest time point at which NASH is diagnosed in our model.

Valuable insights have been acquired from our preliminary RNA-seq study and require further investigation. For example, we have identified two genes, FOXM1 and NELFE, which have not before been implicated in NAFLD studies. Studies have indicated that FOXM1 and NEFLE, through distinct pathways, contribute to HCC pathogenesis (219,223). As an RNA-binding protein, NELFE stabilizes the RNA molecule bound to it. Interestingly, NELFE targets detected in our analysis include important lipid-regulating genes *Ppara* and *Fasn*; however, besides a ChIP study indicating *Ppara* and *Fasn* are NELFE targets, no other associations between the targets and NELFE have been reported (277). Since PPARa plays a crucial role in fatty acid beta-oxidation and the fatty acid synthase controls a key step in *de novo* lipogenesis, studies towards identifying the role of NELFE in their regulation are needed.

The top deregulated genes identified from RNA-seq of NAFLD mouse model present interesting prospects for future studies. For example, argininosuccinate lyase (*Asl*) and energy homeostasis associated (*Enho*) are significantly downregulated in livers of 3-months HFCF-fed mice compared to the livers of 1-month HFCF-fed mice. ASL is highly expressed in liver and catalyzes the hydrolytic cleavage of argininosuccinate into arginine and fumarate, an essential step in detoxifying ammonia via the urea cycle. Deleterious mutations of *Asl* result in argininosuccinic aciduria, the second most common genetic disorder affecting the urea cycle (278). A recent study has demonstrated that dysregulation of the urea cycle occurs in both a rat NAFLD model and NAFLD patients (279). Urea dysregulation can lead to the accumulation of ammonia, a condition called hyperammonemia which can lead to scar tissue development and increase the risk of NAFLD progression (279). Because of this, further studies toward understanding the role of *Asl* and related urea cycle in NAFLD progression are needed.

Enho, another top downregulated gene in the livers of 3-month HFCF-fed mice compared to the livers of 1-month HFCF-fed mice, encodes the secretory signal peptide adropin. Adropin is involved in the regulation of glucose homeostasis and lipid metabolism (280). Studies investigating blood levels of adropin in humans have observed inverse associations of adropin concentrations with carbohydrate consumption (281,282), insulin resistance (283,284) and risk of NAFLD (285,286). Supporting our data is a study which demonstrated that liver ENHO levels are negatively correlated with time on a high-fat diet (287). Overexpressing ENHO or systemic delivery of pharmacological adropin into diet-induced obesity mice can attenuate hepatosteatosis and enhance glucose tolerance (287). Future studies will focus on understanding how *Enho* expression is decreased during NAFL transition to NASH and exploring whether increasing *Enho* levels could be effective for NASH prevention and treatment.

Immune cell functions in NAFLD

We have indicated that macrophages play an important role in inflammation in NASH development. However, during NASH, extrahepatic immune cells infiltrate the liver and exacerbate NASH progression. For example, neutrophil infiltration into the liver helps to clear pathogens but may also enhance macrophage cytotoxicity and exacerbate the inflammatory state (288). In addition, the involvement of adaptive immunity in stimulating adipose tissue inflammation in obesity demonstrated that in the initial phase, the fat-resident macrophages secrete chemokines, which recruit $CD4^+$/$CD8^+$ T lymphocytes and natural killer T cells to the adipose tissue. This, in turn, enhances macrophage activation and proinflammatory mediator release (289). Similarly, in the initiation of inflammation in NASH pathogenesis, one study showed that both macrophages and lymphocytes represent the most frequent inflammatory infiltrates of NASH liver (290). Overall, involvement of adaptive immunity in the processes driving NASH evolution makes T and B cells attractive therapeutic targets for NASH prevention and treatment. Further studies are required to better understand the interaction between innate and adaptive immunity in sustaining hepatic inflammation and promoting fibrosis in NASH. Additionally, since immune cells can secrete profibrogenic factors, further investigation on immune cell to HSC communication are encourages. The studies presented in this dissertation are hepatocyte-centered though we demonstrate the presence of fibrosis within our NAFLD model and $Shp^{Hep-/-}$ models. Based on the literature presented here, further investigations into HSC activation within our animal models are warranted. Of priority are verifying the timepoint at which HSCs switch from quiescent to active in our NAFLD model.

Crosstalk between organs in NAFLD

The studies in this dissertation reveal the nature of the disease as it pertains to the liver since our aims included developing a mouse NAFLD model, uncovering a mechanism behind hepatic steatosis and inflammation, and identifying novel transcriptomic changes in our mouse NAFLD model. However, it is understood that NAFLD is a multisystem disease (291,292); therefore, research using NAFLD models must include a comprehensive examination of all organ systems involved in the disease process. Doing so will provide a more accurate and realistic look at the phenomena occurring during the disease process and provide new approaches for NAFLD reversal or amelioration. For instance, inflammatory mediators released from extra-hepatic organs such as gut and adipose tissue have been implicated in NASH pathogenesis (293). In particular, many pathogenic factors, such as endotoxins resulted from increased gut permeability and dysbiosis, adipokines secreted from adipose tissue, are all considered crucial to the pathogenesis of NASH (294). Currently, several studies have linked NAFLD development and progression to diseases such as type II diabetes mellitus (T2DM), cardiovascular disease (CVD) and chronic kidney disease (CKD). Therefore, further investigations into the contribution of interorgan crosstalk in NASH pathogenesis and pre-dispositions to CVD, CKD, or T2DM using our mouse NAFLD model are warranted.

References

1. Kirpich, I. A., Gobejishvili, L. N., Bon Homme, M., Waigel, S., Cave, M., Arteel, G., Barve, S. S., McClain, C. J., and Deaciuc, I. V. (2011) Integrated hepatic transcriptome and proteome analysis of mice with high-fat diet-induced nonalcoholic fatty liver disease. *J Nutr Biochem* **22**, 38-45
2. Uppal, V., Mansoor, S., and Furuya, K. N. (2016) Pediatric Non-alcoholic Fatty Liver Disease. *Current gastroenterology reports* **18**, 24
3. Younossi, Z. M., Golabi, P., de Avila, L., Paik, J. M., Srishord, M., Fukui, N., Qiu, Y., Burns, L., Afendy, A., and Nader, F. (2019) The global epidemiology of NAFLD and NASH in patients with type 2 diabetes: A systematic review and meta-analysis. *Journal of hepatology* **71**, 793-801
4. Chalasani, N., Younossi, Z., Lavine, J. E., Diehl, A. M., Brunt, E. M., Cusi, K., Charlton, M., and Sanyal, A. J. (2012) The diagnosis and management of non-alcoholic fatty liver disease: practice Guideline by the American Association for the Study of Liver Diseases, American College of Gastroenterology, and the American Gastroenterological Association. *Hepatology* **55**, 2005-2023
5. Younossi, Z. M., Koenig, A. B., Abdelatif, D., Fazel, Y., Henry, L., and Wymer, M. (2016) Global epidemiology of nonalcoholic fatty liver disease-Meta-analytic assessment of prevalence, incidence, and outcomes. *Hepatology* **64**, 73-84
6. Arab, J. P., Arrese, M., and Trauner, M. (2018) Recent Insights into the Pathogenesis of Nonalcoholic Fatty Liver Disease. *Annu Rev Pathol* **13**, 321-350
7. Eslam, M., and George, J. (2020) Genetic contributions to NAFLD: leveraging shared genetics to uncover systems biology. *Nature reviews. Gastroenterology & hepatology* **17**, 40-52
8. Sutti, S., and Albano, E. (2020) Adaptive immunity: an emerging player in the progression of NAFLD. *Nature reviews. Gastroenterology & hepatology* **17**, 81-92
9. Ganz, M., and Szabo, G. (2013) Immune and inflammatory pathways in NASH. *Hepatol Int* **7 Suppl 2**, 771-781
10. Lebensztejn, D. M., Flisiak-Jackiewicz, M., Bialokoz-Kalinowska, I., Bobrus-Chociej, A., and Kowalska, I. (2016) Hepatokines and non-alcoholic fatty liver disease. *Acta biochimica Polonica* **63**
11. Safari, Z., and Gerard, P. (2019) The links between the gut microbiome and non-alcoholic fatty liver disease (NAFLD). *Cell Mol Life Sci* **76**, 1541-1558
12. Lombardi, R., Fargion, S., and Fracanzani, A. L. (2019) Brain involvement in non-alcoholic fatty liver disease (NAFLD): A systematic review. *Dig Liver Dis* **51**, 1214-1222
13. Watt, M. J., Miotto, P. M., De Nardo, W., and Montgomery, M. K. (2019) The Liver as an Endocrine Organ-Linking NAFLD and Insulin Resistance. *Endocr Rev* **40**, 1367-1393
14. McPherson, S., Hardy, T., Henderson, E., Burt, A. D., Day, C. P., and Anstee, Q. M. (2015) Evidence of NAFLD progression from steatosis to fibrosing-steatohepatitis using paired biopsies: implications for prognosis and clinical management. *Journal of hepatology* **62**, 1148-1155

15. Ibrahim, S. H., Hirsova, P., and Gores, G. J. (2018) Non-alcoholic steatohepatitis pathogenesis: sublethal hepatocyte injury as a driver of liver inflammation. *Gut* **67**, 963-972
16. Cha, J. Y., Kim, D. H., and Chun, K. H. (2018) The role of hepatic macrophages in nonalcoholic fatty liver disease and nonalcoholic steatohepatitis. *Lab Anim Res* **34**, 133-139
17. Ore, A., and Akinloye, O. A. (2019) Oxidative Stress and Antioxidant Biomarkers in Clinical and Experimental Models of Non-Alcoholic Fatty Liver Disease. *Medicina (Kaunas)* **55**, 26
18. Yang, J., Fernandez-Galilea, M., Martinez-Fernandez, L., Gonzalez-Muniesa, P., Perez-Chavez, A., Martinez, J. A., and Moreno-Aliaga, M. J. (2019) Oxidative Stress and Non-Alcoholic Fatty Liver Disease: Effects of Omega-3 Fatty Acid Supplementation. *Nutrients* **11**, 872
19. Adolph, T. E., Grander, C., Grabherr, F., and Tilg, H. (2017) Adipokines and Non-Alcoholic Fatty Liver Disease: Multiple Interactions. *Int J Mol Sci* **18**, 1649
20. Grabherr, F., Grander, C., Effenberger, M., Adolph, T. E., and Tilg, H. (2019) Gut Dysfunction and Non-alcoholic Fatty Liver Disease. *Front Endocrinol (Lausanne)* **10**, 611
21. Kosmalski, M., Mokros, L., Kuna, P., Witusik, A., and Pietras, T. (2018) Changes in the immune system - the key to diagnostics and therapy of patients with non-alcoholic fatty liver disease. *Cent Eur J Immunol* **43**, 231-239
22. Day, C. P., and James, O. F. (1998) Steatohepatitis: a tale of two "hits"? *Gastroenterology* **114**, 842-845
23. Zhan, Y. T., and An, W. (2010) Roles of liver innate immune cells in nonalcoholic fatty liver disease. *World J Gastroenterol* **16**, 4652-4660
24. Peverill, W., Powell, L. W., and Skoien, R. (2014) Evolving concepts in the pathogenesis of NASH: beyond steatosis and inflammation. *Int J Mol Sci* **15**, 8591-8638
25. Friedman, S. L. (2013) Liver fibrosis in 2012: Convergent pathways that cause hepatic fibrosis in NASH. *Nature reviews. Gastroenterology & hepatology* **10**, 71-72
26. Jou, J., Choi, S. S., and Diehl, A. M. (2008) Mechanisms of disease progression in nonalcoholic fatty liver disease. *Semin Liver Dis* **28**, 370-379
27. Buzzetti, E., Pinzani, M., and Tsochatzis, E. A. (2016) The multiple-hit pathogenesis of non-alcoholic fatty liver disease (NAFLD). *Metabolism* **65**, 1038-1048
28. Fang, Y. L., Chen, H., Wang, C. L., and Liang, L. (2018) Pathogenesis of non-alcoholic fatty liver disease in children and adolescence: From "two hit theory" to "multiple hit model". *World J Gastroenterol* **24**, 2974-2983
29. Brunt, E. M., Kleiner, D. E., Wilson, L. A., Belt, P., Neuschwander-Tetri, B. A., and Network, N. C. R. (2011) Nonalcoholic fatty liver disease (NAFLD) activity score and the histopathologic diagnosis in NAFLD: distinct clinicopathologic meanings. *Hepatology* **53**, 810-820
30. Liu, J., Han, L., Zhu, L., and Yu, Y. (2016) Free fatty acids, not triglycerides, are associated with non-alcoholic liver injury progression in high fat diet induced obese rats. *Lipids Health Dis* **15**, 27

31. Li, Z. Z., Berk, M., McIntyre, T. M., and Feldstein, A. E. (2009) Hepatic lipid partitioning and liver damage in nonalcoholic fatty liver disease: role of stearoyl-CoA desaturase. *The Journal of biological chemistry* **284**, 5637-5644
32. Swiderska, M., Maciejczyk, M., Zalewska, A., Pogorzelska, J., Flisiak, R., and Chabowski, A. (2019) Oxidative stress biomarkers in the serum and plasma of patients with non-alcoholic fatty liver disease (NAFLD). Can plasma AGE be a marker of NAFLD? Oxidative stress biomarkers in NAFLD patients. *Free Radic Res* **53**, 841-850
33. Nobili, V., Parola, M., Alisi, A., Marra, F., Piemonte, F., Mombello, C., Sutti, S., Povero, D., Maina, V., Novo, E., and Albano, E. (2010) Oxidative stress parameters in paediatric non-alcoholic fatty liver disease. *Int J Mol Med* **26**, 471-476
34. Haghi Aminjan, H., Abtahi, S. R., Hazrati, E., Chamanara, M., Jalili, M., and Paknejad, B. (2019) Targeting of oxidative stress and inflammation through ROS/NF-kappaB pathway in phosphine-induced hepatotoxicity mitigation. *Life Sci* **232**, 116607
35. Arkan, M. C., Hevener, A. L., Greten, F. R., Maeda, S., Li, Z. W., Long, J. M., Wynshaw-Boris, A., Poli, G., Olefsky, J., and Karin, M. (2005) IKK-beta links inflammation to obesity-induced insulin resistance. *Nat Med* **11**, 191-198
36. Li, X. H., McGrath, K. C., Nammi, S., Heather, A. K., and Roufogalis, B. D. (2012) Attenuation of liver pro-inflammatory responses by Zingiber officinale via inhibition of NF-kappa B activation in high-fat diet-fed rats. *Basic Clin Pharmacol Toxicol* **110**, 238-244
37. Chaisson, M. L., Brooling, J. T., Ladiges, W., Tsai, S., and Fausto, N. (2002) Hepatocyte-specific inhibition of NF-kappaB leads to apoptosis after TNF treatment, but not after partial hepatectomy. *J Clin Invest* **110**, 193-202
38. Zhang, X. Q., Xu, C. F., Yu, C. H., Chen, W. X., and Li, Y. M. (2014) Role of endoplasmic reticulum stress in the pathogenesis of nonalcoholic fatty liver disease. *World J Gastroenterol* **20**, 1768-1776
39. Lake, A. D., Novak, P., Hardwick, R. N., Flores-Keown, B., Zhao, F., Klimecki, W. T., and Cherrington, N. J. (2014) The adaptive endoplasmic reticulum stress response to lipotoxicity in progressive human nonalcoholic fatty liver disease. *Toxicol Sci* **137**, 26-35
40. Brenner, C., Galluzzi, L., Kepp, O., and Kroemer, G. (2013) Decoding cell death signals in liver inflammation. *Journal of hepatology* **59**, 583-594
41. Meakin, P. J., Chowdhry, S., Sharma, R. S., Ashford, F. B., Walsh, S. V., McCrimmon, R. J., Dinkova-Kostova, A. T., Dillon, J. F., Hayes, J. D., and Ashford, M. L. (2014) Susceptibility of Nrf2-null mice to steatohepatitis and cirrhosis upon consumption of a high-fat diet is associated with oxidative stress, perturbation of the unfolded protein response, and disturbance in the expression of metabolic enzymes but not with insulin resistance. *Molecular and cellular biology* **34**, 3305-3320
42. Kandel-Kfir, M., Almog, T., Shaish, A., Shlomai, G., Anafi, L., Avivi, C., Barshack, I., Grosskopf, I., Harats, D., and Kamari, Y. (2015) Interleukin-1alpha deficiency attenuates endoplasmic reticulum stress-induced liver damage and CHOP expression in mice. *Journal of hepatology* **63**, 926-933

43. Salomone, F., Godos, J., and Zelber-Sagi, S. (2016) Natural antioxidants for non-alcoholic fatty liver disease: molecular targets and clinical perspectives. *Liver Int* **36**, 5-20
44. Vonghia, L., Michielsen, P., and Francque, S. (2013) Immunological mechanisms in the pathophysiology of non-alcoholic steatohepatitis. *Int J Mol Sci* **14**, 19867-19890
45. Wan, X., Xu, C., Yu, C., and Li, Y. (2016) Role of NLRP3 Inflammasome in the Progression of NAFLD to NASH. *Canadian journal of gastroenterology & hepatology* **2016**, 6489012
46. Gadd, V. L., Skoien, R., Powell, E. E., Fagan, K. J., Winterford, C., Horsfall, L., Irvine, K., and Clouston, A. D. (2014) The portal inflammatory infiltrate and ductular reaction in human nonalcoholic fatty liver disease. *Hepatology* **59**, 1393-1405
47. Bieghs, V., and Trautwein, C. (2013) The innate immune response during liver inflammation and metabolic disease. *Trends Immunol* **34**, 446-452
48. Szymanska, R., and Schmidt-Pospula, M. (1979) [Studies of liver's reticuloendothelial cells by Tadeusz Browicz and Karl Kupffer. A historical outline]. *Arch Hist Med (Warsz)* **42**, 331-336
49. Srodka, A., Gryglewski, R. W., and Szczepariski, W. (2006) Browicz or Kupffer cells? *Pol J Pathol* **57**, 183-185
50. Tacke, F., and Zimmermann, H. W. (2014) Macrophage heterogeneity in liver injury and fibrosis. *Journal of hepatology* **60**, 1090-1096
51. Kazankov, K., Jorgensen, S. M. D., Thomsen, K. L., Moller, H. J., Vilstrup, H., George, J., Schuppan, D., and Gronbaek, H. (2019) The role of macrophages in nonalcoholic fatty liver disease and nonalcoholic steatohepatitis. *Nature reviews. Gastroenterology & hepatology* **16**, 145-159
52. Krenkel, O., and Tacke, F. (2017) Liver macrophages in tissue homeostasis and disease. *Nat Rev Immunol* **17**, 306-321
53. Mouzaki, M., Comelli, E. M., Arendt, B. M., Bonengel, J., Fung, S. K., Fischer, S. E., McGilvray, I. D., and Allard, J. P. (2013) Intestinal microbiota in patients with nonalcoholic fatty liver disease. *Hepatology* **58**, 120-127
54. Henao-Mejia, J., Elinav, E., Jin, C., Hao, L., Mehal, W. Z., Strowig, T., Thaiss, C. A., Kau, A. L., Eisenbarth, S. C., Jurczak, M. J., Camporez, J. P., Shulman, G. I., Gordon, J. I., Hoffman, H. M., and Flavell, R. A. (2012) Inflammasome-mediated dysbiosis regulates progression of NAFLD and obesity. *Nature* **482**, 179-185
55. Schaffert, C. S., Duryee, M. J., Hunter, C. D., Hamilton, B. C., 3rd, DeVeney, A. L., Huerter, M. M., Klassen, L. W., and Thiele, G. M. (2009) Alcohol metabolites and lipopolysaccharide: roles in the development and/or progression of alcoholic liver disease. *World J Gastroenterol* **15**, 1209-1218
56. Zhu, L., Baker, S. S., Gill, C., Liu, W., Alkhouri, R., Baker, R. D., and Gill, S. R. (2013) Characterization of gut microbiomes in nonalcoholic steatohepatitis (NASH) patients: a connection between endogenous alcohol and NASH. *Hepatology* **57**, 601-609
57. Bieghs, V., Rensen, P. C., Hofker, M. H., and Shiri-Sverdlov, R. (2012) NASH and atherosclerosis are two aspects of a shared disease: central role for macrophages. *Atherosclerosis* **220**, 287-293

58. Italiani, P., and Boraschi, D. (2014) From Monocytes to M1/M2 Macrophages: Phenotypical vs. Functional Differentiation. *Frontiers in immunology* **5**, 514
59. Wan, J., Benkdane, M., Teixeira-Clerc, F., Bonnafous, S., Louvet, A., Lafdil, F., Pecker, F., Tran, A., Gual, P., Mallat, A., Lotersztajn, S., and Pavoine, C. (2014) M2 Kupffer cells promote M1 Kupffer cell apoptosis: a protective mechanism against alcoholic and nonalcoholic fatty liver disease. *Hepatology* **59**, 130-142
60. Sica, A., and Mantovani, A. (2012) Macrophage plasticity and polarization: in vivo veritas. *J Clin Invest* **122**, 787-795
61. Xiu, F., Catapano, M., Diao, L., Stanojcic, M., and Jeschke, M. G. (2015) Prolonged Endoplasmic Reticulum-Stressed Hepatocytes Drive an Alternative Macrophage Polarization. *Shock* **44**, 44-51
62. Wenfeng, Z., Yakun, W., Di, M., Jianping, G., Chuanxin, W., and Chun, H. (2014) Kupffer cells: increasingly significant role in nonalcoholic fatty liver disease. *Ann Hepatol* **13**, 489-495
63. Eguchi, A., Wree, A., and Feldstein, A. E. (2014) Biomarkers of liver cell death. *Journal of hepatology* **60**, 1063-1074
64. Kolios, G., Valatas, V., and Kouroumalis, E. (2006) Role of Kupffer cells in the pathogenesis of liver disease. *World J Gastroenterol* **12**, 7413-7420
65. Huang, W., Metlakunta, A., Dedousis, N., Zhang, P., Sipula, I., Dube, J. J., Scott, D. K., and O'Doherty, R. M. (2010) Depletion of liver Kupffer cells prevents the development of diet-induced hepatic steatosis and insulin resistance. *Diabetes* **59**, 347-357
66. Sharifnia, T., Antoun, J., Verriere, T. G., Suarez, G., Wattacheril, J., Wilson, K. T., Peek, R. M., Jr., Abumrad, N. N., and Flynn, C. R. (2015) Hepatic TLR4 signaling in obese NAFLD. *Am J Physiol Gastrointest Liver Physiol* **309**, G270-278
67. Walenbergh, S. M., Koek, G. H., Bieghs, V., and Shiri-Sverdlov, R. (2013) Non-alcoholic steatohepatitis: the role of oxidized low-density lipoproteins. *Journal of hepatology* **58**, 801-810
68. Bieghs, V., Verheyen, F., van Gorp, P. J., Hendrikx, T., Wouters, K., Lutjohann, D., Gijbels, M. J., Febbraio, M., Binder, C. J., Hofker, M. H., and Shiri-Sverdlov, R. (2012) Internalization of modified lipids by CD36 and SR-A leads to hepatic inflammation and lysosomal cholesterol storage in Kupffer cells. *PLoS One* **7**, e34378
69. Bieghs, V., van Gorp, P. J., Walenbergh, S. M., Gijbels, M. J., Verheyen, F., Buurman, W. A., Briles, D. E., Hofker, M. H., Binder, C. J., and Shiri-Sverdlov, R. (2012) Specific immunization strategies against oxidized low-density lipoprotein: a novel way to reduce nonalcoholic steatohepatitis in mice. *Hepatology* **56**, 894-903
70. Rensen, S. S., Slaats, Y., Nijhuis, J., Jans, A., Bieghs, V., Driessen, A., Malle, E., Greve, J. W., and Buurman, W. A. (2009) Increased hepatic myeloperoxidase activity in obese subjects with nonalcoholic steatohepatitis. *Am J Pathol* **175**, 1473-1482
71. Alkhouri, N., Morris-Stiff, G., Campbell, C., Lopez, R., Tamimi, T. A., Yerian, L., Zein, N. N., and Feldstein, A. E. (2012) Neutrophil to lymphocyte ratio: a new marker for predicting steatohepatitis and fibrosis in patients with nonalcoholic fatty liver disease. *Liver Int* **32**, 297-302

72. Ibusuki, R., Uto, H., Arima, S., Mawatari, S., Setoguchi, Y., Iwashita, Y., Hashimoto, S., Maeda, T., Tanoue, S., Kanmura, S., Oketani, M., Ido, A., and Tsubouchi, H. (2013) Transgenic expression of human neutrophil peptide-1 enhances hepatic fibrosis in mice fed a choline-deficient, L-amino acid-defined diet. *Liver Int* **33**, 1549-1556
73. Talukdar, S., Oh da, Y., Bandyopadhyay, G., Li, D., Xu, J., McNelis, J., Lu, M., Li, P., Yan, Q., Zhu, Y., Ofrecio, J., Lin, M., Brenner, M. B., and Olefsky, J. M. (2012) Neutrophils mediate insulin resistance in mice fed a high-fat diet through secreted elastase. *Nat Med* **18**, 1407-1412
74. Meli, R., Mattace Raso, G., and Calignano, A. (2014) Role of innate immune response in non-alcoholic Fatty liver disease: metabolic complications and therapeutic tools. *Frontiers in immunology* **5**, 177
75. Romagnani, S. (1991) Type 1 T helper and type 2 T helper cells: functions, regulation and role in protection and disease. *International journal of clinical & laboratory research* **21**, 152-158
76. Henning, J. R., Graffeo, C. S., Rehman, A., Fallon, N. C., Zambirinis, C. P., Ochi, A., Barilla, R., Jamal, M., Deutsch, M., Greco, S., Ego-Osuala, M., Bin-Saeed, U., Rao, R. S., Badar, S., Quesada, J. P., Acehan, D., and Miller, G. (2013) Dendritic cells limit fibroinflammatory injury in nonalcoholic steatohepatitis in mice. *Hepatology* **58**, 589-602
77. Tang, Y., Bian, Z., Zhao, L., Liu, Y., Liang, S., Wang, Q., Han, X., Peng, Y., Chen, X., Shen, L., Qiu, D., Li, Z., and Ma, X. (2011) Interleukin-17 exacerbates hepatic steatosis and inflammation in non-alcoholic fatty liver disease. *Clinical and experimental immunology* **166**, 281-290
78. Harley, I. T., Stankiewicz, T. E., Giles, D. A., Softic, S., Flick, L. M., Cappelletti, M., Sheridan, R., Xanthakos, S. A., Steinbrecher, K. A., Sartor, R. B., Kohli, R., Karp, C. L., and Divanovic, S. (2014) IL-17 signaling accelerates the progression of nonalcoholic fatty liver disease in mice. *Hepatology* **59**, 1830-1839
79. Rau, M., Schilling, A. K., Meertens, J., Hering, I., Weiss, J., Jurowich, C., Kudlich, T., Hermanns, H. M., Bantel, H., Beyersdorf, N., and Geier, A. (2016) Progression from Nonalcoholic Fatty Liver to Nonalcoholic Steatohepatitis Is Marked by a Higher Frequency of Th17 Cells in the Liver and an Increased Th17/Resting Regulatory T Cell Ratio in Peripheral Blood and in the Liver. *J Immunol* **196**, 97-105
80. Winer, D. A., Winer, S., Chng, M. H., Shen, L., and Engleman, E. G. (2014) B Lymphocytes in obesity-related adipose tissue inflammation and insulin resistance. *Cell Mol Life Sci* **71**, 1033-1043
81. Sutti, S., Jindal, A., Locatelli, I., Vacchiano, M., Gigliotti, L., Bozzola, C., and Albano, E. (2014) Adaptive immune responses triggered by oxidative stress contribute to hepatic inflammation in NASH. *Hepatology* **59**, 886-897
82. Albano, E., Mottaran, E., Vidali, M., Reale, E., Saksena, S., Occhino, G., Burt, A. D., and Day, C. P. (2005) Immune response towards lipid peroxidation products as a predictor of progression of non-alcoholic fatty liver disease to advanced fibrosis. *Gut* **54**, 987-993
83. Winer, D. A., Winer, S., Shen, L., Wadia, P. P., Yantha, J., Paltser, G., Tsui, H., Wu, P., Davidson, M. G., Alonso, M. N., Leong, H. X., Glassford, A., Caimol, M.,

Kenkel, J. A., Tedder, T. F., McLaughlin, T., Miklos, D. B., Dosch, H. M., and Engleman, E. G. (2011) B cells promote insulin resistance through modulation of T cells and production of pathogenic IgG antibodies. *Nat Med* **17**, 610-617
84. Ng, L. G., Sutherland, A. P., Newton, R., Qian, F., Cachero, T. G., Scott, M. L., Thompson, J. S., Wheway, J., Chtanova, T., Groom, J., Sutton, I. J., Xin, C., Tangye, S. G., Kalled, S. L., Mackay, F., and Mackay, C. R. (2004) B cell-activating factor belonging to the TNF family (BAFF)-R is the principal BAFF receptor facilitating BAFF costimulation of circulating T and B cells. *J Immunol* **173**, 807-817
85. Kawasaki, K., Abe, M., Tada, F., Tokumoto, Y., Chen, S., Miyake, T., Furukawa, S., Matsuura, B., Hiasa, Y., and Onji, M. (2013) Blockade of B-cell-activating factor signaling enhances hepatic steatosis induced by a high-fat diet and improves insulin sensitivity. *Laboratory investigation; a journal of technical methods and pathology* **93**, 311-321
86. Kim, D. H., and Do, M. S. (2015) BAFF knockout improves systemic inflammation via regulating adipose tissue distribution in high-fat diet-induced obesity. *Exp Mol Med* **47**, e129
87. Bhattacharjee, J., Kumar, J. M., Arindkar, S., Das, B., Pramod, U., Juyal, R. C., Majumdar, S. S., and Nagarajan, P. (2014) Role of immunodeficient animal models in the development of fructose induced NAFLD. *J Nutr Biochem* **25**, 219-226
88. Szabo, G., and Csak, T. (2012) Inflammasomes in liver diseases. *Journal of hepatology* **57**, 642-654
89. Csak, T., Ganz, M., Pespisa, J., Kodys, K., Dolganiuc, A., and Szabo, G. (2011) Fatty acid and endotoxin activate inflammasomes in mouse hepatocytes that release danger signals to stimulate immune cells. *Hepatology* **54**, 133-144
90. Wree, A., McGeough, M. D., Pena, C. A., Schlattjan, M., Li, H., Inzaugarat, M. E., Messer, K., Canbay, A., Hoffman, H. M., and Feldstein, A. E. (2014) NLRP3 inflammasome activation is required for fibrosis development in NAFLD. *J Mol Med (Berl)* **92**, 1069-1082
91. Kamari, Y., Shaish, A., Vax, E., Shemesh, S., Kandel-Kfir, M., Arbel, Y., Olteanu, S., Barshack, I., Dotan, S., Voronov, E., Dinarello, C. A., Apte, R. N., and Harats, D. (2011) Lack of interleukin-1alpha or interleukin-1beta inhibits transformation of steatosis to steatohepatitis and liver fibrosis in hypercholesterolemic mice. *Journal of hepatology* **55**, 1086-1094
92. Dixon, L. J., Berk, M., Thapaliya, S., Papouchado, B. G., and Feldstein, A. E. (2012) Caspase-1-mediated regulation of fibrogenesis in diet-induced steatohepatitis. *Laboratory investigation; a journal of technical methods and pathology* **92**, 713-723
93. Bataller, R., and Brenner, D. A. (2005) Liver fibrosis. *J Clin Invest* **115**, 209-218
94. Kawada, N. (2015) Cytoglobin as a Marker of Hepatic Stellate Cell-derived Myofibroblasts. *Frontiers in physiology* **6**, 329
95. Safadi, R., and Friedman, S. L. (2002) Hepatic fibrosis--role of hepatic stellate cell activation. *MedGenMed* **4**, 27
96. Ramadori, G., and Saile, B. (2004) Portal tract fibrogenesis in the liver. *Laboratory investigation; a journal of technical methods and pathology* **84**, 153-159

97. Gressner, A. M., and Weiskirchen, R. (2006) Modern pathogenetic concepts of liver fibrosis suggest stellate cells and TGF-beta as major players and therapeutic targets. *J Cell Mol Med* **10**, 76-99
98. Wobser, H., Dorn, C., Weiss, T. S., Amann, T., Bollheimer, C., Buttner, R., Scholmerich, J., and Hellerbrand, C. (2009) Lipid accumulation in hepatocytes induces fibrogenic activation of hepatic stellate cells. *Cell Res* **19**, 996-1005
99. Moreira, R. K. (2007) Hepatic stellate cells and liver fibrosis. *Arch Pathol Lab Med* **131**, 1728-1734
100. Kobold, D., Grundmann, A., Piscaglia, F., Eisenbach, C., Neubauer, K., Steffgen, J., Ramadori, G., and Knittel, T. (2002) Expression of reelin in hepatic stellate cells and during hepatic tissue repair: a novel marker for the differentiation of HSC from other liver myofibroblasts. *Journal of hepatology* **36**, 607-613
101. Dranoff, J. A., Kruglov, E. A., Robson, S. C., Braun, N., Zimmermann, H., and Sevigny, J. (2002) The ecto-nucleoside triphosphate diphosphohydrolase NTPDase2/CD39L1 is expressed in a novel functional compartment within the liver. *Hepatology* **36**, 1135-1144
102. Elpek, G. O. (2014) Cellular and molecular mechanisms in the pathogenesis of liver fibrosis: An update. *World J Gastroenterol* **20**, 7260-7276
103. Bieging, K. T., Fish, K., Bondada, S., and Longnecker, R. (2011) A shared gene expression signature in mouse models of EBV-associated and non-EBV-associated Burkitt lymphoma. *Blood* **118**, 6849-6859
104. Wanninger, J., Neumeier, M., Hellerbrand, C., Schacherer, D., Bauer, S., Weiss, T. S., Huber, H., Schaffler, A., Aslanidis, C., Scholmerich, J., and Buechler, C. (2011) Lipid accumulation impairs adiponectin-mediated induction of activin A by increasing TGFbeta in primary human hepatocytes. *Biochim Biophys Acta* **1811**, 626-633
105. Bansal, R., van Baarlen, J., Storm, G., and Prakash, J. (2015) The interplay of the Notch signaling in hepatic stellate cells and macrophages determines the fate of liver fibrogenesis. *Scientific reports* **5**, 18272
106. Schnabl, B., Bradham, C. A., Bennett, B. L., Manning, A. M., Stefanovic, B., and Brenner, D. A. (2001) TAK1/JNK and p38 have opposite effects on rat hepatic stellate cells. *Hepatology* **34**, 953-963
107. Borthwick, L. A., and Mann, D. A. (2016) Liver: Osteopontin and HMGB1: novel regulators of HSC activation. *Nature reviews. Gastroenterology & hepatology*
108. Guy, C. D., Suzuki, A., Zdanowicz, M., Abdelmalek, M. F., Burchette, J., Unalp, A., Diehl, A. M., and Nash, C. R. N. (2012) Hedgehog pathway activation parallels histologic severity of injury and fibrosis in human nonalcoholic fatty liver disease. *Hepatology* **55**, 1711-1721
109. Kim, K., Kim, K. H., Cho, H. K., Kim, H. Y., Kim, H. H., and Cheong, J. (2010) SHP (small heterodimer partner) suppresses the transcriptional activity and nuclear localization of Hedgehog signalling protein Gli1. *Biochem J* **427**, 413-422
110. Lambert, S. A., Jolma, A., Campitelli, L. F., Das, P. K., Yin, Y., Albu, M., Chen, X., Taipale, J., Hughes, T. R., and Weirauch, M. T. (2018) The Human Transcription Factors. *Cell* **172**, 650-665

111. Vaquerizas, J. M., Kummerfeld, S. K., Teichmann, S. A., and Luscombe, N. M. (2009) A census of human transcription factors: function, expression and evolution. *Nat Rev Genet* **10**, 252-263
112. Lee, T. I., and Young, R. A. (2013) Transcriptional regulation and its misregulation in disease. *Cell* **152**, 1237-1251
113. Mazaira, G. I., Zgajnar, N. R., Lotufo, C. M., Daneri-Becerra, C., Sivils, J. C., Soto, O. B., Cox, M. B., and Galigniana, M. D. (2018) The Nuclear Receptor Field: A Historical Overview and Future Challenges. *Nuclear receptor research* **5**
114. Penvose, A., Keenan, J. L., Bray, D., Ramlall, V., and Siggers, T. (2019) Comprehensive study of nuclear receptor DNA binding provides a revised framework for understanding receptor specificity. *Nat Commun* **10**, 2514
115. Weikum, E. R., Liu, X., and Ortlund, E. A. (2018) The nuclear receptor superfamily: A structural perspective. *Protein Sci* **27**, 1876-1892
116. Tanaka, N., Aoyama, T., Kimura, S., and Gonzalez, F. J. (2017) Targeting nuclear receptors for the treatment of fatty liver disease. *Pharmacol Ther* **179**, 142-157
117. O'Malley, B. W., and Tsai, M. J. (1992) Molecular pathways of steroid receptor action. *Biol Reprod* **46**, 163-167
118. Mangelsdorf, D. J., Thummel, C., Beato, M., Herrlich, P., Schutz, G., Umesono, K., Blumberg, B., Kastner, P., Mark, M., Chambon, P., and Evans, R. M. (1995) The nuclear receptor superfamily: the second decade. *Cell* **83**, 835-839
119. Peters, J. M., Hollingshead, H. E., and Gonzalez, F. J. (2008) Role of peroxisome-proliferator-activated receptor beta/delta (PPARbeta/delta) in gastrointestinal tract function and disease. *Clinical science* **115**, 107-127
120. Repa, J. J., Liang, G., Ou, J., Bashmakov, Y., Lobaccaro, J. M., Shimomura, I., Shan, B., Brown, M. S., Goldstein, J. L., and Mangelsdorf, D. J. (2000) Regulation of mouse sterol regulatory element-binding protein-1c gene (SREBP-1c) by oxysterol receptors, LXRalpha and LXRbeta. *Genes & development* **14**, 2819-2830
121. Yoshikawa, T., Ide, T., Shimano, H., Yahagi, N., Amemiya-Kudo, M., Matsuzaka, T., Yatoh, S., Kitamine, T., Okazaki, H., Tamura, Y., Sekiya, M., Takahashi, A., Hasty, A. H., Sato, R., Sone, H., Osuga, J., Ishibashi, S., and Yamada, N. (2003) Cross-talk between peroxisome proliferator-activated receptor (PPAR) alpha and liver X receptor (LXR) in nutritional regulation of fatty acid metabolism. I. PPARs suppress sterol regulatory element binding protein-1c promoter through inhibition of LXR signaling. *Mol Endocrinol* **17**, 1240-1254
122. Evans, R. M., and Mangelsdorf, D. J. (2014) Nuclear Receptors, RXR, and the Big Bang. *Cell* **157**, 255-266
123. Zhang, Y., Hagedorn, C. H., and Wang, L. (2011) Role of nuclear receptor SHP in metabolism and cancer. *Biochim Biophys Acta* **1812**, 893-908
124. Zou, A., Lehn, S., Magee, N., and Zhang, Y. (2015) New Insights into Orphan Nuclear Receptor SHP in Liver Cancer. *Nuclear receptor research* **2**, 101162
125. Zou, A., Magee, N., Deng, F., Lehn, S., Zhong, C., and Zhang, Y. (2018) Hepatocyte nuclear receptor SHP suppresses inflammation and fibrosis in a mouse model of nonalcoholic steatohepatitis. *The Journal of biological chemistry* **293**, 8656-8671

126. Dajani, A., and AbuHammour, A. (2016) Treatment of nonalcoholic fatty liver disease: Where do we stand? an overview. *Saudi journal of gastroenterology : official journal of the Saudi Gastroenterology Association* **22**, 91-105
127. Cave, M. C., Clair, H. B., Hardesty, J. E., Falkner, K. C., Feng, W., Clark, B. J., Sidey, J., Shi, H., Aqel, B. A., McClain, C. J., and Prough, R. A. (2016) Nuclear receptors and nonalcoholic fatty liver disease. *Biochim Biophys Acta* **1859**, 1083-1099
128. Lopez-Velazquez, J. A., Carrillo-Cordova, L. D., Chavez-Tapia, N. C., Uribe, M., and Mendez-Sanchez, N. (2012) Nuclear receptors in nonalcoholic Fatty liver disease. *Journal of lipids* **2012**, 139875
129. Li, A. C., and Glass, C. K. (2002) The macrophage foam cell as a target for therapeutic intervention. *Nat Med* **8**, 1235-1242
130. Dowman, J. K., Tomlinson, J. W., and Newsome, P. N. (2010) Pathogenesis of non-alcoholic fatty liver disease. *QJM* **103**, 71-83
131. Sanyal, A. J., Chalasani, N., Kowdley, K. V., McCullough, A., Diehl, A. M., Bass, N. M., Neuschwander-Tetri, B. A., Lavine, J. E., Tonascia, J., Unalp, A., Van Natta, M., Clark, J., Brunt, E. M., Kleiner, D. E., Hoofnagle, J. H., Robuck, P. R., and Nash, C. R. N. (2010) Pioglitazone, vitamin E, or placebo for nonalcoholic steatohepatitis. *The New England journal of medicine* **362**, 1675-1685
132. Guy, C. D., Suzuki, A., Abdelmalek, M. F., Burchette, J. L., Diehl, A. M., and Nash, C. R. N. (2015) Treatment response in the PIVENS trial is associated with decreased Hedgehog pathway activity. *Hepatology* **61**, 98-107
133. Hirsova, P., and Gores, G. J. (2015) Ballooned hepatocytes, undead cells, sonic hedgehog, and vitamin E: therapeutic implications for nonalcoholic steatohepatitis. *Hepatology* **61**, 15-17
134. Liu, Y., Wei, R., and Hong, T. P. (2014) Potential roles of glucagon-like peptide-1-based therapies in treating non-alcoholic fatty liver disease. *World J Gastroenterol* **20**, 9090-9097
135. Dyson, J. K., Anstee, Q. M., and McPherson, S. (2014) Non-alcoholic fatty liver disease: a practical approach to treatment. *Frontline Gastroenterol* **5**, 277-286
136. Eslami, L., Merat, S., Nasseri-Moghaddam, S. (2009) Treatment of Non-Alcoholic Fatty Liver Disease (NAFLD): A Systematic Review. *Middle East Journal of Digestive Diseases* **1**, 89-99
137. Vrochides, D., Papanikolaou, V., Pertoft, H., Antoniades, A. A., and Heldin, P. (1996) Biosynthesis and degradation of hyaluronan by nonparenchymal liver cells during liver regeneration. *Hepatology* **23**, 1650-1655
138. Zhang, Y., Liu, C., Barbier, O., Smalling, R., Tsuchiya, H., Lee, S., Delker, D., Zou, A., Hagedorn, C. H., and Wang, L. (2016) Bcl2 is a critical regulator of bile acid homeostasis by dictating Shp and lncRNA H19 function. *Scientific reports* **6**, 20559
139. Kleiner, D. E., Brunt, E. M., Van Natta, M., Behling, C., Contos, M. J., Cummings, O. W., Ferrell, L. D., Liu, Y. C., Torbenson, M. S., Unalp-Arida, A., Yeh, M., McCullough, A. J., Sanyal, A. J., and Nonalcoholic Steatohepatitis Clinical Research, N. (2005) Design and validation of a histological scoring system for nonalcoholic fatty liver disease. *Hepatology* **41**, 1313-1321
140. Smalling, R. L., Delker, D. A., Zhang, Y., Nieto, N., McGuiness, M. S., Liu, S., Friedman, S. L., Hagedorn, C. H., and Wang, L. (2013) Genome-wide

transcriptome analysis identifies novel gene signatures implicated in human chronic liver disease. *Am J Physiol Gastrointest Liver Physiol* **305**, G364-374

141. Sanders, K. A., Delker, D. A., Huecksteadt, T., Beck, E., Wuren, T., Chen, Y., Zhang, Y., Hazel, M. W., and Hoidal, J. R. (2019) RAGE is a Critical Mediator of Pulmonary Oxidative Stress, Alveolar Macrophage Activation and Emphysema in Response to Cigarette Smoke. *Scientific reports* **9**, 231
142. Ding, L., Oligschlaeger, Y., Shiri-Sverdlov, R., and Houben, T. (2020) Nonalcoholic Fatty Liver Disease. *Handb Exp Pharmacol*, 1-37
143. Hebbard, L., and George, J. (2011) Animal models of nonalcoholic fatty liver disease. *Nature reviews. Gastroenterology & hepatology* **8**, 35-44
144. Charlton, M., Krishnan, A., Viker, K., Sanderson, S., Cazanave, S., McConico, A., Masuoko, H., and Gores, G. (2011) Fast food diet mouse: novel small animal model of NASH with ballooning, progressive fibrosis, and high physiological fidelity to the human condition. *Am J Physiol Gastrointest Liver Physiol* **301**, G825-834
145. Van Rooyen, D. M., Larter, C. Z., Haigh, W. G., Yeh, M. M., Ioannou, G., Kuver, R., Lee, S. P., Teoh, N. C., and Farrell, G. C. (2011) Hepatic free cholesterol accumulates in obese, diabetic mice and causes nonalcoholic steatohepatitis. *Gastroenterology* **141**, 1393-1403, 1403 e1391-1395
146. Abdelmalek, M. F., Suzuki, A., Guy, C., Unalp-Arida, A., Colvin, R., Johnson, R. J., Diehl, A. M., and Nonalcoholic Steatohepatitis Clinical Research, N. (2010) Increased fructose consumption is associated with fibrosis severity in patients with nonalcoholic fatty liver disease. *Hepatology* **51**, 1961-1971
147. Ouyang, X., Cirillo, P., Sautin, Y., McCall, S., Bruchette, J. L., Diehl, A. M., Johnson, R. J., and Abdelmalek, M. F. (2008) Fructose consumption as a risk factor for non-alcoholic fatty liver disease. *Journal of hepatology* **48**, 993-999
148. Kohli, R., Kirby, M., Xanthakos, S. A., Softic, S., Feldstein, A. E., Saxena, V., Tang, P. H., Miles, L., Miles, M. V., Balistreri, W. F., Woods, S. C., and Seeley, R. J. (2010) High-fructose, medium chain trans fat diet induces liver fibrosis and elevates plasma coenzyme Q9 in a novel murine model of obesity and nonalcoholic steatohepatitis. *Hepatology* **52**, 934-944
149. Clapper, J. R., Hendricks, M. D., Gu, G., Wittmer, C., Dolman, C. S., Herich, J., Athanacio, J., Villescaz, C., Ghosh, S. S., Heilig, J. S., Lowe, C., and Roth, J. D. (2013) Diet-induced mouse model of fatty liver disease and nonalcoholic steatohepatitis reflecting clinical disease progression and methods of assessment. *Am J Physiol Gastrointest Liver Physiol* **305**, G483-495
150. Asgharpour, A., Cazanave, S. C., Pacana, T., Seneshaw, M., Vincent, R., Banini, B. A., Kumar, D. P., Daita, K., Min, H. K., Mirshahi, F., Bedossa, P., Sun, X., Hoshida, Y., Koduru, S. V., Contaifer, D., Jr., Warncke, U. O., Wijesinghe, D. S., and Sanyal, A. J. (2016) A diet-induced animal model of non-alcoholic fatty liver disease and hepatocellular cancer. *Journal of hepatology* **65**, 579-588
151. Matsusue, K., Kusakabe, T., Noguchi, T., Takiguchi, S., Suzuki, T., Yamano, S., and Gonzalez, F. J. (2008) Hepatic steatosis in leptin-deficient mice is promoted by the PPARgamma target gene Fsp27. *Cell metabolism* **7**, 302-311
152. Wolf Greenstein, A., Majumdar, N., Yang, P., Subbaiah, P. V., Kineman, R. D., and Cordoba-Chacon, J. (2017) Hepatocyte-specific, PPARgamma-regulated

mechanisms to promote steatosis in adult mice. *The Journal of endocrinology* **232**, 107-121

153. Paglialunga, S., and Dehn, C. A. (2016) Clinical assessment of hepatic de novo lipogenesis in non-alcoholic fatty liver disease. *Lipids Health Dis* **15**, 159
154. Kohjima, M., Enjoji, M., Higuchi, N., Kato, M., Kotoh, K., Yoshimoto, T., Fujino, T., Yada, M., Yada, R., Harada, N., Takayanagi, R., and Nakamuta, M. (2007) Re-evaluation of fatty acid metabolism-related gene expression in nonalcoholic fatty liver disease. *Int J Mol Med* **20**, 351-358
155. McGarry, J. D., Leatherman, G. F., and Foster, D. W. (1978) Carnitine palmitoyltransferase I. The site of inhibition of hepatic fatty acid oxidation by malonyl-CoA. *The Journal of biological chemistry* **253**, 4128-4136
156. McGarry, J. D., Mannaerts, G. P., and Foster, D. W. (1977) A possible role for malonyl-CoA in the regulation of hepatic fatty acid oxidation and ketogenesis. *J Clin Invest* **60**, 265-270
157. Foster, D. W. (2012) Malonyl-CoA: the regulator of fatty acid synthesis and oxidation. *J Clin Invest* **122**, 1958-1959
158. Nishigori, H., Tomura, H., Tonooka, N., Kanamori, M., Yamada, S., Sho, K., Inoue, I., Kikuchi, N., Onigata, K., Kojima, I., Kohama, T., Yamagata, K., Yang, Q., Matsuzawa, Y., Miki, T., Seino, S., Kim, M. Y., Choi, H. S., Lee, Y. K., Moore, D. D., and Takeda, J. (2001) Mutations in the small heterodimer partner gene are associated with mild obesity in Japanese subjects. *Proc Natl Acad Sci U S A* **98**, 575-580
159. Yuk, J. M., Shin, D. M., Lee, H. M., Kim, J. J., Kim, S. W., Jin, H. S., Yang, C. S., Park, K. A., Chanda, D., Kim, D. K., Huang, S. M., Lee, S. K., Lee, C. H., Kim, J. M., Song, C. H., Lee, S. Y., Hur, G. M., Moore, D. D., Choi, H. S., and Jo, E. K. (2011) The orphan nuclear receptor SHP acts as a negative regulator in inflammatory signaling triggered by Toll-like receptors. *Nature immunology* **12**, 742-751
160. Yang, C. S., Kim, J. J., Kim, T. S., Lee, P. Y., Kim, S. Y., Lee, H. M., Shin, D. M., Nguyen, L. T., Lee, M. S., Jin, H. S., Kim, K. K., Lee, C. H., Kim, M. H., Park, S. G., Kim, J. M., Choi, H. S., and Jo, E. K. (2015) Small heterodimer partner interacts with NLRP3 and negatively regulates activation of the NLRP3 inflammasome. *Nat Commun* **6**, 6115
161. Ibrahim, S. H., Hirsova, P., Tomita, K., Bronk, S. F., Werneburg, N. W., Harrison, S. A., Goodfellow, V. S., Malhi, H., and Gores, G. J. (2016) Mixed lineage kinase 3 mediates release of C-X-C motif ligand 10-bearing chemotactic extracellular vesicles from lipotoxic hepatocytes. *Hepatology* **63**, 731-744
162. Joshi-Barve, S., Barve, S. S., Amancherla, K., Gobejishvili, L., Hill, D., Cave, M., Hote, P., and McClain, C. J. (2007) Palmitic acid induces production of proinflammatory cytokine interleukin-8 from hepatocytes. *Hepatology* **46**, 823-830
163. Kanda, T., Matsuoka, S., Yamazaki, M., Shibata, T., Nirei, K., Takahashi, H., Kaneko, T., Fujisawa, M., Higuchi, T., Nakamura, H., Matsumoto, N., Yamagami, H., Ogawa, M., Imazu, H., Kuroda, K., and Moriyama, M. (2018) Apoptosis and non-alcoholic fatty liver diseases. *World J Gastroenterol* **24**, 2661-2672

164. Copps, K. D., and White, M. F. (2012) Regulation of insulin sensitivity by serine/threonine phosphorylation of insulin receptor substrate proteins IRS1 and IRS2. *Diabetologia* **55**, 2565-2582
165. Sharfi, H., and Eldar-Finkelman, H. (2008) Sequential phosphorylation of insulin receptor substrate-2 by glycogen synthase kinase-3 and c-Jun NH2-terminal kinase plays a role in hepatic insulin signaling. *Am J Physiol Endocrinol Metab* **294**, E307-315
166. Han, M. S., Jung, D. Y., Morel, C., Lakhani, S. A., Kim, J. K., Flavell, R. A., and Davis, R. J. (2013) JNK expression by macrophages promotes obesity-induced insulin resistance and inflammation. *Science* **339**, 218-222
167. Vernia, S., Cavanagh-Kyros, J., Garcia-Haro, L., Sabio, G., Barrett, T., Jung, D. Y., Kim, J. K., Xu, J., Shulha, H. P., Garber, M., Gao, G., and Davis, R. J. (2014) The PPARalpha-FGF21 hormone axis contributes to metabolic regulation by the hepatic JNK signaling pathway. *Cell metabolism* **20**, 512-525
168. Yan, H., Gao, Y., and Zhang, Y. (2017) Inhibition of JNK suppresses autophagy and attenuates insulin resistance in a rat model of nonalcoholic fatty liver disease. *Mol Med Rep* **15**, 180-186
169. Yuk, J. M., Jin, H. S., and Jo, E. K. (2016) Small Heterodimer Partner and Innate Immune Regulation. *Endocrinol Metab (Seoul)* **31**, 17-24
170. Papa, S., Zazzeroni, F., Pham, C. G., Bubici, C., and Franzoso, G. (2004) Linking JNK signaling to NF-kappaB: a key to survival. *J Cell Sci* **117**, 5197-5208
171. Bubici, C., Papa, S., Pham, C. G., Zazzeroni, F., and Franzoso, G. (2004) NF-kappaB and JNK: an intricate affair. *Cell Cycle* **3**, 1524-1529
172. Nakano, H. (2004) Signaling crosstalk between NF-kappaB and JNK. *Trends Immunol* **25**, 402-405
173. Park, H. J., Lee, H. J., Choi, M. S., Son, D. J., Song, H. S., Song, M. J., Lee, J. M., Han, S. B., Kim, Y., and Hong, J. T. (2008) JNK pathway is involved in the inhibition of inflammatory target gene expression and NF-kappaB activation by melittin. *J Inflamm (Lond)* **5**, 7
174. Kim, J. H., Kim, D. H., Baek, S. H., Lee, H. J., Kim, M. R., Kwon, H. J., and Lee, C. H. (2006) Rengyolone inhibits inducible nitric oxide synthase expression and nitric oxide production by down-regulation of NF-kappaB and p38 MAP kinase activity in LPS-stimulated RAW 264.7 cells. *Biochem Pharmacol* **71**, 1198-1205
175. Pan, Y., Zhang, X., Wang, Y., Cai, L., Ren, L., Tang, L., Wang, J., Zhao, Y., Wang, Y., Liu, Q., Li, X., and Liang, G. (2013) Targeting JNK by a new curcumin analog to inhibit NF-kB-mediated expression of cell adhesion molecules attenuates renal macrophage infiltration and injury in diabetic mice. *PLoS One* **8**, e79084
176. Ansari, A. W., Heiken, H., Meyer-Olson, D., and Schmidt, R. E. (2011) CCL2: a potential prognostic marker and target of anti-inflammatory strategy in HIV/AIDS pathogenesis. *Eur J Immunol* **41**, 3412-3418
177. Thompson, W. L., and Van Eldik, L. J. (2009) Inflammatory cytokines stimulate the chemokines CCL2/MCP-1 and CCL7/MCP-3 through NFkB and MAPK dependent pathways in rat astrocytes [corrected]. *Brain research* **1287**, 47-57
178. Weiskirchen, R., and Tacke, F. (2014) Cellular and molecular functions of hepatic stellate cells in inflammatory responses and liver immunology. *Hepatobiliary surgery and nutrition* **3**, 344-363

179. Saiman, Y., and Friedman, S. L. (2012) The role of chemokines in acute liver injury. *Frontiers in physiology* **3**, 213
180. Wang, Y., Ni, H., Li, H., Deng, H., Xu, L. S., Xu, S., Zhen, Y., Shen, H., Pan, H., and Yao, M. (2018) Nuclear factor kappa B regulated monocyte chemoattractant protein-1/chemokine CC motif receptor-2 expressing in spinal cord contributes to the maintenance of cancer-induced bone pain in rats. *Mol Pain* **14**, 1744806918788681
181. Haukeland, J. W., Damas, J. K., Konopski, Z., Loberg, E. M., Haaland, T., Goverud, I., Torjesen, P. A., Birkeland, K., Bjoro, K., and Aukrust, P. (2006) Systemic inflammation in nonalcoholic fatty liver disease is characterized by elevated levels of CCL2. *Journal of hepatology* **44**, 1167-1174
182. Baeck, C., Wehr, A., Karlmark, K. R., Heymann, F., Vucur, M., Gassler, N., Huss, S., Klussmann, S., Eulberg, D., Luedde, T., Trautwein, C., and Tacke, F. (2012) Pharmacological inhibition of the chemokine CCL2 (MCP-1) diminishes liver macrophage infiltration and steatohepatitis in chronic hepatic injury. *Gut* **61**, 416-426
183. Yang, Z., Koehler, A. N., and Wang, L. (2016) A Novel Small Molecule Activator of Nuclear Receptor SHP Inhibits HCC Cell Migration via Suppressing Ccl2. *Molecular cancer therapeutics* **15**, 2294-2301
184. Miao, J., Xiao, Z., Kanamaluru, D., Min, G., Yau, P. M., Veenstra, T. D., Ellis, E., Strom, S., Suino-Powell, K., Xu, H. E., and Kemper, J. K. (2009) Bile acid signaling pathways increase stability of Small Heterodimer Partner (SHP) by inhibiting ubiquitin-proteasomal degradation. *Genes & development* **23**, 986-996
185. Suh, J. H., Huang, J., Park, Y. Y., Seong, H. A., Kim, D., Shong, M., Ha, H., Lee, I. K., Lee, K., Wang, L., and Choi, H. S. (2006) Orphan nuclear receptor small heterodimer partner inhibits transforming growth factor-beta signaling by repressing SMAD3 transactivation. *The Journal of biological chemistry* **281**, 39169-39178
186. Bell, P., Gao, G., Haskins, M. E., Wang, L., Sleeper, M., Wang, H., Calcedo, R., Vandenberghe, L. H., Chen, S. J., Weisse, C., Withnall, E., and Wilson, J. M. (2011) Evaluation of adeno-associated viral vectors for liver-directed gene transfer in dogs. *Hum Gene Ther* **22**, 985-997
187. Gehrke, N., and Schattenberg, J. M. (2020) Metabolic inflammation - a role for hepatic inflammatory pathways as driver of comorbidities in non-alcoholic fatty liver disease (NAFLD)? *Gastroenterology*
188. Huang, J., Iqbal, J., Saha, P. K., Liu, J., Chan, L., Hussain, M. M., Moore, D. D., and Wang, L. (2007) Molecular characterization of the role of orphan receptor small heterodimer partner in development of fatty liver. *Hepatology* **46**, 147-157
189. Akinrotimi, O., Riessen, R., VanDuyne, P., Park, J. E., Lee, Y. K., Wong, L. J., Zavacki, A. M., Schoonjans, K., and Anakk, S. (2017) Small heterodimer partner deletion prevents hepatic steatosis and when combined with farnesoid X receptor loss protects against type 2 diabetes in mice. *Hepatology* **66**, 1854-1865
190. Moon, Y., Park, B., and Park, H. (2016) Hypoxic repression of CYP7A1 through a HIF-1alpha- and SHP-independent mechanism. *BMB Rep* **49**, 173-178
191. Goodwin, B., Jones, S. A., Price, R. R., Watson, M. A., McKee, D. D., Moore, L. B., Galardi, C., Wilson, J. G., Lewis, M. C., Roth, M. E., Maloney, P. R., Willson,

T. M., and Kliewer, S. A. (2000) A regulatory cascade of the nuclear receptors FXR, SHP-1, and LRH-1 represses bile acid biosynthesis. *Molecular cell* **6**, 517-526

192. Kerr, T. A., Saeki, S., Schneider, M., Schaefer, K., Berdy, S., Redder, T., Shan, B., Russell, D. W., and Schwarz, M. (2002) Loss of nuclear receptor SHP impairs but does not eliminate negative feedback regulation of bile acid synthesis. *Developmental cell* **2**, 713-720
193. Bjorkhem, I., Araya, Z., Rudling, M., Angelin, B., Einarsson, C., and Wikvall, K. (2002) Differences in the regulation of the classical and the alternative pathway for bile acid synthesis in human liver. No coordinate regulation of CYP7A1 and CYP27A1. *The Journal of biological chemistry* **277**, 26804-26807
194. Song, K. H., and Chiang, J. Y. (2006) Glucagon and cAMP inhibit cholesterol 7alpha-hydroxylase (CYP7A1) gene expression in human hepatocytes: discordant regulation of bile acid synthesis and gluconeogenesis. *Hepatology* **43**, 117-125
195. Zhang, Y., Xu, N., Xu, J., Kong, B., Copple, B., Guo, G. L., and Wang, L. (2014) E2F1 is a novel fibrogenic gene that regulates cholestatic liver fibrosis through the Egr-1/SHP/EID1 network. *Hepatology* **60**, 919-930
196. Matsusue, K., Haluzik, M., Lambert, G., Yim, S. H., Gavrilova, O., Ward, J. M., Brewer, B., Jr., Reitman, M. L., and Gonzalez, F. J. (2003) Liver-specific disruption of PPARgamma in leptin-deficient mice improves fatty liver but aggravates diabetic phenotypes. *J Clin Invest* **111**, 737-747
197. Moran-Salvador, E., Lopez-Parra, M., Garcia-Alonso, V., Titos, E., Martinez-Clemente, M., Gonzalez-Periz, A., Lopez-Vicario, C., Barak, Y., Arroyo, V., and Claria, J. (2011) Role for PPARgamma in obesity-induced hepatic steatosis as determined by hepatocyte- and macrophage-specific conditional knockouts. *FASEB J* **25**, 2538-2550
198. Lawrence, T. (2009) The nuclear factor NF-kappaB pathway in inflammation. *Cold Spring Harbor perspectives in biology* **1**, a001651
199. Dela Pena, A., Leclercq, I., Field, J., George, J., Jones, B., and Farrell, G. (2005) NF-kappaB activation, rather than TNF, mediates hepatic inflammation in a murine dietary model of steatohepatitis. *Gastroenterology* **129**, 1663-1674
200. Aguilar-Olivos, N. E., Carrillo-Cordova, D., Oria-Hernandez, J., Sanchez-Valle, V., Ponciano-Rodriguez, G., Ramirez-Jaramillo, M., Chable-Montero, F., Chavez-Tapia, N. C., Uribe, M., and Mendez-Sanchez, N. (2015) The nuclear receptor FXR, but not LXR, up-regulates bile acid transporter expression in non-alcoholic fatty liver disease. *Ann Hepatol* **14**, 487-493
201. Bechmann, L. P., Kocabayoglu, P., Sowa, J. P., Sydor, S., Best, J., Schlattjan, M., Beilfuss, A., Schmitt, J., Hannivoort, R. A., Kilicarslan, A., Rust, C., Berr, F., Tschopp, O., Gerken, G., Friedman, S. L., Geier, A., and Canbay, A. (2013) Free fatty acids repress small heterodimer partner (SHP) activation and adiponectin counteracts bile acid-induced liver injury in superobese patients with nonalcoholic steatohepatitis. *Hepatology* **57**, 1394-1406
202. Benet, M., Guzman, C., Pisonero-Vaquero, S., Garcia-Mediavilla, M. V., Sanchez-Campos, S., Martinez-Chantar, M. L., Donato, M. T., Castell, J. V., and Jover, R. (2015) Repression of the nuclear receptor small heterodimer partner by steatotic

drugs and in advanced nonalcoholic fatty liver disease. *Mol Pharmacol* **87**, 582-594

203. Leamy, A. K., Egnatchik, R. A., and Young, J. D. (2013) Molecular mechanisms and the role of saturated fatty acids in the progression of non-alcoholic fatty liver disease. *Progress in lipid research* **52**, 165-174
204. Baylin, A., Kabagambe, E. K., Siles, X., and Campos, H. (2002) Adipose tissue biomarkers of fatty acid intake. *The American journal of clinical nutrition* **76**, 750-757
205. Huang, S., Rutkowsky, J. M., Snodgrass, R. G., Ono-Moore, K. D., Schneider, D. A., Newman, J. W., Adams, S. H., and Hwang, D. H. (2012) Saturated fatty acids activate TLR-mediated proinflammatory signaling pathways. *Journal of lipid research* **53**, 2002-2013
206. Win, S., Than, T. A., Le, B. H., Garcia-Ruiz, C., Fernandez-Checa, J. C., and Kaplowitz, N. (2015) Sab (Sh3bp5) dependence of JNK mediated inhibition of mitochondrial respiration in palmitic acid induced hepatocyte lipotoxicity. *Journal of hepatology* **62**, 1367-1374
207. Hibi, M., Lin, A., Smeal, T., Minden, A., and Karin, M. (1993) Identification of an oncoprotein- and UV-responsive protein kinase that binds and potentiates the c-Jun activation domain. *Genes & development* **7**, 2135-2148
208. Zhou, Z., Xu, M. J., and Gao, B. (2016) Hepatocytes: a key cell type for innate immunity. *Cellular & molecular immunology* **13**, 301-315
209. Wang, W., Xu, M. J., Cai, Y., Zhou, Z., Cao, H., Mukhopadhyay, P., Pacher, P., Zheng, S., Gonzalez, F. J., and Gao, B. (2017) Inflammation is independent of steatosis in a murine model of steatohepatitis. *Hepatology* **66**, 108-123
210. Mandrekar, P., Ambade, A., Lim, A., Szabo, G., and Catalano, D. (2011) An essential role for monocyte chemoattractant protein-1 in alcoholic liver injury: regulation of proinflammatory cytokines and hepatic steatosis in mice. *Hepatology* **54**, 2185-2197
211. Obstfeld, A. E., Sugaru, E., Thearle, M., Francisco, A. M., Gayet, C., Ginsberg, H. N., Ables, E. V., and Ferrante, A. W., Jr. (2010) C-C chemokine receptor 2 (CCR2) regulates the hepatic recruitment of myeloid cells that promote obesity-induced hepatic steatosis. *Diabetes* **59**, 916-925
212. Kim, S. C., Kim, C. K., Axe, D., Cook, A., Lee, M., Li, T., Smallwood, N., Chiang, J. Y., Hardwick, J. P., Moore, D. D., and Lee, Y. K. (2014) All-trans-retinoic acid ameliorates hepatic steatosis in mice by a novel transcriptional cascade. *Hepatology* **59**, 1750-1760
213. Teufel, A., Itzel, T., Erhart, W., Brosch, M., Wang, X. Y., Kim, Y. O., von Schonfels, W., Herrmann, A., Bruckner, S., Stickel, F., Dufour, J. F., Chavakis, T., Hellerbrand, C., Spang, R., Maass, T., Becker, T., Schreiber, S., Schafmayer, C., Schuppan, D., and Hampe, J. (2016) Comparison of Gene Expression Patterns Between Mouse Models of Nonalcoholic Fatty Liver Disease and Liver Tissues From Patients. *Gastroenterology* **151**, 513-525 e510
214. Xiong, X., Wang, Q., Wang, S., Zhang, J., Liu, T., Guo, L., Yu, Y., and Lin, J. D. (2019) Mapping the molecular signatures of diet-induced NASH and its regulation by the hepatokine Tsukushi. *Molecular metabolism* **20**, 128-137

215. Ahrens, M., Ammerpohl, O., von Schonfels, W., Kolarova, J., Bens, S., Itzel, T., Teufel, A., Herrmann, A., Brosch, M., Hinrichsen, H., Erhart, W., Egberts, J., Sipos, B., Schreiber, S., Hasler, R., Stickel, F., Becker, T., Krawczak, M., Rocken, C., Siebert, R., Schafmayer, C., and Hampe, J. (2013) DNA methylation analysis in nonalcoholic fatty liver disease suggests distinct disease-specific and remodeling signatures after bariatric surgery. *Cell metabolism* **18**, 296-302
216. Suppli, M. P., Rigbolt, K. T. G., Veidal, S. S., Heeboll, S., Eriksen, P. L., Demant, M., Bagger, J. I., Nielsen, J. C., Oro, D., Thrane, S. W., Lund, A., Strandberg, C., Konig, M. J., Vilsboll, T., Vrang, N., Thomsen, K. L., Gronbaek, H., Jelsing, J., Hansen, H. H., and Knop, F. K. (2019) Hepatic transcriptome signatures in patients with varying degrees of nonalcoholic fatty liver disease compared with healthy normal-weight individuals. *Am J Physiol Gastrointest Liver Physiol* **316**, G462-G472
217. Kalin, T. V., Ustiyan, V., and Kalinichenko, V. V. (2011) Multiple faces of FoxM1 transcription factor: lessons from transgenic mouse models. *Cell Cycle* **10**, 396-405
218. Saavedra-Garcia, P., Nichols, K., Mahmud, Z., Fan, L. Y., and Lam, E. W. (2018) Unravelling the role of fatty acid metabolism in cancer through the FOXO3-FOXM1 axis. *Mol Cell Endocrinol* **462**, 82-92
219. Laoukili, J., Stahl, M., and Medema, R. H. (2007) FoxM1: at the crossroads of ageing and cancer. *Biochim Biophys Acta* **1775**, 92-102
220. Shang, R., Pu, M., Li, Y., and Wang, D. (2017) FOXM1 regulates glycolysis in hepatocellular carcinoma by transactivating glucose transporter 1 expression. *Oncol Rep* **37**, 2261-2269
221. Ogura, S., Yoshida, Y., Kurahashi, T., Egawa, M., Furuta, K., Kiso, S., Kamada, Y., Hikita, H., Eguchi, H., Ogita, H., Doki, Y., Mori, M., Tatsumi, T., and Takehara, T. (2018) Targeting the mevalonate pathway is a novel therapeutic approach to inhibit oncogenic FoxM1 transcription factor in human hepatocellular carcinoma. *Oncotarget* **9**, 21022-21035
222. Shirakawa, J., Fernandez, M., Takatani, T., El Ouaamari, A., Jungtrakoon, P., Okawa, E. R., Zhang, W., Yi, P., Doria, A., and Kulkarni, R. N. (2017) Insulin Signaling Regulates the FoxM1/PLK1/CENP-A Pathway to Promote Adaptive Pancreatic beta Cell Proliferation. *Cell metabolism* **25**, 868-882 e865
223. Dang, H., Takai, A., Forgues, M., Pomyen, Y., Mou, H., Xue, W., Ray, D., Ha, K. C. H., Morris, Q. D., Hughes, T. R., and Wang, X. W. (2017) Oncogenic Activation of the RNA Binding Protein NELFE and MYC Signaling in Hepatocellular Carcinoma. *Cancer Cell* **32**, 101-114 e108
224. Iida, M., Iizuka, N., Tsunedomi, R., Tsutsui, M., Yoshida, S., Maeda, Y., Tokuhisa, Y., Sakamoto, K., Yoshimura, K., Tamesa, T., and Oka, M. (2012) Overexpression of the RD RNA binding protein in hepatitis C virus-related hepatocellular carcinoma. *Oncol Rep* **28**, 728-734
225. Giannini, E. G., Testa, R., and Savarino, V. (2005) Liver enzyme alteration: a guide for clinicians. *CMAJ* **172**, 367-379
226. Ahmed, M. (2015) Non-alcoholic fatty liver disease in 2015. *World J Hepatol* **7**, 1450-1459

227. Saeed, N., Nadeau, B., Shannon, C., and Tincopa, M. (2019) Evaluation of Dietary Approaches for the Treatment of Non-Alcoholic Fatty Liver Disease: A Systematic Review. *Nutrients* **11**, 3064
228. Kothari, S., Dhami-Shah, H., and Shah, S. R. (2019) Antidiabetic Drugs and Statins in Nonalcoholic Fatty Liver Disease. *J Clin Exp Hepatol* **9**, 723-730
229. Machado, M., Marques-Vidal, P., and Cortez-Pinto, H. (2006) Hepatic histology in obese patients undergoing bariatric surgery. *Journal of hepatology* **45**, 600-606
230. Donnelly, K. L., Smith, C. I., Schwarzenberg, S. J., Jessurun, J., Boldt, M. D., and Parks, E. J. (2005) Sources of fatty acids stored in liver and secreted via lipoproteins in patients with nonalcoholic fatty liver disease. *J Clin Invest* **115**, 1343-1351
231. Umpleby, A. M., Shojaee-Moradie, F., Fielding, B., Li, X., Marino, A., Alsini, N., Isherwood, C., Jackson, N., Ahmad, A., Stolinski, M., Lovegrove, J. A., Johnsen, S., Jeewaka, R. M. A. S., Wright, J., Wilinska, M. E., Hovorka, R., Bell, J. D., Thomas, E. L., Frost, G. S., and Griffin, B. A. (2017) Impact of liver fat on the differential partitioning of hepatic triacylglycerol into VLDL subclasses on high and low sugar diets. *Clinical science* **131**, 2561-2573
232. Lambert, J. E., Ramos-Roman, M. A., Browning, J. D., and Parks, E. J. (2014) Increased de novo lipogenesis is a distinct characteristic of individuals with nonalcoholic fatty liver disease. *Gastroenterology* **146**, 726-735
233. Neuschwander-Tetri, B. A. (2018) Pharmacologic Management of Nonalcoholic Steatohepatitis. *Gastroenterology & hepatology* **14**, 582-589
234. Goedeke, L., Bates, J., Vatner, D. F., Perry, R. J., Wang, T., Ramirez, R., Li, L., Ellis, M. W., Zhang, D., Wong, K. E., Beysen, C., Cline, G. W., Ray, A. S., and Shulman, G. I. (2018) Acetyl-CoA Carboxylase Inhibition Reverses NAFLD and Hepatic Insulin Resistance but Promotes Hypertriglyceridemia in Rodents. *Hepatology* **68**, 2197-2211
235. Rutkowski, D. T., Wu, J., Back, S. H., Callaghan, M. U., Ferris, S. P., Iqbal, J., Clark, R., Miao, H., Hassler, J. R., Fornek, J., Katze, M. G., Hussain, M. M., Song, B., Swathirajan, J., Wang, J., Yau, G. D., and Kaufman, R. J. (2008) UPR pathways combine to prevent hepatic steatosis caused by ER stress-mediated suppression of transcriptional master regulators. *Developmental cell* **15**, 829-840
236. Ota, T., Gayet, C., and Ginsberg, H. N. (2008) Inhibition of apolipoprotein B100 secretion by lipid-induced hepatic endoplasmic reticulum stress in rodents. *J Clin Invest* **118**, 316-332
237. Pastore, A., Alisi, A., di Giovamberardino, G., Crudele, A., Ceccarelli, S., Panera, N., Dionisi-Vici, C., and Nobili, V. (2014) Plasma levels of homocysteine and cysteine increased in pediatric NAFLD and strongly correlated with severity of liver damage. *Int J Mol Sci* **15**, 21202-21214
238. Mardinoglu, A., Ural, D., Zeybel, M., Yuksel, H. H., Uhlen, M., and Boren, J. (2019) The Potential Use of Metabolic Cofactors in Treatment of NAFLD. *Nutrients* **11**, 1578
239. Honda, Y., Kessoku, T., Sumida, Y., Kobayashi, T., Kato, T., Ogawa, Y., Tomeno, W., Imajo, K., Fujita, K., Yoneda, M., Kataoka, K., Taguri, M., Yamanaka, T., Seko, Y., Tanaka, S., Saito, S., Ono, M., Oeda, S., Eguchi, Y., Aoi, W., Sato, K., Itoh, Y., and Nakajima, A. (2017) Efficacy of glutathione for the treatment of nonalcoholic

fatty liver disease: an open-label, single-arm, multicenter, pilot study. *BMC Gastroenterol* **17**, 96
240. Dou, X., Li, S., Hu, L., Ding, L., Ma, Y., Ma, W., Chai, H., and Song, Z. (2018) Glutathione disulfide sensitizes hepatocytes to TNFalpha-mediated cytotoxicity via IKK-beta S-glutathionylation: a potential mechanism underlying non-alcoholic fatty liver disease. *Exp Mol Med* **50**, 7
241. Seol, W., Choi, H. S., and Moore, D. D. (1996) An orphan nuclear hormone receptor that lacks a DNA binding domain and heterodimerizes with other receptors. *Science* **272**, 1336-1339
242. Lu, T. T., Makishima, M., Repa, J. J., Schoonjans, K., Kerr, T. A., Auwerx, J., and Mangelsdorf, D. J. (2000) Molecular basis for feedback regulation of bile acid synthesis by nuclear receptors. *Molecular cell* **6**, 507-515
243. Wang, L., Liu, J., Saha, P., Huang, J., Chan, L., Spiegelman, B., and Moore, D. D. (2005) The orphan nuclear receptor SHP regulates PGC-1alpha expression and energy production in brown adipocytes. *Cell metabolism* **2**, 227-238
244. Suh, Y. H., Kim, S. Y., Lee, H. Y., Jang, B. C., Bae, J. H., Sohn, J. N., Bae, J. H., Suh, S. I., Park, J. W., Lee, K. U., and Song, D. K. (2004) Overexpression of short heterodimer partner recovers impaired glucose-stimulated insulin secretion of pancreatic beta-cells overexpressing UCP2. *The Journal of endocrinology* **183**, 133-144
245. Kim, Y. D., Park, K. G., Lee, Y. S., Park, Y. Y., Kim, D. K., Nedumaran, B., Jang, W. G., Cho, W. J., Ha, J., Lee, I. K., Lee, C. H., and Choi, H. S. (2008) Metformin inhibits hepatic gluconeogenesis through AMP-activated protein kinase-dependent regulation of the orphan nuclear receptor SHP. *Diabetes* **57**, 306-314
246. Seok, S., Kanamaluru, D., Xiao, Z., Ryerson, D., Choi, S. E., Suino-Powell, K., Xu, H. E., Veenstra, T. D., and Kemper, J. K. (2013) Bile acid signal-induced phosphorylation of small heterodimer partner by protein kinase Czeta is critical for epigenomic regulation of liver metabolic genes. *The Journal of biological chemistry* **288**, 23252-23263
247. Preidis, G. A., Kim, K. H., and Moore, D. D. (2017) Nutrient-sensing nuclear receptors PPARalpha and FXR control liver energy balance. *J Clin Invest* **127**, 1193-1201
248. Lee, J. M., Wagner, M., Xiao, R., Kim, K. H., Feng, D., Lazar, M. A., and Moore, D. D. (2014) Nutrient-sensing nuclear receptors coordinate autophagy. *Nature* **516**, 112-115
249. Ratneswaran, A., Sun, M. M., Dupuis, H., Sawyez, C., Borradaile, N., and Beier, F. (2017) Nuclear receptors regulate lipid metabolism and oxidative stress markers in chondrocytes. *J Mol Med (Berl)* **95**, 431-444
250. Xu, P., Zhai, Y., and Wang, J. (2018) The Role of PPAR and Its Cross-Talk with CAR and LXR in Obesity and Atherosclerosis. *Int J Mol Sci* **19**, 1260
251. Hong, F., Pan, S., Guo, Y., Xu, P., and Zhai, Y. (2019) PPARs as Nuclear Receptors for Nutrient and Energy Metabolism. *Molecules* **24**, 2545
252. Xu, Y., O'Malley, B. W., and Elmquist, J. K. (2017) Brain nuclear receptors and body weight regulation. *J Clin Invest* **127**, 1172-1180

253. Bavner, A., Sanyal, S., Gustafsson, J. A., and Treuter, E. (2005) Transcriptional corepression by SHP: molecular mechanisms and physiological consequences. *Trends Endocrinol Metab* **16**, 478-488
254. Brendel, C., Schoonjans, K., Botrugno, O. A., Treuter, E., and Auwerx, J. (2002) The small heterodimer partner interacts with the liver X receptor alpha and represses its transcriptional activity. *Mol Endocrinol* **16**, 2065-2076
255. Ahmadian, M., Suh, J. M., Hah, N., Liddle, C., Atkins, A. R., Downes, M., and Evans, R. M. (2013) PPARgamma signaling and metabolism: the good, the bad and the future. *Nat Med* **19**, 557-566
256. Wang, Y., Nakajima, T., Gonzalez, F. J., and Tanaka, N. (2020) PPARs as Metabolic Regulators in the Liver: Lessons from Liver-Specific PPAR-Null Mice. *Int J Mol Sci* **21**
257. Lee, Y. J., Ko, E. H., Kim, J. E., Kim, E., Lee, H., Choi, H., Yu, J. H., Kim, H. J., Seong, J. K., Kim, K. S., and Kim, J. W. (2012) Nuclear receptor PPARgamma-regulated monoacylglycerol O-acyltransferase 1 (MGAT1) expression is responsible for the lipid accumulation in diet-induced hepatic steatosis. *Proc Natl Acad Sci U S A* **109**, 13656-13661
258. Pettinelli, P., and Videla, L. A. (2011) Up-regulation of PPAR-gamma mRNA expression in the liver of obese patients: an additional reinforcing lipogenic mechanism to SREBP-1c induction. *J Clin Endocrinol Metab* **96**, 1424-1430
259. Listenberger, L. L., Han, X., Lewis, S. E., Cases, S., Farese, R. V., Jr., Ory, D. S., and Schaffer, J. E. (2003) Triglyceride accumulation protects against fatty acid-induced lipotoxicity. *Proc Natl Acad Sci U S A* **100**, 3077-3082
260. Yamaguchi, K., Yang, L., McCall, S., Huang, J., Yu, X. X., Pandey, S. K., Bhanot, S., Monia, B. P., Li, Y. X., and Diehl, A. M. (2007) Inhibiting triglyceride synthesis improves hepatic steatosis but exacerbates liver damage and fibrosis in obese mice with nonalcoholic steatohepatitis. *Hepatology* **45**, 1366-1374
261. Renga, B., Mencarelli, A., Migliorati, M., Cipriani, S., D'Amore, C., Distrutti, E., and Fiorucci, S. (2011) SHP-dependent and -independent induction of peroxisome proliferator-activated receptor-gamma by the bile acid sensor farnesoid X receptor counter-regulates the pro-inflammatory phenotype of liver myofibroblasts. *Inflammation research : official journal of the European Histamine Research Society ... [et al.]* **60**, 577-587
262. Rizzo, G., Disante, M., Mencarelli, A., Renga, B., Gioiello, A., Pellicciari, R., and Fiorucci, S. (2006) The farnesoid X receptor promotes adipocyte differentiation and regulates adipose cell function in vivo. *Mol Pharmacol* **70**, 1164-1173
263. Chiang, J. Y. (2009) Bile acids: regulation of synthesis. *Journal of lipid research* **50**, 1955-1966
264. Janssen, A. W. F., Houben, T., Katiraei, S., Dijk, W., Boutens, L., van der Bolt, N., Wang, Z., Brown, J. M., Hazen, S. L., Mandard, S., Shiri-Sverdlov, R., Kuipers, F., Willems van Dijk, K., Vervoort, J., Stienstra, R., Hooiveld, G., and Kersten, S. (2017) Modulation of the gut microbiota impacts nonalcoholic fatty liver disease: a potential role for bile acids. *Journal of lipid research* **58**, 1399-1416
265. Magee, N., Zou, A., and Zhang, Y. (2016) Pathogenesis of Nonalcoholic Steatohepatitis: Interactions between Liver Parenchymal and Nonparenchymal Cells. *BioMed research international* **2016**, 5170402

266. Hoeke, M. O., Heegsma, J., Hoekstra, M., Moshage, H., and Faber, K. N. (2014) Human FXR regulates SHP expression through direct binding to an LRH-1 binding site, independent of an IR-1 and LRH-1. *PLoS One* **9**, e88011
267. Anakk, S., Watanabe, M., Ochsner, S. A., McKenna, N. J., Finegold, M. J., and Moore, D. D. (2011) Combined deletion of Fxr and Shp in mice induces Cyp17a1 and results in juvenile onset cholestasis. *J Clin Invest* **121**, 86-95
268. Li, H., Chen, F., Shang, Q., Pan, L., Shneider, B. L., Chiang, J. Y., Forman, B. M., Ananthanarayanan, M., Tint, G. S., Salen, G., and Xu, G. (2005) FXR-activating ligands inhibit rabbit ASBT expression via FXR-SHP-FTF cascade. *Am J Physiol Gastrointest Liver Physiol* **288**, G60-66
269. Ali, A. H., Carey, E. J., and Lindor, K. D. (2015) Recent advances in the development of farnesoid X receptor agonists. *Annals of translational medicine* **3**, 5
270. Jung, G. S., Jeon, J. H., Choi, Y. K., Jang, S. Y., Park, S. Y., Kim, M. K., Shin, E. C., Jeong, W. I., Lee, I. K., Kang, Y. N., and Park, K. G. (2015) Small heterodimer partner attenuates profibrogenic features of hepatitis C virus-infected cells. *Liver Int* **35**, 2233-2245
271. Cipriani, S., Carino, A., Masullo, D., Zampella, A., Distrutti, E., and Fiorucci, S. (2017) Decoding the role of the nuclear receptor SHP in regulating hepatic stellate cells and liver fibrogenesis. *Scientific reports* **7**, 41055
272. Fiorucci, S., Antonelli, E., Rizzo, G., Renga, B., Mencarelli, A., Riccardi, L., Orlandi, S., Pellicciari, R., and Morelli, A. (2004) The nuclear receptor SHP mediates inhibition of hepatic stellate cells by FXR and protects against liver fibrosis. *Gastroenterology* **127**, 1497-1512
273. Fiorucci, S., Rizzo, G., Antonelli, E., Renga, B., Mencarelli, A., Riccardi, L., Orlandi, S., Pruzanski, M., Morelli, A., and Pellicciari, R. (2005) A farnesoid x receptor-small heterodimer partner regulatory cascade modulates tissue metalloproteinase inhibitor-1 and matrix metalloprotease expression in hepatic stellate cells and promotes resolution of liver fibrosis. *J Pharmacol Exp Ther* **314**, 584-595
274. Nishizawa, H., Yamagata, K., Shimomura, I., Takahashi, M., Kuriyama, H., Kishida, K., Hotta, K., Nagaretani, H., Maeda, N., Matsuda, M., Kihara, S., Nakamura, T., Nishigori, H., Tomura, H., Moore, D. D., Takeda, J., Funahashi, T., and Matsuzawa, Y. (2002) Small heterodimer partner, an orphan nuclear receptor, augments peroxisome proliferator-activated receptor gamma transactivation. *The Journal of biological chemistry* **277**, 1586-1592
275. Kim, H. I., Koh, Y. K., Kim, T. H., Kwon, S. K., Im, S. S., Choi, H. S., Kim, K. S., and Ahn, Y. H. (2007) Transcriptional activation of SHP by PPAR-gamma in liver. *Biochem Biophys Res Commun* **360**, 301-306
276. Matsumoto, Y., Ishimi, Y., Suzuki, T., Kobayashi, K. I., Inoue, J., and Yamamoto, Y. (2020) Activation of peroxisome proliferator-activated receptor gamma/small heterodimer partner pathway prevents high fat diet-induced obesity and hepatic steatosis in Sprague-Dawley rats fed soybean meal. *J Nutr Biochem* **75**, 108250
277. Brown, G. R., Hem, V., Katz, K. S., Ovetsky, M., Wallin, C., Ermolaeva, O., Tolstoy, I., Tatusova, T., Pruitt, K. D., Maglott, D. R., and Murphy, T. D. (2015) Gene: a gene-centered information resource at NCBI. *Nucleic Acids Res* **43**, D36-42

278. Erez, A., Nagamani, S. C., and Lee, B. (2011) Argininosuccinate lyase deficiency-argininosuccinic aciduria and beyond. *Am J Med Genet C Semin Med Genet* **157C**, 45-53

279. De Chiara, F., Heeboll, S., Marrone, G., Montoliu, C., Hamilton-Dutoit, S., Ferrandez, A., Andreola, F., Rombouts, K., Gronbaek, H., Felipo, V., Gracia-Sancho, J., Mookerjee, R. P., Vilstrup, H., Jalan, R., and Thomsen, K. L. (2018) Urea cycle dysregulation in non-alcoholic fatty liver disease. *Journal of hepatology* **69**, 905-915

280. Ghoshal, S., Stevens, J. R., Billon, C., Girardet, C., Sitaula, S., Leon, A. S., Rao, D. C., Skinner, J. S., Rankinen, T., Bouchard, C., Nunez, M. V., Stanhope, K. L., Howatt, D. A., Daugherty, A., Zhang, J., Schuelke, M., Weiss, E. P., Coffey, A. R., Bennett, B. J., Sethupathy, P., Burris, T. P., Havel, P. J., and Butler, A. A. (2018) Adropin: An endocrine link between the biological clock and cholesterol homeostasis. *Molecular metabolism* **8**, 51-64

281. Stevens, J. R., Kearney, M. L., St-Onge, M. P., Stanhope, K. L., Havel, P. J., Kanaley, J. A., Thyfault, J. P., Weiss, E. P., and Butler, A. A. (2016) Inverse association between carbohydrate consumption and plasma adropin concentrations in humans. *Obesity (Silver Spring)* **24**, 1731-1740

282. Butler, A. A., St-Onge, M. P., Siebert, E. A., Medici, V., Stanhope, K. L., and Havel, P. J. (2015) Differential Responses of Plasma Adropin Concentrations To Dietary Glucose or Fructose Consumption In Humans. *Scientific reports* **5**, 14691

283. Chen, S., Zeng, K., Liu, Q. C., Guo, Z., Zhang, S., Chen, X. R., Lin, J. H., Wen, J. P., Zhao, C. F., Lin, X. H., and Gao, F. (2017) Adropin deficiency worsens HFD-induced metabolic defects. *Cell Death Dis* **8**, e3008

284. Butler, A. A., Tam, C. S., Stanhope, K. L., Wolfe, B. M., Ali, M. R., O'Keeffe, M., St-Onge, M. P., Ravussin, E., and Havel, P. J. (2012) Low circulating adropin concentrations with obesity and aging correlate with risk factors for metabolic disease and increase after gastric bypass surgery in humans. *J Clin Endocrinol Metab* **97**, 3783-3791

285. Kutlu, O., Altun, O., Dikker, O., Aktas, S., Ozsoy, N., Arman, Y., Ozgun Cil, E., Ozcan, M., Aydin Yoldemir, S., Akarsu, M., Toprak, I. D., Kirna, K., Kutlu, Y., Toprak, Z., Eruzun, H., and Tukek, T. (2019) Serum Adropin Levels Are Reduced in Adult Patients with Nonalcoholic Fatty Liver Disease. *Med Princ Pract* **28**, 463-469

286. Sayin, O., Tokgoz, Y., and Arslan, N. (2014) Investigation of adropin and leptin levels in pediatric obesity-related nonalcoholic fatty liver disease. *J Pediatr Endocrinol Metab* **27**, 479-484

287. Kumar, K. G., Trevaskis, J. L., Lam, D. D., Sutton, G. M., Koza, R. A., Chouljenko, V. N., Kousoulas, K. G., Rogers, P. M., Kesterson, R. A., Thearle, M., Ferrante, A. W., Jr., Mynatt, R. L., Burris, T. P., Dong, J. Z., Halem, H. A., Culler, M. D., Heisler, L. K., Stephens, J. M., and Butler, A. A. (2008) Identification of adropin as a secreted factor linking dietary macronutrient intake with energy homeostasis and lipid metabolism. *Cell metabolism* **8**, 468-481

288. Hwang, S., He, Y., Xiang, X., Seo, W., Kim, S. J., Ma, J., Ren, T., Park, S. H., Zhou, Z., Feng, D., Kunos, G., and Gao, B. (2019) Interleukin-22 Ameliorates

Neutrophil-Driven Nonalcoholic Steatohepatitis Through Multiple Targets. *Hepatology*
289. Sell, H., Habich, C., and Eckel, J. (2012) Adaptive immunity in obesity and insulin resistance. *Nature reviews. Endocrinology* **8**, 709-716
290. Brunt, E. M. (2010) Pathology of nonalcoholic fatty liver disease. *Nature reviews. Gastroenterology & hepatology* **7**, 195-203
291. Danford, C. J., and Lai, M. (2019) NAFLD: a multisystem disease that requires a multidisciplinary approach. *Frontline Gastroenterol* **10**, 328-329
292. Byrne, C. D., and Targher, G. (2015) NAFLD: a multisystem disease. *Journal of hepatology* **62**, S47-64
293. Parthasarathy, G., Revelo, X., and Malhi, H. (2020) Pathogenesis of Nonalcoholic Steatohepatitis: An Overview. *Hepatol Commun* **4**, 478-492
294. Zhang, X., Ji, X., Wang, Q., and Li, J. Z. (2018) New insight into inter-organ crosstalk contributing to the pathogenesis of non-alcoholic fatty liver disease (NAFLD). *Protein Cell* **9**, 164-177